Development of a Chimeric Antigen Receptor (CAR)-based T cell therapy for glioblastoma

Giulia Agliardi

University College London

Supervisors: Prof. John Anderson and Dr Karin Straathof

A thesis submitted to University College London (UCL)

for the degree of

DOCTOR OF PHILOSOPHY

I, Giulia Agliardi, confirm that the work presented in this thesis is my own. Where information has been derived from other sources, I confirm that this has been indicated in the thesis.

Giulia Agliardi

Abstract

High grade gliomas are aggressive brain tumours for which treatment is highly challenging due to the location within the central nervous system (CNS), which may reduce access of cytotoxic chemotherapy, and their infiltrative growth, which precludes complete surgical resection. Current treatment includes surgical removal – wherever possible - followed by radiotherapy and chemotherapy. However, recurrence is common, resulting in a survival of only 12 to 15 months after diagnosis. This highlights the need for new therapies.

Chimeric antigen receptors (CARs) are synthetic molecules which combine the specificity of an antibody to the signalling domains of a T cell receptor (TCR), allowing T cells to directly recognise tumour antigens with no need for co-stimulation. CAR-T cells have shown promising responses in the treatment of haematological malignancies, inducing complete and durable responses in patients with chemo-refractory disease treated with CD19-redirected T cells. This therapeutic approach may be highly suitable for high grade gliomas as T cells have the ability to track to distant tumour sites. However, translation of this technology to solid tumours is proving more difficult, due to several challenges, including: requirement for an effective infiltration of CAR-T cells within the tumour and the immunosuppressive environment provided by solid malignancies. In this work, we developed an immunocompetent animal model of glioma, to study kinetics of migration and infiltration of CAR-T cells and the interplay between CAR-T cells, the tumour and the endogenous immune system to inform the design of T cell immunotherapy for this brain tumours.

The tumour specific variant III of the epidermal growth factor receptor (EGFRvIII) – a mutation found in 30% of glioblastomas – was used as model antigen. A murine CAR was constructed based on the single chain fragment variant (ScFv) of EGFRvIII-specific antibody MR1.1 linked with a CD8 stalk to CD28-CD3ζ activation domains. A murine marker gene (truncated CD34) was co-expressed to allow for *ex vivo* analysis as well as firefly luciferase for *in vivo* tracking of CAR T-cells.

The mouse glioma cell line GL261 was modified to express the mouse version of EGFRvIII and used to establish orthotopic tumours.

After validation of function and specificity *in vitro*, efficacy of CAR-T cells was tested *in vivo*. Both bioluminescence imaging (BLI) and flow cytometry

demonstrated that CAR T cells accumulated within the tumour in an antigen-dependent manner. MRI demonstrated that CAR T cells delayed tumour growth and increased survival. However, tumours were not consistently eradicated. Both immunohistochemistry and BLI indicated lack of long term persistence of T cells within the tumour. Analysis of tumour infiltrating lymphocytes (TILs) phenotype suggested that decreased functionality of CAR-T cells could be a result of their exhaustion *in situ*.

We hypothesised that additional strategies were required to improve efficacy and persistence of CAR-T cells. We postulated that CAR-T cell fitness may be prolonged by:

- Incorporation of 41BB as additional co-stimulatory domain in the CAR to provide a pro-survival signal.
- Combination therapy with PD1 blockade to overcome T cell exhaustion (both on CAR and endogenous T cells) *in situ*.

While the employment of third-generation CAR did not significantly improve survival and showed increased toxicity, combination therapy of CAR-T cells and PD-1 blockade promoted complete clearance of tumours resulting in long term survival. Immunohistochemistry and flow cytometry analysis suggested that combination therapy may increase persistence of CAR-T cells, leading to a more rapid and consistent tumour eradication compared to CAR-T cell administration alone. However, data presented here did not demonstrate a synergistic effect of CAR-T cell therapy and PD1 blockade, as an effect of PD1 blockade alone was also observed. Therefore, additional experiments are required to examine this further.

Acknowledgments

This project is the result of a collaboration with many labs within UCL. I had the fortune and privilege to work with many people, the list is long but I wouldn't be where I am without each of them.

Firstly, I would like to thank both my supervisors, for their support, enthusiasm and helpful advice throughout my PhD. Particularly, thanks to Karin for teaching me to always be rational and honest towards my results. You were enthusiastic about my data, often when I wasn't and I am very grateful for your encouragement and supervision. Thanks to John for allowing me to work in the lab and learn from your knowledge and expertise.

A great contribution to this project came from Martin and Sergio. Thanks to Martin, for his invaluable help and constant ideas. Thank to Sergio, for always sparing some time for me to go through my data, discuss them and challenge me as a scientist.

I would also like to thank Angela and all the staff at IQPath at Institute of Neurology: their histopathology service has always been very professional and incredibly reliable.

A big thank you goes to all the people in CABI, who made these years so enjoyable. Particularly, thank to Tom, Raj and Bernard for their help with the ICON, and all the time they spent to optimise sequences for my animal model. Thanks to Alice for her support and help during my experiments and to Tammy for her advice during these years.

A big thank goes to my colleagues in ICH: Barry, Christine, Jon, Denton, Anna and Pierre. And, of course, Aysha: we shared so many frustrations and joys together, you were always there for me, as a colleague I could trust and as a friend. Thanks to all the members of Kerry Chester's lab, I always felt welcomed in your lab. Particularly thanks to Tom: my days at the Cancer Institute wouldn't be the same without the chats over a coffee with you. You always comforted me and told me how wise I am, it's probably not true, but it really helped me in my down moments.

Thanks to the members of Sergio Quezada's lab, for teaching me all I know about flow cytometry. Particularly, thanks to Dafne for her patience with me on those long days on the flow cytometer.

Finally, thanks to all the members of the Pulelab. Particularly to Gordon: you always find time for me and for any of my questions, even when stupid. And, of course, thanks to Alastair: thank you for always be there to discuss about my data and my doubts, and for your help with experiments and your advice while writing this thesis. I feel incredibly lucky to be working so closely with you.

A huge thank goes to my friends, either in London or anywhere else. Particularly to Eleonora: I wouldn't have made through all this without you, I know I can always count on you and I am so grateful for that.

Thanks to Sara, Valentina, Francesca, Elena and Vittoria: I miss you all so much, but I know that even if we now live in different countries I can always count on your help and support, just like when we were at uni.

Thanks to Alberto. I am so grateful for the last six years together and all the beautiful moments we shared. Thank you for always being next to me, even when far away, and for always being so supportive.

Finally, a huge thank to my parents: I probably don't show it as much as I should, but I wouldn't be in this position were it not for you both. Thank you for always believing in me and making me the person I am.

Table of contents

List of figures

List of tables

List of abbreviations

Ab	Antibody
ACT	Adoptive cell therapy
ADCC	Antibody-dependent cell-mediated cytotoxicity
Akt	Protein Kinase B
ALL	Acute Lymphocytic Leukaemia
APC	Antigen presenting cell
ATRX	Alpha-thalassemia X-linked mental retardation protein
BCR	B cell receptor
BLI	Bioluminescence imaging
CAR	Chimeric Antigen Receptor
CAR	Chimeric Antigen Receptor
CCR2,4…	CC-Chemokine receptor 2,4…
CD4,8…	Cluster of Differentiation4,8…
CDCC	Complement-dependent cell-mediated cytotoxicity
CEACAM1	Carcinoembryonic antigen-related cell adhesion molecule 1
CLL	Chronic Lymphocytic Leukaemia
CNS	Central Nervous System
ConA	Concanavalin A
cTEC	Cortical thymic epithelial cells
CTL	Cytotoxic T lymphocyte
CTLA-4	Cytotoxic T lymphocyte associated antigen 4
DAG	Diacylglycerol
DAXX	Death domain associated protein
DC	Dendritic cell
DIPG	Diffuse Intrinsic Pontine Glioma
DNA	Deoxyribonucleic acid
EBV	Epstein-Barr virus
EGFR	Epidermal growth factor receptor
EGFRvIII	Epidermal growth factor receptor variant three
ELISA	Enzyme-linked immunosorbent assay
ER	Endoplasmic reticulum
FACS	Fluorescence Activated Cell Sorting
FasL	Fas ligand
FBS	Foetal Bovine Serum
FLuc	Firefly Luciferase
FSC	Forward Scatter
GBM	Glioblastoma Multiforme
GFP	Green fluorescent protein
Gy	Gray
GzmB	Granzyme B
H&E	Haematoxylin and Eosin

HGG	High grade glioma
HLA	Human leukocyte antigen
HRP	Horseradish peroxidase
ICOS	Inducible T cell costimulator
IDH1/2	Isocitrate dehydrogenase 1 and 2
IFNγ	Interferon gamma
IHC	Immunohistochemistry
IL-2,7…	Interleukin 2,7…
ip	Intraperitoneal
IRES	Internal ribosome site entry
ITAM	Immunoreceptor tyrosine-based activation motif
ITIM	immunoreceptor tyrosine-based inhibitory motif
iv	Intravenous
KD	Knock-down
KO	Knock-out
L/D	Live dead staining
LAG3	Lymphocyte-activation gene 3
Lck	Lymphocyte-specific protein tyrosine kinase
LN	lymph node
LTR	Long Terminal Repeat
MAGE A3	Melanoma Associated antigen A3
MAPK	Mitogen-activated protein kinase
MART 1	Melanoma antigen recognised by T cells 1
MFI	Maedian Fluorescence Intensity
MHC-I/II	Major Histocompatibility class I and II
MRI	Magnetic Resonance Imaging
mTOR	Mammalian target of Rapamacyn
NFAT	Nuclear factor of activated T cells
NK	Natural Killer cells
O/N	Over night
PBS	Phosphate Buffer Saline
PCR	Polymerase Chain Reaction
PD-L1	Programme Cell Death Ligand 1
PD1	Programme Cell Death
PDGFR	Platelet-derived growth factor
PI3K	Phospho
PMA	PHORBOL 12-MYRISTATE 13-ACETATE
pMHC	peptide-major histocompatibility complex
RAG	Recombination activating gene
RARE	Rapid Acquisition with Relaxation Enhancement
Rb	Retinoblastoma
ROI	Region of interest
SAR	Scaffold Attachment Region
ScFv	Single chain Fragment variant

SPL	Splenocytes
SSC	Side scatter
TAA	Tumour Associated Antigen
TBI	Total body irradiation
TCM	Central memory T cells
TCR	T cell receptor
TEM	Effector memory T cells
TERT	Telomerase reverse transcriptase
TGF-b	Transforming growth factor beta
Th1,2	Type1,2… T helper cell
TIL	Tumour infiltrating lymphocytes
TM	Transmembrane domain
TME	Tumour microenvironment
TNFα	Tumour necrosis factor alpha
Treg	Regulatory T cell
Trp1,2	Tyrosinase-related protein 1,2
TSA	Tumour-specific Antigen
Zap70	Zeta-chain-associated protein kinase of 70kDa

Chapter 1

Introduction

1 Introduction

1.1 High grade gliomas

High grade gliomas are a common type of primary brain tumours, both in adults and in children. Among these, glioblastoma multiforme (GBM) is the most aggressive form with the most dismal survival with current standard treatments (12 to 15 months after diagnosis). Therefore, development of new therapeutic approaches is fundamental.

High grade gliomas arise from cells of glial lineage and, according to the World health organisation (WHO), they can be classified in four grades based on their histological features:

- Grade I: *pilocytic astrocytoma*
- Grade II: *diffuse astrocytoma*
- Grade III: *anaplastic astrocytoma*
- Grade IV: *glioblastoma (GBM)*

Grade I and II are classified as low grade gliomas (LGGs), while grade III and IV are considered as high grade gliomas (HGGs). Histologic criteria for high-grade gliomas include hypercellularity, nuclear atypia, and mitotic activity. In addition, GBM present with either microvascular proliferation and/or tumour necrosis. HGGs can either arise *de novo* as fully malignant tumours or they can develop from a previous low-grade glioma (secondary GBMs). Primary GBM arise in elderly patients, while secondary GBMs are more common in younger patients (45 years or less). Despite differences in clinical course, primary and secondary GBMs are histologically indistinguishable.

GBM is the most common and aggressive form of primary brain tumour in adults, with an average of about 7 new cases/100,000 individuals per year in the United Kingdom, accounting for 45-50% of all primary brain tumours. Incidence of this tumour is higher in individuals between 60 and 80 years old and slightly higher in men than women (sex ratio:1.4) and in Caucasians more than in individuals of African descent (Porter et al., 2010).

These tumours are characterised by a high infiltrative nature: invading tumour cells escape at the periphery of the tumour mass and diffusely infiltrate the brain parenchyma (Osswald et al., 2015). This feature makes tumour

recurrence after surgical resection almost inevitable, leading to a median overall survival of only 15-17 months after diagnosis.

1.1.1 High grade gliomas in adults and children

High-grade gliomas predominate in adults, while in children low-grade malignancies are more common. Despite being quite rare in children (one individual every 100,000), HGGs in young individuals still retain dismal prognosis, especially when they arise in the brainstem. The main difference between HGGs in children and adults is the location: supratentorial tumours mainly occur in adults, while infratentorial (brainstem and cerebellum) tumours mainly occur in children. Indeed, brainstem gliomas represent only 1% of adult HGGs, but 10% of paediatric HGG. The most common (50% of cases) form of grade IV glioma in paediatric patients is *diffuse intrinsic pontine glioma* (DIPG), a particularly aggressive form of cancer due to its location and infiltrative nature that makes resection impossible: in these cases, radiation is the only therapy available, leading to a median survival of only 9 to 12 months.

For a long time, gliomas in adults and children have been considered as indistinguishable diseases. However, recent findings have demonstrated that, despite shared histopathological appearance and shared key pathways involved, paediatric gliomas possess peculiar molecular features that make them a distinct disease.

Recent genome-wide sequencing studies identified mutations in the genes encoding for chromatin proteins histone H3 variants H3.3 and H3.1 (Wu et al., 2012; Schwartzentruber et al., 2012) as unique to children and young adults. 44% of paediatric tumours analysed in the study contained mutations in the H3.3-ATRX-DAXX pathway. Histone H3 mutations occur at two residues: the lysine at position 27 (K27M) and the glycine at position 34 (G34R or G34V). A recent study demonstrated that the K27M mutation ablates the tri-methylation usually occurring at this site: lack of this epigenetic modification impairs the interaction with the Polycomb repressive complex 2 (PRC2), thus leading to a deregulation of gene expression (Lewis et al., 2013). These findings demonstrated for the first time that paediatric gliomas are a molecularly and functionally distinct disease compared to adult forms.

1.1.2 Diagnosis and clinical symptoms of GBM

GBMs are most common in cerebral hemispheres which may lead to impaired cognitive functions, including memory loss and confusion and personality changes. Moreover, seizures and headaches (due to increased intracranial pressure) are also frequent.

Diagnosis is confirmed by magnetic resonance imaging (MRI). Standard techniques used in clinical settings are:

- **T2-weighted MR**. The lesions appear hyperintense, due to higher cellular density, increased nucleus/cytoplasm ratio and interstitial oedema
- **Contrast-enhanced T1-weighted MR**: gadolinium is the most common contrast agent used for this acquisition. This technique is particularly useful for volumetric studies at diagnosis and before surgery. The lesions appear hypointense due to accumulation of the contrast agent in the presence of local disruption of the blood brain barrier.
- **Fluid attenuated inversion recovery (FLAIR)** sequences. This method is particularly useful as it allows to null fluids. For this reason, this technique provides a better definition between oedema and tumour.

On MRI, lesions appear quite heterogeneous in shape and are usually limited to one lobe, characterised by a central area of necrosis surrounded by a wide area of oedema that can cross over other lobes. At the time of surgery tissue is obtained to determine the histopathological diagnosis.

In cases where imaging is non-diagnostic, a biopsy is now usually performed to establish diagnosis at a histopathological and molecular level and aid surgical planning. Biopsies can also be performed after surgery to confirm the type of tumour at a histopathological and molecular level. These tumours are typically characterised by the presence of both neoplastic and stromal tissue.

Figure 1.1 Standard MRI sequences used for diagnosis of HGG
(A) Axial T2-weighted image (**B**) FLAIR (**C**) Contrast-enhanced T1-weighted MRI.

1.1.3 Standard treatment

The treatment of malignant gliomas is currently an unmet clinical need, as the survival of patients is still very poor and the median survival remains 12 to 15 months after diagnosis. Standard therapy for newly diagnosed patients includes surgical removal of the tumour mass where possible, followed by radiotherapy and/or chemotherapy. Radiotherapy has shown to increase the survival from a range of 3 to 4 months to a range of 7 to 12 months.

The most common chemotherapeutic agent is *temozolomide*. Its administration in combination with surgery and radiotherapy has led to modest survival improvement (6 to 10% increase in the 1-year survival rate) (Stupp et al., 2005).

Nevertheless, despite the use of combinatorial treatment, tumours usually recur within two centimetres from resection borders. This is due to the highly infiltrative nature of these tumours within the brain parenchyma, which makes the complete resection of the mass usually not possible.

This peculiar feature makes the development of new treatments pivotal. Recent insights into the molecular pathways involved in high grade gliomas offer the chance to develop new targeted therapies which can improve both efficacy and toxic side effects.

1.1.4 Molecular characterisation

So far, high grade gliomas have been largely classified based on their histological features. However, it has become evident that, despite sharing the same morphological features, gliomas can be further characterised based on their molecular alterations (Aldape et al., 2015).

HGGs present the classical alterations in pathways involved in proliferation, apoptosis, invasion and angiogenesis. Some of these mutations are common to all forms of gliomas, while others are restricted to specific subgroups.

Understanding the molecular pathways altered in gliomas can also provide the opportunity for targeted therapies, including immunotherapy, as explored in this thesis.

The next sessions will briefly describe the main pathways altered in high grade gliomas.

Oncosuppressors

p53 is one of the most common oncosuppressors involved in cancer development. Recent studies have demonstrated that mutations/alterations of this pathway are found in 87% of GBMs (Ludwig and Kornblum, 2017). Not only were p53 mutations observed, but also mutations in other proteins in the upstream and downstream pathway, such as ATM, ATR, MDM2 and $p14^{ARF}$ (Figure 1.2).

Alterations of the Retinoblastoma (**Rb**) have been observed in 78% of GBMs. Only 20% of GBMs are mutated at the Rb locus, while inactivating mutations of the upstream regulator $p16^{INK4a}$, or activating mutations in the downstream factors CDK4 or cyclin D are very common (Figure 1.2).

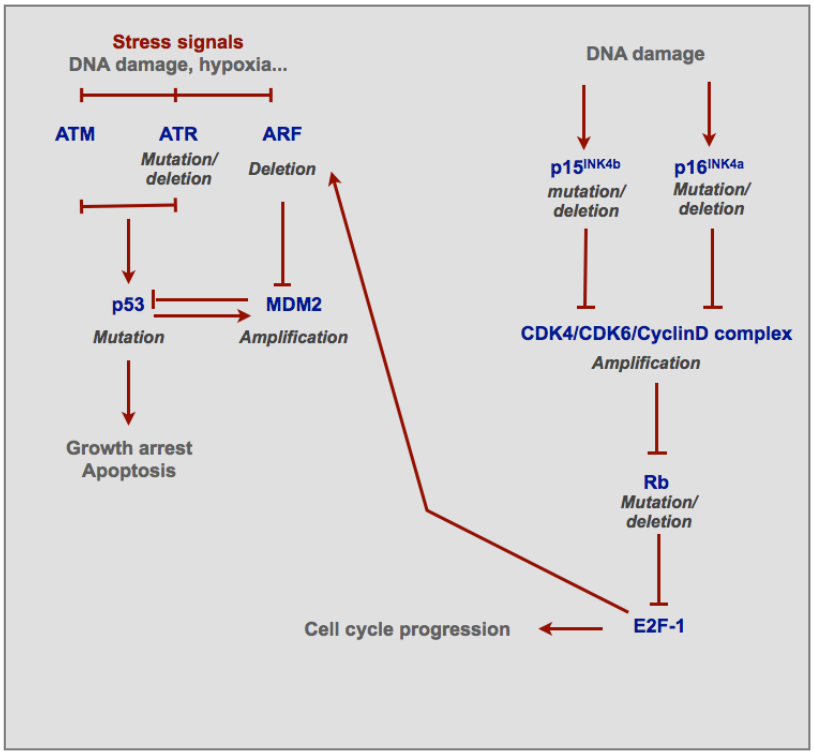

Figure 1.2 Alteration in the p53/Rb pathways in GBM.

The p53 and Rb pathways are often deregulated in many tumours, including glioblastoma (reviewed in Aldape et al., 2015; Ludwig and Kornblum, 2017; Mao et al., 2012).
(**A**) p53 activation is induced after DNA damage and cytotoxic stress. Its activation induces cell cicle arrest and apotosis.
Mutations in p53 itself can occur, however, in 78% of GBM mutations occur in upstream regulators of p53. MDM2 is a negative regulator of p53 (it mediates its degradation through its E3 ubiquitin ligase activity). Amplifications of MDM2 have been observed in 10% of GBM with wild type p53. The tumour suppressor ARF regulates the activity of p53 by directly binding and inhibiting MDM2. Deletion or mutation are common in both low-grade and high-grade gliomas. ATR is another important inducer of p53 actitivity in response to DNA damage. Mutations in this gene have been observed in grade II and III gliomas as well as in secondary GBM.
(**B**) The Rb pathway is another important pathway involved in the inhibition of cell cycle progression. When active, Rb binds and inhibits transcription factors of the E2F family. Mutations in this pathway have been found in 20% of GBM.
In addition to mutations to Rb itself, other mutations have been identified in upstream regulators. During G1 phase, Rb is inhibited by the CDK4/CDK6/CyclinD complex, which phosphorilates Rb leading to its release from E2F with consequent entrance in phase S. Either INK4b or INK4a - which are CDK inhibitors - form a complex with CDK4 or CDK6, thus preventing the activation of the CDKs complex. Both inactivation of CDK2A and CDKN2B locus (encoding for INK4b and INK4a, respectively) and amplification in CDK4 and CDK6 are common in GBM.

Oncogenes

Activation of oncogenic pathways have also been linked to development of GBM. Particularly, mutations and amplification of receptor tyrosine kinases (RTKs) are one of the most common genetic alterations in this kind of malignancy.

The most prevalent alteration occurring in these receptors is the one involving the Epidermal growth factor receptor (**EGFR**). About 40% of adult GBMs present high-level genomic amplification of its locus. This can be associated in some cases (30-50% of patients with amplification) to a constitutively active mutation known as EGFR variant three (EGFRvIII) (Aldape et al., 2015). This mutation will be discussed in further details in the next section.

Another RTK often altered in GBM is the platelet-derived growth factor receptor (**PDGFR**).

Of note, alterations in EGFR are rarely found in paediatric tumours, while PDGFR alterations are more often found in paediatric forms and in Diffuse Intrinsic Pontine Glioma (DIPG).

Moreover, most of GBMs exhibit deregulation of the RTKs downstream pathways PI3K-AKT-mTOR and RAS-MAPK. Approximately 15% of GBMs carry activating mutations of PI3K, while about 30% of cases present silencing mutations of PTEN, the main inhibitor of the PI3K pathway (Figure 1.3). Mutation or deletion of the neurofibromin 1 (NF1) gene, a Ras inhibitor, have also been identified in 15-18% of primary GBMs (Comprehensive genomic characterization defines human glioblastoma genes and core pathways, 2008).

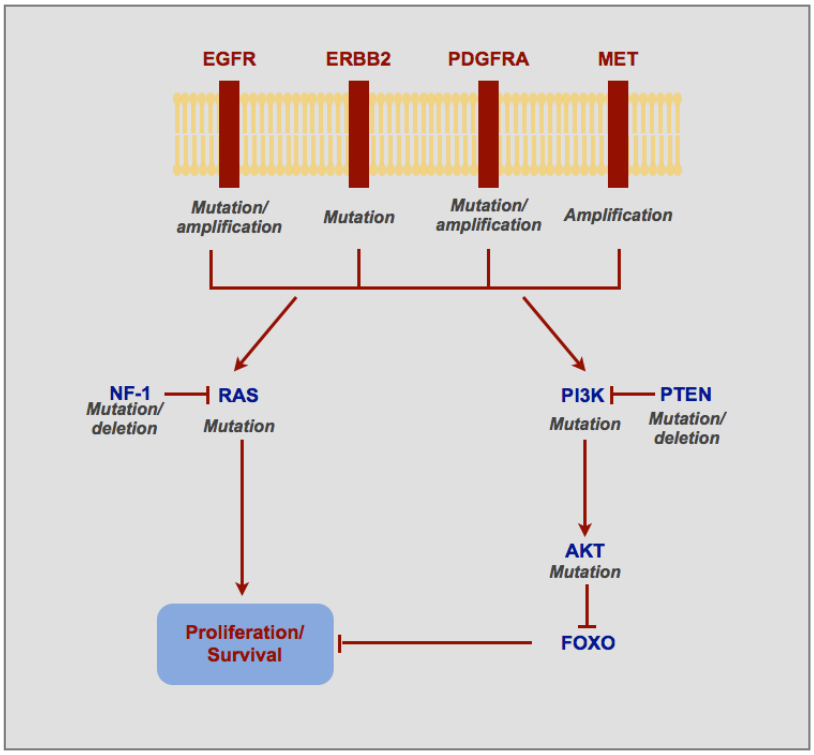

Figure 1.3 Alteration in the RTK/RAS/PI3K pathaways in GBM.
Adapted from (Aldape et al., 2015).

EGFRvIII mutation

Amplification of EGFR is one of the most common alterations observed in glioblastoma. The majority of patients with amplified EGFR also present re-arrangements of this gene, resulting in a tumour that express both wild type and mutated EGFR. EGFRvIII is the most common of these mutations (about 50% of gene mutations). The overall frequency of EGFRvIII mutation is approximately 30% in the adult population, making this mutation quite an attractive target for the treatment of adult HGGs. Of note, this mutation is always accompanied by EGFR amplification.

EGFRvIII is the result of an in-frame deletion of exons 2 to 7 where 801 base pairs are removed, leading to a protein with truncated extracellular domain. This creates a constitutively active form that does not need the ligand to dimerise. The junction between exons 1 and 8 results into a new glycine inserted in between (Figure 1.4).

Expression of this mutant form leads to constitutive autophosphorylation and activation of the Shc–Grb2–Ras and PI3K pathways, which results in

increased proliferation and tumorigenesis (Huang et al., 1997; Narita et al., 2002).

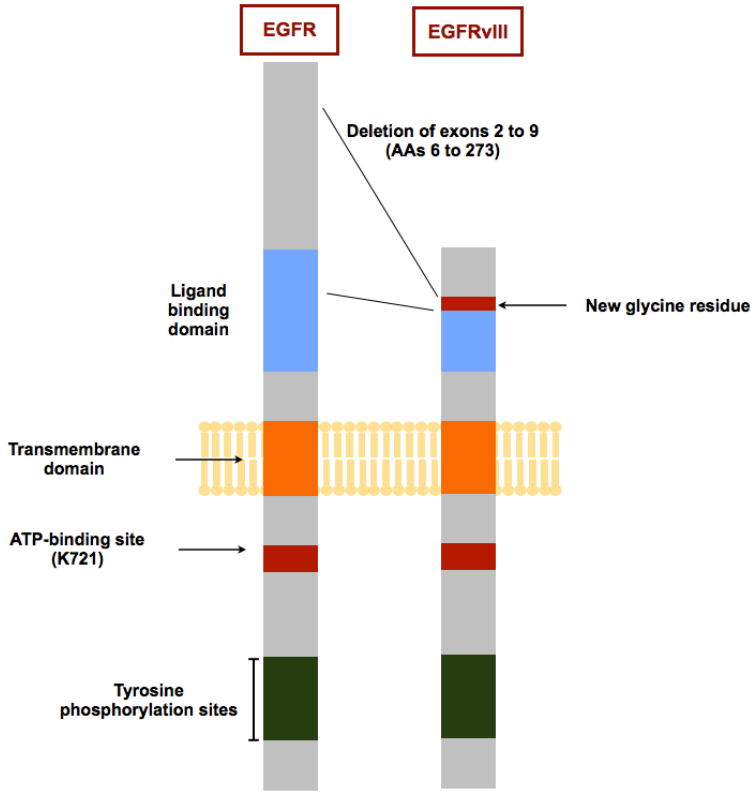

Figure 1.4 The EGFRvIII mutation
Adapted from (Gan et al., 2009)

Isocitrate dehydrogenase 1 and 2 (IDH1/2) mutation

The alteration in the IDH1/2 genes consist in a point mutation which results in an amminoacid substitution (histidine to arginine). This gives the enzyme an additional function whereby it converts alpha-ketoglutarate (α-KG), the normal product, to D-2-hydroxy-glutarate (D-2HG). The mechanism by which the mutant enzyme can promote tumorigenesis is still not entirely clear, but it is believed to be related to the inhibition of demethylases activity, thus resulting in hypermethylated DNA regions (Noushmehr et al., 2010).

The discovery of point mutations in IDH1/2 genes has given important new insight to the molecular sub-classification of GBMs, as alterations of this protein are, in fact, very common in grade II and III diffuse gliomas (70-90%) and secondary GBMs derived from lower glade gliomas (85%). Most of primary

GBMs are, on the other hand, IDH wild type (Louis et al., 2016). IDH mutation is generally mutually exclusive to EGFR amplification/mutations.

Based on these findings, GBMs can now be classified based on their IDH1/2 status. A correlation between IDH1/2 mutation and clinical course is summarised in

Table 1.1.

Table 1.1 Clinical develpoment and molecular features of IDH-wild type and IDH-mutant GBMs
Adapted from (Louis et al., 2016)

	IDH WT GBM	**IDH mutant GBM**
Synonym	Primary GBM	Secondary GBM
Precursor lesion	Not identifiable	Diffuse astrocytoma/ Anaplastic astrocytoma
Proportion of GBM	90%	10%
Median age at diagnosis	62 years	44 years
Male/Female ratio	1.4:1	1.05:1
Mean length of clinical history	4 months	15 months
Median survival (with standard therapy	9-15 months	24-31 months
Location	Supratentorial	Preferentially frontal
TERT promoter mutations	72%	26%
P53 MUTATIONS	27%	81%
ATRX mutations	Exceptional	71%
EGFR amplification	35%	Exceptional
PTEN mutations	24%	Exceptional

1.2 T-cell biology

T cells, together with B cells, comprise the adaptive immune response. While innate immunity – which includes macrophages, NK cells and neutrophils – can mount rapid responses after recognition of pathogen/risk-associated signals, adaptive immunity intervenes at a later stage and is able to recognise unique antigens. This specificity is given by the T cell receptor (TCR).
Besides recognition of pathogens-associated antigens, T cells can recognise aberrantly expressed or mutated antigens which are associated with cancer. This feature makes them an important player in tumour control. This section will describe the basic biology of T cells, while sections 1.3 and 1.4 will describe their role in tumour control and strategies that can be employed to enhance their anti-tumour activity.

1.2.1 Organisation of the adaptive immune response

Tissue-resident dendritic cells (DCs) are specialised cells which, like macrophages, are activated through innate immune receptors (such as Toll-like receptors). Once activated, DCs take up antigens from the inflamed tissue and migrate to the draining lymph nodes where they present the antigens to antigen-specific naive T cells through MHC. T cells that recognise peptides presented by DCs undergo proliferation and enter the circulation and reach the inflamed tissue (Janeway and Murphy, 2011). The activation mechanisms and effector functions of T cells will be described in detail in the next sections.
The second arm of an adaptive immune response is mediated by B cells. To be activated, B cells require signalling both through the B cell receptor (BCR) and through the interaction with helper T cells (called follicular helper T cells, T_{FH}) (Janeway and Murphy, 2011).
Opsonized pathogenic antigens are transported to the lymph nodes through the afferent lymph or to the spleen through the blood, where they are retained either through direct interaction with complement receptors expressed by follicular dendritic cells or by specialised macrophages which retain the antigen on the surface rather than internalising it (Gordon et al., 2015). Once the BCR has engaged with its specific antigen, it is internalised and the antigen is processed for presentation on MHC-II. Activated B cells migrate to the

boundary with the T cell area where they enter in contact with T_{FH} cells. Here, antigen-specific T_{FH} cells recognise their cognate peptide/MHC-II complex expressed by B cells and mediate full activation of B cells through expression of CD40L and production of cytokines. This interaction gives rise to a germinal centre reaction in the follicle where B cells undergo isotype switching and affinity maturation. This process gives rise to plasma cells, specialised B cells which secrete high-affinity antibodies, and memory B cells. This represents the humoral phase of the adaptive immune response, which is mediated by the effector functions of the different antibody subclasses (in human: IgM, IgD, IgG1, IgG3, IgG4, IgA and IgE). These include: neutralisation (IgG and IgA), opsonisation (IgG1 and IgG3 mainly), sensitisation for killing by NK cells (IgG1 and 3), sensitisation of mast cells (IgE), activation of complement system (IgM and IgG3) (Janeway and Murphy, 2011).

1.2.2 T cell receptor

The TCR is a heterodimeric membrane-anchored protein formed by α and β chains, linked by disulphide bonds. Both the α and β chains consist of a constant region which spans the plasma membrane and a variable extracellular region, which confers specificity to a unique antigen (Davis and Bjorkman, 1988).

As opposed to the B-cell receptor (BCR), which recognises native antigens, the TCR recognises processed peptides presented by major histocompatibility complex (MHC) molecules.

Similarly to antibody heavy-chain pools, different genes encode for the α and β chains. These are located on different chromosomes and comprises separate *V* (variable), *D* (diversity, on the β chain) and *J* (joining) genes segments, which are brought together by site-specific recombination during T cell development in the thymus. Recombined V(D)J genes are found in the complementarity-determining regions (CDR) of the TCR chains (Schatz et al., 1992). Particularly, the CDR3 region is involved in the antigen specificity.

TCRs, however, do not undergo somatic hypermutation after antigen encounter, therefore the affinity for the antigen remains low (Janeway and Murphy, 2011).

Figure 1.5 αβ TCR structure.
From (Garcia et al., 1996).

1.2.3 Major histocompatibility complexes (MHC) class I and II

T cells do not recognise antigens in their native form, but they do recognise processed antigens presented by MHCI or II, depending on their co-receptors.

Class I MHC (**MHC-I**) has a transmembrane α chain and a small extracellular protein, β_2-microglobulin, which does not span the plasma membrane and is non-covalently associated to the α chain. The β_2-microglobulin gene is not part of the MHC genes cluster.

The α chain comprises a transmembrane domain and 3 globular extracellular domains, called α_1, α_2 and α_3. The α_1 and α_2 domains are responsible of binding the peptide and presenting to cytotoxic T lymphocytes ($CD8^+$, see 1.2.6) (Figure 1.6A)

Class II MHC (**MHC-II**), on the other hand, has two transmembrane chains, α and β. In contrast to class I MHC, class II MHC chains are encoded by genes within the MHC cluster. The α_1 and β_1 domains constitute the peptide binding site and present it to $CD4^+$helper T cells (Figure 1.6B) (Yin et al., 2012).

Both class I and class II MHC can bind different peptides and present them to T cells. MHC-I binds to 8 to 10 amino acid long peptides, which lie in the cleft in an elongated form stabilised at both ends by contacts with invariants portions of the MHC-I molecule (Janeway and Murphy, 2011).

On the other hand, MHC-II binds to peptides at least 13 amino acids long or more. The peptide is not bound at its extremities to the MHC-II cleft (Figure 1.6), but it is kept in place by amino acids side chains that protrude into pockets lined by polymorphic residues and by interactions between the peptide backbone and side chains of conserved amino acids within the binding cleft.

MHC-I and II expression profiles are also different. MHC-I is expressed on all nucleated cells and platelets (however expression in brain and kidney is lower). MHC-II expression, on the other hand, is restricted to cells of the immune system, including: dendritic cells, macrophages, activated B cells and thymus epithelium.

Figure 1.6 Structure and schematic representation of class I and class II MHC. MHC-I and MHC-II binding cleft structures are from Janeway and Murphy, 2011.

1.2.4 TCR maturation and central tolerance

Once produced within the bone marrow, T cells precursors undergo a process of maturation in the thymus to select functional TCRs and eliminate potentially self-reactive TCRs.

T cell maturation can be divided into three main processes: *a)* thymus colonisation of early T lineage progenitors (ETP) and T cell commitment, *b)* β selection and *c)* MHC-dependent positive and negative selection (reviewed in Carpenter and Bosselut, 2010).

The thymic stroma is responsible for the organisation of the first step, by providing structural support to migrating progenitors (at this stage called thymocytes) and by producing different chemokines which promote cell migration. At this point, thymocytes are called double negative (DN) cells as they do not express either CD4 nor CD8. T lineage commitment involves the sustained repression of alternative gene expression pathways specific of other cell lineages. Thymic stroma is responsible for the production of proteins such as Delta-like 4 (DL4) which interacts with Notch1, a transcription factor considered one of the most important driving forces for T cell commitment (reviewed in Carpenter and Bosselut, 2010; Radtke et al., 2010).

The crucial rearrangements of the variable gene segments (by homologous recombination) occur during the second phase of thymocytes maturation. Because most of the rearrangements at this stage give rise to non-functional proteins, only functional pre-TCRs (consisting of a correctly rearranged TCRβ chain, CD3 chains and the pre-Tα chain), despite not recognising any ligand, are able to signal through oligomerisation and, therefore, are positively selected. This process is known as β-selection.

DNs that pass β-selection become double positive (DP) by expressing both CD4 and CD8 co-receptors and start rearrangements of the α chain. This leads to expression of the final αβ TCR. At this stage cells undergo three additional steps of selection: *a)* positive selection of TCRs interacting with peptide-MHC complexes expressed by cortical thymic epithelial cells (cTEC) and dendritic

cells; (*b)* negative selection of TCRs with affinity for self-antigens in the medullary thymus; (*c)* lineage differentiation (CD4 or CD8). During *(a)*, those TCRs that do not bind self pMHC complexes die by neglect, as failure of interactions results in lack of signal transduction and, ultimately, apoptosis. To avoid autoimmunity resulting from TCRs reactive for self-antigens, a negative selection process has evolved: positively selected thymocytes migrate to the medullar thymus, where medullary thymic epithelial cells (mTEC) present tissue-specific antigens not normally found in the thymus. This process is dependent on expression of AIRE (*autoimmune regulator*), a transcription factor that controls the ectopic expression of self-antigens normally present in peripheral tissues (Anderson et al., 2002). More recently, another transcription factor, Fezf2, was identified as another major regulator of the expression of self-antigens by mTEC in an AIRE-independent manner (Takaba et al., 2015). TCRs with the highest avidity for self pMHC undergo TCR-induced programmed cell death. Moreover, antigens that induce partial TCR activation promote the induction of thymic regulatory T cells ($_tT_{reg}$) (Aschenbrenner et al., 2007). The current model for $_tT_{reg}$ differentiation suggests that transient high affinity TCR engagement induces $_tT_{reg}$ formation, while continuous antigen stimulation induces cell death (reviewed in Li and Rudensky, 2016).

These processes contribute to the formation of central tolerance.

Finally, thymocytes which survive this negative selection will become single positive for one co-receptor (CD4 or CD8), based on their affinity for MHC-I or MHC-II.

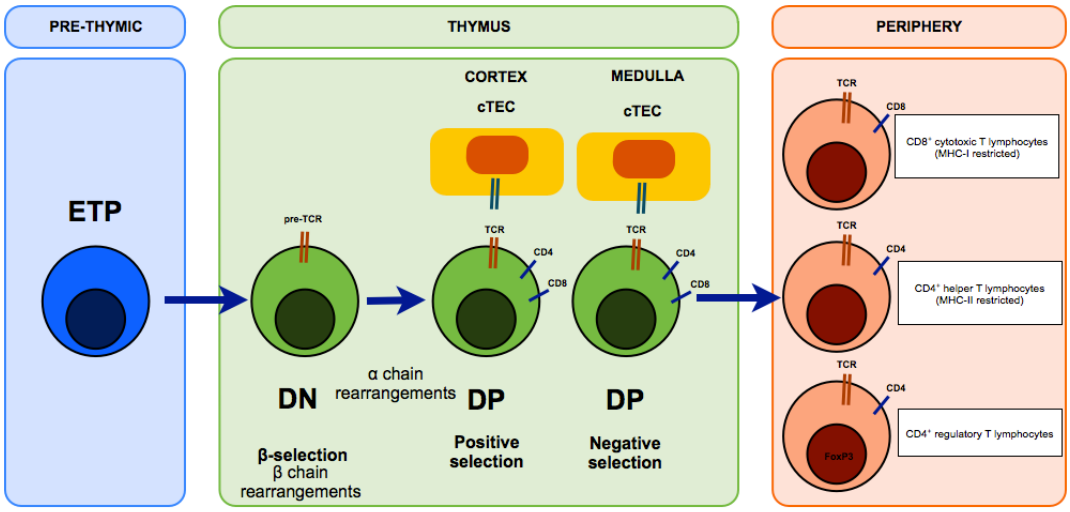

Figure 1.7 Lymphocytes maturation within the thymus.

1.2.5 TCR-MHC interaction and T cell activation

The TCR endodomain does not possess signalling properties. The signalling cascade is dependent on other components part of the so-called TCR complex. The TCR is associated with CD3 molecules: δ, ε, γ and ζ, where the ζ chain contains immunoreceptor tyrosine-based activation motifs (ITAMs) responsible for the signalling cascade in response to TCR engagement (reviewed in Smith-Garvin et al., 2009)

Other two important co-receptors are CD4 and CD8, which are differentially expressed on helper and cytotoxic T cells, respectively. CD4 binds to MHC-II, while CD8 binds to MHC-I and their role in T cells activation relies in both stabilising the TCR-pMHC interaction and bringing the lymphocyte-specific protein tyrosine kinase (Lck) in proximity of the TCR complex (Figure 1.8) (Artyomov et al., 2010). Once either CD4 or CD8 bind to the pMHC, Lck phosphorylates the ITAMs on the CD3ζ chains. These, in turn, recruit the cytosolic zeta-chain-associated protein kinase of 70kDa (ZAP70), which is also phosphorylated by Lck. In this form, ZAP70 is active and can in turn phosphorylate two adaptor molecules: linker of activated T cells (LAT) and SH2 domain containing leukocyte protein of 76kDa (SLP-76). In the active form these proteins form a complex together with phospholipase C gamma 1 (PLCγ1), which produces inositol trisphosphate (IP3) and diacylglycerol (DAG). Production of these substrates activates three different transcription factors: nuclear factor of activated T cells (NFAT), NFκB and activator protein 1 (AP-1), via different pathways (Figure 1.8) (Smith-Garvin et al., 2009; Malissen and Bongrand, 2015)

a) IP3 induces calcium release from the endoplasmic reticulum into the cytosol. This activates calcineurin, a phosphatase which is able to activate NFAT.
b) DAG can de-inhibit NFκB, which is normally retained within the cytosol by inhibitor of NFκB members (IκB). Binding of DAG to PKCθ induces localisation of this protein at the plasma membrane where it gets activated. Activated PKCθ phosphorylates CARMA1, leading to

recruitment of Bcl10 and MALT1 and subsequent formation of the CBM complex. This complex is responsible for the ubiquitinylation and subsequent degradation of the regulatory subunit of the IκB kinase (IKK) complex, which releases the catalytic subunits of the IKK complex. This mediates phosphorylation and degradation of IκB, thus resulting in NFκB nuclear translocation.

c) DAG can also activate *Ras*, leading to activation of the MAPK cascade, which results in activation of AP-1.

Activation of these transcription factors results in their nuclear translocation and initiation of transcription pathways leading to proliferation and enhanced survival and cytokine production (Figure 1.8) (Malissen and Bongrand, 2015).

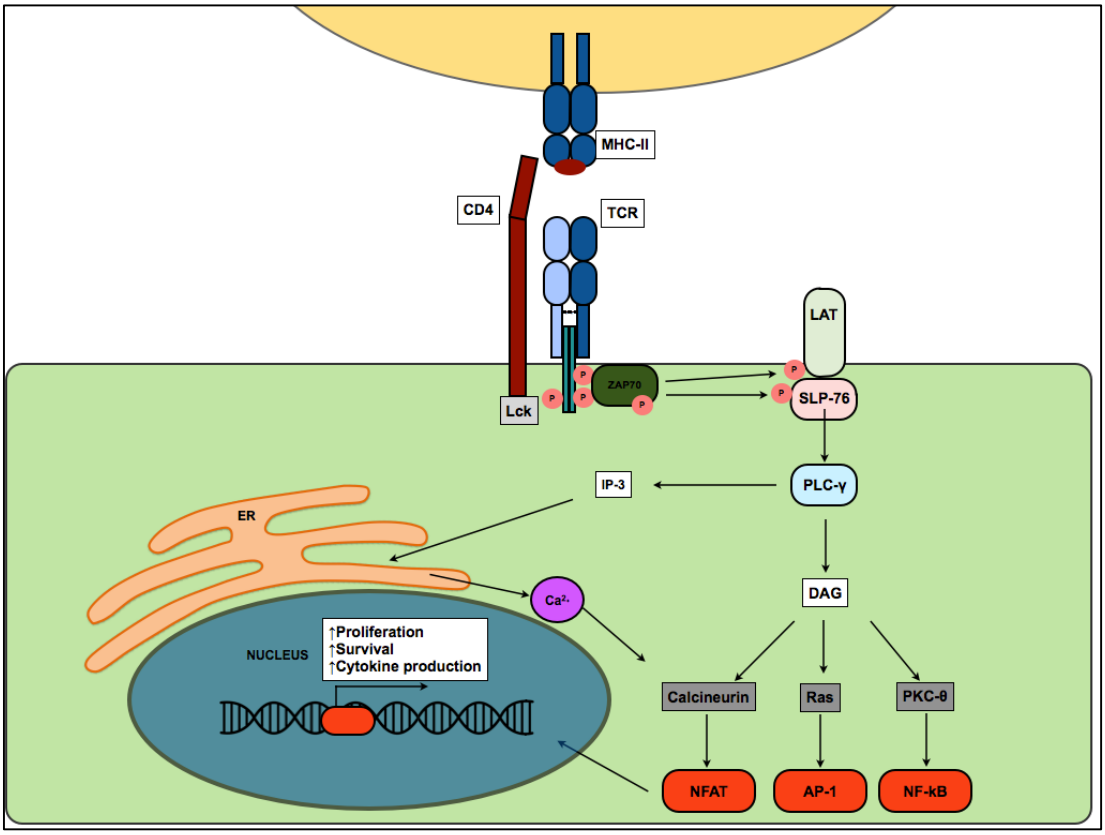

Figure 1.8 Simplified signalling cascade following TCR engagement.

Co-stimulation

TCR stimulation alone, however, is not sufficient to promote a full and efficient activation/proliferation, resulting in T cell anergy. Alongside the presentation of peptide-MHC complex, antigen presenting cells (APCs) have to provide a series of additional co-stimulatory signals. One of the most robust pathways is

the CD80/CD86-CD28. CD80/CD86 - expressed by APCs - interact with CD28, expressed on T cells. The intracellular domain of CD28 does not possess catalytic activity, but presents highly conserved tyrosine and proline-rich sequences important for its downstream signalling. Engagement of CD28 results in the amplification of the signalling pathways downstream of TCR engagement (reviewed in Smith-Garvin et al., 2009). CD28 signalling induces conversion of PIP_2 into PIP_3 and subsequent activation of the Akt pathway: this leads to increased NFκB nuclear translocation and increased transcription of NFAT-regulated genes such as IL2.

Other co-stimulatory pathways are present and are important for a full activation. CD28 is, however, the only molecule that is constitutively expressed on the cell surface. Other receptors include: ICOS (Inducible costimulatory), 41BB and OX40.

ICOS belongs to the CD28 superfamily, but, unlike CD28, is induced only after T cells activation. Engagement of this molecule activates the Akt pathway similarly to CD28. However, ICOS does not promote IL2 transcription mediated by NFAT.

OX40 and 41BB belong to the tumour necrosis factor receptor (TNFR) family. The expression of both these proteins is induced after stimulation and consequent to TCR signalling. Unlike CD28 and ICOS, these proteins do not directly interact with protein kinases, but they rather associate with adaptor proteins such as TRAF (TNFR-associated factor).

41BB expression is induced in activated $CD8^+$ and $CD4^+$ T cells, but also on T_{reg}, B and NK cells. Following engagement with its ligand (41BBL), 41BB forms a heterotrimer complex consisting of two TNF-receptor associated factor (TRAF)-2 and TRAF-1. Formation of this complex recruits the leukocyte specific protein-1 (LSP-1), leading to potentiation of the signalling of c-Jun N-terminal kinase (JNK), extracellular signal-regulated kinase (ERK), β-catenin and AKT. All these pathways converge on NF-κB with consequent amplification of the TCR signalling (reviewed in Bartkowiak and Curran, 2015). Moreover, 41BB has a pivotal role in T cell survival: its engagement prevents activation-induced cell death (AICD) through NFκB-mediated transcription of Bcl-X_L and Bfl-1, two pro-survival members of the BCL family (Watts, 2005).

Similarly to 41BB, the interaction of OX40 with its ligand leads to the its trimerisation, which leads to clustering of the intracellular domain of OX40 creating a docking site for TRAF adaptor proteins (reviewed in Willoughby et al., 2017). Interaction with TRAF proteins is dependent on the QEE motif present in the intracellular portion of both human and mouse OX40. TRAF 2, 3 and 5 have been shown to be localised with OX40. In particular, TRAF 2 and 5 are able to activate the NFκB pathway, while TRAF3 has an inhibitory effect (Kawamata et al., 1998).

Activation of the NF-kB signalling pathway leads to suppression of apoptosis through increased expression of Bcl-2, Bcl-xL and Bfl-1. Moreover, OX40 signalling can enhance the pathways downstream of TCR signalling, such as PI3K/PKB and NFAT. Signalling of PKB signalling from OX40 and TCR has been shown to mediate longevity of T cells through increased expression of Survivin and Aurora B kinase (Song et al., 2005). Additionally, signalling downstream of OX40 increases calcium influx with consequent enhanced NFAT activation and increased production of cytokines such as IL2, IL4 IL5 and IFNγ (So et al., 2006).

The role of 41BB and OX40 in T cells activation seems, therefore, to propagate a long term and efficient response, while CD28 is involved in early stages of T cell activation.

Modulation of T cell activation: inhibitory checkpoints

In a physiological immune response, after antigen encounter and rapid activation and expansion of T cells, this needs to be down-regulated to avoid excessive tissue damage and autoimmunity. Different proteins are involved in this regulatory pathway. These are called inhibitory checkpoints. Here, the most important negative regulators and their mechanisms of action will be discussed, whilst their role in cancer immunotherapy will be discussed later (section 1.4.5).

The checkpoint receptor *cytotoxic T lymphocytes antigen 4* (**CTLA-4**) molecule is one of the most important regulatory feedback mechanism which inhibits excessive activation of T cells. The overall homology between murine and human CTLA-4 is 76%, but the intracellular domain presents complete identity. CTLA-4 is a homologue of CD28, but it binds to its ligands – CD80 and CD86 – with higher affinity than CD28. CTLA-4 is not constitutively expressed on the

surface of naïve T cells, however, after TCR engagement, it is rapidly mobilised and expressed on the cell surface from intracellular vesicles (Mead et al., 2005; Śledzińska et al., 2015).

CTLA-4 competes with CD28 for binding to CD80 and CD86 and therefore inhibits T cell activation by inhibiting CD28 signalling. The signalling downstream of CTLA-4 remains, however, unclear. Recent reports have shown that in T cells from CTLA-4 deficient mice only 9 genes were downregulated when compared to cells from wild type mice, suggesting that no obvious negative pathway is regulated by CTLA-4 (Corse and Allison, 2012).

CTLA-4 is thought to act through a cell-extrinsic mechanism: CTLA-4 captures CD80 and CD86 from APCs and mediates their internalisation within the CTLA-4-expressing cells via trans-endocytosis. These findings suggest that through this mechanism CTLA-4-expressing cells can inhibit activation of other effector T cells (Qureshi et al., 2011).

Moreover, both human and murine regulatory T cells (T_{reg}) constitutively express CTLA-4 and are thought to downregulate the immune response by sequestration of CD80/CD86.

Programmed cell death 1 (**PD1**) is another important inhibitor checkpoint molecule. PD1 is a transmembrane protein with an N-terminal IgV-like domain and a cytoplasmic domain which contains an immunoreceptor tyrosine-based inhibitory motif (ITIM) and an immunoreceptor tyrosine-based switch motif (ITSM).

PD1 has two known ligands, PD-L1 and PD-L2: PD-L1 is expressed by T, B and myeloid cells in response to activation. Moreover, it is expressed by a wide range of human cancer types, which are known to use this mechanism to inhibit the immune response (Sznol and Chen, 2013).

Once it binds to its ligand, two tyrosines within the intracellular portion of PD1 are phosphorylated and recruit two SH2 domain-containing tyrosine phosphatases: SHP-1 and SHP-2. Recruitment of these two proteins mediates the inhibitory function of PD1, by downregulation of TCR signalling, but mainly the CD28 activation pathway and the PI3K-Akt cascade (Riley, 2009; Hui et al., 2017). Knock-out (KO) mice demonstrated that PD1 has a crucial function

in maintaining peripheral tolerance and in regulating T cell exhaustion (Śledzińska et al., 2015).

The *lymphocyte activation 3* (**LAG3**) protein is a type I transmembrane protein belonging to the immunoglobulin super family and its structure closely resembles the CD4 molecule both in human and in mouse. LAG3 binds to MHC-II with higher affinity than CD4, both in human (Baixeras et al., 1992) and in mouse (Workman et al., 2002). $CD4^+$ and $CD8^+$ T cells upregulate LAG3 after activation both in mouse (Workman and Vignali, 2005) and in human (Triebel et al., 1990). In human, it has been demonstrated that LAG3 associates with the TCR/CD3 complex and it inhibits the calcium release in response to CD3 stimulation (Hannier et al., 1998). However, the downstream pathway remains largely unknown and the role of LAG3 in T cell homeostasis is still not entirely clear.

The T cell Immunoglobulin and Immunoreceptor tyrosine-based inhibitory motif (ITIM) domain (**TIGIT**) is a protein of the immunoglobulin superfamily and consists of two ITIMs, a transmembrane domain and an immunoglobulin variable (IgV) domain. Homology between mouse and human is 58% (Yu et al., 2009). In both species, TIGIT is expressed on both activated $CD4^+$ and $CD8^+$ T cells, in association with other exhaustion markers such as PD1 and TIM-3.

TIGIT binds to nectins (such as CD155, CD112 and CD113) with higher affinity than CD226 and CD96 (Yu et al., 2009). Binding of TIGIT by one of its ligands results in the downregulation of T cells proliferation and pro-inflammatory cytokine production. TIGIT seems to downregulate T cell response by inhibiting expression of the α chain of the TCR.

The T cells Ig and Mucin domain proteins (**TIMs**) represent a family of type I transmembrane proteins, containing a single IgV domain followed by a variable length mucin domain and cytoplasmic tail with tyrosine-based signalling motif. In mice, four members of TIMs have been identified (TIM 1 to 4), while in human only three members have been identified (TIM-1, 3 and 4). I will focus here on TIM-3, as its inhibitory role in T cells activation is well established. TIM-3 expression is induced upon activation on $CD8^+$ T cells mainly, but on $CD4^+$ T_h1 T cells as well. Its expression has been associated with an

exhausted phenotype of T cells in the context of viral infection in human (Jones et al., 2008).

One of the inhibitory effects of TIM-3 is mediated by the binding of IgV domain to the High- Mobility Group Box 1 (HMGB1) protein, which blocks the trafficking of nucleic acids into the endosomes, decreasing toll-like receptors stimulation and therefore suppressing the activation of dendritic cells (Gorman and Colgan, 2014). TIM-3 also binds to Galectin-9 and this interaction has been linked to cell death in both activated $CD4^+$ (Zhu et al., 2005) and $CD8^+$ (Sehrawat et al., 2010) T cells. More recently, it has been demonstrated that the interaction between TIM3 and **CEACAM1** (Carcinoembryonic antigen-related cell adhesion molecule 1) – another inhibitor of T cell activation - is important for its binding to galectin-9 and consequent signalling (Huang et al., 2015). The inhibitory functions of TIM3 rely on recruitment at the ITIM motif of the phosphatase SHP-2, which downregulates the TCR signalling.

These proteins are fundamental players of the immune peripheral tolerance. However, their upregulation and persistent expression in the context of cancer has been linked to exhaustion of tumour infiltrating lymphocytes and, therefore, to their failure in controlling tumour growth. This aspect will be discussed in more detail in section 1.4.5.

1.2.6 The production of effector T cells

Once their maturation is completed within the thymus, T cells circulate in the periphery, moving between lymph nodes, blood and spleen. T cells are activated when the innate response fails to control pathogen infections or cancer. Mature T cells that have not encountered their cognate antigen are called naïve T cells and are activated when they recognise their cognate antigen presented on MHC-I or II by professional antigen presenting cells (dendritic cells) within the lymph nodes. Once activated, they are recruited by specific chemokine patterns at the site of inflammation where they orchestrate the adaptive immune response. Here, they are re-activated by both pMHC-I complexes expressed by target cells (infected cells or tumour cells) or by pMHC-II complexes expressed by antigen presenting cells *in situ* (either resident dendritic cells or activated macrophages). According to their co-

receptor (CD4 or CD8), naïve T cells differentiate into different effector cells: CD8 cells differentiate into cytotoxic T lymphocytes (CTL), while $CD4^+$ T cells differentiate into either helper T cells or regulatory T cells, depending on the cytokines present at the time of activation.

$CD8^+$ cytotoxic T lymphocytes (CTLs)

$CD8^+$ T cells are major players in targeted killing of infected or malignant cells. Their function is exploited by direct lysis through release of cytolytic factors, which are pre-synthetized and compartmentalised into lytic granules and secreted after activation. This mechanism requires, therefore, direct interaction between T cells and the target. Cytolytic factors include perforin - a toxin that is thought to form pores into the membrane of target cells - and serine proteases such as Granzyme B (GzmB) (Lopez et al., 2013). Perforin and granzymes act in a synergistic manner, where perforin allows efficient entry of granzymes into the target cell. The mechanisms through which this happens are still not entirely clear: perforin could form pores in the target cell plasma membrane, but also mediate endocytosis and then release of GzmB in the cytosol (Trapani and Smyth, 2002). Apoptosis is triggered through activation of caspases: GzmB cleaves and activates Caspase 3, which in turns activates the caspase proteolytic cascade leading to apoptosis (Andersen et al., 2006). In addition to direct killing mediated by cell to cell contacts, CTLs also produce cytokines of the TNFα family, such as TNFα, FasL and TRAIL, which can also induce apoptosis once they bind to their receptors on target cells. Moreover, CTLs produce IFNγ which inhibits viral proliferation directly, augments surface expression of MHC-I and activates macrophages.

Importantly, CTLs kill infected/malignant cells in a very precise way: after TCR engagement, CTLs orient their Golgi apparatus and microtubule-organising centre to direct specific secretion of GzmB and perforin only at the point of contact with the target cell. This feature is very important to avoid excessive damage of neighbour normal cells (Trapani and Smyth, 2002; Andersen et al., 2006).

$CD4^+$ helper T cells

$CD4^+$ T cells are called helper cells as they do not present direct killing capabilities as opposed to $CD8^+$ T cells, but they rather support other immune cells (both from innate and adaptive response) in their function.

Naïve $CD4^+$ T cells can differentiate into different subsets depending on the microenvironment (i.e. presence of polarising cytokines) at the time the TCR is engaged. These subsets are functionally distinct and present different cytokine profiles (Janeway and Murphy, 2011):

- T_h1 cells produce pro-inflammatory cytokines such as IFNγ and TNFα, which are pivotal stimulators of the function of the cells of the innate response such as macrophages, promote the cytotoxic activity of $CD8^+$ T cells and induce IgG2a production by B cells (Wan and Flavell, 2009).
- T_h2 cells' signature cytokine is IL4, but they also produce IL5, IL9, IL10 and IL13. They promote B cells proliferation and antibody class-switching to IgG1 and IgE antibodies. Moreover, T_h2 cytokines are involved in the alternate polarisation of macrophages into type-2 macrophages (M2), which have an immunomodulatory function, as they are implicated in tissue remodelling, angiogenesis and tumour progression (Mantovani et al., 2002).
- T_h17 T cells signature cytokine is IL17, but they also produce IL21 and IL22. T_h17 are pro-inflammatory cells which are involved in the protection from extracellular pathogens/fungi, as opposed to T_h1, which are active against intracellular pathogens. Their role in autoimmunity has been suggested (Zambrano-Zaragoza et al., 2014).
- A particular subset of $CD4^+$ T cells has the opposite role of downregulating the immune response. Regulatory T cells (T_{reg}) can either develop during thymic maturation (natural T_{reg}, see 1.2.4) or differentiate when naïve T cells are activated in presence of TGFβ and IL10. T_{reg} cells are pivotal to maintain self-tolerance and to maintain immune homeostasis. T_{reg} cells are characterised by the expression of the specific transcription factor Foxp3 (forkhead box 3), a master regulator of T_{reg} development, maintenance and function (Hori et al., 2003; Fontenot et al., 2003). Both in human and mouse, lack of FoxP3 results in a sever autoimmune-like lymphoproliferative disease:

immunodysregulation polyendocrinopathy enteropathy X-linked syndrome (IPEX) in human, while mice present with a phenotype called *scurfy* (Bennett et al., 2001; Wildin et al., 2001).

In mice, T_{reg} cells are identified as $CD25^{+}Foxp3^{+}$. In human, on the other hand, both CD25 (α chain of the IL2 receptor) and FoxP3 are also upregulated in recently activated (non-regulatory) T cells. It was shown that only $CD25^{high}$ T cells possess regulatory function (Baecher-Allan et al., 2005). Moreover, CD127 was also identified as marker for human T_{reg} cells, as lack of CD127 correlates with expression of FoxP3 (Liu et al., 2006; Seddiki et al., 2006). Therefore, in human, T_{reg} cells are identified as $CD25^{high}Foxp3^{+}CD127^{-/low}$.

Moreover, both in human and in mouse T_{reg} cells are positive for CTLA-4, which contributes to their function (Sakaguchi et al., 2010; Tai et al., 2012).

T_{reg} cells downregulate the immune response through a variety of mechanisms: secretion of immunosuppressive cytokines such as TGFβ and IL10, limitation of co-stimulation trough binding (and sequestering) of CTLA-4 to CD80/86 on APCs, sequestration of IL2 through constitutive expression of CD25. Dysfunction or depletion of T_{reg} cells result in development of autoimmune disease. On the other hand, tumours often recruit T_{reg} cells, contributing to tumour immune evasion.

1.2.7 The production of memory T cells

A physiological immune response to a pathogen or a potential cancer comprises an initial effector phase where antigen-specific T cells expand followed by a contraction phase, where 90-95% of T cells die via apoptosis after pathogen clearance. A small fraction of antigen-specific T cells, however, survive and become memory T cells. Memory formation is a pivotal step mediated by the adaptive immune response which allows a more rapid response to pathogens that have been encountered previously. Memory T cells can survive in the absence of the antigen that originally induced them.

Central and effector memory T cells

$CD8^+$ memory T cells are a heterogeneous population comprising effector memory (T_{EM}) and central memory (T_{CM}) T cells. These two subtypes differ in chemokine receptor expression: T_{CM} express CCR7, a chemokine receptor involved in migration to secondary lymphoid organs. These cells have limited effector functions, but they possess a greater potential to proliferate and differentiate into effector T cells. Conversely, T_{EM} do not express CCR7 and express chemokine receptors that promote migration to inflamed tissues - such as β_1 and β_2 integrins- and receptors for inflammatory cytokines. These cells have less proliferative capacity than T_{CM}, but are better able to rapidly produce effector cytokines and lyse target cells after antigen re-encounter (Janeway et al., 2011).

Models for memory T cells formation

The pathway leading to memory T cells formation is still matter of debate and not entirely clear.

The first model provides that after an initial expansion phase where antigen-specific T cells become effector T cells, T cells undergo a contraction phase and only a small fraction of de-differentiated T cells survive to form a memory subset (Youngblood et al., 2013; Restifo and Gattinoni, 2013) (Figure 1.9A).

An alternative model proposes a linear differentiation pathway where memory T cells arise directly from naïve T cells which do not experience a full-strength or repeated antigenic stimulation in a highly inflammatory milieu (Restifo and Gattinoni, 2013) (Figure 1.9B). This model is supported by findings from *in vivo* cell-fate tracking. These studies demonstrated that antigen-specific naïve T cells which undergo massive proliferation tend to generate short-lived effector cells, while minimally expanded T cells preferentially form long-lived memory T cells (Buchholz et al., 2013; Gerlach et al., 2013).

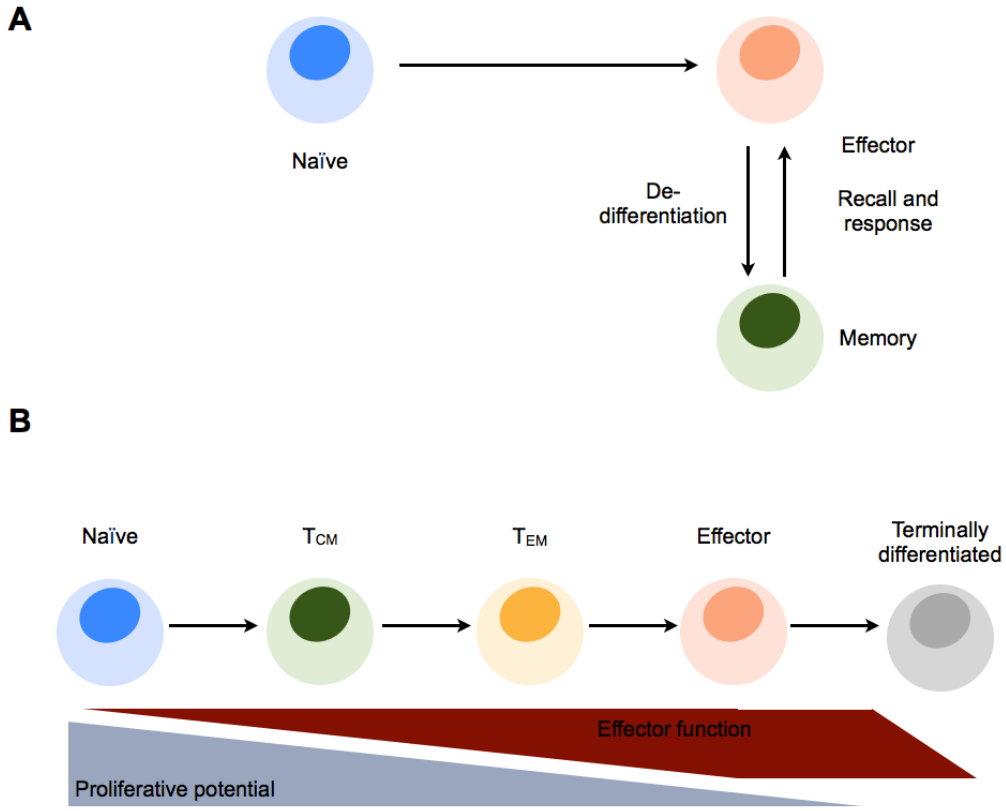

Figure 1.9 Two models for memory T cells formation.
(**A**) De-differentiation model. (**B**) Linear differentiation model.

A better understanding of the dynamics of memory formation is fundamental as it has been demonstrated that functional status and degree of differentiation of adoptively transferred T cells for cancer treatment can significantly affect their efficacy (Gattinoni et al., 2011; Sommermeyer et al., 2016) (see Chapter 3).

1.3 Immune surveillance of cancer

Tumours present a repertoire of either aberrantly expressed or mutated proteins. This characteristic makes them visible to the immune system, which has long been known not only to be interacting with tumour cells, but also to sculpt tumour immunogenicity. This process is known as immunoediting and consists of three phases: elimination, equilibrium and escape (Dunn et al., 2004).

Elimination phase

Pivotal studies that demonstrated a role of the immune system in the control of tumour growth were performed on IFNγ and perforin knock out mice, which showed that deficiency in these pathways enhanced mice susceptibility to chemically induced and spontaneous tumours (Kaplan et al., 1998). Studies performed on immunocompromised RAG-2 (Recombination activating gene 2) deficient mice further demonstrated that lymphocytes play a major role in this process. Depletion of NK cells demonstrated that the innate response is also important for immune surveillance. Tumour elimination consists of an initial response by innate cells such as NK and NKT cells, which respond to local inflammation by producing pro-inflammatory cytokines such as IFNγ. Tumour cell apoptosis causes the release of tumour-specific antigens which are processed by dendritic cells (DC), which then migrate to lymph nodes where they will present processed antigens to T cells. Antigen-specific T cells are activated and subsequently migrate to the tumour site where they will amplify the immune response against the tumour.

Equilibrium

The equilibrium phase is reached when the initial immune response is not able to promote a complete eradication of the tumour. The definitive proof of this process was published in a paper by Koebel and co-workers (Koebel et al., 2007), which showed that mice that rejected Methylcholanthrene (MCA)-induced tumours but that then received antibodies depleting $CD4^+$ and $CD8^+$ T cells and neutralising IFNγ, subsequently developed tumours in more than 50% of cases.

During this phase, the complex interaction between the immune system and the tumour shapes the mutational evolution of the tumour. This is due to the

high genetic instability of cancer, which constantly produces new variants selected for their ability to escape the immune control (Dunn et al., 2004).

Escape

The final phase is represented by the uncontrolled tumour growth which results in a clinical manifestation. At this stage, tumours have accumulated several additional mutations which allow them to overcome the immune response (Dunn et al., 2004). Several mutations have been associated to tumour escape.

Tumours are known to downregulate antigen presentation via reduced expression of MHC-I and MHC-II (Algarra et al., 2000) or the components of the antigen processing pathways (Seliger et al., 2001).

They can also downregulate proteins involved in apoptosis signalling or overexpressing proteins involved in the resistance to apoptosis, thus becoming resistant to CTL-induced apoptosis (Fulda, 2009).

Moreover, tumours can promote immune dysfunction by several mechanisms including (Joyce and Fearon, 2015):

- Production of immunosuppressive cytokines such as TGFβ and IL10 (Khong and Restifo, 2002)
- Production of chemokines which recruit immunosuppressive cells such as T_{reg} cells and myeloid-derived suppressor cells (Gabrilovich and Nagaraj, 2009)
- Expression of PD-L1 by myeloid and cancer cells can down-regulate immune response of PD1-expressing T cells
- Myeloid and cancer cells can also produce Indole 2,3-dioxygenase (IDO) which catabolises tryptophan to generate kynurenine. Expression of this enzyme has been correlated to many effects: removal of tryptophan and generation of its metabolic product inhibit clonal expansion of T cells and promotes differentiation of naïve T cells into T_{reg}.

1.4 Cancer immunotherapy

The impact of cancer immunotherapy has rapidly grown in the past decade. From the formalisation of the concept of cancer immunoediting, many research groups have attempted to boost the immune response against tumours as therapeutic approach. Broadly speaking, cancer immunotherapy can be classified in three main approaches:

- Vaccination against tumour antigens to promote an endogenous immune response
- Adoptive T cell therapy, which can be further divided in two main categories:
  - Infusion of naturally occurring *tumour infiltrating lymphocytes* (TILs) expanded *ex vivo*
  - Infusion of genetically-modified T cells produced *ex vivo*
- Antibody therapy, which can be further divided in five categories:
  - Antibodies blocking specific tumour-associated antigens and associated signalling pathways. Examples in this category include *cetuximab*, an antibody binding to EGFR which blocks its downstream pathway and *trastuzumab*, which binds to HER2 (human epidermal growth factor 2) and blocks its dimerization
  - Antibodies targeting the tumour blood supply, such as *Bevacizumab* which binds to VEGFR (vascular endothelial growth factor receptor).
  - Antibodies mediating direct lysis of target-expressing cells through ADCC (antibody-dependent cytotoxicity) and CDC (complement-dependent cytotoxicity). Examples falling into this category include *Rituximab*, which targets CD20 and has been approved for Non-Hodgkin lymphoma and *alemtuzumab* which targets CD52 and has been approved for CLL (chronic lymphocytic leukaemia).
  - Antibodies armed with cytotoxic agents such as toxins or radio-isotopes, for selective delivery of cytotoxic payloads
  - Checkpoint blockade: antibodies blocking negative immune regulators such as CTLA-4 and PD1
  - Antibodies which can stimulate the immune system: agonistic antibodies for 41BB and OX40 have been shown to promote a

reactivation of the immune system in preclinical models and are currently tested in clinical trials, in combination with other immunotherapeutic approaches (reviewed in Bartkowiak and Curran, 2015; Willoughby et al., 2017).

This section will cover T cell therapy and checkpoint blockade as these approaches were the main focus of this work.

1.4.1 Adoptive T cell therapy: TILs therapy

This approach is based on the idea that removing TILs from the immunosuppressive environment created by the tumour should rescue their ability to activate and expand. The protocol involves the isolation of infiltrating T cells from tumour biopsies. T cells can be expanded over other types of infiltrating immune cells such as NK and myeloid-derived suppressor cells (MDSCs) by growing them in medium containing IL-2 (Figure 1.10). This strategy has shown promising results in the treatment of patients with metastatic melanoma, with objective responses in 50 to 70% of patients and complete and sustained tumour regression in over 20% of treated patients (Dudley et al., 2008; Rosenberg et al., 2011).

Several studies demonstrated that lymphodepletion is fundamental for efficacy of this therapy (Dudley et al., 2008; Rosenberg et al., 2011). The effects of total body irradiation (TBI) or chemotherapy seem to be multiple and include:

- Removal or reprogramming of myeloid-derived suppressor cells (MDSCs) and promotion of inflammation at tumour site
- Depletion of T cells and NK cells to promote homeostatic expansion of transferred T cells (Dummer et al., 2002)
- Production of IL7 and IL15 in response to lymphodepletion directly affects anti-tumour functions of transferred T cells (Gattinoni et al., 2005)

Despite the encouraging results obtained in melanoma, the efficacy of this therapy appears to be restricted to this cancer. This may be related to the high mutation rate of melanoma, a feature that renders it particularly susceptible to recognition by TILs (Restifo et al., 2012; Alexandrov et al., 2013). Isolating TILs from less immunogenic tumours may be difficult, therefore alternative ways of generating tumour-specific T cells have been developed through viral gene transfer.

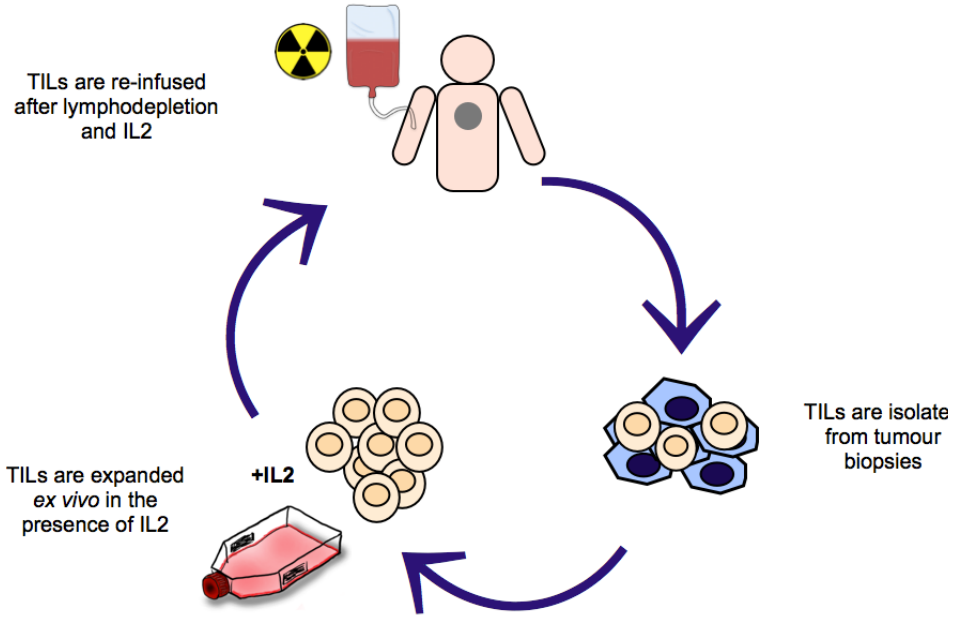

Figure 1.10 Adoptive cell therapy with naturally occurring tumour infiltrating lymphocytes.

1.4.2 Adoptive cell therapy: TCR gene therapy

Genetic modification has been used to graft specificity for tumour antigens onto peripheral blood lymphocytes. Once a TCR recognising a MHC-peptide complex is identified, it can be introduced on polyclonal lymphocytes to re-direct them against the tumour

Several clinical trials have been conducted mainly in patients with metastatic melanoma. Reports demonstrated successful treatments with T cells transduced with a HLA-A2-restricted TCR specific for MART1 (melanoma antigen recognised by T cells 1) (Dudley et al., 2002; Morgan et al., 2006; Johnson et al., 2009). Responses varied between 13% (Morgan et al., 2006) to 30% when using a higher avidity MART1 TCR (Johnson et al., 2009).

Other antigens that have been targeted include: the melanoma antigen gp100 (Johnson et al., 2009), the cancer/testis antigen NY-ESO-1 (Robbins et al., 2011) and MAGE-A3 (Morgan et al., 2013).

Data from these clinical trials suggested that TCR therapy can be effective in controlling tumour growth, however efficacy was reported in only a subset of patients (reviewed in Duong et al., 2015).

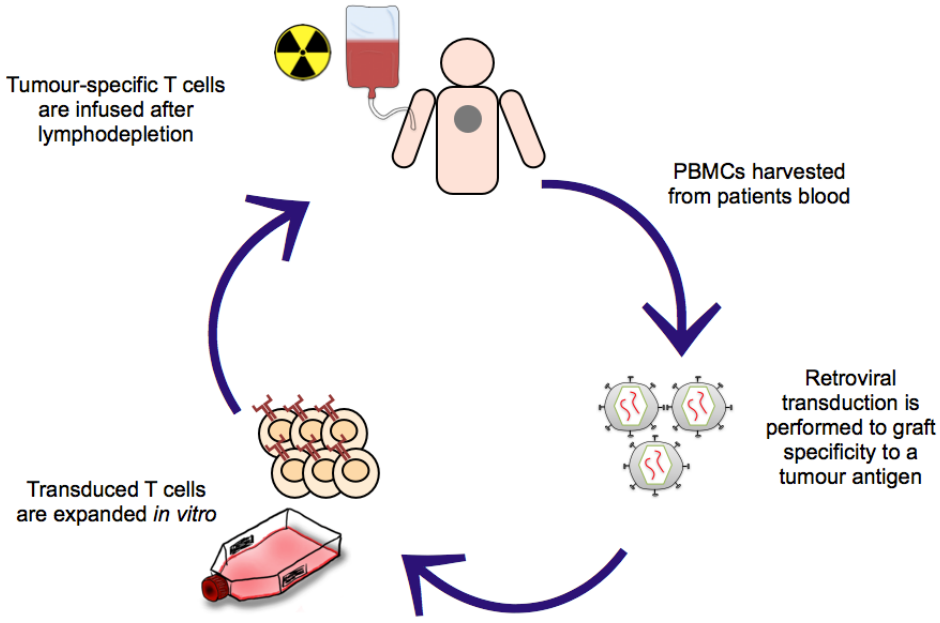

Figure 1.11 Adoptive cell therapy with genetically modified T cells.

In the same way as TILs therapy, TCR therapy has been mainly restricted to melanoma patients, with only few reports in other cancers, such synovial sarcoma (Robbins et al., 2011) and colorectal cancer (Parkhurst et al., 2011).

Limitations of TCR adoptive cell therapy

Several limitations may have contributed to the relatively disappointing results obtained by TCR cell therapy and its restriction to melanoma. Most of the TCR used in clinical trials target tumour associated antigens (TAAs), which are non-mutated antigens associated with specific tissues (like melanoma differentiation antigens such as gp100 and MART1). This feature makes them universal antigens for every patient, but, at the same time, TCRs specific for these antigens are subject to central and peripheral tolerance to avoid autoimmunity and often possess very low avidity for their cognate antigen (Träger et al., 2012; Zhu et al., 2013). Indeed TCRs with increased avidity have shown better response in patients (Johnson et al., 2009). Targeting tumour specific antigens (TSAs), which are mutated antigens only expressed by a certain tumour, would therefore be an advantage, but this approach would make this therapy patient-specific (Heemskerk et al., 2012).

Another limitation of TCR therapies relies on their MHC class restriction, which allows their use only in specific subsets of patients. Moreover, cancers are known to downregulate HLA/MHC as mechanism of immune escape (Algarra et al., 2000; Seliger et al., 2001), which can limit their efficacy in controlling tumour growth.

1.4.3 Adoptive cell therapy: Chimeric Antigen Receptors (CARs)

CARs are obtained by the fusion of the single chain fragment variant of a monoclonal antibody to the intracellular activation domain of the TCR complex, provided by the CD3ζ. This fusion allows for direct recognition of the antigens with no need for presentation through MHC-I MHC-II molecules. This feature is particularly important in the context of immunotherapy, as MHC down-regulation is a mechanism often observed in tumours. Moreover, as they do not require recognition of targets that have undergone antigen processing, CARs are more broadly applicable to HLA-diverse patient populations. A drawback of this is that CARs, in contrast to TCRs, can only recognise antigens expressed on the membrane surface.

The first generation of CARs only included the ScFv fused with the ζ chain of the TCR/CD3 complex (Eshhar et al., 1993). This was sufficient to drive T cell activation, but it was later demonstrated that it is not sufficient to induce a strong cytokine response and T cell expansion.

In a physiological T cell activation, after TCR engagement, co-stimulation is required to prevent anergy of T cells and to produce effective amounts of cytokines as IL2 and IFNγ (see section 1.2.5). Additional co-stimulatory domains were therefore added, such as CD28, 41BB and OX40 (Finney et al., 1998, 2003; Maher et al., 2002; Imai et al., 2004). The addition of a co-stimulatory signal is required to induce full T cell activation after repeated antigen exposure (Maher et al., 2002) and to mediate efficient proliferation and cytokine production (Haynes et al., 2002; Milone et al., 2009).

The benefits of using additional co-stimulation has been demonstrated *in vivo* in both preclinical animal models (Haynes et al., 2002; Carpenito et al., 2009; Milone et al., 2009) and in clinical trials (Savoldo et al., 2011).

Third generation CARs, encompassing two co-stimulatory domains combined with an activation domain in their cytoplasmic domain, have also been developed (Figure 1.12). It has been shown that the additional co-stimulatory domain confers higher potency to CAR-expressing T cells both *in vitro* and *in vivo* (Pulè et al., 2005; Carpenito et al., 2009; Zhong et al., 2010).

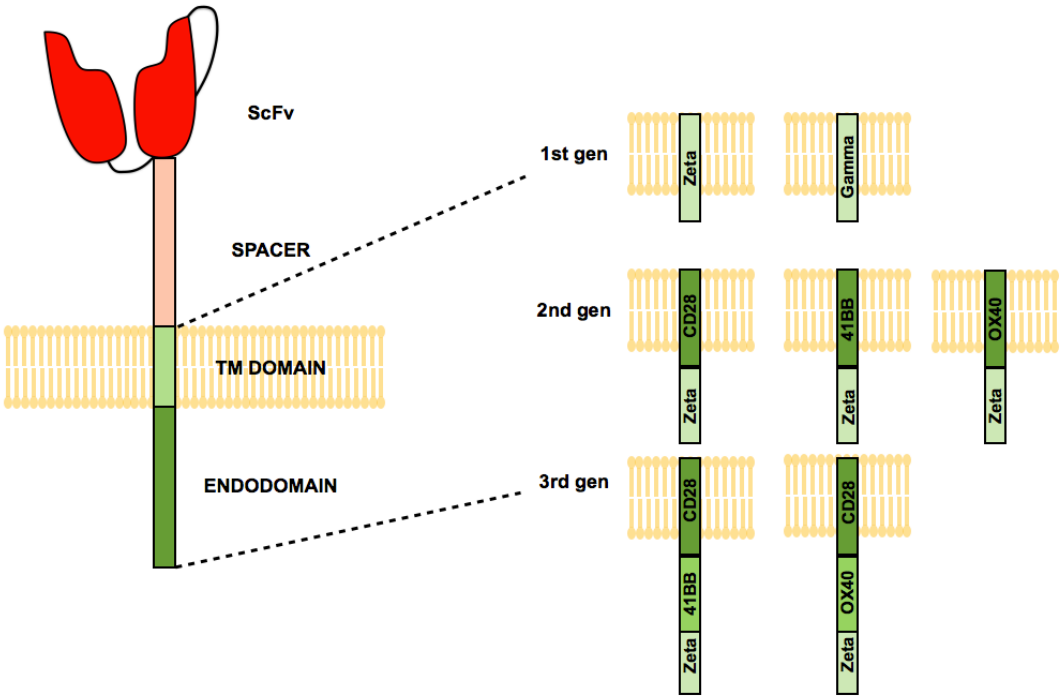

Figure 1.12 Structure of a chimeric antigen receptor.
Adapted from (Ghorashian et al., 2015)

The CD19 paradigm

CD19 is a tumour associated antigen which is expressed by B cells and a range of B cell malignancies. CD19 is not expressed by other haematopoietic populations nor non-haematopoietic cells, therefore making it an ideal target for CAR-T cell therapy, with no toxicity to the bone marrow and non-haematopoietic organs (Ghorashian et al., 2015).

The majority of studies performed with CAR-T cells so far have targeted CD19. Our knowledge of kinetics and efficacy of CAR-T cells mainly comes from studies conducted in CD19-positive malignancies, both in preclinical models and in clinical trials.

Clinical studies have been published on patients with chronic lymphocytic leukaemia (CLL), Non-Hodgkin Lymphoma (NHL) and Acute Lymphoblastic Leukaemia (ALL). In all cases, patients received preparative lymphodepletion prior to CAR-T cells administration. So far, the highest response rates have been observed in ALL patients, with percentage varying between 50 to 90% of cases (Brentjens et al., 2013; Grupp et al., 2013; Davila et al., 2014; Maude et

al., 2014; Lee et al., 2015). Responses in NHL and CLL have been lower (Brentjens et al., 2011; Porter et al., 2011; Savoldo et al., 2011; Kochenderfer et al., 2013). This could be due to the inhibitory tumour microenvironment observed in NHL (Burger and Gribben, 2014).

The main reported adverse effects are:

- B cell aplasia, due to CD19 expression on B cells.
- Cytokine release syndrome (CRS), which can be managed with corticosteroids and, in severe cases, *tocilizumab* (monoclonal antibody blocking IL6 receptor). Severe CRS has been observed – more commonly in patients with higher disease burden.
- Neurotoxicity: this remains a poorly understood problem which has been observed also in patients without overt CNS disease. Brain imaging results normal, however lymphocytosis (composed in part by CAR-T cells) has been observed in the cerebrospinal fluid (CSF). Interestingly, infiltration of CAR-T cells was found also in patients without overt CNS disease. Neuropathies can vary in severity from aphasia to delirium and seizures. (Davila et al., 2014). This seems to resolve spontaneously without specific therapy. However, a recent clinical trial from Juno Therapeutics (Seattle) (NCT02535364) has been suspended for severe neurotoxicity, resulting in the death of 5 patients (http://ir.junotherapeutics.com/phoenix.zhtml?c=253828&p=irol-newsArticle&ID=2225491). The causes of these severe adverse effects are still not known and will require further investigation.

Experience from these initial clinical trials has led to the definition of key parameters which can predict efficacy of CAR-T cells in this context (reviewed in Ghorashian et al., 2015; Lim and June, 2017):

- Persistence and proliferation of transferred CAR-T cells is fundamental for durable responses (Maude et al., 2014; Porter et al., 2015)
- The duration of B cell aplasia has also been correlated to higher responses (Maude et al., 2014)
- The 41BB endodomain is believed to mediate more sustained proliferation and longer persistence of CAR-T cells. Persistence of CD28ζ CAR-T cells was reported to be up to 4 months (Davila et al.,

2014), while 41BB ζ CAR-T cells persisted up to 2 years (Maude et al., 2014). However, this needs further investigation and a clinical trial is currently ongoing to directly compare these co-stimulatory domains (NCT004664531).

- Relapses with antigen-negative tumours are possible (Maude et al., 2014; Yu et al., 2017). Future strategies will have to focus on different approaches to overcome this problem, possibly by targeting two different antigens to avoid relapses.

Translating CAR-T cell therapy to solid tumours

Data from initial clinical trials suggest that targeting CD19-positive malignancies has been particularly successful for several reasons:

- Migration and infiltration of CAR-T cells in the bone marrow and lymph nodes is easier than in solid tumours (Lim and June, 2017).
- CD19-positive B cells provide an optimal target to mediate efficient proliferation of CAR-T cells once infused into the patients. B cells can also provide co-stimulation through expression of CD80/CD86, thus facilitating long term persistence of CAR-T cells (Lim and June, 2017).
- Haematological malignancies represent a less immunosuppressive environment compared to other solid cancers. This might also be the reason why CLL and NHL have shown lower responses compared to ALL (Burger and Gribben, 2014).

The first clinical trials for solid tumours are currently ongoing. Some tumour responses have been observed, however it is becoming clear that translation of CAR-T cell therapy to solid tumours will require additional strategies and optimisation of the CAR construct to enhance efficacy and achieve the remarkable clinical responses obtained in haematological malignancies (Jackson et al., 2016; Lim and June, 2017).

Table 1.2 summarises the current ongoing clinical trials for solid tumours and the antigens targeted.

Among these, mesothelin-directed CAR-T cells have shown some initial response, but patients then relapsed (Beatty et al., 2014). Another clinical trial is currently testing efficacy of mesothelin-specific CAR-T cells locally injected into the pleural space, as pre-clinical data suggested more potent effect

through this route of administration (Adusumilli et al., 2014). The disialoganglioside GD2 has also been targeted for neuroblastoma, showing responses in 3 out 11 patients treated (Louis et al., 2011). The human epidermal growth factor 2 (HER2) has also been tested in patients with late-stage sarcoma and colon cancer, but opposing results have been observed so far. Concerns arose when a patient died due to acute respiratory failure following administration of a third-generation CAR (Morgan et al., 2010), however, another clinical trial with a second-generation CAR specific for HER2 has shown no adverse effects and remissions up to 16 months in three out 17 patients (Ahmed et al., 2015).

Based on the experience of haematological malignancies and first clinical trial in solid tumours, different parameters are becoming apparent which need to be taken into consideration to increase efficacy in solid cancers. These are summarised in Figure 1.13.

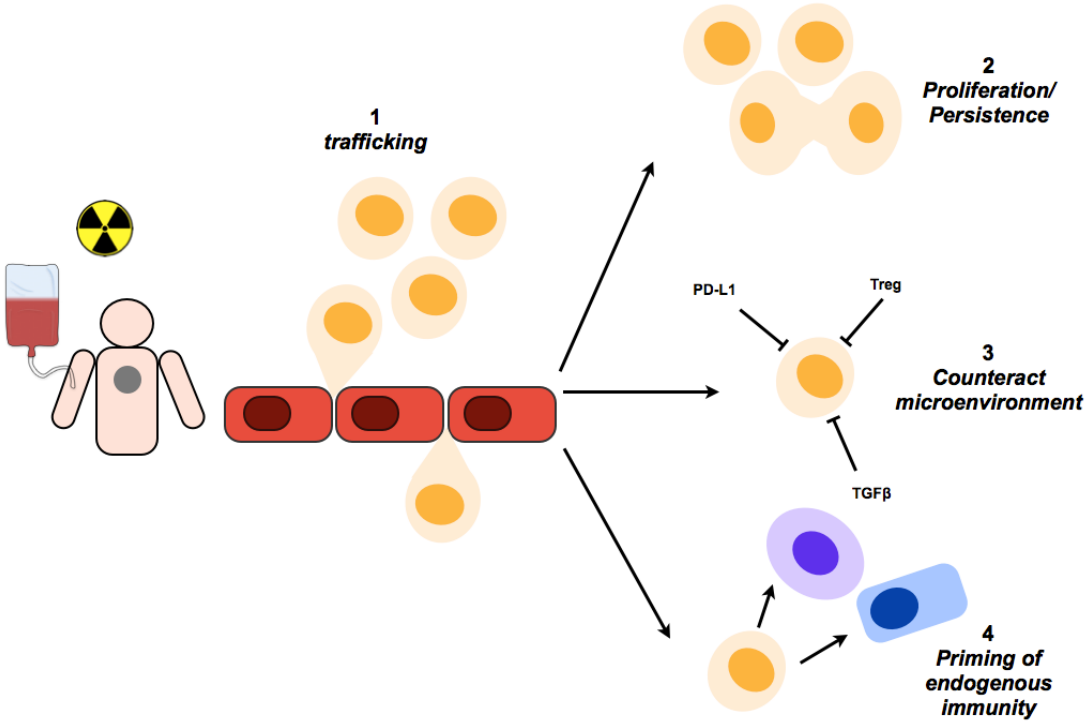

Figure 1.13 Functional needs for optimal anti-cancer T cell therapy
Adapted from (Lim and June, 2017).

Table 1.2 Clinical trials ongoing with CAR-T cells for solid tumours
Adapted from (Jackson et al., 2016)

Target	Malignancy	CAR structure	Reference
PSMA	Prostate Cancer	CD3ζ and CD28	NCT01140373 NCT00664196
Mesothelin	Mesothelioma/Pancreatic Cancer/Ovarian Cancer	CD3ζ and CD28 CD3ζ and 41BB CD3ζ, 41BB and CD28	NCT01355965 NCT02465983/ NCT02159716 NCT02414269 NCT01583686
FAP	Mesothelioma	CD3ζ and CD28	NCT01722149
EGFRvIII	Glioma	CD3ζ and 41BB CD3ζ, 41BB and CD28	NCT02209376 NCT01454596
CEA	Liver metastasis	CD3ζ and CD28	NCT02146466
CD171	Neuroblastoma	CD3ζ and 41BB CD3ζ, 41BB and CD28	NCT02311621
GD2	Sarcoma/Glioblastoma	CD3ζ, OX40 and CD28 CD3ζ, OX40 and CD28 virus-specific CD3ζ and CD28	NCT02107963 NCT01822652 NCT01953900 NCT02761915
HER2	Glioblastoma/Sarcoma	CD3ζ and CD28 CD3ζ, Ox40, CD28, virus specific	NCT00902044 NCT02442297 NCT01109095
IL-13	Glioma	RαCD3ζ and 4-1BB	NCT02208362

1- Improve trafficking

Solid tumours represent an additional challenge to effective T cell migration, as some tumours are known to be more fibrotic and therefore more difficult to penetrate, while others can actively suppress chemokine signalling (Lim and June, 2017). Two studies reported that incorporation of a chemokine receptor (CCR2 or CCR4) enhances tumour infiltration (Di Stasi et al., 2009; Moon et al., 2011).

2- Proliferation and persistence of CAR-T cells

Initial clinical trials with neuroblastoma patients have demonstrated that persistence of CAR-T cells is fundamental also in the context of solid tumours (Louis et al., 2011). In this study, Brenner and colleagues showed that longer persistence of CAR-T cells (over 6 weeks) was associated with better clinical outcome.

It has become clear that the phenotype of T cells at the time of injection can affect their persistence. Central memory T cells (T_{CM}) have higher proliferative

capacity compared to effector memory T cells (T_{EM}) (see section 1.2.7). In primates, it has been shown that antigen-specific $CD8^+$ T_{CM} cells, but not T_{EM}, expand long term, reacquire phenotypic and functional properties of memory T cells and occupy memory T cell niches (Berger et al., 2008). In a recent study, CAR-T cells derived from distinct subtypes of $CD4^+$ and $CD8^+$ T cells had different anti-tumour activity and proliferation potential, both *in vivo* and *in vitro*. Combination of the most potent $CD4^+$ (naïve) and $CD8^+$ (central memory) displayed synergistic effect *in vivo* (Sommermeyer et al., 2016).

Moreover, in human it has been suggested that a population of stem-like memory T cells retains even higher proliferative potential i*n vivo*; human CAR-T cells derived from this population mediated a more potent anti-tumour activity in immunocompromised mesothelioma-bearing mice (Gattinoni et al., 2011).

An alternative approach to improve persistence of CAR T cells is the use of T cells with anti-viral specificity, to provide cells with a physiological T cell activation through the TCR. Epstein Barr Virus (EBV)-specific first-generation CAR-T cells specific for GD2 (Pule et al., 2008) and CD19 have shown better persistence *in vivo*, especially following EBV-directed vaccination (Rossig et al., 2017).

3- *Overcoming an immunosuppressive environment and priming endogenous immune system*

As discussed in section 1.3 (Immunoediting), solid cancers present an immunosuppressive environment which can evolve to down-regulate the immune response (reviewed in Joyce and Fearon, 2015).

Different strategies have been explored to overcome this barrier and improve function of CAR-T cells in the context of solid cancers.

- Additional co-stimulation: incorporation of a constitutively active 41BBL (Zhao et al., 2015) or CD40L (Curran et al., 2015) co-stimulation molecules increased efficacy of CAR-T cells *in vivo*. For 41BBL, the effect seems to be mediated by induction of IFNβ pathway (Zhao et al., 2015).

- Co-expression of cytokines: T cells transduced with a bicistronic vector to produce both the CAR and a pro-inflammatory cytokine that can remodel the microenvironment. IL12 is one of the most potent anti-tumour cytokines, however systemic effects can be highly toxic in humans. CAR-T cells engineered to produce IL12 either in a constitutive way (through an IRES)

(Pegram et al., 2012) or only in response to activation (through and inducible promoter, NFAT) (Chmielewski et al., 2011) have been shown to mediate a more potent anti-tumour effect. However, toxicities due to IL12, especially combined with CAR-T cells, should be taken into consideration.

- Another approach – which is explored in this thesis – is the combination of CAR-T cell therapy and checkpoint blockade: as discussed below (section) the use of antibodies blocking CTLA-4 and PD1 has shown striking responses in patients with melanoma and lung cancer. Combining this strategy with adoptive T cell therapy is therefore a promising approach to improve efficacy in solid tumours.

Methods to introduce CAR constructs into T cells

Several methods have been used to introduce CARs within the cells, each of them has advantages and disadvantages (reviewed in Ghorashian et al., 2015; Wang and Rivière, 2016).

- Integrating viral vectors. γ-retroviral and lentiviral vectors are the most commonly used methods of gene transfer. These are integrating vectors, therefore the CAR construct is stably expressed into the transduced cells.

γ-retroviral vectors require cells to be in mitosis, while lentiviral vectors can also transduce quiescent cells. However, the current protocols for transduction of T cells employ strong mitogenic activation stimuli, hence this advantage might not be of practical relevance.

Lentiviral vectors are in theory safer as their integration preference is less focussed on transcriptional start sites and they are typically self-inactivating, meaning that after insertion the viral promoters are truncated. However, the long-term safety of transduction with γ-retroviral vectors has been demonstrated in patients treated with CAR-T cells (Scholler et al., 2012).

The advantage of γ-retroviral vectors is that it is possible to generate a packaging cell line, which allows indefinite production of the viral vector. On the other hand, production of lentiviral vectors relies on transient transfection.

- *In vitro* transcribed messenger RNA electroporation (mRNA). This technique only allows transient expression of the transgene. This feature has advantages and disadvantages. Since the CAR is not stably expressed, the anti-tumour effect can be limited. On the other hand, however, this can reduce toxicity. One

application of this method could be for the detection of unexpected side effects before administration of permanently modified T cells.

- Transposon-based integration. This system allows stable expression of the transgene without the employment of a viral vector. This is achieved by electroporation of the DNA on interest together with DNA or RNA which encodes for a transposase. The CAR construct is flanked by specific regions which are recognised by the transposase and this allows the insertion of the cassette into the genome.

The advantage of this system is that it is cheaper compared to viral vectors. However, a disadvantage is that such protocols are more toxic for the T cells and require prolonged culture to recover the cells.

- CRISPR/Cas9. A recent approach described by Sadelain and colleagues described the use of the CRISPR/Cas9 system to knock out the endogenous T cell receptor α constant (TRAC) locus and direct replacement with the CAR construct (following a 2A self-cleaving peptide) through an adenovirus associated virus (AAV) repair matrix. This system resulted in more physiological expression of the CAR on the cell surface, leading to retention of a more undifferentiated phenotype, lower tonic signalling and delayed exhaustion of CAR-T cells. This translated to a superior activity *in vivo* compared to cells transduced with a randomly integrating retroviral vector (Eyquem et al., 2017).

This paper highlighted for the first time the importance of the method of gene transfer and expression levels of the CAR, linking it to *in vivo* efficacy. This aspect will need to be taken into consideration in the future.

1.4.4 TCR and CAR: advantages and disadvantages

T cell therapy with TCR has the advantage of being able to target any tumour-associated or tumour-specific protein, both expressed on the cell surface or intracellularly.

However, this approach is HLA-restricted, a feature that limits its broad use in clinic. Moreover, a common escape mechanism of many tumours is downregulation of MHC-I and MHC-II, which therefore reduces the ability of TCR-transduced T cells to target tumour antigens.

Another drawback is that, by targeting tumour associated antigens, TCRs used in T cell therapy have often low affinity as they have undergone central tolerance during thymic development.

On the other hand, CAR T cells are not HLA-restricted, a feature that widens their use to virtually all patients that express a specific antigen. Moreover, since they can recognise the antigen in its native form, they do not require antigen processing and presentation, therefore they are less susceptible to tumour escape. A major drawback of CAR-T cells is that they can only recognise antigens expressed on the cell surface, as they rely on antibody binding. This feature restricts their application to a limited number of targets.

1.4.5 Checkpoint blockade

As described in section 1.2.5, checkpoint inhibitors are regulators of the immune response important for the maintenance of peripheral tolerance. Chronic exposure to antigens, such as in the case of viral infections and in cancer, has been associated with exhaustion of T cells, which results in a suboptimal T cells activation and, therefore, tumour escape.
The ligands for these inhibitory receptors are often upregulated on tumours and on non-malignant cells in the tumour microenvironment, providing a mechanism by which tumours can modulate immune response.

Clinical use of checkpoint blockade
Antibodies blocking these inhibitory receptors have shown profound responses in melanoma patients.
Ipilimumab is a fully human monoclonal antibody blocking CTLA-4. A phase III clinical trial where 676 patients were treated showed increased survival (46% at 1 year and 24% at 2 years) of patients of patients receiving Ipilimumab compared to patients receiving a vaccine against gp100 (25% at 1 year, 14% at 2 years) (Hodi et al., 2010). These results led to FDA (Food and Drug agency) approval in 2011 and EMA (European Medicine Agency) approval in 2013.
It has been shown that CTLA-4 blockade can “release the brakes” and reactivate TILs (Kitano et al., 2013), However, a double effect on the tumour microenvironment has also been proposed: *Ipilimumab* is an IgG1 isotype, which is able to mediate antibody-dependent cell-mediated cytotoxicity (ADCC) and it has been shown that this feature promote lysis of T_{reg} cells, which constitutively express high levels of CTLA-4 (Simpson et al., 2013).
Lack of ADCC might be one the reasons underlying the less promising results obtained by another CTLA-4 blocking antibody (*Tremelimumab*) (Ribas et al., 2013).
The PD1/PD-L1 pathway has also been successfully targeted in the clinic.
Nivolumab and *Pembrolizumab* are two antibodies blocking PD1. Several studies have demonstrated efficacy of this treatment with acceptable toxicities in patients with metastatic melanoma (Hamid et al., 2013) and, more recently, in non-small lung cancer (Garon et al., 2015) and advanced renal cell carcinoma (Motzer et al., 2015).

Moreover, combination of CTLA-4 and PD1 blockade has shown synergistic effects in a Phase III clinical trial (Larkin et al., 2015).

Criteria for efficacy of checkpoint blockade

Clinical experience with checkpoint blockade agents led to the definition of key points which can predict efficacy of immunotherapy in human cancers and, therefore can serve as biomarkers for the choice of therapy.

The first and most important parameter is the "*tumour foreignness*", which defines the degree of neo-antigens present within a tumour. A correlation between mutational load, a surrogate marker for neo-antigen load, and efficacy of checkpoint blockade has been established (Blank et al., 2016).

Indeed, cancers with high mutational load such as melanoma and non-small lung cancer (Alexandrov et al., 2013) (Figure 1.14) have shown the greatest response to checkpoint blockade. However, despite being a good predictor, mutational load does not take into account a possible contribution of self-antigen recognition to tumour control, therefore low mutational load does not necessarily mean low foreignness (Blank et al., 2016).

Another important parameter to take into consideration is T cells infiltration: infiltration of $CD8^+$ T cells is associated with improved outcome in melanoma upon therapy with PD1-blocking antibody (Blank et al., 2016). Only highly infiltrated tumours (which are most likely escaping the immune response by inhibiting T cells function) will respond to checkpoint blockade.

Figure 1.14 Mutation load signature of human cancers.
From (Alexandrov et al., 2013)

1.5 Scientific rationale and aims

Despite the success in recent years, immunotherapy has proven to be more difficult in the context of neurooncology.

There are specific challenges to brain tumour immunity, mainly related to the concept that the central nervous system (CNS) is an immune-privileged site. However, several observations that challenge this dogma have been proposed (Ransohoff and Engelhardt, 2012), including capability of the immune system to patrol the CNS in search for pathogens and damaging agents that would disrupt homeostasis (Ousman and Kubes, 2012), and the ability of T cells reactive for myelin antigens to efficiently enter the brain parenchyma and mount an inflammatory response, such as in the case of the autoimmune disease multiple sclerosis (Ransohoff and Engelhardt, 2012).

An additional challenge relies on the relatively low mutational load of GBM, which renders the recognition of this tumour by the immune system more difficult (see section 1.4.5).

Nonetheless, the field of immunotherapy in the context of neurooncology has rapidly grown and recent findings have shown that mounting an immune response to glioma-specific antigens (EGFRvIII and IDH1) is possible through a tumour-specific vaccine (Sampson et al., 2011; Schumacher et al., 2014).

The use of CAR-modified T cells in this context represents a valuable alternative to break the immune tolerance to GBM and induce an effective inflammatory response. In most cases, CAR-T cells for GBM were directly delivered to the tumour, except for few cases where T cells were systemically infused (Sampson et al., 2014; Johnson et al., 2015). None of the previous studies, however, evaluated effective migration, proliferation and persistence of CAR-T cells within the tumour.

This project was designed to evaluate the feasibility and efficacy of a CAR-based immunotherapy for GBM. A syngeneic mouse model of GBM was developed to enable study of the kinetics of migration and persistence of CAR-T cells in the context of a functional immune system. Specifically, the aims of this project were:

- Establish an immunocompetent glioma mouse model expressing EGFRvIII.

- Test specificity and function of murine T cells expressing an EGFRvIII-specific murine CAR
- Evaluate migration properties of systemically administered CAR-T cells
- Study the persistence and function of adoptively transferred CAR-T cells within the tumour microenvironment.
- Based on observations from these experiment, we sought to explore strategies to improve persistence and efficacy. Two approaches were followed:
    - Employment of a third-generation CAR to provide an additional survival signal (41BB).
    - Evaluation the effect of combining CAR therapy with PD1 blockade to improve efficacy and promote long term survival

Chapter 2

Materials and Methods

2 Materials and Methods

2.1 Molecular cloning

The splicing retroviral SFG vector was used for all constructs. SFG plasmid contained ampicillin resistance gene which was used as selection marker for transformed bacteria. A list of constructs made is summarised in

Table 2.1. The maps for all constructs used can be found in Chapter 8, Appendix.

All CAR constructs were included into BamHI and MluI restriction sites, with the ScFv being included into a BamHI and NcoI site.

The maps for all constructs used are shown in chapter 8, Appendix.

Table 2.1 Plasmids used in this study

Plasmid ID	NAME	DESCRIPTION
15616	SFG.m_dEGFRvIII	Truncated mouse EGFRvIII in plain SFG
19711	SFG.muCD34ddGPI.I2.eGFP	Amino-terminus of murine CD34 on a GPI anchor
19712	SFG.mu_dCD34d.I2.eGFP	Signal peptide carboxy-terminal half of murine CD34 ectodomain
20493	SFGmR.mu_dCD34d-2A-aEGFRvIII_MR1-muCD8STK-muCD28Z	Mouse truncated CD34 co-expressed with MR1.1 anti-EGFRvIII 2nd generation CAR
20504	SFGmR.mu_dCD34d-2A-aEGFRvIII_MR1-muCD8STK-muCD28Z-2A-FLucX5red	Mouse truncated CD34 co-expressed with MR1.1 aEGFRvIII 2nd generation CAR and red-shifted FLuc
25063	SFGmR.mu_dCD34d-2A-aEGFRvIII_MR1-muCD8STK-muCD28-41BBZ	Mouse truncated CD34 co-expressed with MR1.1 aEGFRvIII 3rd generation CAR
25128	SFGmR.mu_dCD34d-2A-aEGFRvIII_MR1-muCD8STK-muCD28-41BBZ-2A-FLucX5red	Mouse truncated CD34 co-expressed with MR1.1 aEGFRvIII 3rd generation CAR and red-shifted FLuc
27962	SFGmR.mu_dCD34d-2A-ahCD19_4G7-muCD8STK-muCD28-41BBZ-2A-FLucX5red	Mouse truncated CD34 co-expressed with 4G7 ahCD19 2nd generation CAR and red-shifted FLuc

2.1.1 *De novo* gene synthesis

De novo gene synthesis was performed by polymerase chain reaction (PCR) of overlapping oligos (IDTDNA). Oligos were reconstituted at 100μM in nuclease-free H_2O, then diluted to 25μM, 12.5μM or 6.125μM and mixed together. Three separate PCR reactions were set up as follows:

- 36.5μL nuclease-free water
- 10uL Phusion HiFid buffer (Thermofisher Scientific)
- 2μL of pool template (either 25μM, 12.5μM or 6.25μM)
- 1μL of dNTPs
- 0.5μL of Phusion hot-start polymerase (Thermofisher Scientific)
-

PCRs were performed as follows:

- 98°C for 2 minutes
- 98°C for 1 minute
- 65°C for 45 seconds
- 72°C for 60 seconds
- Repeat to #2 35 times
- 72°C for 10 minutes
- 4°C forever

The DNA products from the above PCRs were cleaned up with a clean-up Kit (Qiagen) according to manufacturer's protocol.

The amplification PCR was set up as follows:

- 35.5μL Nuclease-free water
- 10μL Phusion HiFid buffer
- 2μL of cleaned-up template above
- 1μL first (Forward) Primer (25μM)
- 1μL last (Reverse) Primer (25μM)
- 1μL of dNTPs
- 0.5μL of Phusion polymerase

PCR was performed as follows:

- 98°C for 2 minutes
- 98°C for 1 minute
- 65°C for 45 seconds
- 72°C for 60 seconds
- repeat to #2 35 times
- 72°C for 10 minutes
- 4°C forever

Amplified products were run on a 1% agarose gel and the best condition (25μM, 12.5μM or 6.125μM) was chosen. Three additional amplification PCRs were performed at the best condition. PCR products were pooled and digested with the appropriate endonucleases.

2.1.2 DNA digestion and ligation

All endonucleases were obtained from New England Biolabs (NEB). DNA digestion reactions (both of vector or the insert) were set up as follows:

- Nuclease-free water: up to 50μL
- Buffer: 5μL

- Enzyme 1: 1μL
- Enzyme 2: 1μL
- DNA: volume to 1μg

Digestion was performed at 37°C for 2 hours. The digestion products were run on a 1% agarose gel and the correct band was isolated using a dark reader blue transilluminator (Clare Chemical Research). The DNA was isolated using a QIAquick Gel Extraction Kit (Qiagen).

The vector was de-phosphorylated using an Alkaline Phosphatase (Thermofischer Scientific) as follows:

- DNA: 30μL (as extracted from gel)
- Buffer: 3μL
- FastAP: 1μL

De-phosphorylation was performed at 37°C for 10 minutes, then the enzyme was inactivated at 75°C for 5 minutes.

Quick ligase was obtained from New England Biolabs. Ligation reaction was set up as follows:

- Vector: 1μL
- Insert: 7μL
- Ligase Buffer: 10μL
- Ligase: 1μL
- Nuclease-free water: 1μL (8μL in vector only control)

Ligation was performed at room temperature for 5 to 10 minutes.

2.1.3 Transformation of competent *E.Coli* cells

High efficiency chemically competent *E.Coli* (DH5α, New England Biolabs) were transformed by adding 2 μL of ligation product to 25 μL of bacteria and incubated on ice for 10 minutes. Heat shock was performed by placing cells at 42°C for 35 seconds, then on ice for 2 minutes. Cells were plated on LB-agar plates with ampicillin and grown overnight at 37°C.

2.1.4 Plasmids purification

Single colonies were picked and grown overnight in 4mL of Luria Broth (LB) bacteria medium containing Ampicillin 100μg/mL. Plasmid DNA was isolated using QIAprep Spin Miniprep Kit (Qiagen). DNA was digested with restriction enzymes to discriminate the new construct from the original plasmid and to

verify correct ligation. When de novo gene synthesis was performed, DNA was sequenced to verify absence of point mutations (Source Bioscience).
Correct minicultures were inoculated into 100mL of LB medium containing Ampicillin 100μg/mL and DNA was isolated the following day using a NucleoBond® Xtra Midi kit (Macherey-Nagel).

2.2 Cell culture

2.2.1 Generation of retroviral vectors

Retroviral vector production for mouse splenocytes
Phoenix Eco packaging cells were obtained from Hans Stauss, UCL Division of Infection and Immunity.
These cells were originally obtained by stable transfection of the human 293T cell line (a human embryonic kidney line transformed with adenovirus E1a) with DNA encoding for the *gag-pol* proteins as well as the ecotropic virus envelope (Nolan laboratories). These packaging cells are easily transfected with DNA for the production of retroviruses.
Cells were plated on 10 cm dishes in complete IMDM ($1.5x10^6$ cells/plate) and, when about 50-60% confluent, were transfected with 2.7 μg of *pClEco* packaging plasmid and 4.68 μg of plasmid of interest. For each plate, 470μl of plain medium were mixed with 30μl of Genejuice (Novagen) for 5 minutes at room temperature, then the DNA was added and incubated for additional 15 minutes at RT, then the mixture was added drop wise on the cells. 18 hours post transfection, IMDM was replaced with 5 ml of complete RPMI.
48 hours post transfection, supernatants containing the retroviral vectors were collected and stored at 4ºC o/n, 5 ml of fresh RPMI were added to the plates and new supernatants were collected at 72 hours. Both supernatants were mixed together, spun at 400g to get rid of any residual cell, aliquoted into 2 ml tubes and stored at -80ºC.

Retroviral vector production for adherent tumour cell lines.
HEK293T cells were plated on 10 cm dishes in complete IMDM ($1.5x10^6$ cells/plate) and, when about 50-60% confluent, were transfected with three different plasmids:
- *Envelope VSV-G*: 3.125 μg/plate

- *Gagpol*: 4.68µg / plate
- Construct of interest: 4.68µg/plate

For each plate, 470µL of plain medium were mixed with 30µL of Genejuice (Novagen) for 5 minutes at room temperature, then the DNA was added and incubated for additional 15 minutes at RT, then the mixture was added drop wise on the cells. Supernatant containing retroviral particles was collected 48 hours and 72 hours post transfection.

Retroviral vector production for human suspension cells

The same protocol was followed as per the adherent tumour cell line (see). A different envelope was used:

- *Envelope RD114*: 3.125 µg/plate
- *Gagpol*: 4.68µg / plate
- Construct of interest: 4.68µg/plate

2.2.2 Murine tumour cell lines

GL261 were a gift of Sergio Quezada (UCL Cancer Institute). GL261 were cultured in complete DMEM with no antibiotics. Wild type cells were transduced with a retroviral plasmid to stably express a truncated form of EGFRvIII. Briefly, cells were plated on 6-well plates at $3x10^5$ cells/well. 24 hours after seeding, the old medium was removed and 2 ml of retroviral supernatant (with VSV-G envelope) were added. 1 µL of Polybrene 10mg/ml was added to each well. 72 hours post transduction, viral supernatant was removed and cells transferred to a flask and analysed for transduction efficiency using FACS.

EGFRvIII- positive cells were sorted with a BD ARIA cell sorter. Up to $3x10^6$ cells were stained with MR1.1 monoclonal antibody for 30 minutes at room temperature, then washed twice with PBS and stained with secondary antibody AlexaFluor 647 goat anti mouse IgG2a for 20 minutes in the dark. Cells were finally washed twice and re-suspended in DMEM 2% FCS for sorting.

To obtain a homogeneous population, single cell dilution was performed. Cells were re-suspended at $1x10^6$ cells/mL and diluted to 1.67 cells/mL and plated in 200 µL on flat-bottom 96 well plates. Two weeks later, clones were transferred to a 12-well plate first and then to 6-well plates. Clones were tested

for EGFRvIII expression and two high expressing clones were chosen for expansion.

2.2.3 Transduction of mouse splenocytes

Splenocytes were isolated from the spleen of C57Bl/6 female mice. A single cell suspension was obtained smashing the spleen using a 70µm cell strainer. After lysis of red blood cells with ACK buffer (Lonza), splenocytes were re-suspended in complete RPMI medium at $1x10^6$ cells/ml and activated with Concanavalin A (Sigma) 2 µg/ml and IL-7 (Peprotech) 1 ng/ml for 24 hours.
Non-tissue culture treated 24-well plates were pre-coated with Retronectin (Takara) overnight at 4ºC, then blocked with 2% BSA in PBS for 30 minutes and washed twice with PBS.
Cells were collected, washed once with PBS and re-suspended directly in 750 µl of neat retroviral supernatant at $2x10^6$ cells/well. After seeding, cells and retroviral particles were spun at 800g for 90 minutes without brake at 32 ºC. After 18 hours, each well was topped-up with 1.25ml of complete RPMI containing IL-2 (Peprotech) to a final concentration of 100 U/ml.
Cells were harvested 72 hours post-transduction, washed once in PBS and split 1:2 into tissue culture treated 24-well plates for further experiments.

2.2.4 Transduction of suspension human cells

SupT1 cells were cultured in complete RPMI medium and transduced when in exponential growth phase.
As per murine splenocytes, non-tissue culture treated 24-well plates were pre-coated with Retronectin (Takara) overnight at 4ºC. The following day, Retronectin was aspirated and 250µL of viral supernatant were added. The viral supernatant was incubated for 30 minutes at room temperature, then removed and 500 µL of cells were added at a concentration of $6x10^5$ cells/mL ($3x10^5$ cells/well). In each well 1.5mL of viral supernatant were added to a final volume of 2mL. The plate was spun at 1,000g for 40 minutes at room temperature.
Cells were harvested 72 hours after transduction and transferred to a flask.

Table 2.2 List and composition of complete media

MEDIUM	SUPPLIER	FBS	SUPPLEMENTS	SUPPLIER
IMDM	Sigma	10%	none	/
DMEM	Sigma	10%	*1 mM Sodium Pyruvate*	Life Technologies
RPMI	Sigma	10%	10 mM HEPES, *βMercaptoethanol*	Life Technologies

2.2.5 Expression and purification of EGFRvIII_mIgG2a

KF562 cells transduced to express mouse EGFRvIII ectodomain fused with mouse IgG2a-Fc were expanded to $1x10^8$ cells, then transferred into a bioreactor (CELLine) in phenol-free medium (Lonza**)** and low IgG FBS.

Cells were harvested weekly and spun at 400g for 5 minutes, then the supernatant was centrifuged at maximum speed for 10 minutes, then filtered first through a 0.45 μm filter and then through a 0.2μm filter. The protein was purified using 1 ml HiTrap columns (GE Healthcare) according to manufacturer's protocol. Purified protein was dialysed over/night in PBS using a dialysis cassette with 20,000 molecular weight cut off (Thermo Fisher Scientific).

Purity of the protein was then assessed by Sodium dodecyl sulphate (SDS)-Polyacrylamide gel electrophoresis (PAGE).

Purified protein was directly labelled to AF488 dye using an Antibody Labelling Kit (Thermo Fisher Scientific) according to manufacturer's protocol.

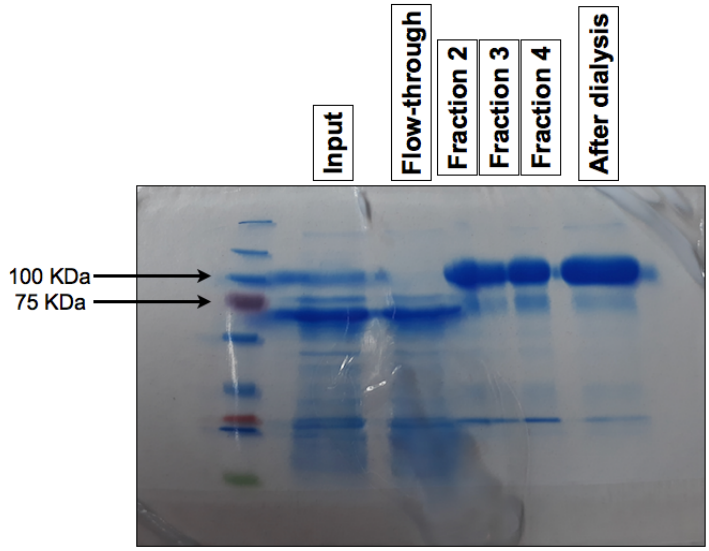

Figure 2.1 Purification of mEGFRvIII-mIgG2A
All fractions of the purification process were loaded: input (supernatant from bioreactor), column flow-through, elution fraction 2,3 and 4, protein after purification.

2.3 *In vitro* functional assays

2.3.1 ^{51}Chromium cytotoxicity assay.

Target cells (either GL261 or EGFRvIII-expressing GL261) were incubated with ^{51}Cr (20 µL/1x10^{6}cells, corresponding to 3.7 MBq) for 1 hour at 37ºC in PBS/0.5% BSA. Cells were washed 5 times with 4 ml of complete medium.

Effectors were prepared (either untransduced or CAR-expressing splenocytes) at 32:1, 16:1, 8:1 and 4:1 effector/target ratio. Splenocytes were re-suspended at 1.6x10^6 cells/ml and 200µL were aliquoted into appropriate number of wells in row A of a V-bottom 96-well plate; cells were then serially diluted in RPMI complete medium to reach the desired concentration. 1% Triton X-100 was used as positive control for lysis, while targets only were included to see background release.

After labelling with ^{51}Cr, target cells were counted, re-suspended at 5x10^4 cells/ml and 100 µL added to effector cells.

The plate was incubated at 37ºC for 4 hours, after which 50µL of supernatant from each well were transferred to a white-sided, clear-bottomed 96-well plate. 150µl of scintillation solution were added to each well and the solutions were left overnight to mix.

The release of ^{51}Cr was measured using a γ counter and calculated as follow:

$$\frac{\text{(Experimental release – Background release)}}{\text{(Maximum release-Background release)}} * 100$$

2.3.2 Assessment of IFNγ release

Effector and target cells were co-cultured at a 2:1 ratio into 24-well plates. Target cells (400,000 cells, either GL261 or EGFRvIII expressing GL261) were co-cultured with 800,000 effector cells (either untransduced or CAR-transduced splenocytes) in RPMI complete medium without IL2. Supernatant from each condition was collected 24 hours after co-culture set-up, diluted 1:1,000 and IFNγ release was analysed by ELISA (Biolegend,) according to manufacturer's protocol.

2.3.3 *In vitro* proliferation assay

Transduced splenocytes were labelled with *CellTrace Violet* (thermos Fisher Scientific) according to manufacturer's protocol. Effector and target cells were co-cultured at a 2:1 ratio into 24-well plates (see above, section 2.3.2). Proliferation was evaluated 72 hours after co-culture set by dilution of the dye.

2.4 *In vivo* animal work

2.4.1 Mice

Animal protocols were approved by local institutional research committees and in accordance with U.K. Home Office guidelines. C57BL/6 mice aged between 6 and 8 weeks were obtained from Charles River and housed in individually ventilated cages (IVCs) with access to food and water ad libitum.

Mice were sacrificed when 20% loss in weight was observed or when other clinical signs appeared (significant hunch and reduced movement).

Preliminary experiments (cohorts no larger than 4 mice per group) were performed to evaluate the variability of the system (i.e. tumour growth kinetics with or without treatment). Based on preliminary results and data from other groups using the same cell line (vom Berg et al., 2013; Wainwright et al., 2014), subsequent survival experiments were scaled up to 6 mice per group to reach significance. Independent experiments were repeated two to three times to ensure reproducibility of the data.

2.4.2 Establishment of an intracranial tumour model

Intracranial injection

6-8 weeks old female mice were anesthetized with 4% isoflurane in an induction chamber. Mice were then placed into a stereotactic frame (David Kopf Instrument), where anaesthesia was maintained at 2% isoflurane delivered through a nose adaptor. The head was sterilised with 4% chlorhexidine and the skin was cut with a sterile scalpel to expose the skull. Coordinates were taken using a blunt-ended Hamilton syringe (Hamilton, 75N, 26s/2"/3, 5 µL): 2 mm right and 1 mm anterior to bregma corresponding to the right caudate nucleus. A hole was made using a 25-gauge needle, then the Hamilton syringe was lowered into the burr hole to a depth of 4 mm below the dura surface and retracted 1 mm to form a small reservoir.

$2x10^4$ EGFRvIII-expressing GL261 were injected in a volume of 2 µL over two minutes. After leaving the needle in place for 2 min, it was retracted at 1 mm/min. The burr hole was closed with bone wax (Aesculap; Braun) and the scalp wound was closed using Vicryl Ethicon sutures 6/0.

Total body irradiation and splenocytes injection in vivo

On day 11 post tumour implantation, mice received 5Gy total body irradiation. The dose delivered in one minute (integrated dose) was calculated with a *UNIDOS^{atto} Electrometer* (PTV) and the time of exposure was calculated as follow:

$$\text{Time (minutes)} = \frac{\text{Dose desired (5Gy)} \times 13.89}{\text{Integrated dose}}$$

On the same day, CAR-transduced splenocytes (six days after transduction) were harvested, counted and washed at least three times with PBS to remove serum before intravenous tail injection in mice. $5x10^6$ bulk splenocytes were injected in 200µL of PBS using a winged infusion set.

Anti-PD1 antibody administration

Anti PD1 antibody (clone RMP1-14, *InVivo* MAb, BioXCell) was diluted to 1mg/ml in sterile PBS. Mice received a total of four doses (200µg each) by intraperitoneal injection on the day of T cells administration and then at day 3, 6 and 14 post infusion.

2.4.3 *In vivo* imaging

Bioluminescence (BLI)

Luciferin 10mg/ml (Stratech) was injected intraperitoneally (200 µL) and mice were scanned after 15 minutes using a PhotonIMAGER™ optical imaging system (Biospace Lab). A region of interest (ROI) was drawn around the head of each mouse to measure the photons/sec/sr for each animal.

Magnetic Resonance Imaging (MRI)

Images were acquired on a low magnetic field small animal 1T ICON MRI (Bruker) scanner with a 26 mm diameter mouse head coil. Images were acquired using a T_2 – weighted sequence (TR = 3201.5ms, TE = 85ms, flipangle = 90°, 20x20 mm^2 field of view = 2cm, 96x96 matrix, slice thickness = 0.5 mm, 15 or 30 averages were acquired with an acquisition time of 6 or 13 min, depending on number of averages). Differences in structure and the higher water content of the tumour translate in a longer relaxation time (T2) of the tumour compared to brain parenchyma. Tumour volumes were calculated using the software *Amira*.

2.4.4 Preparation of samples for *ex vivo* analysis

Mice were deeply anesthetised with pentobarbital and cardially perfused with ice-cold PBS containing 2mM EDTA, followed by 4%PFA to fix tissues for subsequent histopathological analysis. Brains were post-fixed overnight in 4%PFA, then stored in PBS containing 0.01% Sodium Azide until embedding. If fresh tissues were needed to isolate tumour infiltrating lymphocytes, brains were removed after perfusion with PBS 2mM EDTA and stored in HBSS on ice until processing.

2.5 FACS analysis

2.5.1 Sample preparation

a) For FACS analysis of suspension cells in culture, cells were collected from the culture flasks or wells, centrifuged at 400g for 5 minutes. Then the supernatant was removed and the cells were washed twice with PBS and counted with Trypan blue (Sigma-Aldrich): about $2x10^5$ cells/condition were transferred to 96-well U-bottom plates.

b) Adherent cells were first trypsinised, then washed and counted as for suspension cells.

c) Isolation of tumour infiltrating lymphocytes from intracranial tumours: brains perfused with PBS 2mM EDTA were chopped using a blunt razor and digested in HBSS (containing $Ca^{2+}$and Mg^{2+}) with Collagenase D 400 µg/ml (Roche) and DNAse type I 200 µg/ml (Roche) for 30 minutes at 37°C, after which EDTA (final concentration 5mM) was added to stop the reaction. Samples were homogenised through an 18-gauge needle, then spun at 500g for 10 minutes. The pellet was stratified on a Percoll (GE Healthcare) gradient (in HBSS) in a 15 mL tube. Briefly, the pellet was re-suspended in 4 mL of 37% Percoll, 4 mL of 70% Percoll was under-layered, then 4mL of 30% Percoll were added to top up. The gradient was spun at 500g for 30 minutes without brake at 4°C. After removal of myelin and debris from the 30% surface, the interphase between 70% and 37% was collected and washed three times with 10 mL of complete RPMI. Cells were counted with trypan blue and used for subsequent analysis.

2.5.2 Staining

Cells were washed with 200 µL FACS buffer by spinning the plate at 500 g for 2 minutes and decanting the supernatant. Cells were stained with the appropriate dilution of fluorophore-conjugated antibodies (see Table 2.4) in superblock buffer (Table 2.3) containing fixable viability dye eFluor780 diluted 1:1,000 (eBioscience). The final incubation volume was 40 µL/well. Incubation time was 30 minutes on ice in the dark. Cells were then washed three times with FACS buffer. For intracellular staining, cells were fixed and permeabilised with Fix/Perm buffer and Perm buffer (eBioscience) according to manufacturer's protocol. Intracellular staining was performed by dilution of antibodies in perm buffer containing 10% superblock.

For re-stimulation assay *ex vivo*, isolated TILs were incubated for 4 hours either with PMA 50ng/ml (Biolegend) and and ionomycin (1µg/mL) or with target cells. After two hours, GolgiStop (BD Bioscience) was added according to manufacturer's protocol.

Acquisition was performed with a Cyan™ Analyzer (Beckman Coulter, Inc.), LSRII or Fortessa flow cytometers (both from BD Biosciences). Data were analysed with FlowJo (Tree Star) v10.

Table 2.3 Composition of superblock buffer

COMPONENT	FINAL CONCENTRATION in PBS
FBS	2%
Normal Rat Serum	5%
Mouse serum	5%
Rabbit serum	5%
2.4G2 anti-Fcr mAb	25µg/mL
Sodium Azide	0.1%

Table 2.4 List of fluorophore-conjugated antibodies used for FACS.

Antigen	Clone	Fluorophore	Cat.No.	Source/Isotype	Dilution
CD3	17A2	BV785	Biolegend 100232	Rat IgG2b k	1:100
CD4	RM4-5	V500	BD Bioscience 560783	Rat IgG2a k	1:300
CD8	53-6.7	BV650	BioLegend 100742	Rat IgG2a k	1:300
CD45	30-F11	PECy7	BD Bioscience 561868	Rat IgG2b	1:200
CD45.1	A20	PECy7	Biolegend 110729	Mouse IgG2a k	1:200
CD45.2	104	AF700	Biolegend 109821	Mouse(SJL)IgG2a k	1:200
CD11b	M1/70	BV711	Bioloegend 101242	Rat IgG2b k	1:100
PD1	29F.1A12	PECy7	Biolegend 135215	Rat IgG2a k	1:100
PD1	J43	PercP-eF710	eBioscience 46-9985	Hamster IgG	1:100
LAG3	C9B7W	PE	eBioscience 12-2231	Rat IgG1 k	1:100
GzmB	GB12	PE	Invitrogen MHGB04	Mouse IgG1	1:100
Ki67	SolA15	eFluor450	eBioscience 48-5698-80	Rat IgG2a k	1:100
CD34	RAM34	AF647	BD Bioscience 560233	Mouse IgG2a k	1:100
EGFRvIII CAR	na	AF488	*Produced in house*	Mouse IgG2a	0.5 μL/sample
IFNγ	XMG1.2	PE	Biolegend 505807	RatIgG1 k	1:100
CD44	IM7	PECy7	Biolegend 103029	Rat IgG2b k	1:200
CD62L	MEL-14	APC	Biolegend 104411	Rat IgG2a k	1:100

2.6 Histopathology and immunohistochemistry

Brains were handed over to UCL Institute of Neurology IQPath for processing and paraffin embedding, sliced and stained. Full thickness sections of brain (coronally sliced in 0.5cm increments, guided by reference MRI images) were fixed in 10% formal saline for 24 hours. The orientation of the slices was maintained using biowraps (Thermo Fisher). The tissue was then processed through alcohol/chloroform dehydration and embedded in paraffin wax. Sections were cut using a Sakura Accu Cut SRM® manual microtome at 5μm thickness, and mounted on VWR superfrost® adhesive slides.

Cells pellets were made by fixing $4x10^7$ transduced Supt1 over night in 3 ml of 10% formal saline. The cell pellets were mixed with 2% low gelling agarose (Sigma) and spun at 7,000 rpm on a top bench centrifuge.

2.6.1 Haematoxylin and eosin staining

All slides were H&E stained using a Leica ST5010 Autostainer XL, and coverslipped using a Leica CV5030 coverslipper. The Leica ST5010 was programmed to dewax slides in xylene, and incubate slides in Haematoxylin for 5 minutes, "blue" nuclei for 5 minutes in water, and then counterstain in eosin for 5 minutes. Slides were then dehydrated through 99% ethanol and mounted in Pertex mounting medium.

2.6.2 Immunohistochemistry staining

Slides were de-waxed in xylene and de-hydrated in 100% and 70% ethanol. Endogenous peroxidases were blocked with 10% H_2O_2 for 15 minutes. Antigen retrieval step was performed with sodium citrate buffer pH6.9 in a pressure cooker.

Primary antibody was incubated for 1 hour at room temperature, then washed in PBS-tween 0.5%, then secondary staining was performed for with:

- DAKO HRP EnVision polymer (Dako) for rabbit/mouse was added for 30 minutes at room temperature when a rabbit primary antibody was used
- HRP-conjugated goat anti rat II antibody for 1 hour at room temperature when rat primary antibody was used

Slides were washed twice with PBS/tween, then the DAB substrate was added according to manufacturer's protocol (Dako) for a maximum of 5 minutes. Slides were then rinsed with distilled water and counterstained with Mayer's haematoxylin, dehydrated and mounted in DPX.

Automated staining was performed using a Ventana automated immunostainer.

The Protocol included: de-paraffinisation with dewax solution, antigen retrieval with ER2 (pH9) for 5 minutes, peroxide block (H_2O_2) for 5 minutes, incubation with primary antibody for 15 minutes at RT, secondary antibody for 8 minutes and streptavidin HRP for 8 minutes. Detection was performed with Bond Intense R (mixed DAB refine) for 5 minutes. Counterstain was performed with Mayer's haematoxylin.

Slides were examined on a Nikon Eclipse E600 microscope with multi-header functionality. Histology photographs were taken with a Leica DMD108 photographic microscope.

Table 2.5 List of primary antibodies used for immunohistochemistry.

Antigen	Clone	Cat.No.	Source/Isotype	Dilution
CD3	17A2	Biolegend 100232	Rat IgG2b k	1:100
CD34	RAM34	Thermo Fisher 14-0341-82	Rat IgG2a k	1:100
EGFRvIII	L84A	Absolute Antibody	Mouse IgG1kappa	1:1000

2.7 Statistical analysis

Data was analyside in GraphPad Prism 6, which was also used to generate graphs including means, medians, standard deviations and to perform statistical analysis. Unpaired students t-tests were calculated for data sets, Kaplan-Meier survival curves and mantel-Cox tests were performed for survival data. Differences were considered statistically significant when p values were <0.05 (significance was represented by *: <0.05, **: <0.01, ***: <0.001, ****: <0.0001).

Chapter 3

Results:

In vitro functional characterisation of a murine CAR for high grade gliomas

3 Results: *In vitro* functional characterisation of a murine CAR for high grade gliomas

3.1 Introduction

3.1.1 EGFRvIII-targeted therapies

Since EGFRvIII expression is restricted only to tumour cells, targeting this mutation is particularly attractive in the context of a tumour as glioblastoma in a delicate location such as the CNS.

The EGFRvIII mutation has been widely used for a targeted therapy for glioblastoma, both as tumour-specific antigen for antibody therapy and as a vaccine to boost the endogenous immune system.

As the EGFRvIII mutation is always associated with EGFR overexpression/amplification, both antigens have been targeted in glioblastoma: the EGFR-specific antibodies *Cetuximab*, *Panitumumab*, and *Nimotuzumab* bind to the extracellular portion of the receptor and cross-react with EGFRvIII. Their use in the treatment of glioblastoma has been, however, relatively unsuccessful and failed to show improved progression-free survival and durable responses (Neyns et al., 2009).

EGFRvIII-specific targeted therapies have also been explored. The ScFv from the EGFRvIII-specific antibody MR1.1 (see below, Beers et al., 2000a) fused to *Pseudomonas* exotoxin domains II and III has been used to target EGFRvIII-expressing cells in a orthotopic syngeneic mouse model. Preclinical data showed that intra-tumour delivery of the immunotoxin promoted tumour clearance. Interestingly, the effect was partially abrogated by depletion of $CD4^+$ and $CD8^+$ T cells, thus suggesting that anti-tumour activity was mediated not only by direct cytotoxic effect of the toxin, but also by the subsequent activation of the immune response (Ochiai et al., 2008). A clinical trial is currently undergoing on patients with recurrent GBM to receive local EGFRvIII immunotoxin via Convection-Enhanced Delivery (CED) (NCT02303678).

The EGFRvIII mutation has also been employed as a tumour-specific vaccine. The peptide-based vaccine Rindopepimut® [EGFRvIII peptide conjugated to the adjuvant keyhole limpet hemocyanin (KLH) administered with granulocyte–macrophage colony-stimulating factor (GM-CSF)] has been used in a phase I-

II clinical trial, showing development of EGFRvIII humoral responses (Sampson et al., 2010, 2011). However, a phase III clinical trial failed to show improved survival and therefore it has been terminated (Weller et al., 2016).

3.1.2 CAR-T cell therapy for GBM

Pre-clinical data have demonstrated that CAR-T cells can control the growth of orthotopic gliomas (Ahmed et al., 2010; Chow et al., 2013; Johnson et al., 2015). These studies used a xenograft model for GBM and targeted different antigens: HER2 (Ahmed et al., 2010), Ephrin A2 receptor (Chow et al., 2013). The interleukin-13 receptor alpha 2 (IL13Rα2) has also shown promising results as a GBM-specific target for CAR-T cell therapy, both in pre-clinical and clinical settings (Kong et al., 2012; Brown et al., 2016).

All these studies showed an effect of CAR-T cells when directly injected into the tumour. Only one study tested efficacy of systemically infused CAR-T cells, but they failed to control tumour growth (Chow et al., 2013). This work, however, did not address the question of why systemically infused CAR-T cells failed to control tumour growth. This could have been due to either lack of effective migration or persistence within the tumour.

In the context of EGFRvIII-specific CAR-T cells therapy, two pre-clinical studies report the use of EGFRvIII-specific CAR T cells (Sampson et al., 2014; Johnson et al., 2015). Both these studies showed efficacy in tumour control of EGFRvIII-specific CAR-T cells, in both a subcutaneous and an intracranial model. In particular, the report from Johnson and colleagues (Sampson et al., 2014) used mouse T cells to express a murine third-generation CAR and demonstrated efficacy in controlling both subcutaneous and intracranial tumours in a immunocompetent mouse model for glioblastoma (Sampson et al., 2014).

Rationale and aims

Here, we followed a similar approach and tested a second-generation murine CAR specific for EGFRvIII, in order to test efficacy and kinetics in the context of a fully functional immune system.

A variety of antibodies specific for EGFRvIII are available, including L8A4, Y10 and H10. These antibodies, however, cross react with wild-type EGFR and possess a low affinity for the target (K_D 26 to 117 nM). One of the most

characterised antibodies against EGFRvIII is MR1.1, an high affinity (K_D 1.5 nM) ScFv (Beers et al., 2000b), derived by random mutagenesis of the complementary determining region (CDR) of the MR1 ScFv, derived by phage display (Lorimer et al., 1996). This antibody is specific for EGFRvIII, however, some degree of cross-reactivity with EGFR has been reported (Klausz et al., 2011). This antibody specifically recognises the junctional portion of the EGFRvIII mutation, therefore, since the sequence of the junctional portion of the EGFRvIII mutation is the same for both human and mouse versions, the same antibody generated for the human version could be used in a murine setting. Our lab already had extensive knowledge and experience with MR1.1-based human CAR-T cells, so the same ScFV was employed in the murine setting.

In order to avoid possible toxicity as previously described for third generation CAR T-cell therapy for glioblastoma (Morgan et al., 2010), in first instance a second generation CAR carrying a CD8 stalk and the CD28-CD3ζ intracellular domain (Ahmed et al., 2010; Chow et al., 2013) was used.

Prior to testing the function of CAR-T cells *in vivo*, we first evaluated their activity and phenotype *in vitro*. The mouse glioma cell line (described in more detail in chapter 4.1) was chosen as target cell line.

Specifically, the aims of the experiments described in this chapter were:

- Generation of EGFRvIII-expressing GL261, as these cells do not physiologically express this antigen
- Generation of a murine CAR against EGFRvIII (based on the ScFv of the high affinity antibody MR1.1) and test of its function *in vitro.*
- Generation of murine CAR to be used as negative control. The unrelated human CD19 antigen was chosen as target. The ScFv from the 4g7 antibody was used (MEEKER et al., 1984).
- Characterisation of phenotype of CAR-transduced splenocytes prior to injection *in vivo*

3.2 Generation of an EGFRvIII-expressing murine glioma cell line

Parental GL261 were transduced with a retroviral vector carrying the VSV-G envelope. The sequence of the junctional portion of the EGFRvIII mutation is the same for both human and mouse versions, therefore the same antibody generated for humans could be used in a murine setting. The mutated portion of EGFRvIII was fused with the transmembrane domain of the mouse EGFR (see Appendix, page 187) to obtain cells which expressed the epitope on the surface. GL261 were first transduced, then sorted for EGFRvIII expression (stained with full MR1.1 antibody) and single cell cloned to obtain a homogeneous population (Figure 3.1).

Two single-cell clones with high expression of EGFRvIII were chosen and expanded. However, only one clone was used in this project for all experiments, both *in vitro* and *in vivo*.

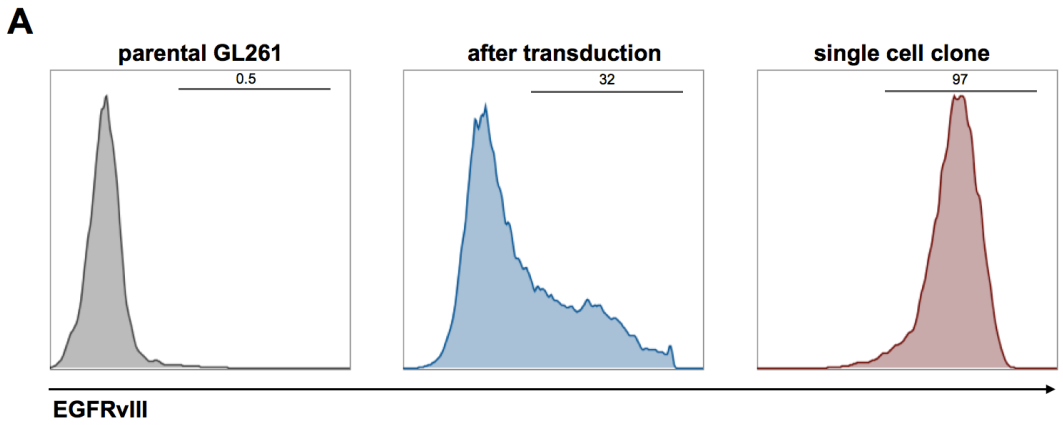

Figure 3.1 (A) Murine EGFRvIII expression in parental and transduced GL261. GL261 were transduced with a retroviral vector to express the murine version of EGFRvIII. Cells were stained with the monoclonal antibody MR1.1. After transduction, 32% of cells were positive (middle panel), therefore cells were FACS-sorted and a single cell clone (obtained by limiting dilution) with high and homogenous expression (right panel) was chosen.

3.3 Generation and validation of a murine marker gene for CAR-expressing T cells

We designed a marker gene to be able to distinguish transferred cells from the endogenous compartment. As we chose an immunocompetent mouse model, we opted for a murine protein, rather than an exogenous marker such as green fluorescence protein (GFP) to avoid possible immunogenicity that could result in a rejection of CAR-T cells once transferred *in vivo*.

CD34 was chosen as it is not expressed on mature haematopoietic cells nor neural tissue. To limit the size of the construct, we designed two versions: one containing the N-terminal part and one containing the C-terminal part of the CD34 gene and tested which one could be detected with the monoclonal antibody RAM34, with established use in immunohistochemistry (Park et al., 2006). The N-terminal part was cloned as Glycosylphosphatidylinositol (GPI)-anchored protein, while the C-terminal part was expressed as a type I transmembrane protein. In this case, the endodomain was de-functionalised by modification of tyrosines required for downstream signalling into alanines (see chapter 8: Appendix). HEK293T cells were transiently transfected with the two constructs which also co-expressed eGFP via an IRES, as positive control for transfection. Figure 3.2 shows that the C-terminal part was sufficient to be recognised by RAM34. Conversely, the N-terminal part was not recognised by the antibody. The C-terminal part of murine CD34 was therefore chosen as marker gene for CAR-transduced T cells. This was transferred into the CAR plasmid backbone (see chapter 3.4).

To validate this marker gene for future use *ex vivo* in immunohistochemistry, SupT1 cells were transduced to express the C-terminal part of CD34. Agar cell pellets were prepared and slices were stained with RAM34. CD34 membrane stain was observed in approximately 50% of cells, which reflected transduction efficiency as measured by flow cytometry (Figure 3.2B and C). SupT1 were used as they are readily transduced and, as being of T-lymphoblastic origin, have a shape similar to that of mouse splenocytes.

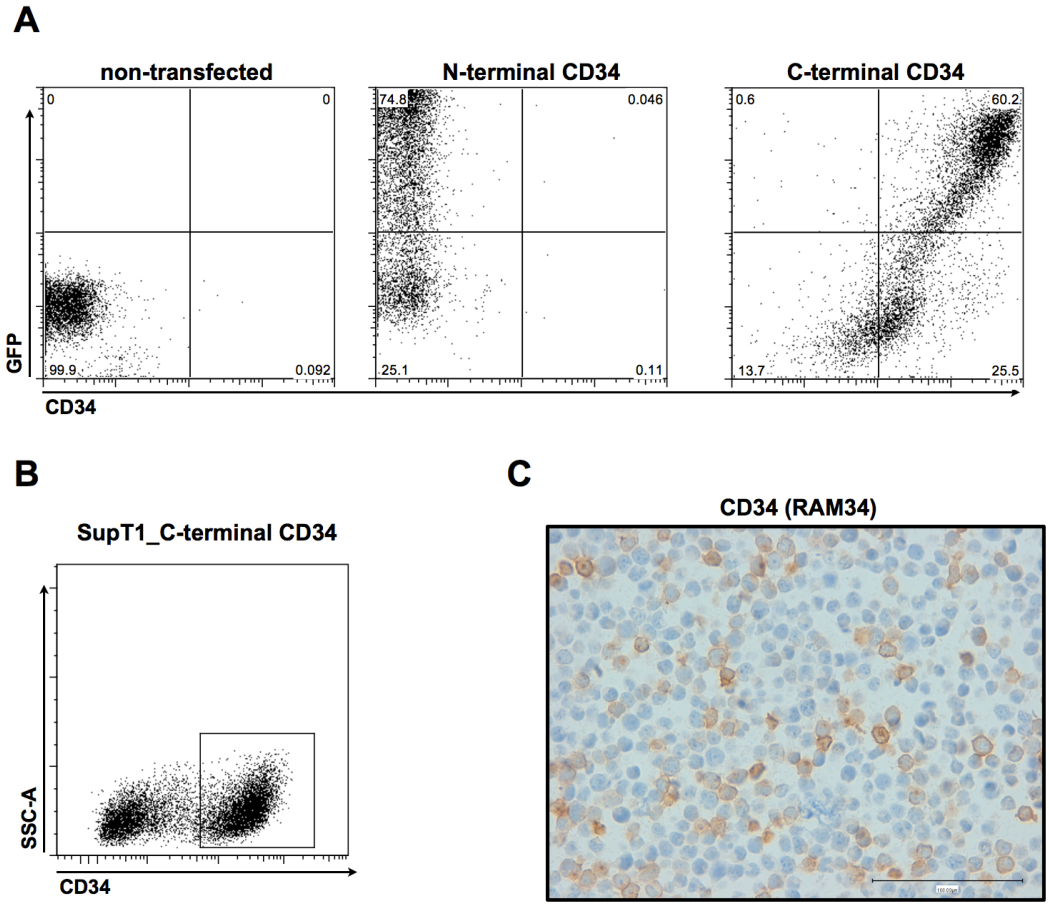

Figure 3.2 Validation of murine CD34 as marker gene for CAR-T cells.
(**A**) HEK293T were transfected with a plasmid encoding eGFP and either the N-terminal portion or the C-terminal portion of the murine CD34. Cells were stained with the monoclonal antibody RAM34. (**B**) SupT1 cells were transduced with a retroviral vector to stably express the C-terminal portion of the murine CD34, transduction efficiency was tested by staining with the antibody RAM34. (**C**) Agar pellets from SupT1 cells transduced to express mCD34 were paraffin-embedded and stained with RAM34. Membrane staining is observed in transduced cells.

3.4 Generation and characterisation of a murine chimeric antigen receptor (CAR) against EGFRvIII.

To generate an EGFRvIII-specific chimeric antigen receptor, the single chain fragment variant (ScFv) from the high affinity antibody MR1.1 was used (Beers et al., 2000). To avoid immunogenicity *in vivo*, we designed a second-generation murine CAR to be expressed by murine splenocytes. This included:

- CD8 stalk as transmembrane domain
- CD28-CD3ζ, as co-stimulatory activation domains

An irrelevant CAR was also generated as negative control: this carried the same murine activation domains of the EGFRvIII CAR, but recognised an irrelevant human antigen, CD19. The ScFv of the monoclonal antibody 4g7 was used (MEEKER et al., 1984).

Upstream of the CAR sequence, the C-terminal portion of the mouse CD34 was included as marker gene for *ex vivo* analysis (see chapter 3.3). For *in vivo* tracking, a red-shifted firefly luciferase was incorporated downstream of the CAR construct. The three genes were separated by two different 2A peptides, one from the *Thosea asigna virus* (T2A) and one from the *Equine rhinitis virus A* (E2A) (Figure 3.3A). These are self-cleaving peptides which allow simultaneous translation and subsequent cleavage of several genes within a multicistronic construct (Szymczak et al., 2004).

3.4.1 Validation of *in vitro* function of CAR-transduced T cells

Splenocytes were activated with Concanavalin A and IL7 for 24 hours, then transduced with ecotropic retroviral vector to stably express the CAR and both marker genes. This activation protocol mainly produced $CD8^+$ T cells, therefore the great majority (77%±14) of CAR-expressing cells were cytotoxic T lymphocytes (CTLs) (Figure 3.3B).

Transduction efficiency was measured 3 days post transduction by double staining for CD34 and CAR. CAR expression was verified using the purified EGFRvIII protein fused to a mouse IgG2A (directly conjugated to AF488). For the negative control CAR, cells were instead stained with supernatant from K562 transduced to secrete hCD19 protein fused to a rabbit IgG2A, then with

a secondary antibody against rabbit IgG2A. Consistent and high expression levels were obtained for both the CAR and CD34 (Figure 3.3B). Figure 3.3 shows average transduction efficiencies obtained for all constructs used: 51.9%±10.4 for MR1.1 CAR, 56.3%±10.2 for MR1.1 CAR_FLuc and 59.6%±0.3 for 4g7 CAR_FLuc.

Specificity and efficacy was first tested *in vitro* in a chromium (^{51}Cr) release assay. Data from Figure 3.4A (left panel) shows that both CARs (with and without FLuc) were effective in lysing EGFRvIII-expressing GL261, but not the parental cell line. Percentage of lysis spanned from 50% at the higher effector to target ratio (54±7 for MR1.1 CAR, 51±5 for MR1.1 CAR_FLuc) to 30% at the lower ratio (30±11 for MR1.1 CAR, 33±9 for MR1.1 CAR_FLuc). Background lysis of EGFRvIII$^-$ GL261 was 8±5 for MR1.1 CAR and 10±4 for MR1.1 CAR_FLuc. No lysis was observed for activated untransduced splenocytes, both of GL261 and GL261_EGFRvIII (5±4 and 7±3, respectively, Figure 3.4A, middle panel). Similarly, no lysis of GL261 and GL261_EGFRvIII was observed for the hCD19 CAR, while effective cytotoxic activity was observed when co-cultured with hCD19-expressing SupT1 (4±2, 5±4, and 58±17, respectively.Figure 3.4, right panel).

IFNγ production was measured by ELISA 24 hours after co-culture set up. Specific IFNγ release was only observed in response to EGFRvIII-expressing GL261 (Figure 3.4B).

When co-cultured in the presence of GL261_EGFRvIII for 72 hours (without IL2), CAR-expressing T cells proliferated to a small extent (Figure 3.4C), which was demonstrated by dilution of CellTrace® Violet dye. However, no clear proliferation peaks were observed. An explanation for this might be that, after antigen encounter, murine CAR-T cells mainly activate towards a cytotoxic profile rather than proliferating, especially after they have already gone through one round of proliferation prior to transduction.

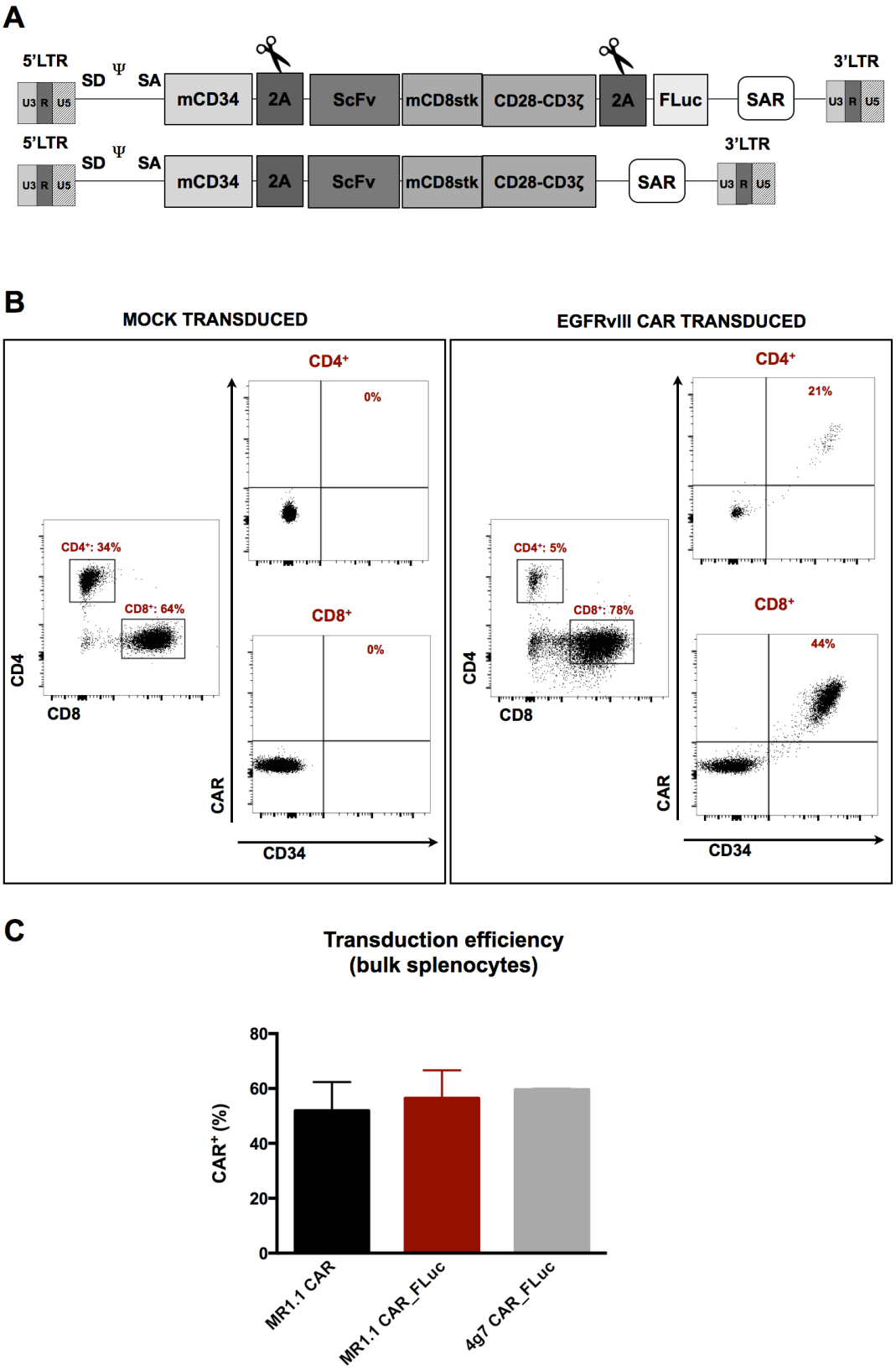

Figure 3.3. Consistent CAR expression in transduced mouse T cells.
(A) Constructs used in this study: the C-terminal portion of the murine CD34 was included and separeted by a T2A peptide from the CAR construct, which included MR1.1 as ScFv specific for EGFRvIII, a CD8 STALK as transmembrane domain and the CD28-CD3ζ as activation domains. Firefly luciferase was also included (top row), separed by a E2A peptide. **(B)** Transduction efficiency of mock-transduced

splenocytes (left panel) and EGFRvIII-CAR-transduced splenocytes. Although the majorty of of CAR T-cells were $CD8^+$, both $CD4^+$ and $CD8^+$ expressed the EGFRvIII-CAR. Shown is a representative example of 7 separate transductions. **(C)** Shown is the mean and standard deviation of 7 transduction. Average transduction efficiency was consistent for between all constructs used (range 40 and 60%).

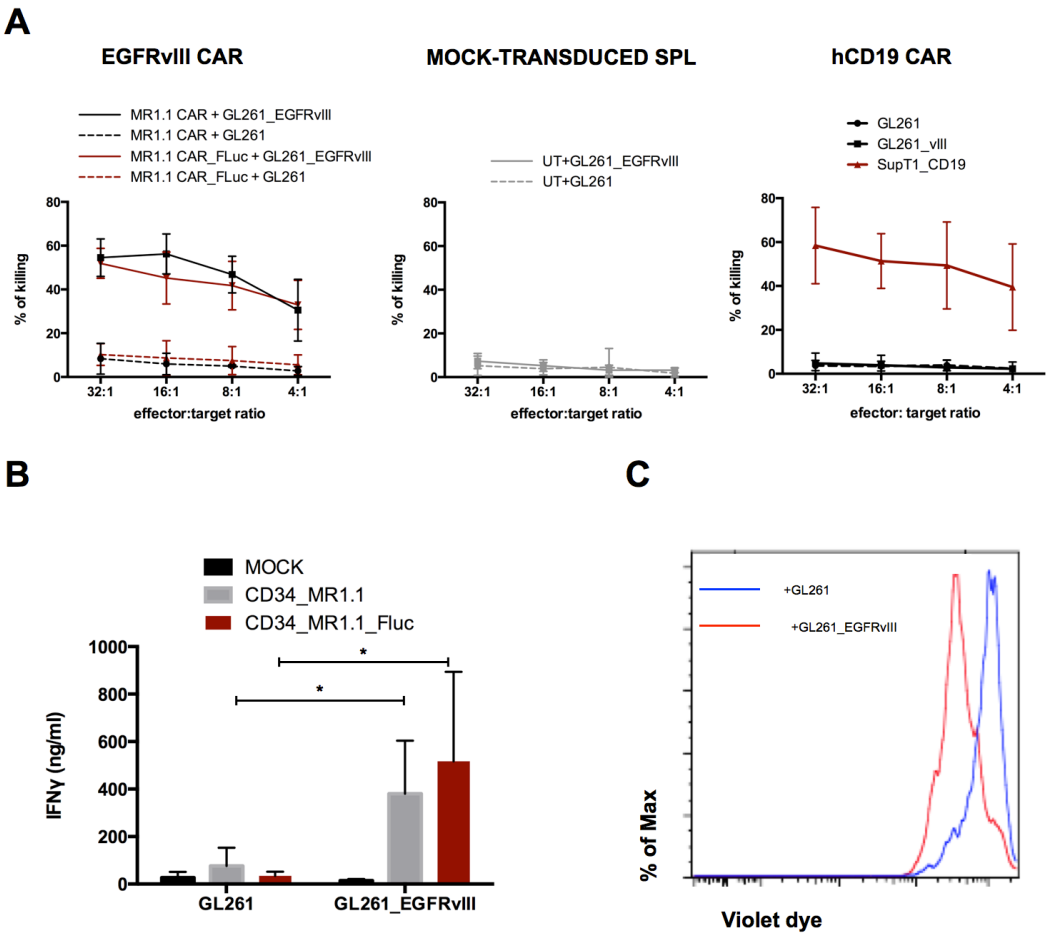

Figure 3.4 Specific cytotoxic activity of CAR-T cells *in vitro*.
(A) Chromium release assay showing specific lysis of EGFRvIII-expressing GL261 by both MR1.1 and MR1.1 CAR_FLuc T cells, but not parental cell line GL261 (left panel), no lysis by untransduced splenocytes (middle panel) nor by 4g7 CAR T cells, which in turn specifically lysed hCD19-expressing SupT1 (right panel). Shown are average and standard deviation of three independent experiments.
(B) IFNγ release was only observed when CAR-expressing T cells were co-cultured with EGFRvIII-positive GL261. No release was observed in response to parental GL261. No background production was observed when both GL261 and GL261_EGFRvIII were cultured in the presence of untransduced splenocytes ($p \leq 0.05$). Shown are mean and standard deviation of three independent experiments.
(C) Proliferation of CAR-transduced T cells in response to antigen stimulation 72 hours after co-culture set-up: dilution of CellTrace Violet dye was only observed when CAR-T cells were co-cultured with GL261_EGFRvIII. One representative experiment is shown of two.

3.4.2 Phenotype of CAR-transduced T cells

Phenotype of transduced T cells was analysed at day 6 post transduction, the day before systemic infusion in the mice (see 4.2.1).

CAR-expressing $CD8^+$ T cells expressed higher levels of the activation/exhaustion markers PD1 and LAG3 compared to untransduced T cells in the same well (Figure 3.5A): PD1 MFI for CAR^+ cells was 1273 versus 314 for CAR^- cells, while LAG3 MFI was 2044 versus 931, respectively.

This data suggests that, despite absence of the antigen, CAR-T cells tend to be more activated than CAR^- T cells.

Similarly, CAR-expressing cells exhibited a smaller population of $CD44^+CD62L^+$ central memory population compared to CAR^- cells (23.1%±2.9 versus 35.6%±1.3, respectively - Figure 3.5B, top panel).

CAR-expressing cells were functional, as antigen encounter led to increased expression of markers such as CD44, PD1 and LAG3 and decrease in CD62L, thus indicating an overall activation in response to antigen stimulation. PD1 MFI increased to 26892, while LAG3 MFI increased to a lesser extent (2231). At the same time, activation in response to antigen stimulation resulted in a diminished percentage of $CD44^+CD62L^+$ central memory cells (9%±4).

Activation markers were only up regulated by CAR^+ T cells, suggesting that lysis is mainly mediated by antigen recognition and no bystander effect was occurring in this context.

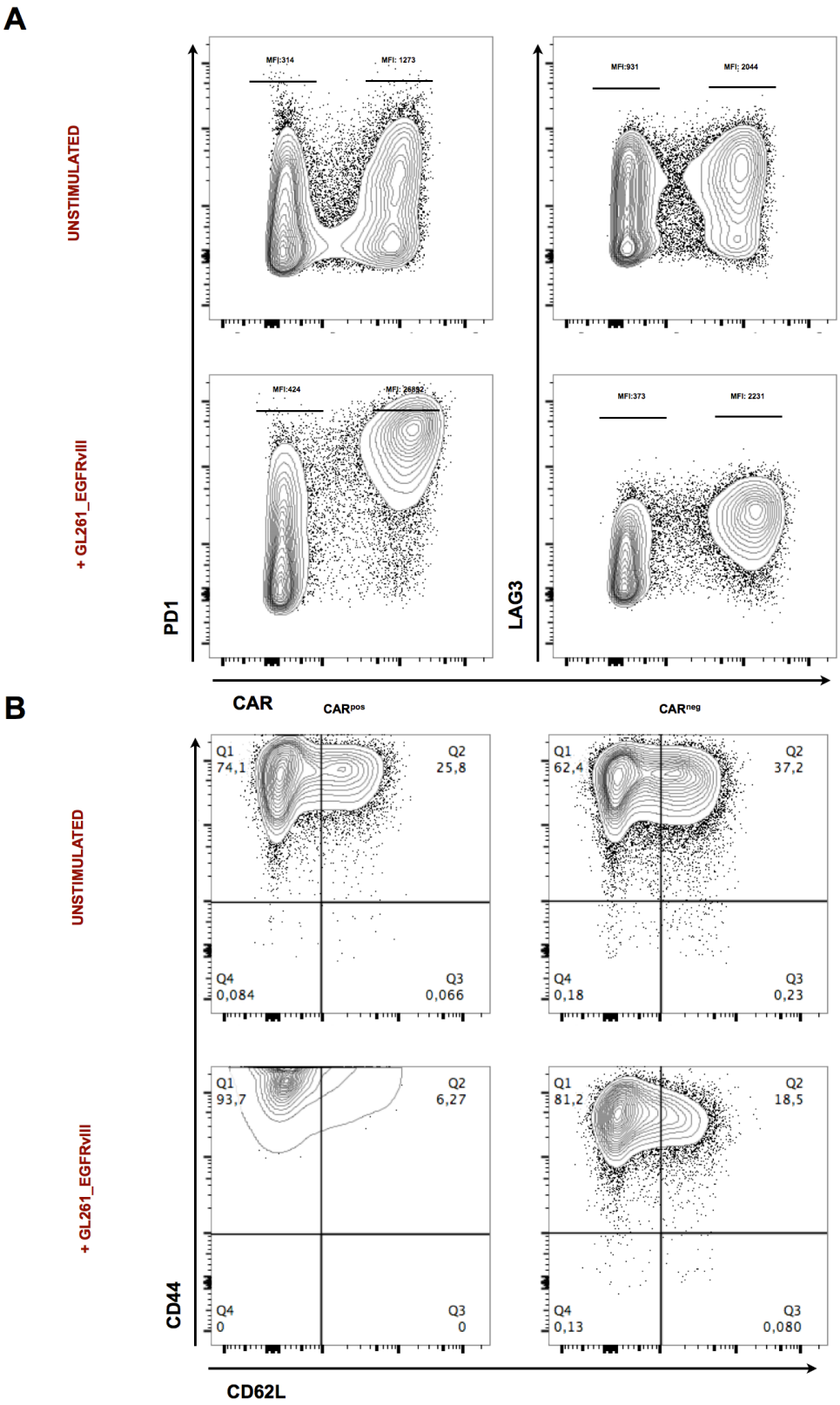

Figure 3.5 Activation and memory markers.
(A) PD1 and LAG3 expression was analysed at day 6 post transduction. Unstimulated cells were cultured in the presence of IL2 100U/mL, while stimulated cells were co-cultured for 3 days with GL261_EGFRvIII in the absence of IL2. **(B)** CD44 and CD62L expression in unstimulated cells (top panel) and cells co-cultured with GL261_EGFRvIII (bottom panel). A representative example of 3 independentexperiments is shown.

3.5 Summary and conclusions

Data from this chapter demonstrated that activated murine splenocytes were consistently transduced to express the CAR and the marker gene CD34.

Antigen specificity was confirmed with different *in vitro* assays, including ^{51}Cr release assay, ELISA and proliferation assay: MR1.1 CAR-T cells responded only to EGFRvIII-expressing targets, while 4g7 CAR-T cells only responded to hCD19-expressing targets.

Activation with ConA mainly produced $CD8^+$ cytotoxic T lymphocytes, therefore the majority of CAR-T cells were cytotoxic T lymphocytes (CTLs), which resulted in an efficient lysis of antigen-expressing targets *in vitro* and production of IFNγ. It has recently been demonstrated that a combination of both $CD4^+$ and $CD8^+$ T cells is important to promote an effective response both *in vitro* and *in vivo* (Turtle et al., 2016; Sommermeyer et al., 2016): while $CD8^+$ T cells are mainly efficient in lysing target cells, $CD4^+$ T_{helper} cells produce cytokines such as IFNγ, TNFα and IL2. Sommermeyer et al. demonstrated that CAR-expressing $CD4^+$ T_{helper} cells are able stimulate proliferation of CAR-expressing $CD8^+$ T cells *in vitro* and are necessary to promote potent responses *in vivo*. These findings might suggest that activation with ConA is not an ideal method as, despite generating very potent EGFRvIII-specific CTLs *in vitro*, lack of $CD4^+$ T_{helper} cells may lead to reduced activity *in vivo*. The next chapter will describe efficacy of CAR-T cells produced with this method *in vivo* and will discuss the effects of lack of T_{helper} cells in more detail.

In terms of phenotype, CAR-T cells were positive for activation markers such as PD1 and LAG3 even in the absence of antigen stimulation.

PD1 expression is physiologically induced both in response to TCR engagement (Vibhakar et al., 1997) and to common gamma-chain cytokines (IL2, IL15, IL21 and IL7) (Kinter et al., 2008). Therefore, high expression of this marker on CAR-expressing cells might be the result of background signalling of the CD28-CD3ζ intracellular domains. Similarly, LAG3 is induced after T cell activation (Workman et al., 2002). Antigen stimulation resulted in a further upregulation of these markers, thus suggesting that PD1 and LAG3 expression reflects the activation status of CAR-expressing T cells. PD1 and LAG3 have been extensively associated with exhaustion of T lymphocytes both in chronic viral infections (Wherry et al., 2007) and in cancers (Topalian et al., 2015;

Śledzińska et al., 2015). In particular, the PD1 pathway has been successfully targeted alongside CTLA-4 (see section 1.4.5) to release the immunological breaks that inhibit an effective immune response and obtain potent anti-tumour responses in several types of solid cancers, especially melanoma (Śledzińska et al., 2015).

In vitro functional assays described in this chapter demonstrated that CAR-T cells are fully functional at the time of systemic infusion into mice, however high expression of PD1 and LAG3 may result in CAR-T cells exhaustion after exposure to an immunosuppressive environment *in vivo*. The next chapter will evaluate this issue in more detail.

The composition of the T cells product at the time of *in vivo* infusion has also been associated with efficacy of adoptively transferred T cells (Gattinoni et al., 2011; Sommermeyer et al., 2016), with central memory and naïve-like T cells been associated with better engraftment and proliferation capabilities *in vivo* compared to effector memory and terminally differentiated T cells.

Activation with ConA and expression of EGFRvIII-CAR resulted in the majority of cells being effector memory, however a population of central memory $CD44^{+}CD62L^{+}$ was retained in these conditions.

In summary, expression of CAR was observed in both CTLs and T_{helper} cells and in a consistent fraction of central memory T cells. *In vitro* validation demonstrated efficient cytolytic activity, cytokine release and a degree of proliferative activity in an EGFRvIII-specific manner.

To correlate *in vitro* function to efficacy *in vivo*, we decided to move into an orthotopic mouse model of glioma. The next chapter will describe the establishment of intracranial tumours by direct implantation of GL261_EGFRvIII to test efficacy of EGFRvIII-specific CAR-T cells *in vivo*.

Chapter 4

Results:

Evaluation of *in vivo* functionality and efficacy of a murine αEGFRvIII CAR

4 Results: *In vivo* model set up

4.1 Introduction

4.1.1 Mouse models for GBM

Xenograft models

The majority of previous studies of CAR-T cells for GBM have been performed with xenograft models using either established human GMB cell lines such as U87 and U373 or patient-derived GBM cancer stem cells.

U87MG, **U251MG** and **U373MG** are human glioma cell lines which were derived from patient biopsies and cultured as monolayer before intracranial implantation (Stylli et al., 2015). These cells have been widely used for the study of GBM, however in recent years it has become clear that they do not recapitulate the typical features of human GBM, particularly they lack the infiltrative nature when growing *in vivo* (Lee et al., 2006). Detailed genomic analysis revealed that growing glioma cells in presence of FBS results in the acquisition of genetic mutations such as loss of heterozygosity and chromosomal aberrations (Lee et al., 2006; Li et al., 2008). These findings led researchers to prefer the use of patient-derived cancer stem-cells cultured in serum-free medium in the presence of specific growth factors such as epidermal growth factor (EGF) and basic fibroblast growth factor (bFGF) (Lee et al., 2006; Pollard et al., 2009). These models have shown to retain the genetic hallmarks of the original tumour and better recapitulate the growth pattern *in vivo* (Lee et al., 2006).

Syngeneic models

To study the immunology of brain tumours and immunotherapy approaches, syngeneic models have been developed. These were generated via chemical induction, through injection of carcinogenic agents directly into the brain (Seligman et al., 1939).

One of the most common mouse glioma cell line is the **GL261**, which was originally induced by implantation of 3-methylcholantrene pellets in the brain of C57Bl/6 mice and maintained by serial syngeneic transplantation of small tumour pieces (Ausman et al., 1970). GL261 have a poorly differentiated

morphology similar to GBM and demonstrate a relatively diffuse and infiltrative pattern into surrounding normal brain (Zagzag et al., 2003). As in human GBM, GL261 carry point mutations of p53 and K-Ras, with consequent increased activation of the PI3K pathway and phosphorylation of Akt (reviewed in Maes and Van Gool, 2011; Oh et al., 2014). GL261 are considered a moderate immunogenic model, as cells express MHC-I, but their expression of MHC-II and co-stimulatory molecules is limited (Szatmári et al., 2006).

Syngeneic models have the advantage of recapitulating the complex interaction between the tumour and the immune system, which is particularly important when evaluating immunotherapy approaches.

4.1.2 Animal models for CAR-T cells in the context of GBM

The majority of previous studies of CAR-T cells in GBM employed human CAR-expressing T cells in the context of an orthotopic xenograft model, using either established human glioma cell lines or patient-derived cells.

Several studies reported the ability of human CAR-T cells to eradicate tumours when injected intracranially (Ahmed et al., 2010; Kong et al., 2012; Chow et al., 2013; Hegde et al., 2016). Chow et al. also tested the efficacy of systemically infused CAR-T cells, but reported that CAR-T cells did not increase survival with this route of administration. The authors, however, did not investigate the causes underlying their failure in controlling tumour growth, therefore leaving open the question whether T cells did not migrate to the tumour or just failed to control tumour growth *in situ*.

The evaluation of efficacy of CAR-T cells in the context of an immunocompromised animal model, however, lacks an important component of this therapeutic approach, which is the interplay between transferred T cells and the endogenous immune system/tumour microenvironment.

4.1.3 Rationale and aims

We chose the GL261 model as the most well characterised immunocompetent animal model for immunotherapy of GBM (Maes and Van Gool, 2011; Oh et al., 2014) to evaluate kinetics and efficacy of CAR-T cells in the context of an intact immune system.

In this chapter, I will describe the development of a pre-clinical model to investigate kinetics of migration, accumulation and persistence of CAR-T cells

in an orthotopic model of high grade glioma. Specifically, the aims of the experiments described in this chapter were:

- Establish an orthotopic model by implanting EGFRvIII-expressing GL261 into the striatum of C57Bl/6 mice
- Evaluate magnetic resonance imaging (MRI) as a tool to monitor tumour engraftment and growth
- Assess migration kinetics of CAR-T cells following systemic infusion
- Evaluate efficacy of CAR-T cells to control tumour growth
- Assess phenotype of CAR-T cells and endogenous TILs *in situ*

4.2 Assessment of tumour growth kinetics

The first step was to determine at which time point post orthotopic injection tumours consistently engrafted as well as their growth rate. These in vivo growth kinetics will then inform the optimal therapeutic window to test efficacy of CAR T cell therapy.

EGFRvIII-expressing GL261 were stereotactically implanted into the right striatum of C57Bl/6 female mice.

A 1T magnetic resonance imaging system (ICON™, Bruker) was used to monitor tumour engraftment and growth over time by serial imaging.

The tumour was clearly distinguishable from normal brain tissue on a standard T2-weighted sequence (RARE, 15 averages, acquisition time 6 minutes). The tumour appeared hyperintense compared to normal brain parenchyma. Within tumours, localised regions of very high signal (Figure 4.1A, white arrow) were observed most likely corresponding to oedema or haemorrhage. Increased intracranial pressure was apparent, which caused ventricle displacement (Figure 4.1A, blue arrow).

After tumour implantation, mice were scanned at different time points: the earliest time point at which tumour masses were clearly distinguishable from brain parenchyma was day 10 post implantation (Figure 4.1A). Tumour progression over time is shown in three representative mice (only one representative slice per time point is shown). Tumour volumes were measured based on the ROIs on each slice and by converting voxels into mm^3 (Figure 4.1B). H&E staining (Figure 4.1C) confirmed tumour engraftment and growth over time. Tumours appeared as formed by big glomerular-like structures and stromal areas, with regions of extracellular matrix deposition, typical of high grade gliomas in humans.

To verify EGFRvIII retention *in vivo*, tumour slices were stained with the monoclonal antibody L8A4. Strong antigen expression was observed in all tumour cells, but not on brain tissue as well as in blood vessels and stroma (Figure 4.1D).

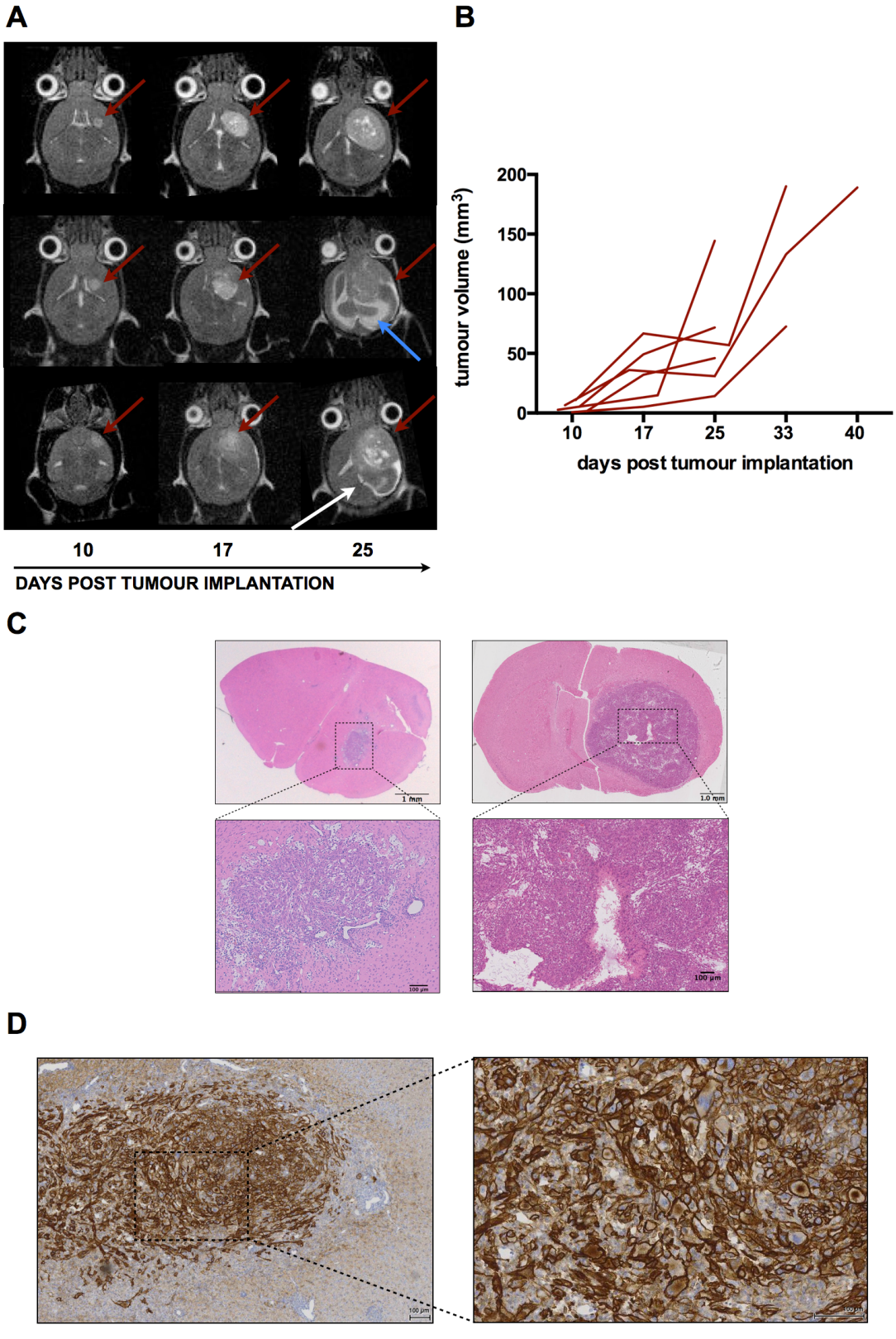

Figure 4.1 Assessment of tumour growth kinetics.
(**A**) Tumour growth over time in three representative mice. In T2-RARE sequences, tumours appeared as hyperintense (red arrows) compared to normal brain parenchyma. Middle row: blue arrow indicates ventricles displacement due to increased pressure. Bottom row: hyperintense areas (white arrow) indicate regions of haemmorage (**B**) Tumour growth kinetics of untreated mice. Tumour volumes were

measured by drawing ROIs on each slice. Mice were culled when tumours exceeded 150 mm^3 or when developed first clinical signs (**C**) H&E of tumours at day 10 and 25 post tumour implantation. To confirm tumour engraftment and growth, mice were sacrificed at day 10 and 25 post implantation. Tumours appear as formed by big glomerular cells and stromal areas, with regions of extracellular matrix deposition (arrows). (**D**) To validate retention of the antigen *in vivo*, tumour slices were stained for EGFRvIII with the monoclonal antibody L8A4, then with secondary anti-rat HRP-conjugated antibody. No staining was observed in normal brain tissue.

4.2.1 Assessment of CAR-T cells migration to tumour site

To evaluate migration and accumulation of CAR-T cells following intravenous infusion, T cells co-expressing CAR and FLuc were employed in initial experiments. After evaluation of tumour engraftment on day 10 post implantation, mice received intravenous infusion of $5x10^6$ bulk splenocytes.
Pre-conditioning with 5Gy irradiation was given prior to cells infusion to promote T cells expansion in response to lymphodepletion, as it has been demonstrated that host pre-conditioning is essential for efficacy of adoptive cell therapy (Gattinoni et al., 2005; Dudley et al., 2008; de Witte et al., 2008).
Bioluminescence imaging (BLI) showed that EGFRvIII-specific CAR-T cells accumulated at the tumour site, in contrast to T cells expressing the control CAR against hCD19. Figure 4.2B shows that from day 3 post cells infusion, EGFRvIII-specific CAR T cells migrated to the tumour, while hCD19-specific CAR-T cells did not accumulate. The total flux quantification at three time points is shown in Figure 4.2C. Differences in BLI signal were statistically significant at day 12 post T cells injection: mice receiving EGFRvIII-specific CAR-T cells had an average photons/second of $3.14x10^6 \pm 2.8\ x10^6$, while mice receiving hCD19-specific CAR-T cells had an average photons/second of $3.9x \pm 4.1\ x10^4$. Despite variability being relatively high among mice, there were 2 log differences between the two groups ($p \leq 0.05$). Specificity of migration was confirmed both by immunohistochemistry and flow cytometry.
Mice were sacrificed at day 15 post systemic injection and tumour slices were stained for CD34 as marker gene for CAR-T cells (Figure 4.2D). CD34 stains for endogenous blood vessels, therefore it was used as internal positive control for immunohistochemistry, as endothelium of capillaries and T cells can clearly be distinguished based on their morphology. In addition to $CD34^+$ capillaries (dotted arrows), tumours from mice receiving CAR-T cells specific for EGFRvIII exhibited $CD34^+$ round-shaped T cells (solid arrows). On the other hand, tumours from mice that received CAR-T cells specific for human CD19 only showed capillaries positivity.
To further validate antigen-specific CAR-T cells accumulation, tumour infiltrating lymphocytes (TILs) were isolated at day 9 post transfer. Lymphocytes were pre-gated on $CD45^+CD11b^{low}$ to exclude macrophages and microglia (vom Berg et al., 2013), then the percentage of CAR-T cells was

evaluated in $CD8^+$ and $CD4^+$ cells (Figure 4.3A). Similarly to observations *in vitro*, the vast majority of CAR-T cells were $CD8^+$ cytotoxic lymphocytes, thus suggesting that, in this model, $CD4^+$ helper lymphocytes were not involved. Staining for EGFRvIII-specific CAR-T cells was performed by double staining with RAM34 and EGFRvIII-mIgG2, to stain for both the marker gene and the actual CAR through its binding site. Conversely, staining for hCD19-specific CAR-T cells was performed only with single staining for the marker gene CD34. Average percentages of CAR-T cells on total $CD3^+$ T cells is shown in Figure 4.3B: 35.6 ± 16 for mice receiving EGFRvIII-specific CAR-T cells, 3.5 ± 2.6 for mice receiving hCD19-specific CAR-T cells ($p \leq 0.005$, unpaired T test). Taken together, these data suggest that CAR infiltration within the tumour is specific and antigen-dependent.

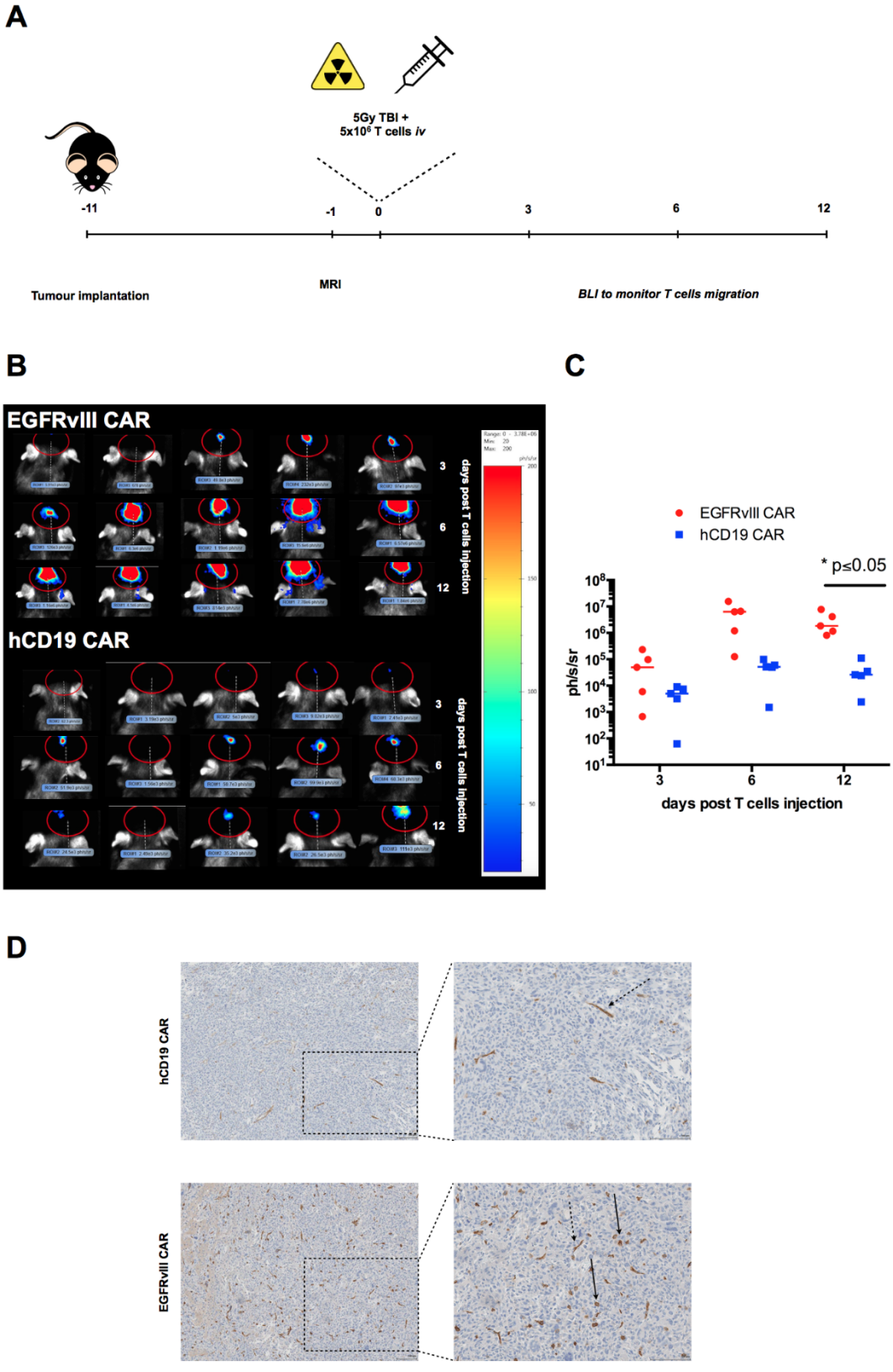

Figure 4.2 CAR-T cells efficiently migrate to tumour site.
(**A**) Timeline of experiment. Upon evaluation of tumour engraftment, mice received 5Gy sublethal total body irradiation followed by intravenous infusion of $5x10^6$ CAR-T cells. Bioluminescence imaging was used to monitor CAR-T cells migration to the tumour site. (**B**) Specific migration of EGFRvIII-specific CAR- T cells. Bioluminescence imaging (BLI) at day 3, 6 and 12 after T cells transfer showing

specific accumulation of EGFRvIII-specific CAR-T cells as opposed to anti human CD19-specific CAR (negative control). (**C)** BLI signal quantification. Each data point represents one mouse, horizonatl arrows represent median. Statistically significant differences were observed at day 12 post T cells infusion ($p \leq 0.05$, unpaired T test). (**D**) $CD34^+$ T cells observed only in EGFRvIII-specific CAR-treated mice. Tumour slices were stained with the monoclonal antibody RAM34. Dotted arrows indicate blood vessels (used as positive internal controls). T cells-shaped T cells were only observed in tumours from mice treated with EGFRvIII-specific CAR T cells (bottom panels), but not hCD19-specific CAR-T cells.

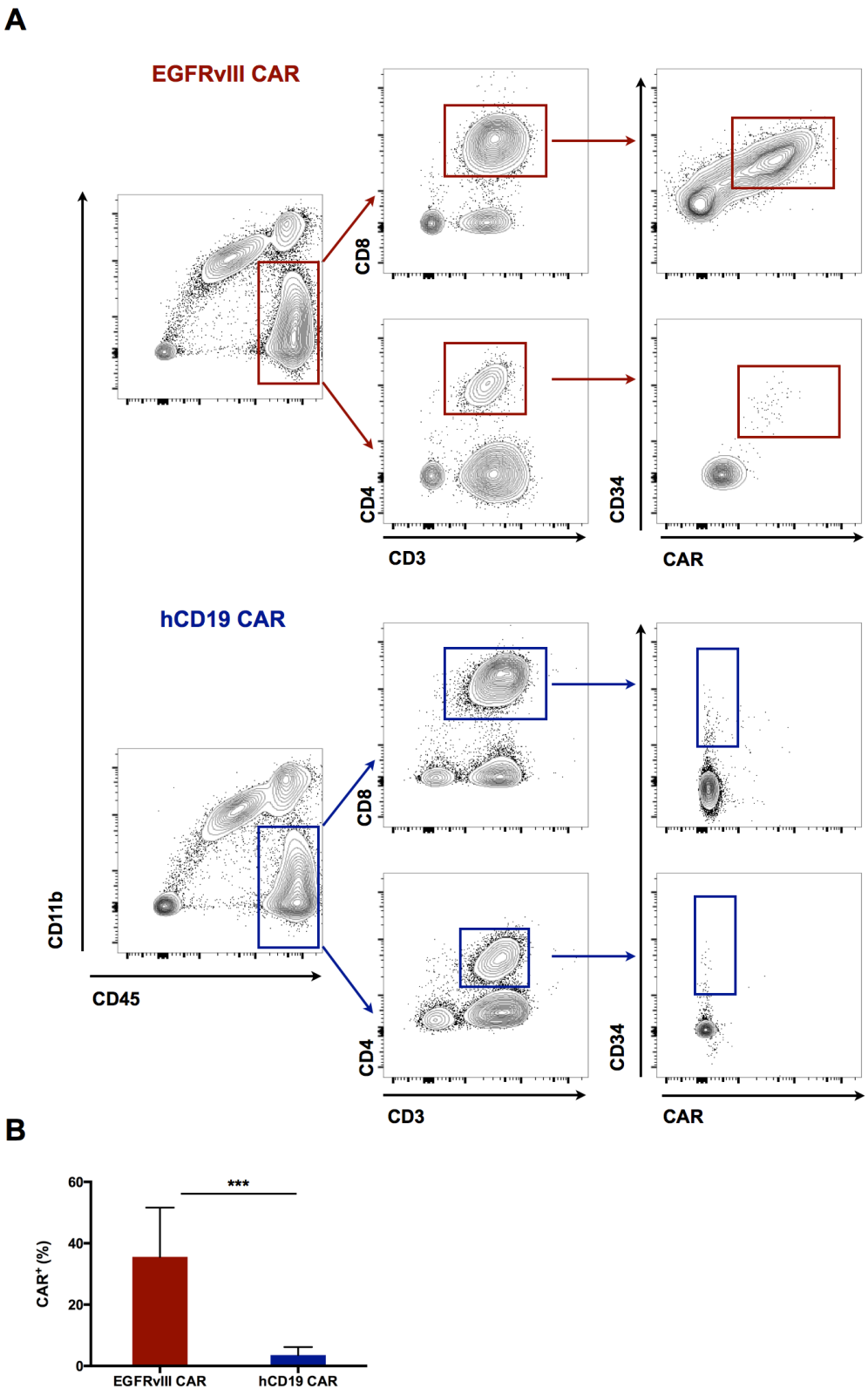

Figure 4.3 Specific infiltration of EGFRvIII CAR-T cells within intracranial tumours.

(**A**) Representative FACS plots showing tumour infiltrating lymphocytes. Gating strategy was: live, $CD45^{+}CD11b^{low}$, then $CD3^{+}CD4^{+}$ and $CD3^{+}CD8^{+}$. Transferred cells were identified as $CD34^{+}CAR^{+}$. CAR staining with EGFRvIII-mIgG2 was always performed both extracellularly and intracellularly, to account for receptor

internalisation following triggering and signalling. hCD19 CAR-T cells were only identified as $CD34^+$ cells. The majority of CAR^+ T cells were $CD8^+$ T cells.
(**B**) Average percentage of CAR^+ cells on total $CD3^+$ T cells in mice receiving EGFRvIII-specific (red) and hCD19-specific (blue) T cells (n=8), day 9 post infusion. $p \leq 0.005$, unpaired T-test.

4.3 Efficacy to control tumour growth

Upon confirmation of efficient migration of CAR-T cells at tumour site, we evaluated whether CAR-T cells infiltrating the tumour were sufficient to control tumour growth and promote long term survival.

The timeline from the previous experiment was followed (Figure 4.4A) and mice were sacrificed when tumours exceeded 150 mm^3 or whenever clinical signs developed, whichever appeared first.

MRI was performed weekly to follow tumour growth.

Survival rates were significantly higher for mice receiving EGFRvIII-specific CAR-T cells than in mice receiving TBI alone (Figure 4.4C, $p \leq 0.01$): while all TBI-only controls were sacrificed by day 38 post tumour implantation, with a median survival of 34 days, mice receiving EGFRvIII CAR had a median survival of 50 days.

At day 14 post T cells infusion, mice receiving TBI only had an average tumour volume of 61 ± 45 mm^3, mice treated with the control CAR had an average tumour size of 39 ± 44 mm^3, while mice receiving EGFRvIII-specific CAR-T cells had an average tumour volume of 23 ± 8 mm^3. However, tumour volumes were not statistically significant at this time point (Figure 4.4B).

Figure 4.5 exhibits three representative EGFRvIII CAR-treated mice with different patterns of tumour growth. Figure 4.5A shows one mouse with initial tumour reduction (day 21 post T cells injection), however the tumour grew back again at day 42. Figure 4.5B shows a mouse with a slower growth pattern, while Figure 4.5C shows a faster growing tumour.

Surprisingly, administration of hCD19 CAR seemed to improve survival curves, (median survival of 38 days), even though this was not statistically significant compared to TBI only treated mice (Figure 4.4C). However, this effect resulted in lack of significance in survival of mice receiving EGFRvIII-CAR compared to mice receiving control CAR.

Considering that by day 14 post T cells infusion no hCD19 CAR-T cells were detected within the tumours (Figure 4.2D), the minimal effect of the control CAR could be explained by some degree of initial unspecific migration (Figure 4.2B and C), due to activation of CAR-T cells, even in the absence of the antigen (Figure 3.5A). Total body irradiation (TBI) could induce immunogenic cell death at the tumour site and enhanced trafficking of T cells in general to

the tumour, resulting in increased inflammation at the tumour site and consequent delayed tumour growth.

In summary, although CAR-T cells administration enhanced survival, tumours were not completely eradicated, which resulted in the lack of long term survivors. This observation, combined with differences observed in tumour growth patterns suggests that, despite efficiently reaching the tumour, CAR-T cells effect on tumour growth is variable and may fail due to the influence of tumour microenvironment (TME).

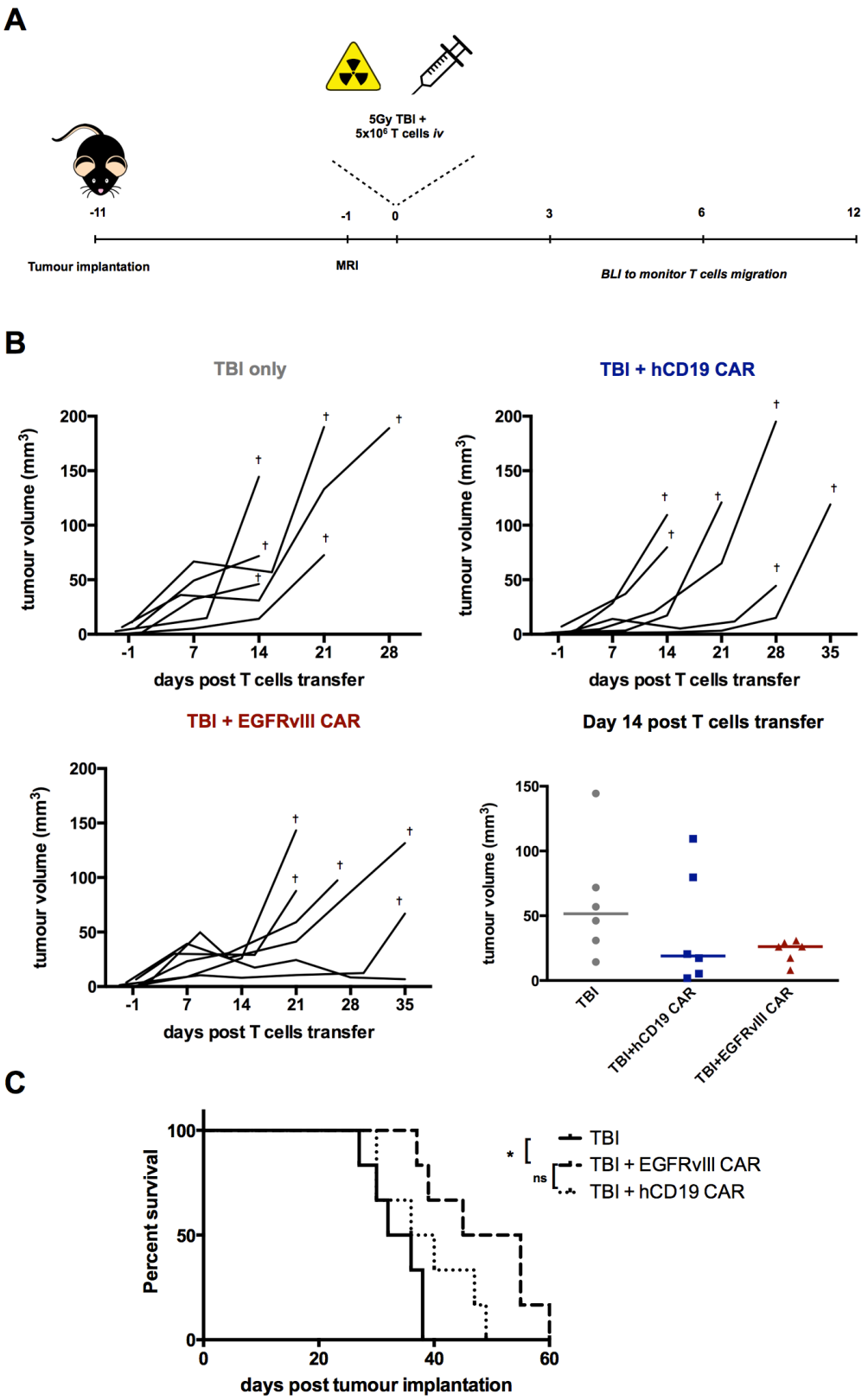

Figure 4.4 CAR-T cells administration delays tumour growth.
(**A**) Timeline of experiment. After T cells administration, MRI was performed weekly to monitor tumour growth. (**B**) Tumours volumes measured weekly. Administration of CAR-T cells after TBI delayed tumour growth if compared to TBI only treated mice. A minimal effect in growth curves was observed for mice treated with hCD19 CAR-T cells.

(**C**) Survival curves for mice treated with EGFRvIII-specific CAR-T cells, hCD19-specific CAR-T cells or TBI-only. Mice were sacrificed when tumours exceeded 150mm^3 or when clinical signs developed. (n=6) (** p≤0.01, Mantel-Cox test).

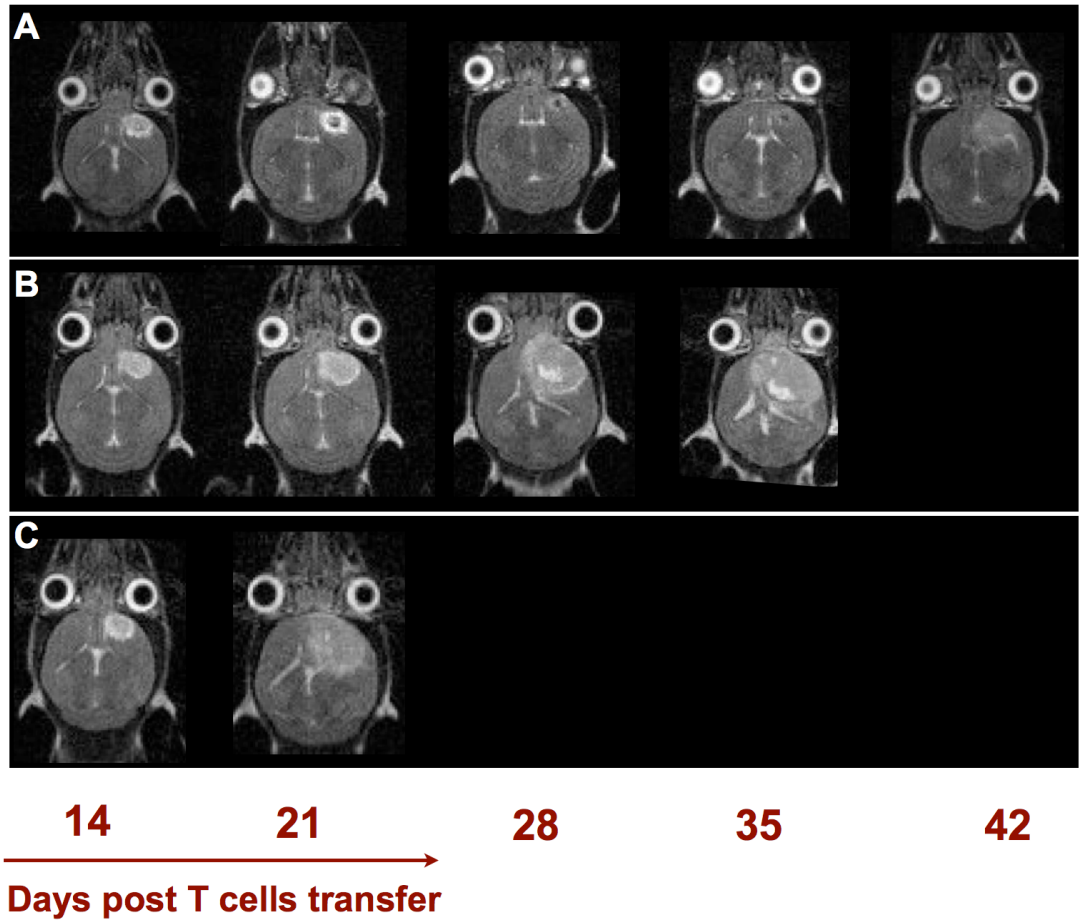

Figure 4.5 Tumour growth patterns in three representative mice receiving EGFRvIII-specific CAR-T cells
(**A**) Tumour reduction was observed in one mouse out of six, however tumour eventually grew again (**B**) Slow-growing tumour (**C**) Faster-growing tumour. This mouse had to be sacrificed at day 28 post T cells transfer due to development of clinical signs.

4.3.1 Assessment of functionality of CAR-T cells at tumour site

Data from Figure 4.4 demonstrated that, despite efficiently infiltrating the tumour (Figure 4.3), CAR-T cells failed to mediate complete remission. Therefore, we decided to assess a phenotype characterisation of tumour infiltrating lymphocytes (TILs), to verify whether CAR-T cells were functional *in situ*. TILs were isolated at day 9 post cells infusion, based on preliminary studies (Figure 4.2 and Figure 4.3) showing high infiltration at this time point.

Figure 4.6A shows gating strategy: cells were gated on live, then on $CD45^{+}CD11b^{low}$ to exclude macrophages and microglia, then $CD3^{+}CD8^{+}$ and $CD3^{+}CD4^{+}$. CAR^{neg} were considered as endogenous T cells, even though this identification system does not allow to distinguish between endogenous and transferred non-transduced T cells.

Granzyme B (GzmB) expression was evaluated on $CD8^{+}$ T and $CD4^{+}$ T cells as a marker for cytolytic activity.

Percentage of GzmB-positive cells was very high in both transferred CAR-T cells and endogenous $CD8^{+}$ T cells (identified as CAR^{neg}) (Figure 4.6B and C) Interestingly, not only CAR-T cells had a higher fraction of $GzmB^{+}$ cells compared to endogenous $CD8^{+}$ T cells from TBI only-treated mice (91%$\pm$5 versus 55$\pm$12, respectively, $p \leq 0.005$), but also CAR^{neg} $CD8^{+}$ cells had a significantly higher proportion of $GzmB^{+}$ cells (82%$\pm$13, $p \leq 0.01$). Moreover, the median fluorescence intensity (MFI) for GzmB was significantly higher in CAR^{+} T cells compared to other T cell populations (37,700$\pm$13,360, while endogenous $CD8^{+}$ T cells from treated mice were 16,000$\pm$8,000, $CD8^{+}$ T cells from mice receiving hCD19 CAR-T cells were 10,000$\pm$5,000 and $CD8^{+}$ T cells from TBI-only treated mice were 1,600$\pm$1,000). This indicates that both CAR^{+} and CAR^{-} CD8 T cells produce higher amounts of this proteinase associated with cytolytic activity. These observations suggest that CAR-T cells administration was able to promote an overall activation of the endogenous immune system. Interestingly, $CD8^{+}$ T cells from mice receiving hCD19 CAR-T cells exhibited a more activated profile compared to cells from TBI-only mice (Figure 4.6C, $GzmB^{+}$ 69.2%$\pm$10, $p \leq 0.05$). This observation was in line with previous data from the survival experiment (Figure 4.4), suggesting that the administration of an irrelevant CAR is still able to induce some degree of activation over the untreated condition.

Ki67 expression was also investigated as a marker for proliferating cells: proliferation levels were more variable and not consistently different between groups. Percentages of $Ki67^+$ cells were: 82±12 for mice only receiving TBI, 63±14 for $CD8^+$ T cells from mice receiving TBI+hCD19 CAR, 66±25 for $CD8^+$ T cells from mice receiving TBI+EGFRvIII CAR and 68±29 for EGFRvIII CAR-T cells (Figure 4.6C). No statistically significant differences were observed in this case. This observation suggests that endogenous tumour infiltrating lymphocytes already proliferate to a certain extent. Addition of CAR-T cells did not seem to improve proliferative capabilities of TILs. Interestingly, Ki67 percentages of expression were quite variable particularly for EGFRvIII-specific CAR T cells. Of note, a high variability in the percentage of Ki67 expression was observed between different experiments rather than within the same experiment (Figure 4.6C, bottom panel), with one experiment showing high percentages of proliferating cells in all mice (n=4, 93.7%±0.4) and the other showing lower levels of Ki67 expression in all mice (n=4, 43±16).

Similar findings were observed in $CD4^+$ T_{helper} cells (Figure 4.6D and E). EGFRvIII-specific CAR-T cells administration significantly increased both the percentage of GzmB-expressing $CD4^+$ T cells (49%±31) and the amount of GzmB produced (MFI 1,800±1,300) compared to mice receiving TBI only (17%±8, MFI 211±60, $p \leq 0.05$). As per $CD8^+$ cytotoxic T cells, hCD19-specific CAR T cells administration resulted in a minimal effect on $CD4^+$ T cells, although differences were not statistically significant compared to untreated controls (41%±27 and MFI 800±900).

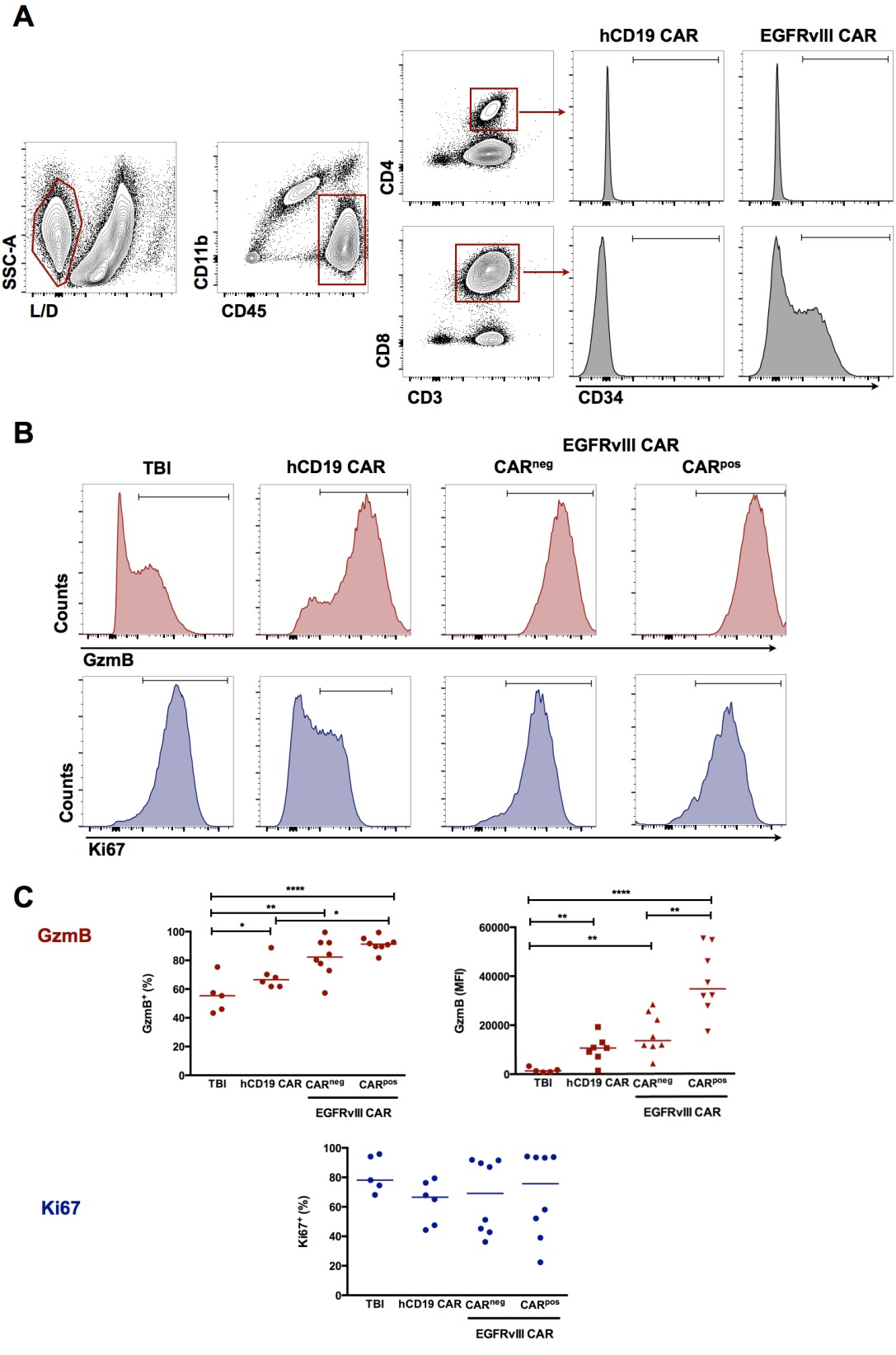
A
hCD19 CAR
EGFRvIII CAR
SSC-A
L/D
CD11b
CD45
CD4
CD8
CD3
CD34
B
TBI
hCD19 CAR
CAR^neg
CAR^pos
EGFRvIII CAR
Counts
GzmB
Counts
Ki67
C
GzmB
GzmB+ (%)
GzmB (MFI)
TBI
hCD19 CAR
CAR^neg
CAR^pos
EGFRvIII CAR
Ki67
Ki67+ (%)

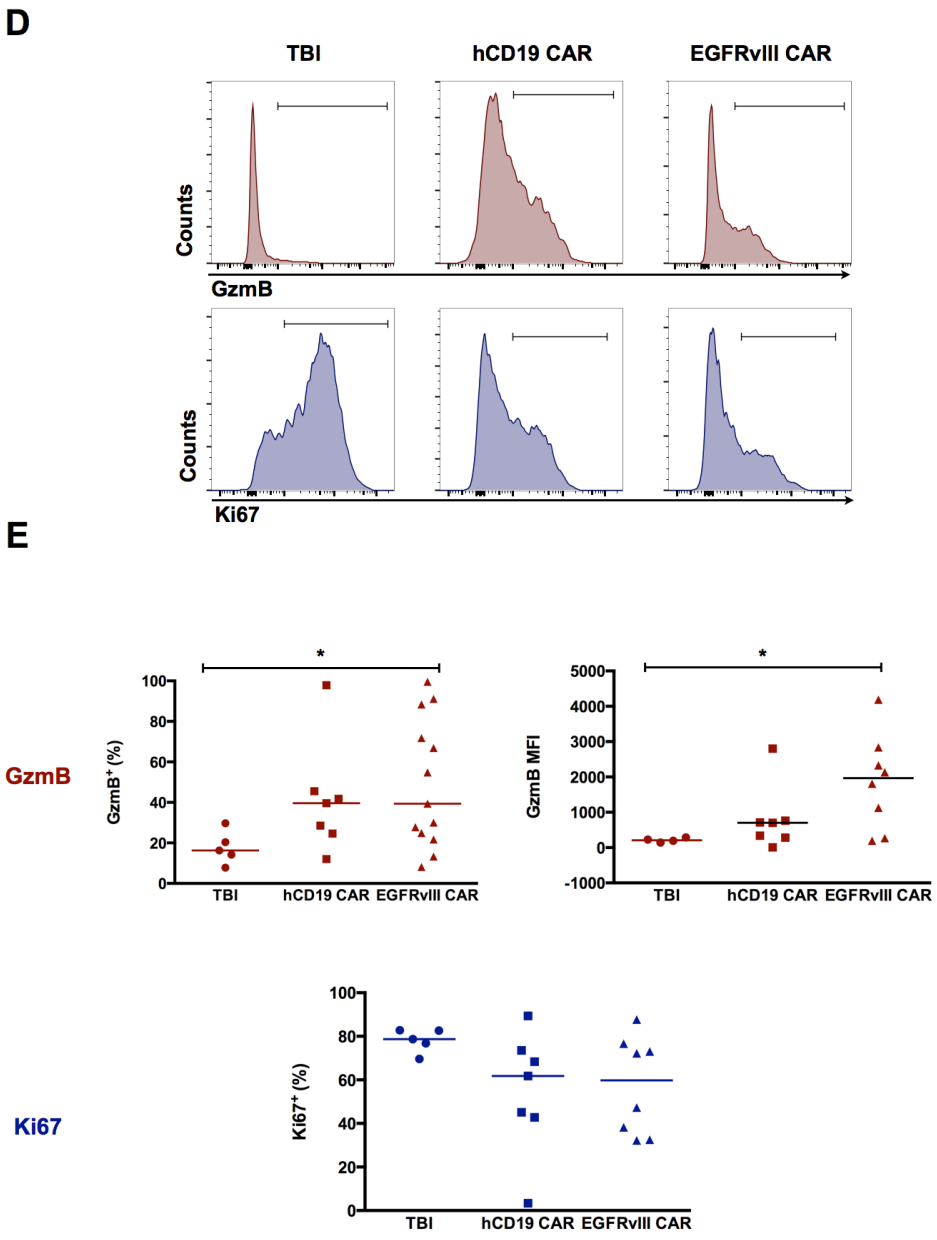

Figure 4.6 CAR-T cells are highly activated within the tumour.

(**A**) Gating strategy: cells were gated on live, $CD45^{+}CD11b^{low}$, then on $CD3^{+}CD4^{+}$ and $CD3^{+}CD8^{+}$, then on CD34 as marker gene for the CAR. (**B**) Representative histograms showing Granzyme B (GzmB) (top row) and Ki67 expression (bottom row) by $CD3^{+}CD8^{+}$T cells in different treatment groups: TBI only, TBI+hCD19 CAR-T cells and TBI+EGFRvIII CAR-T cells. In the latter group $CD3^{+}CD8^{+}$ are diveded as CAR^{pos} and CAR^{neg} based on CD34 expression. (**C**) Percentage of expression of GzmB and Ki67 in $CD3^{+}CD8^{+}$ T cells. (Unpaired T test,*p≤0.05) (**D**) Representative histograms showing Granzyme B (GzmB) (top row) and Ki67 expression (bottom row) by $CD3^{+}CD4^{+}$T cells in different treatment groups. (**E**) Percentage of expression and MFI of GzmB and percentage of Ki67-expressing $CD3^{+}CD4^{+}$ T cells. Individual data points from three independent experiments as well as the median (horizontal line) are shown.

Assessment of reactivation potential of TILs

To establish whether TILs were fully functional within the tumour, after isolation TILs were stimulated for 4 hours with PMA-ionomycin and IFNγ production was measured by intracellular cytokine staining. PMA-ionomycin is a strong unspecific stimulus which can be used to test potential of T cells to be reactivated.

Figure 4.7B shows that both CAR^+ and CAR^- $CD8^+$ T cells produced IFNγ (CAR^+ 94%±5 and CAR^- 90%±2,

Figure 4.7A and B). As expected, $CD4^+$ T cells also expressed IFNγ, but to a lesser extent (42%±10).

Upon confirmation of their activation potential, next was tested whether TILs were also able to produce IFNγ in response to antigen stimulation. TILs were therefore stimulated for 4 hours with EGFRvIII-expressing GL261.

Figure 4.7C shows percentages of $IFN\gamma^+$ cells in CAR^+ and CAR^- $CD8^+$ T cells and $CD4^+$ T cells. As expected, percentages of $IFN\gamma^+$ cells were lower in response to a specific stimulus: CAR^+ 9%±7, CAR^- 3%±2 and $CD4^+$ 1.5±1.

These data suggest that TILs can still respond to EGFRvIII-expressing cells. However, it has to be noted that viability of TILs after 4 hours stimulation with tumour cells was very low and we encountered technical problems repeating this experiment. Therefore, these data might not reflect the actual reactivation potential of TILs.

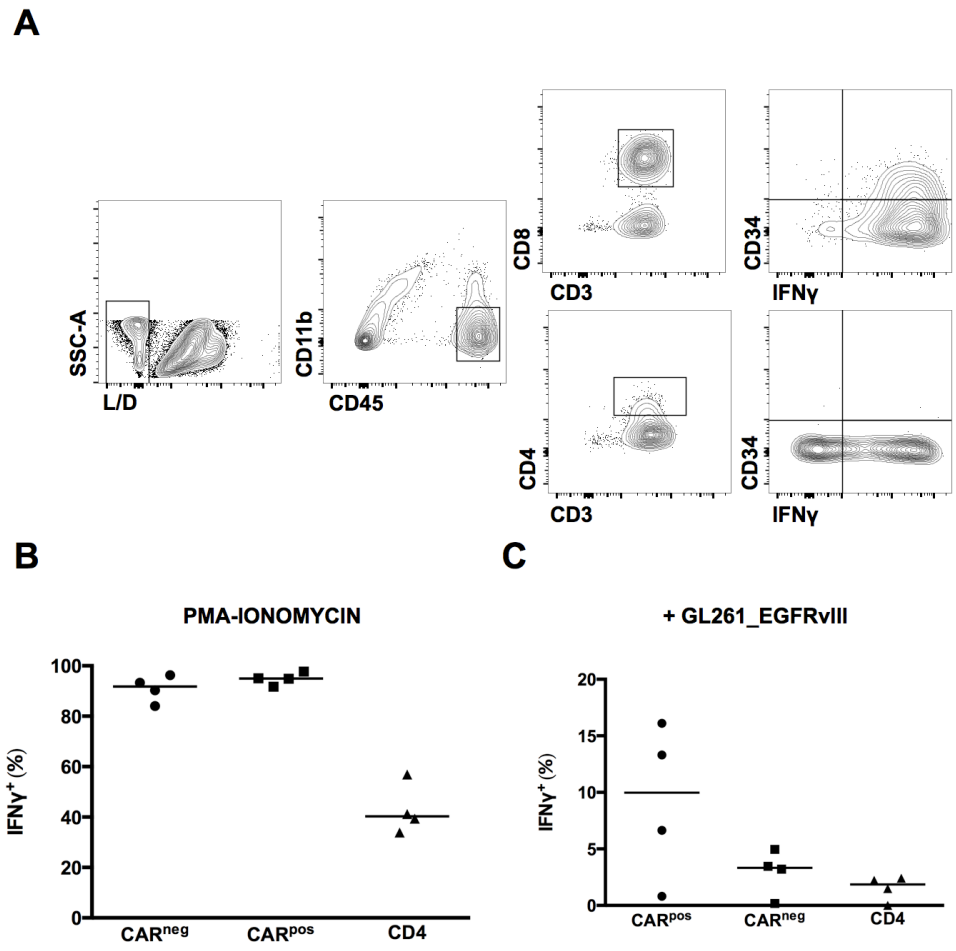

Figure 4.7 IFNγ production in response to PMA-ionomycin and GL261_EGFRvIII.
(**A**) Representative plots showing gating strategy. Cells were gated on live, then on $CD45^{+}CD11bl^{ow}$, then on $CD3^{+}CD8^{+}$ and CD34 or $CD3^{+}CD4^{+}$ and CD34.
(**B**) Percentages of $IFN\gamma^{+}$ CAR^{+} and CAR^{-} $CD8^{+}$ T cells and $CD4^{+}$ T cells after stimulation with PMA-ionomycin.
(**C**) Percentages of $IFN\gamma^{+}$ CAR^{+} and CAR^{-} $CD8^{+}$ T cells and $CD4^{+}$ T cells after stimulation with EGFRvIII-expressing GL261. Individual data points (each one mouse) and median are shown.

4.3.2 Lack of long-term persistence of CAR-T cells at tumour site

Survival experiments were initially carried out employing CAR-T cells co-expressing FLuc to monitor the long-term fate of the cells after infusion.

Mice were monitored weekly with BLI to evaluate CAR-T cells persistence within the tumour.

Figure 4.8A and B show a general trend where BLI signal decreased at later time points, leading to an almost complete drop in the BLI signal just before the clinical signs developed and mice had to be sacrificed.

These data suggested that one of the causes underlying the failure of CAR-T cells to completely eradicate tumours might be their lack of persistence within the tumour.

To confirm this hypothesis, immunohistochemistry for CD34 was performed on tumour slices at the time of sacrifice. Figure 4.8C and D show that very few $CD34^{+}$CAR-T cells were found within the tumour at the time mice developed clinical signs. This in contrast to presence of TIL at the earlier time point (15 days post T cells infusion, see Figure 4.2),

To assess whether lack of persistence was due to antigen loss, tumour slices were also stained for EGFRvIII. Figure 4.8 E shows that even after treatment with EGFRvIII-specific CAR-T cells, the antigen expression was retained by the tumour, and therefore does not explain the lack of persistence of CAR T-cells at the tumour site.

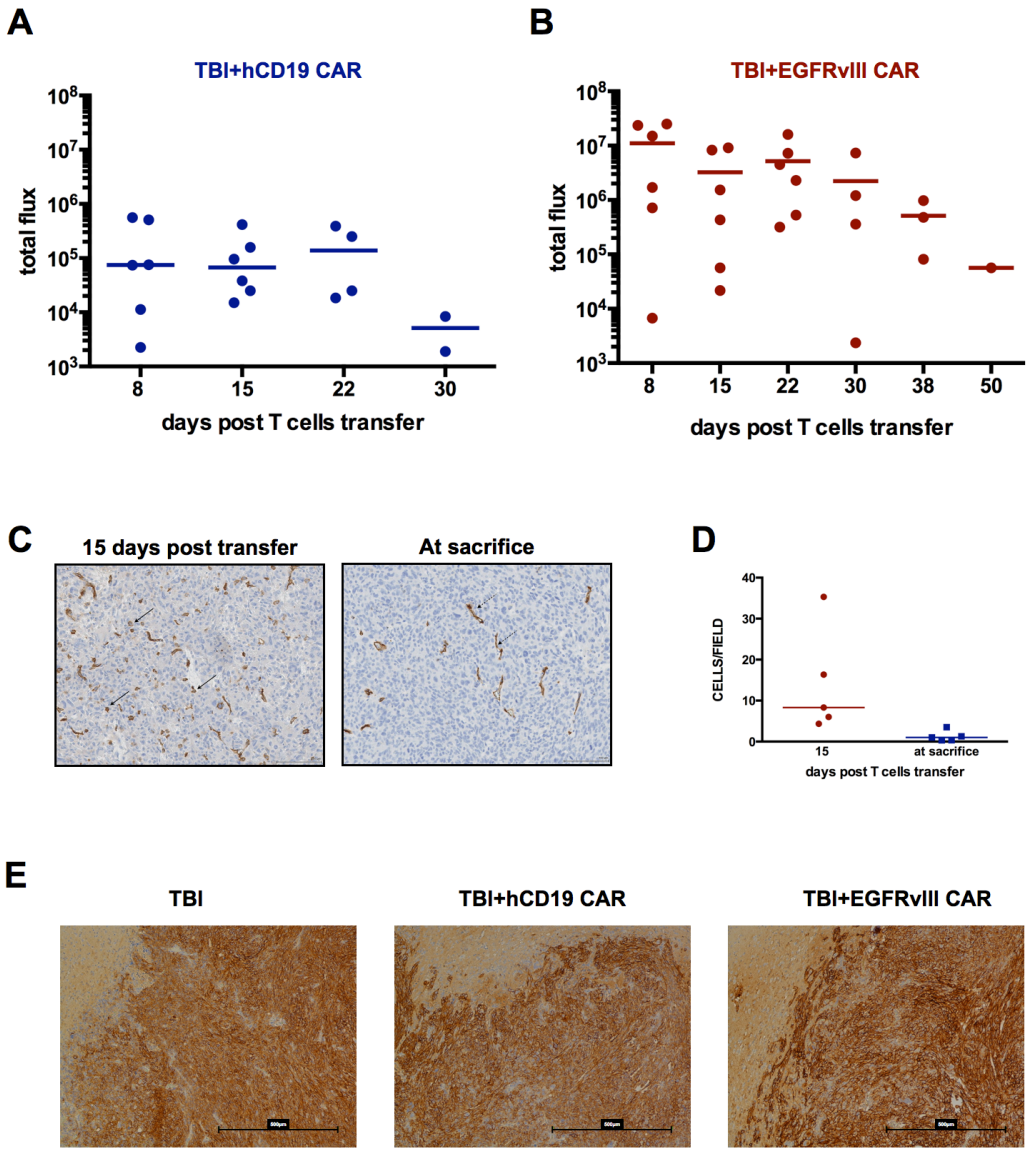

Figure 4.8 Lack of persistence of CAR-T cells.
(**A**) and (**B**) CAR-T cells co-expressing FLuc (hCD19 CAR, A, EGFRvIII CAR, B) were employed to track their long term fate in a survival experiment. Individual data points from three independent experiments as well as the median (horizontal line) are shown.
(**C**) Immunohistochemistry for CD34. Left panel shows infiltration of $CD34^+$ CAR-T cells at day 15 post administration (solid arrows), while right panel shows lack of persistence at the time of sacrifice. Dotted arrows show blood capillaries.
(**D**) Quantification of **C**. Each point indicates the average of cells counted in four randomly selected $50\mu m^2$ areas on the tumour slice.
(**E**) EGFRvIII staining on tumour slices. Antigen expression was retained in mice receiving TBI, TBI+hCD19 CAR and TBI+EGFRvIII CAR.

4.3.3 Assessment of functionality of CAR-T cells at later time point

CAR-T cells clearly infiltrated the tumour at day 9 post infusion. Increased GzmB and Ki67 expression on endogenous CTLs indicates that not only CAR-T cells were active *in situ*, but their administration was also able to drive an overall activation of the endogenous immune system (Figure 4.6).

Lack of long-term persistence within the tumour, however, suggested that these cells might get exhausted due to chronic antigen exposure, leading to incomplete tumour eradication.

To test this hypothesis, we analysed phenotype of TILs at a later time point: 17 days post transfer was chosen as an optimal time point to avoid losing mice due to excessive tumour growth.

We investigated GzmB and Ki67 expression to compare percentages of positive T cells at the two different time points. Figure 4.9B and C show a marked decrease in the expression of both markers at day 17 if compared to day 9, in both CAR^{pos} and CAR^{neg} T cells. This observation, together with the expression of PD1 at both time points (Figure 4.9D) may suggests that, after initial activation, both CAR-T cells and endogenous CTLs become exhausted due to chronic antigen exposure.

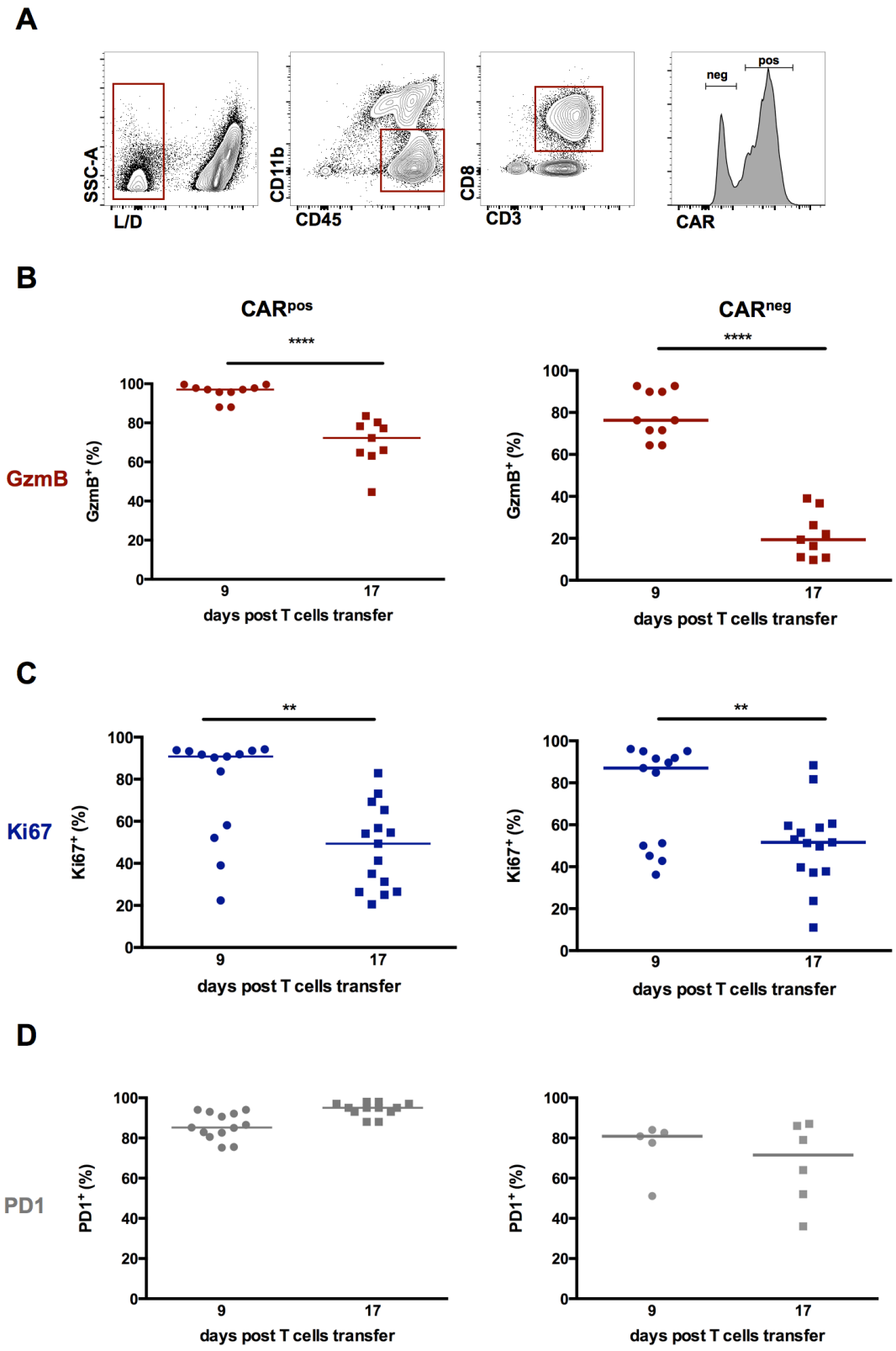

Figure 4.9 Decreased activation markers in TILs.
(**A**) Gating strategy. Cells were gated on live, then on $CD45^{high}CD11b^{-}$, $CD3^{+}CD8^{+}$ and CAR. (**B**) GzmB and Ki67 expression comparison at day 9 and 17 post T cells infusion in CAR^{pos} T cells. (**C**) GzmB and Ki67 expression comparison at day 9 and 17 post T cells infusion in CAR^{neg} T cells. (**D**) PD1 expression. Individual data points

from three independent experiments as well as the median are shown. (Unpaired T test * $p \leq 0.05$, ** $p \leq 0.01$, **** $p \leq 0.0001$).

4.3.4 Lack of migration to the draining lymph nodes

Despite effective infiltration within the tumour, we did not observe any migration of CAR-T cells in draining cervical lymph nodes at day 9 post T cells transfer (Figure 4.10A).

To verify that our staining protocol was sensitive enough to detect even small numbers of CAR-T cells, we performed a titration of CAR-T cells in a naïve spleen, where we mixed increasing amounts of CAR-T cells to naïve splenocytes (Figure 4.10B). This experiment showed that our staining protocol was able to detect cells even at a low ratio (0.5:100), therefore we could conclude that CAR-T cells did not migrate to lymph nodes in our experimental settings.

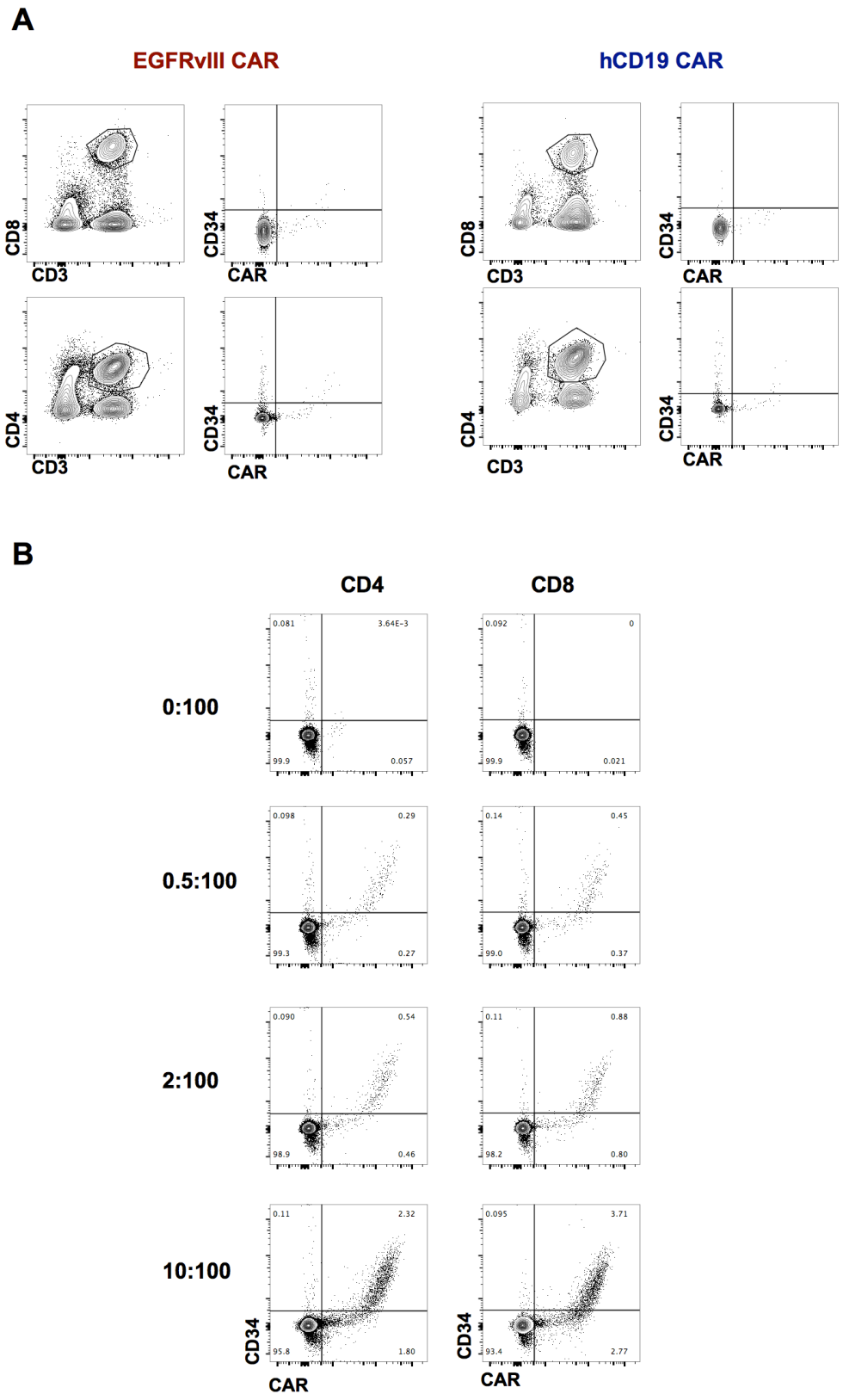

Figure 4.10 Lack of migration of CAR-T cells to draining lymph nodes.
(**A**) Staining for CAR and CD34 in cervical lymph nodes from mice receiving either EGFRvIII-specific or hCD19-specifc T cells showed no migration of cells to this site. (**B**) Titration of CAR-T cells in a naïve spleen. CAR-transduced T cells were mixed with a splenocytes at different CAR:spl ratios (0.100; 0.5:100; 2:100;10:100).

4.4 Summary and conclusions

Taken together, data from this chapter show that EGFRvIII-expressing GL261 consistently engrafted in the striatum of C57Bl/6 mice and EGFRvIII expression was retained *in vivo*. A bench-top 1T MRI system was shown to be a suitable and reliable tool to monitor tumour growth over time. Initial migration studies confirmed that intravenously injected CAR-T cells efficiently infiltrated the tumour in an antigen-dependent manner.

Initial background migration of hCD19-specific CAR-T cells was observed (Figure 4.2B and C). This could be due to some level of background activation given by the presence of the CAR signalling domain (see paragraph 3.4.2), which could explain migration of CAR-expressing T cells to an inflamed site such as the tumour. Nonetheless, both immunohistochemistry and flow cytometry confirmed that antigen recognition is essential for a persistent accumulation of CAR-T cells within the tumour at later time points (day 12 and 15 post T cells administration).

These preliminary data suggest that systemic administration is a suitable route of administration of CAR-T cells for intracranial tumours such as glioblastoma. The majority of previous studies using CAR-T cells in this context opted for a direct injection of cells within the brain, with only three cases describing systemic administration of CAR-T cells (Chow et al., 2013; Sampson et al., 2014; Johnson et al., 2015). Chow et al. reported no effect of systemically injected CAR-T cells, while the other two studies reported partial or complete response. The latter two studies reported efficacy of systemically infused CAR-T cells. Both these reports targeted the EGFRvIII mutation. The report from Sampson et al. used a similar approach to ours and tested efficacy of murine T cells expressing a third-generation murine CAR in an immunocompetent intracranial glioma model (SMA-560 is a murine glioma cell line developed in VM/Dk mice). This work highlighted the need for host pre-conditioning with radiotherapy for CAR-T cells to be effective. Data from this paper demonstrated that EGFRvIII-specific CAR-T cells are able to promote long term survival when systemically injected. Moreover, tumour-cured mice were protected from re-challenge with EGFRvIII-negative SMA-560 cells, suggesting a capability of CAR-T cells to promote antigen spreading and generation of host immune memory.

Despite describing an interesting approach to the study of a CAR-based therapy, Sampson's et al's study did not provide any insight into the kinetics of migration and persistence of CAR-T cells in the context of an immunocompetent mouse model, nor did it provided an analysis of the effect of CAR-T cells on the endogenous compartment.

Here, we sought to investigate infiltration of CAR-T cells within the tumour and their interaction with the endogenous immune system. Phenotype analysis of TILs by flow cytometry showed that at day 9 post T cell infusion CAR-T cells constituted up to 50% of total $CD3^+$ within the tumour. Interestingly, virtually all CAR-T cells within the tumour were $CD8^+$ CTLs (Figure 4.3). This was not unexpected, since the original infused product mainly comprised $CD8^+$ cells (Figure 3.3). We propose that the CD8 predominance was a consequence of the activation protocol with ConA. The ratio CD8/CD4 seemed to increase even further *in vivo*, where no $CD4^+$ CAR-T cells were found within the tumour (Figure 4.3). A similar observation was recently reported in a clinical trial for multiple myeloma: in this report, Kochenderfer and colleagues described that, despite a ratio CD8:CD4 of 1, engrafted CAR-T cells were mainly $CD8^+$T cells, but did not hypothesize the mechanism behind this (Ali et al., 2016).

In this tumour model, the majority of TILs within the tumour were $CD8^+$ T cells, even in the endogenous compartment (Figure 4.3, Figure 4.6 and, later, Figure 6.8), suggesting that $CD8^+$ CTLs preferentially infiltrate the tumour and play an important role in tumour control. This feature may explain why the ratio CD8/CD4 is even more pronounced in the CAR-T cell compartment. The causes underlying this phenomenon should be further investigated, especially since previous reports demonstrated that a combination of CAR-expressing $CD8^+$ and $CD4^+$ T cells is important to promote a more potent anti-tumour response (Moeller et al., 2005, 2007). In particular, the requirement for CD4 was mediated by IL2 production, which might sustain proliferation and persistence of $CD8^+$ CAR-T cells (Moeller et al., 2007). More recently, another group described similar results (Sommermeyer et al., 2016; Turtle et al., 2016). This observation might be important for our findings of lack of long term persistence of CAR-T cells within the tumour (Figure 4.8).

Administration of CAR-T cells following total body irradiation was able to increase survival (Figure 4.4, $p \leq 0.01$ compared to TBI group). However, due

to variability of tumour growth kinetics, no statistically significant differences in tumour volumes were observed at any time point.

We did not observe complete tumour eradication in this experimental setting. Lack of tumour clearance correlated with loss of CAR-T cells within the tumour at time of sacrifice. This was confirmed by both BLI and IHC for mCD34 (Figure 4.8). This data is in contrast with a recent published study which showed that in mice not controlling tumour growth, CAR-T cells were still present at the time of sacrifice (Cherkassky et al., 2016). These differences might be due to the different animal model used: Cherkassky et al. used an immunocompromised xenograft for lung cancer, therefore lack of endogenous immune system might affect persistence of CAR-T cells. Moreover, location within the CNS might be an additional challenge for T cell persistence.

Functional analysis of TILs showed that initial infiltration within the tumour results in an overall activation of both CAR-T cells and endogenous immune system, as demonstrated by increased expression of GzmB in both $CD8^+$ and $CD4^+$ in mice receiving EGFRvIII-specific CAR-T cells (Figure 4.6). However, markers for activation and proliferation dropped drastically when we analysed TILs at a later time point, 17 days post T cells administration (Figure 4.9). This was observed in both CAR-T cells and endogenous CTLs, suggesting that both compartments might have lost functionality.

To prove T cell exhaustion, lack of production of cytokines upon *ex-vivo* re-stimulation should have been demonstrated. However, sample processing from brain tumours (from cardiac perfusion to isolation of TILs) is a long procedure which results in the loss of many cells and consequent low number of recovered viable cells. Additional 4 hours re-stimulation resulted in further 80% loss of viable cells compared to samples stained fresh. Due to these technical issues, it was difficult to obtain a solid IFNγ staining which could allow a reliable quantification of cytokine production. Therefore, it was not possible to definitely establish T cell exhaustion at a later time point.

This finding was in line with those of Cherkassky et al., which showed exhaustion of CAR-T cells *in vivo*, resulting in decreased cytokine release after exposure to the tumour. This was observed particularly for CAR-T cells carrying CD28 co-stimulatory domain as opposed to 41BB (Cherkassky et al., 2016), thus suggesting that 41BBζ CAR-T cells might have enhanced fitness

in vivo. Similar findings were found by Long et al., 2015, who demonstrated that the CD28 domain drives early exhaustion of CAR-T cells during *ex vivo* expansion through tonic signalling, resulting in poor cytokine production and poor persistence and efficacy *in vivo*. Exhaustion of CAR-expressing T cells was ameliorated by introduction of a 41BB co-stimulatory domain which enhanced efficacy *in vivo* (Long et al., 2015). This effect was observed for a specific CAR carrying a particular ScFv (14gA, which recognises GD2) which led to constant tonic signalling, therefore this does not necessary apply to all CARs. More recently, another study from Carl June's group demonstrated that CD28-based CARs have shorter *in vitro* persistence, which is associated with glycolytic activity, while 41BB-based CARs have enhanced persistence and selectively induce mitochondrial biogenesis. Interestingly, two recent papers demonstrated that CD28 is the main target downstream of PD1 signalling (Hui et al., 2017) and that rescue of exhausted CD8 T cells by PD1 blockade is dependent on CD28 signalling (Kamphorst et al., 2017), thus corroborating the hypothesis that CD28-based CARs might be more sensitive to exhaustion through PD1 signalling.

Finally, in this experimental setting, we did not observe any migration of CAR-T cells to the draining lymph nodes. A possible explanation for this phenomenon might be the fact that the CAR-T cells activation mechanism does not require antigen presentation by dendritic cells or antigen presenting cells, resulting in lack of migration to the draining lymph nodes. Accumulation of CAR-T cells was only observed within the tumour, the only site where the antigen is expressed and where CAR-T cells encounter an immunosuppressive microenvironment which may drive their exhaustion.

However, this aspect was not investigated further as it was not the main purpose of this project and would therefore need future research.

In conclusion, CAR-T cells therapy can increase survival of treated mice, however additional strategies are needed to enhance efficacy. The next two chapters will describe two different approaches that were explored to improve CAR-T cell therapy in this context.

Chapter 5

Results:

Improving efficacy of CAR-T cells using a third-generation CAR

5 Results: Improving efficacy of CAR-T cells using third generation CAR

5.1 Introduction

Data from chapter 4 suggested that, despite being highly activated *in vitro* and when they first reached the tumour, CAR-T cells may get exhausted over time. This correlated with lack of systemic engraftment and poor persistence *in situ*. Based on these data, we hypothesised that poor CAR-T cells persistence could be due to:

a) Insufficient stimulation of CAR-expressing CAR-T cells. Efficacy *in vivo* may require additional survival signals. We therefore added a second co-stimulatory domain - 41BB – to provide an additional survival signal to CAR-expressing T cells. Third-generation CARs have been shown to have increased Bcl-X_L activation and enhanced potency *in vivo* in large established tumours. Moreover, they have been associated to better persistence (Carpenito et al., 2009; Zhong et al., 2010).

b) Alternatively, since working in the context of an immunocompetent mouse model, it was possible that luciferase expression in CAR-T cells could lead to recognition of transferred T cells as exogenous. The mount of an endogenous immune response could ultimately lead to lack of long term persistence.

5.1.1 Rationale and aims

Specifically, in the context of glioblastoma, a previous study from Sampson et al. demonstrated that EGFRvIII-specific CAR-T cells carrying a third generation CAR were able to mediate long term survival of mice bearing orthotopic tumours (Sampson et al., 2014). We therefore sought to investigate whether addition of 41BB could enhance efficacy *in vivo* and improve persistence of CAR-T cells *in situ* in our model. Specifically, the aims of the experiments described in this chapter are:

- Test and characterise T cells expressing a third-generation CAR, by comparison to a second-generation CAR
- Evaluate efficacy *in vivo*
- Assess phenotype of TILs *in situ*

- Evaluate effects of luciferase expression on CAR-T cells persistence within the tumour

5.2 Validation of *in vitro* function of 3rd generation CAR-transduced T cells

The same constructs were designed as per the 2nd generation version, one including FLuc for *in vivo* tracking (Figure 5.1A).

All *in vitro* validation experiments were carried out using 2nd generation CAR-transduced T cells as reference.

Chromium release assay showed no differences in cytotoxic capabilities of splenocytes transduced with third-generation CAR compared to second-generation, with percentages of chromium release similar at all effector to target ratios (Figure 5.1B).

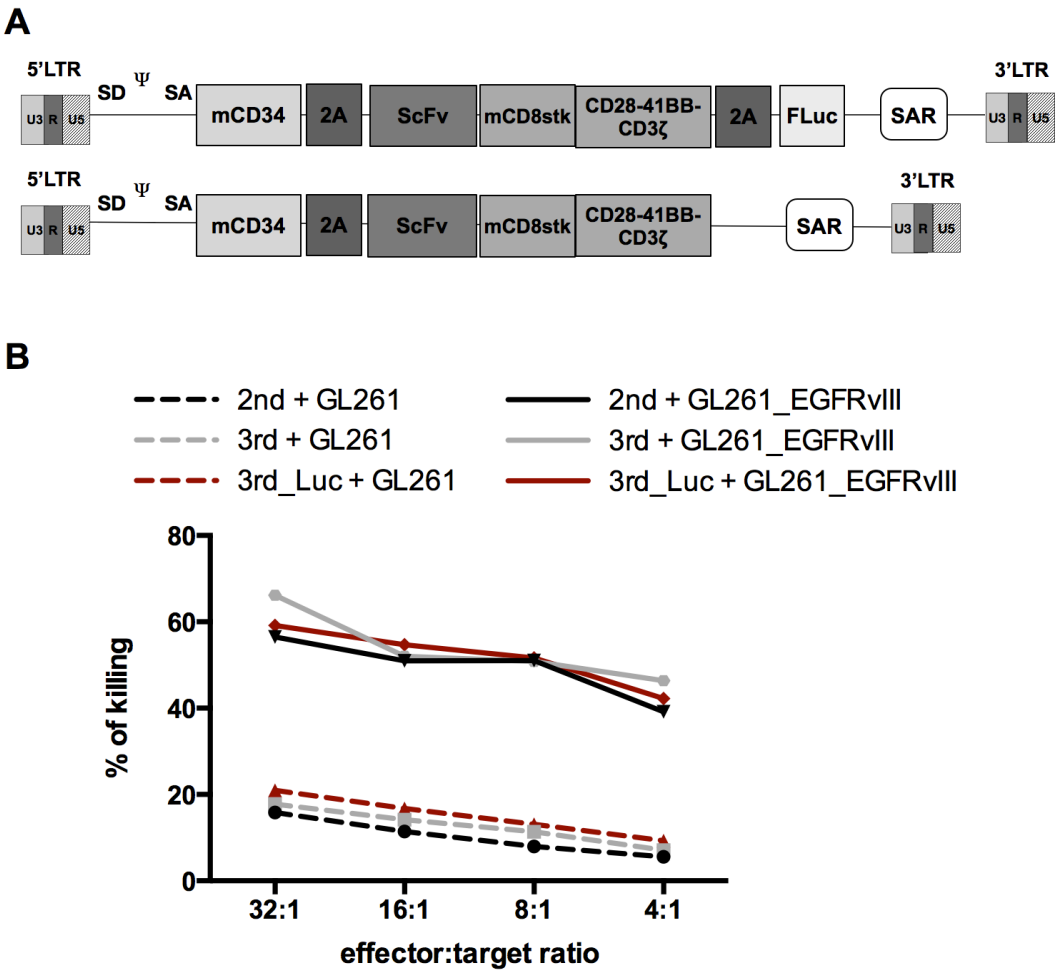

Figure 5.1 Third-generation CAR validation *in vitro*.
(**A**) Constructs used in this study. Both constructs included the murine CD34 as marker gene, while luciferase was included for *in vivo* tracking. (**B**) Chromium release assay was performed to compare cytotoxic activity of 2nd and 3rd generation CAR-T cells against both GL261 and GL261_EGFRvIII.

5.3 *In vitro* phenotype of third-generation CAR-transduced T cells

Further characterisation of activation/exhaustion markers PD1 and LAG3 showed a generally higher expression in CAR-expressing T cells compared to non-transduced cells in the same well (Figure 5.2A), similarly to T cells transduced with 2nd generation CAR (Figure 5.2C).

Cells were analysed at day 6 post transduction, one day prior to systemic infusion into mice (see section 5.4) When unstimulated, CAR-T cells had a PD1 MFI of 2524 compared to 395 of untransduced T cells. Likewise, LAG3 had an MFI of 3145 versus 513 in untransduced cells. Overall, these data sugest that CAR-expressing T cells have a more activated profile compared to untransduced cells, even when exposed to the same conditions. PD1 was further upregulated in response to antigen stimulation (3 days stimulation), with an MFI of 48725. Conversely, LAG3 expression was not upregulated (MFI: 2236). If compared to 2nd generation CAR-transduced T cells, cells expressing 3rd generation CAR presented a more activated profile: when unstimulated, PD1 MFI for 2nd generation CAR was 1273 and LAG3 MFI was 2043.

Similarly, in response to antigen stimulation, 2nd generation CAR-T cells upregulated PD1, but MFI was lower if compared to 3rd generation CAR-T cells (26892 versus 48725, respectively), while LAG3 MFI was very similar for both CARs (2231 versus 2236, respectively).

CD44 and CD62L expression was also assessed to evaluate memory phenotype of transduced cells. Similarly to T cells expressing 2nd generation CAR, CAR-T cells expressing 3rd generation CAR had decreased percentages of $CD44^{+}CD62L^{+}$ compared to untransduced T cells (22%$\pm$7 versus 47% $\pm$0.5, respectively).

Table 5.1 summarises MFIs and percentages for both constructs. Taken together, these data suggest that T cells expressing a 3rd generation CAR have an overall more activated profile.

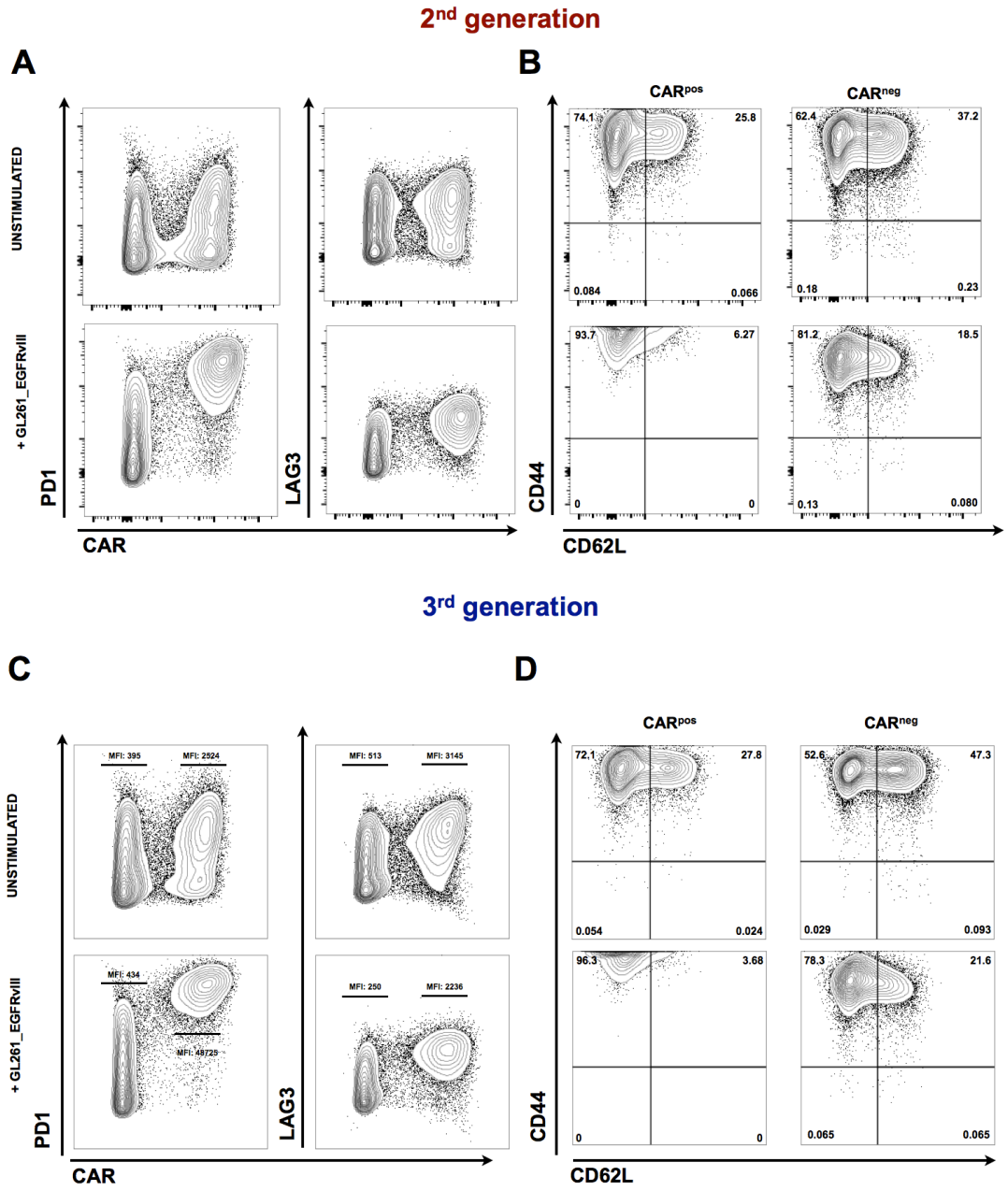

Figure 5.2 Comparison of phenotype of 2nd and 3rd generation and CAR T cells *in vitro*.
(**A**) 2nd generation CAR: PD1 and LAG3 expression in in CAR^+ and CAR^- T cells at day 6 post transduction. (**B**) 2nd generation CAR: CD44 and CD62L expression defines effector memory T cells. (**C**) 3rd generation CAR: PD1 and LAG3 expression in in CAR^+ and CAR^- T cells at day 6 post transduction. (**D**) 3rd generation CAR: CD44 and CD62L expression defines effector memory T cells.

Table 5.1 Activation and effector memory profile of 2nd and 3rd generation CAR-transduced T cells.

	PD1 MFI		LAG3 MFI		CD44 MFI		%CD44$^+$CD62L$^+$	
	CAR$^+$	CAR$^-$	CAR$^+$	CAR$^-$	CAR$^+$	CAR$^-$	CAR$^+$	CAR$^-$
2nd generation: unstimulated	1273	314	2044	531	60050	50531	24±1.6	36±1.6
3rd generation: unstimulated	2524	395	3145	513	78540	71926	22±7	47±0.5
2nd generation: stimulated	26892	424	2231	373	195463	44548	9.6±4.7	27±12
3rd generation: stimulated	48725	434	2236	250	261573	55687	11.3±10	25±5

5.4 Evaluation of efficacy of 3rd generation CAR-transduced T cells *in vivo*.

5.4.1 Efficacy of third-generation CAR T cells

To test whether the addition of the co-stimulatory domain 41BB could give an advantage to CAR-T cells *in vivo*, mice were orthotopically injected with GL261_EGFRvIII, then received either 2nd or 3rd generation CAR-T cells (Figure 5.3A).

MRI was performed weekly to evaluate differences in tumour growth, while FLuc+ T cells were employed to monitor persistence at tumour site.

No statistically significant reduction in tumour size was observed in mice receiving 3rd generation CAR-T cells compared to mice receiving 2nd generation CAR at day 14 post T cell administration (Figure 5.3B and C).

Similarly, no differences were observed in tumour persistence of 3rd generation CAR-T compared to 2nd generation, as measured by BLI (Figure 5.3D). Similar results were obtained on immunohistochemistry for CD34 at time of sacrifice at day 30 post tumour implantation (Figure 5.3E).

We were not able to assess long term differences of second versus third generation CAR-T cells as the experiment had to be terminated (14 days post T cell administration), as three mice in the cohort treated with third generation CAR-T cells died unexpectedly. Unfortunately, this time point was too early to assess whether the presence of an additional co-stimulatory domain is enough to promote long term persistence within the tumour.

Post-mortem histopathology depicted that mice treated with 3rd generation CAR that died unexpectedly presented extensive haemorrhage in areas within and around the tumour (Figure 5.3F), which most likely was the cause of death. This finding raises concerns about the use of 3rd generation CAR-T cells for intracranial tumours, as over-activated cells in such a delicate location could cause a great damage leading to dangerous side effects.

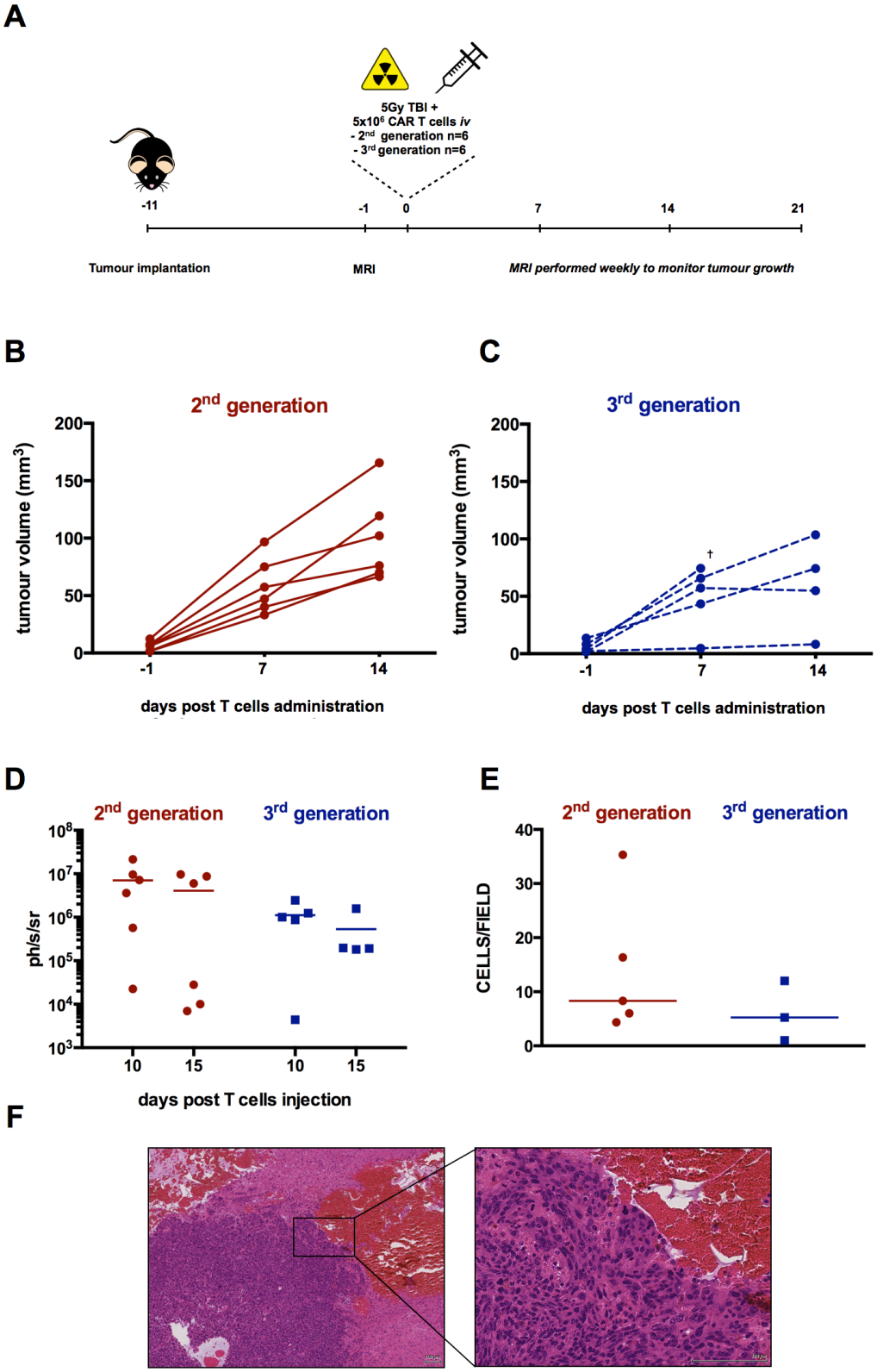

Figure 5.3 Comparison of 2nd and 3rd generation CAR-T cells *in vivo*.
(**A**) Timeline of the experiment: on day 11 post tumour implantation, mice received 5Gy TBI and either 2nd or 3rd generation CAR-T cells *iv*. MRI and BLI were performed weekly to monitor tumour growth and persistence of CAR-T cells. (**B**) Tumour volumes of mice treated with 2nd generation CAR. (**C**) Tumour volumes of mice treated with 3rd generation CAR. (**D**) BLI at day 10 and 15 post T cells infusion. Individual data

points as well as the median are shown (**E**) Quantification of $CD34^+$ CAR-T cells within the tumour at sacrifice. Each value represents an average of 4 fields ($50\mu m^2$ each). (**F**) H&E showing extensive haemorrhage in mice receiving 3rd generation CAR-T cells.

5.4.2 Systemic engraftment

To evaluate whether addition of 41BB could affect systemic engraftment, we analysed the spleens from mice receiving either second or third-generation CAR-T cells at day 17 post T cells injection. To identify CAR-T cells, we performed staining for CD34 and CAR. Only double positive cells were considered as CAR^+ transferred T cells, while single positive populations were considered as the result of unspecific staining. Mice receiving third-generation CAR exhibited a small, but consistent percentage of double positive $CD8^+$T cells (Figure 5.4A and B). Similarly to what was observed in the brain, no CAR-T cells were observed within the $CD4^+$ population.

Conversely, a significantly lower percentage of CAR-T cells was observed in mice receiving second-generation CAR-T cells (Figure 5.4A and B).

These data suggest that addition of 41BB might affect systemic engraftment of tumour-specific T cells.

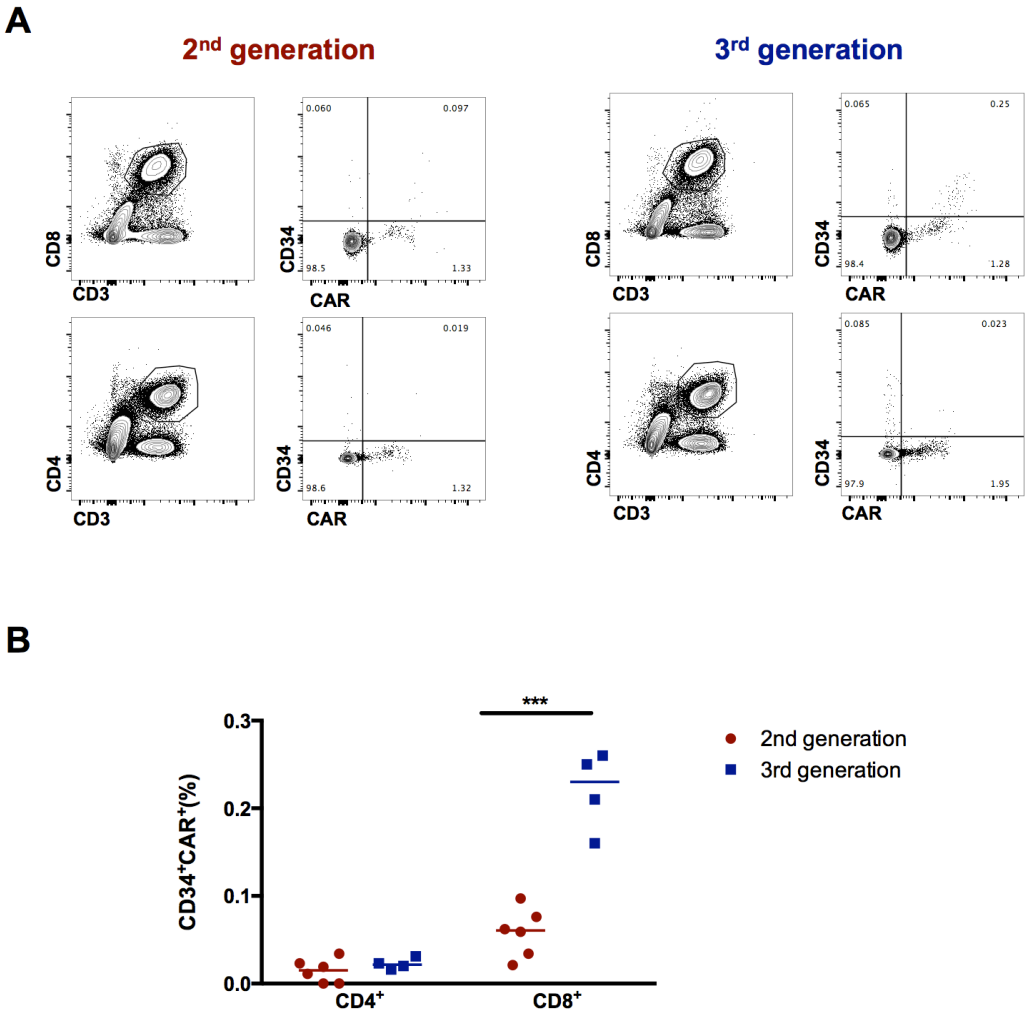

Figure 5.4 Systemic engraftment of transferred CAR-T cells
(**A**) Representative FACS plots showing CAR^+CD34^+ in CD8 and CD4 T cells. Left panel: mice receiving second-generation CAR-T cells; right panel: mice receiving third-generation CAR-T cells.
(**B**) Quantification of double positive CAR^+CD34^+ in the two treated groups. Individual data points as well as the median are shown. Only one experiemnt was performed. Unpaired T test (*$p \leq 0.001$).

5.4.3 Assessment of phenotype of 3rd generation CAR-T cells *in vivo*

Data from Figure 4.9 suggested that, despite being active soon after reaching the tumour, CAR-T cells lost functionality over time (day 17 post cells infusion). To address whether addition of 41BB as second co-stimulatory domain could prevent exhaustion of CAR-T cells *in situ*, we analysed phenotype of TILs at day 17 post T cells infusion.

Surprisingly, CAR-T cells expressing a 3rd generation CAR-T cells exhibited a lower expression of GzmB (Figure 5.5B). Conversely, Ki67 expression was higher in 3rd generation CAR-T cells (Figure 5.5C), suggesting that the additional co-stimulatory domain may improve proliferation capabilities of CAR-T cells, but not their cytotoxic activity.

In terms of activation/exhaustion markers, no statistically significant differences were observed in the two groups, which both exhibited PD1 expression in almost all CAR^+ T cells (Figure 5.5D), while LAG3 MFI was similar (Figure 5.5E).

Phenotype of CAR^- $CD8^+$ T cells was also analysed: the endogenous compartment resulted less activated compared to CAR-T cells, however, no significant differences were observed in the two treatment groups. This suggests that administration of 3rd generation CAR-T cells does not affect the functionality of tumour infiltrating lymphocytes.

To evaluate whether the presence of 41BB could improve persistence of 3rd generation CAR-T cells, absolute numbers of CAR-T cells within the tumour were calculated (normalised on tumour volumes, measured one day before sacrifice, Figure 5.5F): no statistically significant differences were observed in CAR-T cells numbers (Figure 5.5G).

Taken together, these data indicate that administration of 3rd generation CAR-T cells did not confer enhanced efficacy when compared to 2nd generation CAR-treated mice.

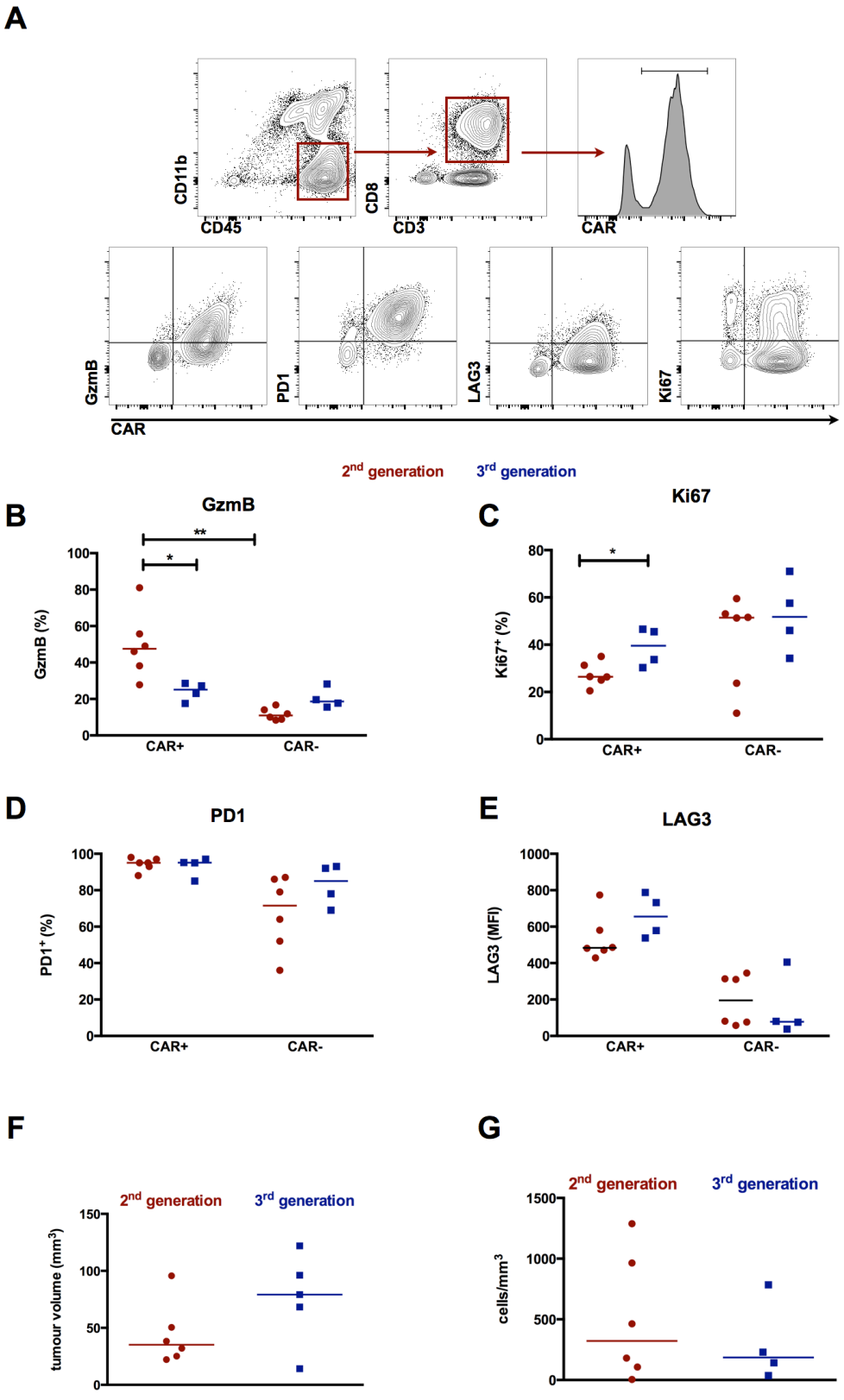

Figure 5.5 Characterisation of 2nd and 3rd generation CAR-T cells *in vivo*.
(**A**) Representative FACS plots of tumour infiltrating lymphocytes at day 17 post T cells infusion. Cells were gated on live, then $CD45^{high}CD11b^{low}$, then $CD3^{+}CD8^{+}$. CAR-expressing cells were identified by intracellular staining with EGFRvIII-mIgG2A. (**B**) GzmB expression (% of total cells) in CAR^{+} and CAR^{-} cells. (**C**) Ki67 expression (% of total cells) in CAR^{+} and CAR^{-} cells. (**D**) PD1 expression (% of total cells) in CAR^{+}

and CAR^- cells. (**E**) LAG3 MFI in CAR^+ and CAR^- cells. (**F**) Tumour volumes measured one day prior sacrifice (**G**) CAR-T cells counts were normalised on tumour volumes. Individual data points from one experiment as well as the median are shown. (Unpaired T test * $p \leq 0.05$).

5.5 Evaluating effect of luciferase on CAR-T cells persistence *in vivo*

Data from chapter 4.3.2 suggested that CAR-T cells failed to persist within the tumour, despite efficiently migrating to the brain after systemic infusion (Figure 4.2 and Figure 4.8).

Since the GL261 is an immunocompetent animal model, one possibility is that an immune reaction occurred against transferred T cells. Luciferase is an exogenous gene that, despite being expressed intracellularly, could be recognised as exogenous by the endogenous immune system which could therefore mount a response against $FLuc^+$ T cells.

To evaluate whether expression of FLuc could affect persistence and efficacy of CAR-T cells *in vivo*, both $FLuc^+$ and $FLuc^-$ CAR-T cells were compared in the same experiment. Both 2^{nd} and 3^{rd} generation CAR-T cells were used.

This experiment was performed alongside the comparison between second and generation CAR described in chapter 5.4.1 (graphs in Figure 5.6 showing tumour volumes in the cohort treated with second and third generation CAR-T cells co-expressing luciferase are the same as shown in Figure 5.3).

Figure 5.6 shows tumour volumes in the 4 different groups: growth kinetics suggest that expression of FLuc may impair long term activity of CAR-T cells. Mice receiving $FLuc^-$ CAR-T cells exhibited a better tumour control compared to mice receiving $FLuc^+$ CAR-T cells, even though differences were not statistically significant. However, while in the $FLuc^+$ groups all mice eventually grew, in the $FLuc^-$ group some mice showed a tumour reduction at day 14 post T cells administration. Unfortunately, due to unexpected deaths within the group treated with third generation CAR (see section 5.4), the experiment was terminated early and we could not assess long term effects of luciferase expression in CAR-T cells. Immunohistochemistry for CD34 at time of sacrifice did not show statistically significant differences in CAR-T cells infiltration.

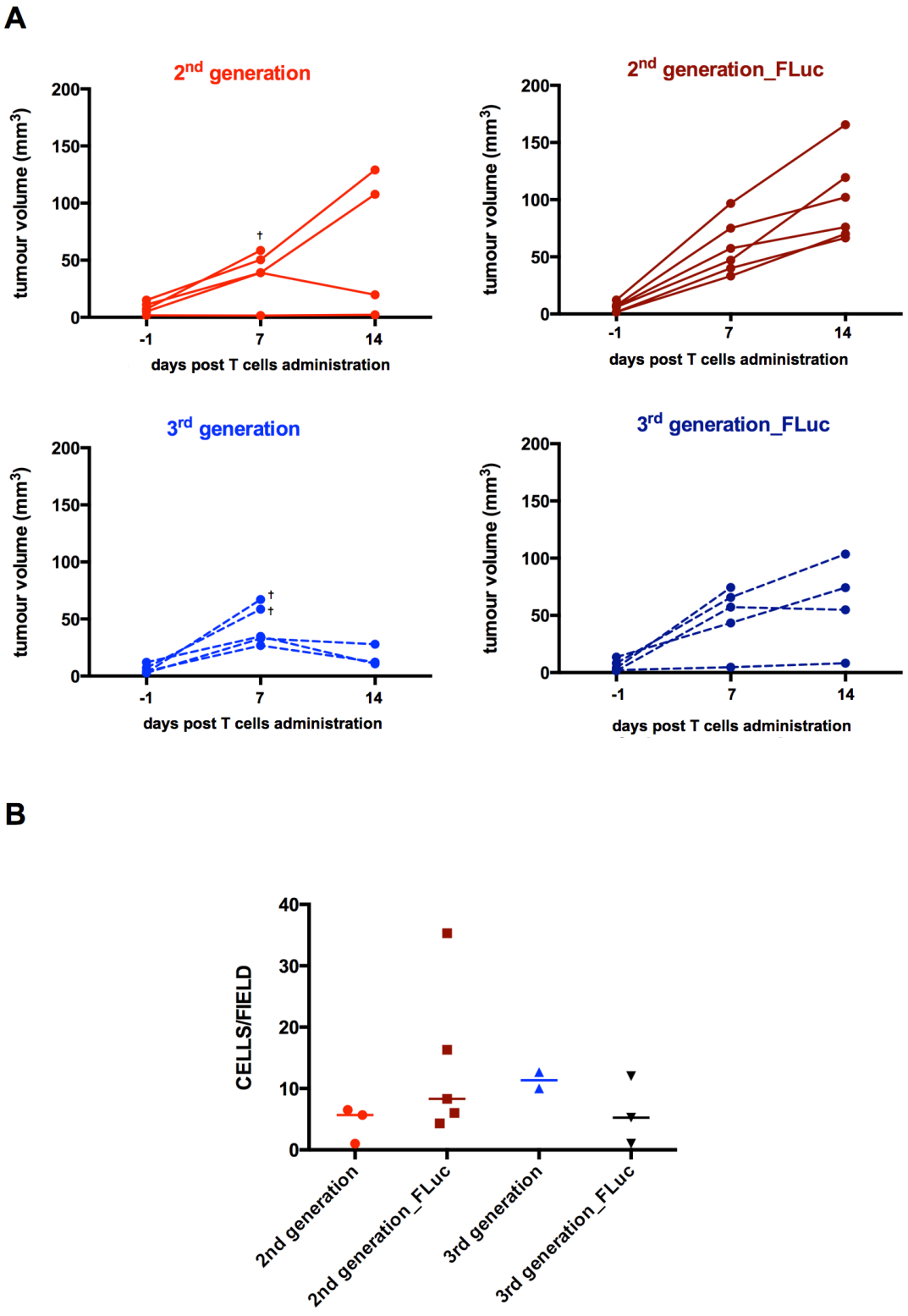

Figure 5.6 Effects of FLuc expression on CAR-T cells function and persistence (**A**) Tumour growth curves in mice receiving second generation CAR-T cells (either with or without FLuc), top panel, or third generation CAR-T cells (with or without FLuc),

bottom panel. (**B**) IHC for CD34 to evaluate CAR-T cells within the tumour. Each dot represent one mouse (cells/field average counts of 4 areas randomly chosen within the tumour).

5.6 Summary and conclusions

Data from this chapter demonstrate that T cells expressing a third-generation CAR have similar cytolytic activity *in vitro* and may have a more activated profile compared to second generation CAR-T cells when unstimulated (Table 5.1).

No statistically significant differences were observed in tumour growth at the time points analysed. Similarly, CAR-T cells infiltration/persistence measured by BLI and IHC was not affected by incorporation of a second co-stimulatory domain. However, as the study had to be terminated in advance due to unexpected side effects in the mice treated with third-generation CAR, it is not possible to infer that 41BB did not improve T cells persistence *in situ*. In particular, when we studied the phenotype of TILs at day 17 post T cell infusion, T cells expressing third generation CAR exhibited higher expression of Ki67, suggesting that 41BB incorporation might affect proliferation *in situ* (Figure 5.5C). Conversely, GzmB expression was significantly lower in third-generation CAR-T cells (Figure 5.5B), indicating that third-generation endodomain might affect functionality of CAR-T cells, possibly due to early exhaustion. This hypothesis should, however, be investigated further. Interestingly, incorporation of a second co-stimulatory domain induced a better T cell systemic engraftment (Figure 5.4). Whether this effect was mediated by incorporation of a second co-stimulatory domain or by 41BB signalling *per se* should be further investigated.

The benefit of using third-generation over second-generation CARs has not yet been demonstrated (Till et al., 2012). Contrasting studies have been published with some studies have reported that incorporation of 41BB can decrease functionality of CAR-T cells (Kochenderfer et al., 2009; Haso et al., 2013).

Differences between studies might be CAR and model-specific, as it was in the case of (Long et al., 2015), where early exhaustion mediated by CD28 was only observed in GD2 CAR but not in CD19 CAR. Similar considerations should be taken into account for evaluation of toxicity *in vivo*. A case report

described serious adverse effects following administration of a HER2-specific third-generation CAR T cells, where a treated patient died to respiratory failure (Morgan et al., 2010). Toxicities observed in this case were most likely due to the high dose infused (10^{10} CAR-T cells) and to expression of HER2 by the lung endothelium, which led to over activation of CAR-T cells in this critical site. Nevertheless, this study highlighted the importance of carefully evaluating possible side effects of CAR-T cells.

In our hands, although third-generation CAR-T cells were able to offer similar (and in some cases better) tumour control, they showed more severe toxicity, with cases of extensive haemorrhages within the brain which were the most likely cause of death and illness in some mice.

Moreover, the additional co-stimulatory domain did not provide any benefit in terms of persistence within the tumour, at least at this stage, nor improved functionality of CAR-T cells *in situ*, although third-generation CAR-T cells seemed to proliferate more *in vivo*.

Based on these data, a second-generation CAR was used for future experiments.

On a separate note, we also evaluated whether incorporation of luciferase could *a)* affect CAR-T cells function and *b)* affect CAR-T cells persistence due to possible immunogenicity.

Due to early termination of the experiment, we could not definitively determine whether luciferase expression affected long-term persistence of CAR-T cells within the tumour (Figure 5.6B). However, tumour volumes measurements up to day 14 post T cells administration may suggest that T cells only expressing CD34 and CAR performed better than T cells also expressing luciferase (Figure 5.6A), as both 2^{nd} and 3^{rd} generation CAR-T cells not expressing FLuc were able to mediate tumour regression in some cases, while in the $FLuc^{+}$ treated groups, all tumours eventually grew. Differences in functionality *in vivo* could be due to the big size of the construct incorporated into the cells (Figure 3.3A) which may affect fitness of T cells *in vivo*.

Since initial experiments had demonstrated the kinetics of migration of EGFRvIII-specific T cells administrated i.v., a CAR construct without the co-expression of luciferase was used for future experiments.

Chapter 6

Results:

Improving CAR-T cells efficacy: combination with PD1 blockade

6 Results: Improving CAR-T cells efficacy: combination with PD1 blockade

6.1 Introduction

6.1.1 Combination of PD1 blockade with adoptive cell therapy

Antibodies blocking inhibitory checkpoints (CTLA-4 and PD1) - both in monotherapy or in combination - have recently shown dramatic results in tumours harbouring a high mutational load: melanoma was the first tumour type to be successfully targeted, but impressive results have been achieved in non-small cell lung cancer (Garon et al., 2015) and renal cell- carcinoma (Motzer et al., 2015) (see section1.4.5).

It has been shown that treatment with PD1 blockade increase accumulation and proliferation of $CD8^+$ T cells within the tumour (Hamid et al., 2013; Tumeh et al., 2014).

As described in section 1.4.3, the challenge of translating adoptive cell therapy to solid tumours requires that T cells receive additional co-stimulation to survive and be functional within an immunosuppressive microenvironment.

Blocking the PD1/PD-L1 pathway has been one of the approaches that have been explored to enhance T cells activity in solid tumours. A recent clinical study reported effective expansion and rescue of efficacy of CD19-specific CAR-T cells in a patient with refractory diffuse large B-cell lymphoma (Chong et al., 2017).

Two pre-clinical studies have employed syngeneic pre-clinical model to study the effect of combination of PD1 blockade and adoptive cell therapy, either with Pmel1-specific T cells (Peng et al., 2012) or HER2-specific CAR-T cells (John et al., 2013). These studies report different effects of administration of a PD1 antibody. Peng et al. described enhanced migration and proliferation within the tumour of Pmel1-specific T cells in response to concomitant PD1 blockade. This effect was related to increased production of IFNγ-induced chemokines such as CXCL10. On the other hand, John et al. did not observe any significant difference in the accumulation/persistence of CAR-T cells in the presence of PD1 blockade. The authors reported, however, a decrease in the

percentage of $CD11b^{+}Gr\text{-}1^{+}$ myeloid-derived suppressor cells (MDSCs). This observation, though, is to be considered as an indirect effect of PD1 blockade on the myeloid compartment.

6.1.2 Rationale and aims

Previous reports of combination therapy with PD1 blockade and ACT (Peng et al., 2012; John et al., 2013) did not investigate the effect of PD1 blockade on the endogenous TILs. Here, we combined CAR-T cell administration with the PD1-blocking antibody RMP1-14 to evaluate effect on both transferred T cells and endogenous compartment. Data from chapter 4 demonstrated that both CAR-T cells and endogenous T cells express PD1 *in situ* and suggested that lack of long-term persistence might be responsible for the failure of CAR-T cells in promoting complete tumour regression. We therefore wanted to evaluate whether combination with PD1 blockade could improve persistence and function of CAR-T cells at the tumour site.

6.2 PD-L1 expression by GL261 and myeloid cells

First, we investigated whether PD1-expressing TILs do encounter PD-L1 *in situ*, to confirm that combination with PD1 blockade was a suitable strategy to improve CAR-T cell therapy in this context.

PD-L1 expression was tested on both target cells (GL261_EGFRvIII) and myeloid cells infiltrating the tumours.

GL261_EGFRvIII did not constitutively express PD-L1, but upregulated it in response to IFNγ (Figure 6.1

), suggesting that PD-L1 expression on GL261 is induced in an inflammatory environment.

PD-L1 expression was also evaluated *ex vivo,* on tumour infiltrating cells from mice receiving either TBI only or TBI and systemic administration of CAR-T cells.

Virtually all $CD11b^+$ myeloid cells expressing MHCII were also $PD\text{-}L1^+$, irrespective of treatment received (

Figure 6.1B). These data suggest that TILs do encounter an immunosuppressive environment which might downregulate their activity *in situ*. PD-L1 staining on tumour cells *in vivo*, however, proved to be technically difficult, most likely due to the isolation method with Percoll® gradient and lack of a suitable marker for GL261_EGFRvIII *in vivo*. Optimisation of this protocol is currently undergoing to validate that tumour cells also express PD-L1 *in vivo*.

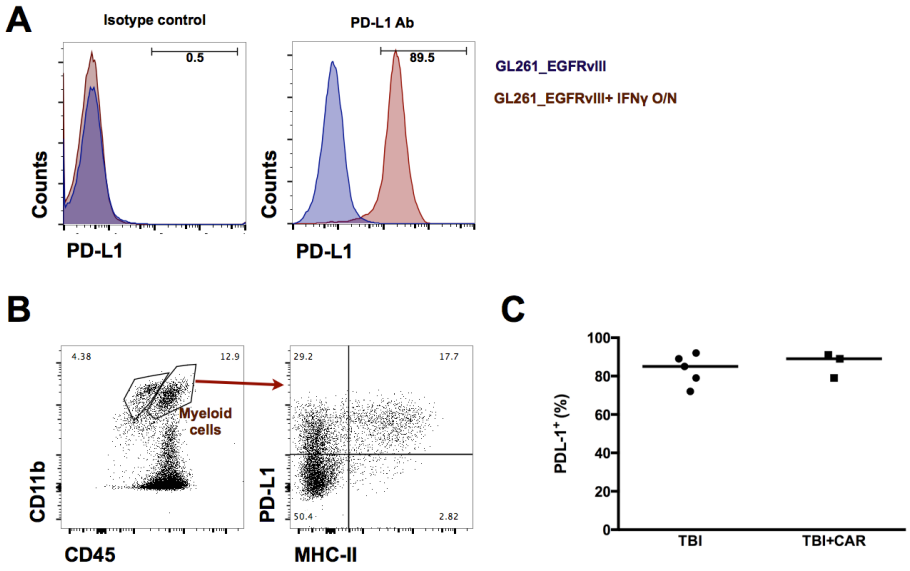

Figure 6.1 PD-L1 expression on GL261_EGFRvIII and myeloid cells
(**A**) GL261_EGFRvIII were incubated O/N with IFNγ 1ng/mL and staining with αPD-L1 antibody or isotype control. (**B**) Representative FACS plot showing myeloid cells, identified as $CD45^{+}CD11b^{+}$ cells. $CD45^{low}CD11b^{+}$ were gated out as microglia. (**C**) Percentage of $PD\text{-}L1^{+}$ cells was evaluated on $CD11b^{+}MHCII^{+}$gated cells. Shown are data point for individual tumours treated either with TBI only or TBI and CAR T-cells as well as the maedian of these as a horizontal line.

6.3 Combination of CAR-T cells therapy with PD1 blockade

Mice received 4 intraperitoneal doses of the PD1-blocking antibody RMP1-14 on the day of T cells administration and on day 3, 6 and 14 after transfer (Figure 6.2A). MRI was performed weekly to monitor tumour growth.

Data shown in this section are the result of three independent experiments. In the first two batches, mice were sacrificed when clinical signs developed and both experiments were terminated at day 35 post treatment administration for histopathology analysis (CAR and CAR+PD1: n=7 mice per group, PD1 only: n=5). For the third batch, instead, responding mice were monitored for up to four months to evaluate long-term survival (n=5 mice per group).

Figure 6.2B shows tumour growth curves in the different treatment groups. At day 14 post treatment administration, average tumour volumes were: $36\pm47mm^3$ for mice receiving PD1-blockade, 40 ± 31 mm^3 for mice receiving CAR, 16 ± 19 mm^3 for mice receiving combination therapy (CAR+PD1 blockade).

CAR-T cells administration delayed tumour growth in treated mice compared to mice receiving TBI only. However, reduction in tumour size was observed in only 3 out of 12 mice treated. The combination of CAR-T cells and PD1 blockade promoted complete clearance of the tumours in 8 out of 12 treated mice. However, PD1 blockade alone also induced a marked response, with 5 out of 10 treated mice showing a reduction in tumour size at day 14 post treatment administration. This effect was not unexpected, considering GL261 is a moderately immunogenic model (Maes and Van Gool, 2011) and partial effect of PD-L1 blockade has been recently demonstrated (Wainwright et al., 2014).

Survival curves reflected tumour growth patterns (Figure 6.2C). CAR-T cells administration increased survival, however only 3 out of 12 treated mice were long-term survivors. On the other hand, combination therapy induced long-term survival in 8 out 12 mice. Differences within the two groups were statistically significant ($p\leq0.05$ Mantel-Cox test).

It is important to note that the 4 mice that did not respond to the combination treatment were all part of the same experiment, while in the other two sets of experiments mice receiving CAR+PD1 consistently responded to the

treatment. This observation suggests that there might have been some technical problems with that experiment.

Difference in survival between the mice treated with a combination of CAR T-cells and PD-1 blockade compared to treatment with PD-1 blockade alone was not significant. Interestingly, however, within the PD1 blockade alone group, 4 out 6 mice which responded to the treatment exhibited tumour reduction by day 14 post treatment administration, but tumours started growing again at day 35 post treatment administration. This observation suggests that although PD1 blockade was able to control tumour growth, this may not have the same effect as the combination with CAR-T cells.

For the first two batches, upon sacrifice, brains were processed for histology. No tumour was observed in mice responding to combination therapy and there were signs of scar tissue (Figure 6.3C, black arrows). CD34 staining showed that CAR-T cells were still infiltrating the tumour site at the time of sacrifice. Interestingly, mice that did not respond to the combinatorial therapy (Figure 7.3C, bottom row) still exhibited some degree of CAR-T cells infiltration at the time of sacrifice, as opposed to mice receiving CAR-T cells alone (Figure 7.3A).

CD3 staining was performed to evaluate the degree of immune infiltration within the tumour. All three groups exhibited high levels of CD3 positivity (Figure 7.3).

Figure 6.4 shows MR images of representative mice receiving either CAR alone (Figure 6.4A), PD1 blockade alone (Figure 6.4B) or CAR+PD1 blockade (Figure 6.4C). Images showed that mice responding to treatment exhibited tumour regression by day 14 post T cells infusion (day 25 post tumour implantation). The site of tumour injection was still visible at day 50 post T cells injection as hyperintense spot corresponding to scar tissue.

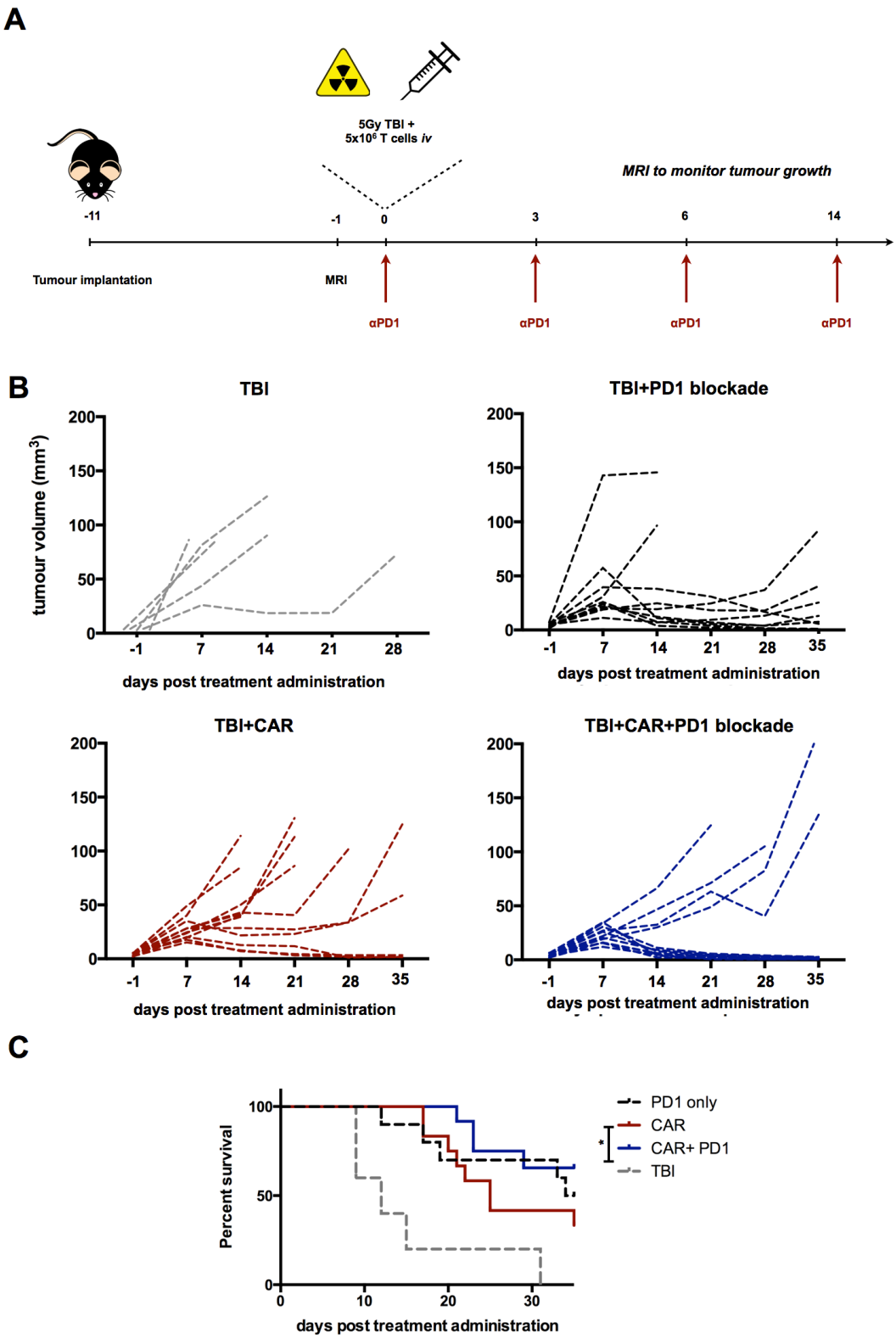

Figure 6.2 Combination of CAR-T cells with PD1 blockade.
(**A**) Experimental timeline: upon tumour engrafment confirmation at day 10 post implantation, mice received 5Gy TBI followed by systemic infusion of $5x10^6$ bulk splenocytes. Intraperitoneal injections of the anti PD1 antibody RMP1-14 were performed at day 0,3,6 and 14 post T cells infusion. (**B**) Tumour volumes measured with MRI in 4 different groups: TBI (n=5), TBI+PD1 blockade (n=10), TBI+CAR (n=12),

TBI+CAR+PD1 blocade (n=12). Individual growth curves from three independent experiments are shown. Tumour volumes are are shown up to day 35 post treatment administration, a time point where all surviving mice from the first two experiments were sacrificed for histopathology analysis.
(**C**) Survival proportions in the 4 different goups (*p≤0.05, Mantel Cox test). Individual growth curves from three independent experiments are shown.

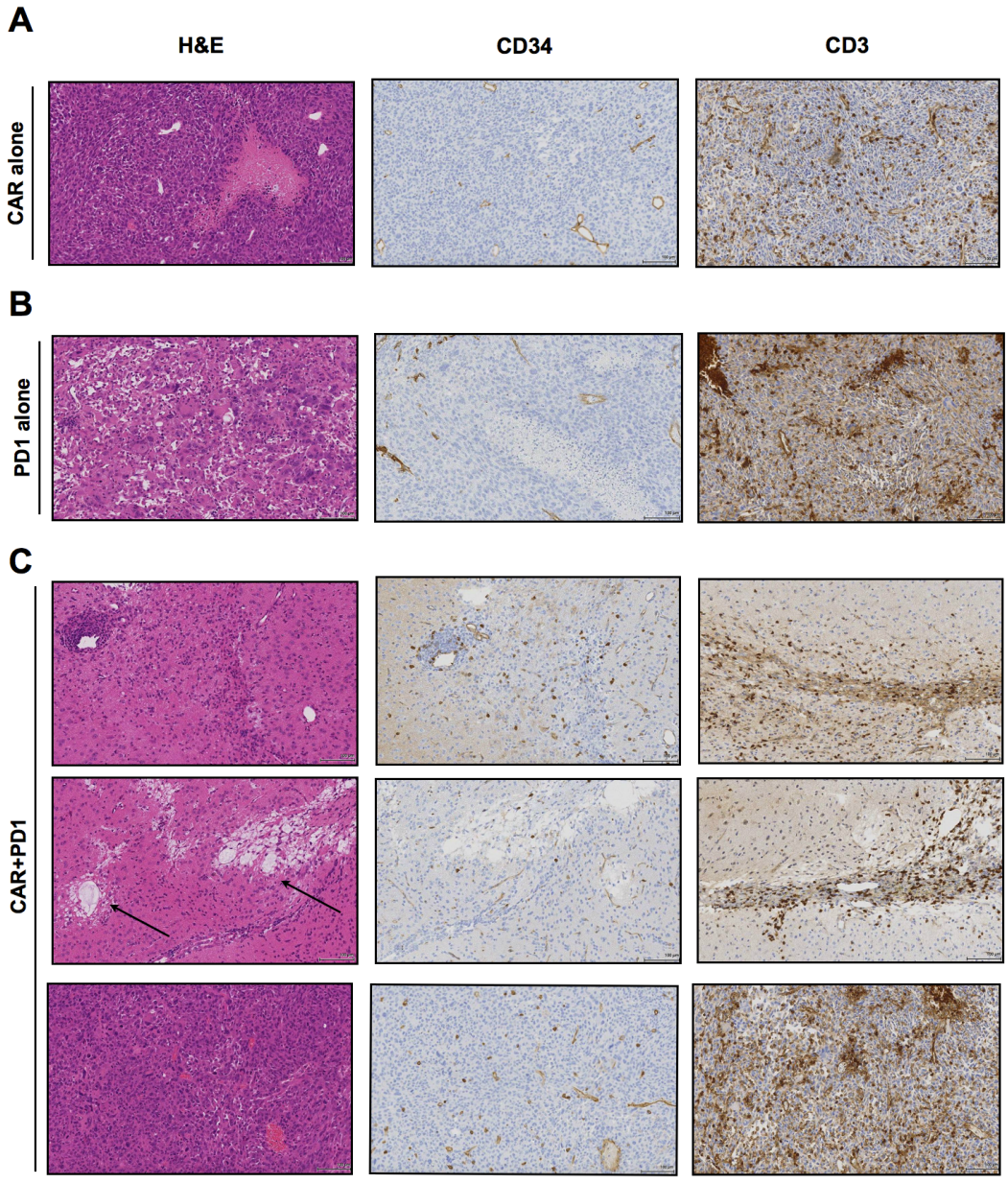

Figure 6.3 CAR-T cells and CD3$^+$ T cells infiltration in treated tumours.
H&E, CD34 and CD3 staining in tumours from mice treated with CAR (**A**), PD1- (**B**) and CAR+PD1 (**C**). Histopathology was perfromed at the time mice were sacrificed due to clinical signs development in the case of non-responding mice, ar at day 40 post tumour implantation for mice responding to treatment.

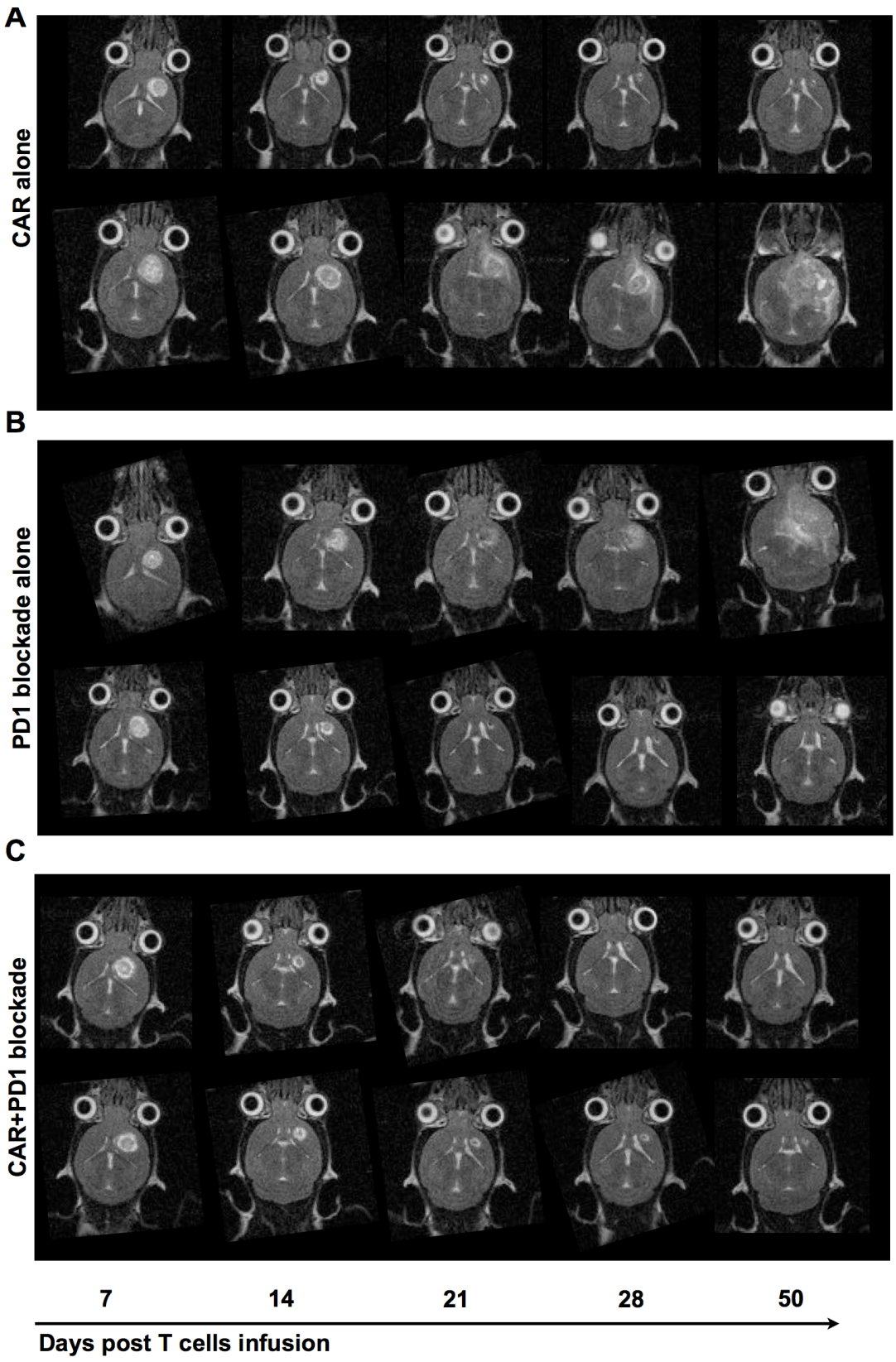

Figure 6.4 Representative MR images of treated images.
(**A**) MRI of two representative mice treated with CAR-T cells only: top row shows a mouse with tumour shrinkage, bottom row shows a mouse where T cells administration only delayed tumour growth.
(**B**) MRI of two representative mice treated with PD1 blockade alone, one showing delayed tumour growth (top row), the other showing complete remission.

(**C**) MRI of two representative mice treated with combination therapy CAR+PD1 blockade, both showing complete remission of tumour.

6.3.1 Long-term survival of treated mice

In the third cohort of treated mice (PD1 alone: n=5, CAR: n=5, CAR+PD1 n=5), we monitored mice with regressed tumour for development of clinical signs for up to 4 months after tumour implantation. Mice were scanned one last time before sacrifice to confirm tumour regression (Figure 6.5). Histopathology was carried out to verify absence of viable tumour, while CD34 IHC was performed to investigate persistence of CAR-T cells within the brain even in the absence of the antigen. No tumours were observed, both on MRI and on H&E. No CD34 positivity was observed, thus confirming that persistence of CAR-T cells in the brain is dependent on presence of the antigen.

Interestingly, mice responding to monotherapy (either CAR alone or PD1 blockade alone) also showed long-term effect of the treatment, with no signs of tumour re-growth.

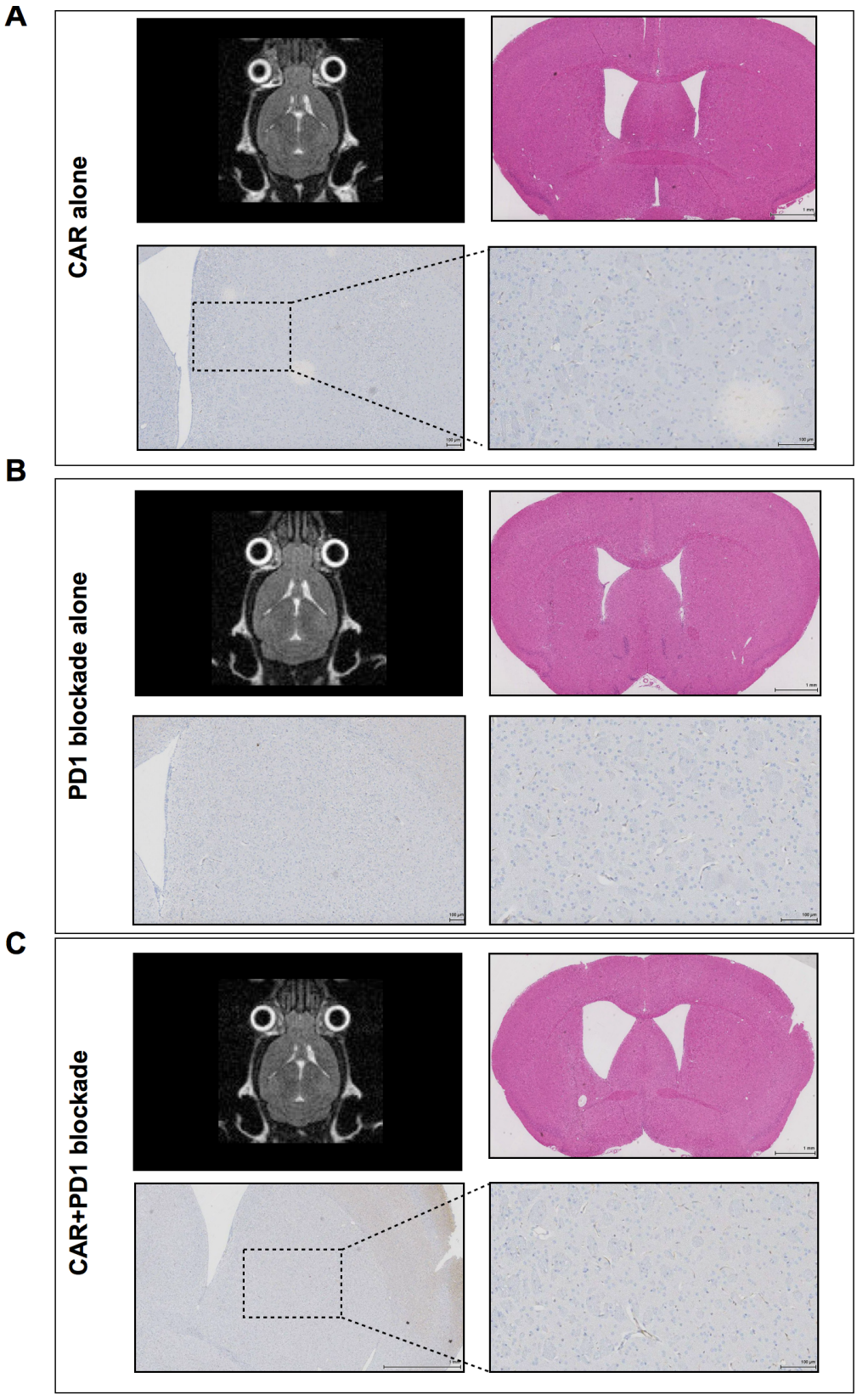

Figure 6.5 MRI, H&E and CD34 IHC of long term survivors (day 120 post tumour implantation)
Complete clearance of the tumour was confirmed by both MRI and by H&E staining. Immunohistochemistry for CD34 confirmed that no CAR-T cells were still present within the brain at day 120 post implantation. (**A**): CAR-T cells administration alone; (**B**) PD1 blockade alone; (**C**) Combination therapy.

6.4 Assessment of PD1 blockade effect on TILs

Combinatorial therapy with CAR-T cells and PD1 blockade had a marked effect on tumour growth and survival (Figure 6.2). However, PD1 blockade alone also promoted tumour clearance in some cases, suggesting that release of the brakes on endogenous T cells plays an important role in the effect observed in survival experiments. To investigate whether PD1 blockade mainly acts on the endogenous compartment or on the transferred cells, or both, an experiment was designed where mice were sacrificed at different time points (either 9 or 17 post T cells infusion) and TILs were isolated and their phenotype was analysed by flow cytometry.

In this set of experiments, CAR-T cells were generated from CD45.1 congenic mice in order to be able to clearly distinguish adoptively transferred cells from endogenous T cells (which express CD45.2).

To evaluate whether *in vivo* administration of RMP1-14 antibody could affect staining with the anti PD1 antibody J43 used for FACS staining *ex vivo*, CAR-T cells stimulated *in vitro* with EGFRvIII-expressing GL261 were pre-incubated with RMP1-14 antibody, then stained with J43 (Figure 6.6). No differences in percentage of $PD1^+$ cells were observed when cells were pre-incubated with RMP1-14. We therefore concluded that the RMP1-14 does not compete with J43 for binding to PD1.

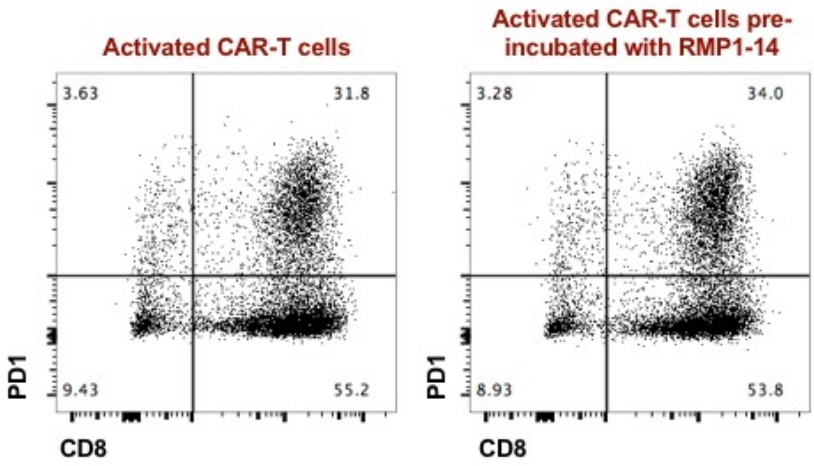

Figure 6.6 RMP1-14 clone does not compete with clone J43 for binding to PD1. CAR-expressing splenocytes were stimulated over night with GL261_EGFRvIII to upregulate PD1. Cells were pre-incubated with the anti PD1 antibody RMP1-14 (used for *in vivo* administration) at a concentration of 10μg/ml for 30 minutes on ice, then they were stained with J43. Left panel shows staining in absence of RMP1-14, right panel shows staining with pre-incubation with RMP1-14.

Figure 6.7 shows phenotype of both endogenous and transferred T cells at day 9 post infusion. Cells were gated on live, then on $CD45.2^+CD11b^-$ (endogenous lymphocytes,
Figure 6.7A), while transferred T cells were distinguished as $CD45.1^+$(
Figure 6.7B). As previously observed (Figure 4.6C), administration of CAR-T cells induced an overall activation of the endogenous $CD8^+$ T cells (percentage of $GzmB^+$ cells) when compared to TBI-only treated mice (
Figure 6.7C). As expected, PD1 blockade alone had a similar effect on T cells. The combination of CAR-T cells and PD1-blocking antibody, however, did not show any synergistic effect (
Figure 6.7C, TBI: 55%±12; PD1:67%±24; CAR: 79%±12; CAR+PD1:71%±12). On the contrary, when looking at GzmB MFI, combination therapy seemed to rather decrease levels of GzmB production in $CD8^+$T cells (
Figure 6.7C, CAR: 4,359±1,600; PD1: 3,659±2,300; CAR+PD1: 2,800±1,300), even though differences were not statistically significant.
In this experimental dataset, no variations were observed on $CD4^+T_{helper}$ cells. On the other hand, combination with PD1 blockade did not alter GzmB expression in CAR-T cells, expressed both as percentage of positive cells (CAR: 95%±4; CAR+PD1: 93.6%±6) and as MFI (CAR: 14,000±6,000; CAR+PD1: 13,700±5,600).
Neither mono nor combination therapy affected proliferation of either endogenous or CAR-T cells (
Figure 6.7D). As previously observed (Figure 4.6C and E), the majority of TILs (82%±12) from mice receiving TBI only were $Ki67^+$ and administration of either PD1 or CAR, alone or in combination, did not increase the percentage of proliferating cells.
In this experimental dataset, no differences were observed in the phenotype of $CD4^+$helper T cells (
Figure 6.7C and D).
We also investigated PD1 and LAG3 expression as markers for activation/ exhaustion of infiltrating T cells. Double positive ($PD1^+LAG3^+$) cells were considered as potentially exhausted cells. TILs from mice receiving only TBI showed the lower percentage of double positive cells (27%±18): this

phenotype correlated with lower levels of GzmB expression, suggesting that TILs from untreated mice are less activated rather than less exhausted. Treatment with either CAR or PD1 blockade increased the percentage of double positive cells (PD1:36±26; CAR:52±11), which correlated with higher levels of GzmB production. Surprisingly, combination therapy did not have a synergistic effect, but it rather resulted in a diminished percentage of $PD1^{+}LAG3^{+}$ cells, even though this was not statistically significant (p=0.051) (Figure 6.8A). To assess whether the double positive cells were a population of exhausted or rather more activated/differentiated cells, we looked at GzmB expression differences in double positive and double negative cells and observed that within the double positive population a higher percentage of $CD8^{+}$ T cells were $GzmB^{+}$ (Figure 6.8B). This suggests that, at this stage, PD1 and LAG3 expression was indicative of activation of tumour infiltrating lymphocytes.

When looking at $CD45.1^{+}$ CAR-T cells, co-administration of PD1-blocking antibody did not affect expression of PD1 and LAG3, with both groups showing the same percentage of double positive cells (CAR: 56%±14; CAR+PD1: 55%±13).

These data suggest that PD1 blockade may not affect functionality and activation of CAR-T cells at this particular time point. Unexpectedly, co-administration of PD1-blocking antibody with CAR-T cells resulted in a reduced activation of endogenous $CD8^{+}$ T cells when compared to both PD1 blockade alone and CAR alone, even though differences were not statistically significant.

A possible explanation for this could be that PD1 blockade is acting on CAR-T cells (which are the populations within the tumour that express the higher levels of PD1, see Figure 4.9), even though differences were not visible at this time point. In a context where CAR-T cells are more functional, they could be able to better control tumour growth, therefore endogenous $CD8^{+}$ T cells could be less active and, possibly, less exhausted.

Previous reports suggested that PD1 blockade can modulate accumulation of $CD8^{+}$T cells within the tumour and their proliferation *in situ* (Hamid et al., 2013; Tumeh et al., 2014).

To test whether this was the case in this experimental setting, we assessed absolute numbers of $CD8^+$, $CD4^+$ and CAR^+ T cells in all four groups (Figure 6.8C). No significant variations were observed in any of these compartments, suggesting that neither CAR-T cells administration nor PD1 blockade affected T cells infiltration at this time point.

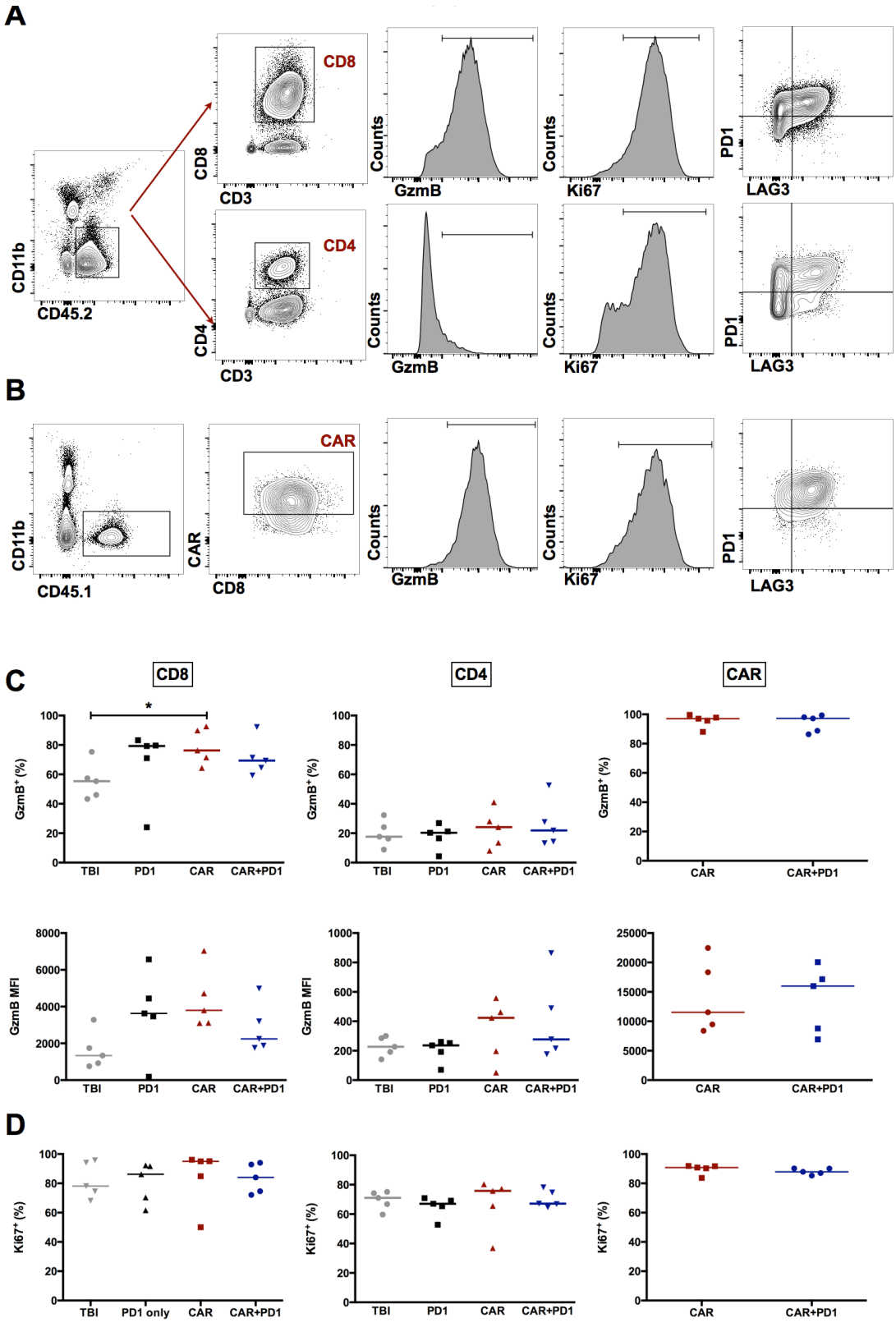

Figure 6.7 Functional analysis of TILs with and without PD1 blockade: day 9 post infusion

(**A**) and (**B**) Gating strategy: endogenous and transferred T cells were discriminated based on CD45.2 and CD45.1 expresion, respectively.

(**C**) Percentage of GzmB^{+} cells and GzmB MFI in endogenous CD8+ and Cd4+ T cells and transferred CAR-T cells

(**D**) Percentage of Ki67+ cells in endogenous $CD8^+$ and $CD4^+$ T cells and transferred CAR-T cells.
Shown are individual data point from x number of independent experiments as well as median as a horizontal line (* $p \leq 0.05$, unpaired T test).

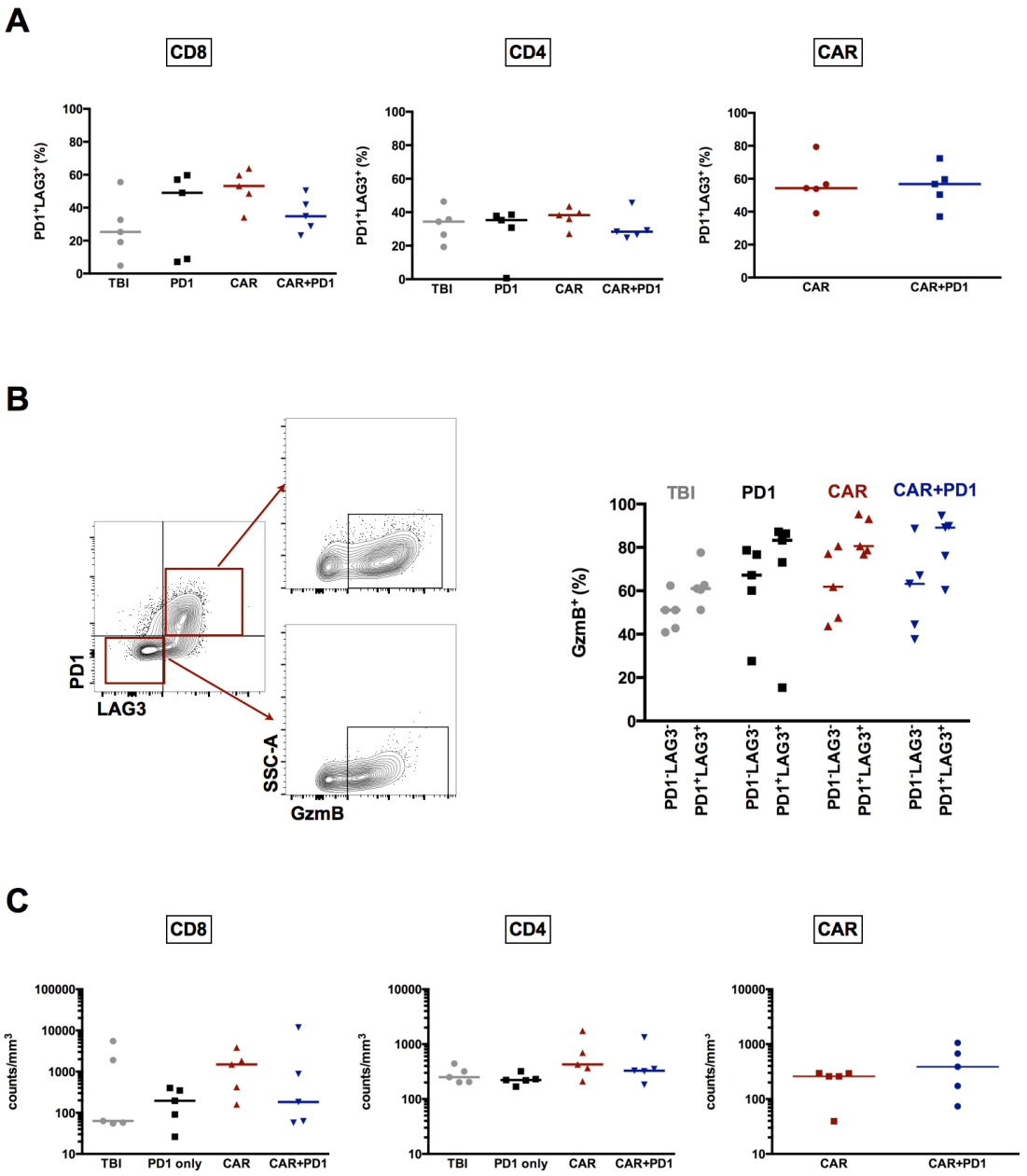

Figure 6.8 Activation and TILs numbers with and without PD1 blockade: day 9 post infusion
(**A**) Percentage of $PD1^+LAG3^+$ in endogenous $CD8^+$ and $CD4^+$ T cells and transferred CAR-T cells.
(**B**) GzmB expression was assessed in double positive and double negative populations to assess their activation status.
(**C**) Absolute numbers of $CD8^+$ and $CD4^+$ T cells and transferred CAR-T cells. Cells were counted based on absolute counting beads.
Shown are individual data point and the median as a horizontal line.

To investigate whether PD1 blockade affected phenotype of TILs at later time points, we isolated cells at day 17 post T cells infusion, a time point at which effects of combination therapy were already visible in terms of tumour volumes (Figure 6.9A).

Analysis at this later time point showed that CAR-T cells from combination treatment exhibited significantly lower percentages of $Ki67^+$ cells (Figure 6.9B and Figure 6.10C, $p \leq 0.00001$) and lower GzmB MFI (Figure 6.10B $p \leq 0.05$) - despite no actual differences in percentages of $GzmB^+$ cells (Figure 6.10B) - when compared to cells from mice receiving CAR-T cells alone. Moreover, fewer $PD1^+LAG3^+$ double positive cells were observed in CAR-T cells from mice receiving combination therapy (Figure 6.9B and Figure 6.10D). These observations, combined with the reduced size of tumours within the combination group, may suggest that CAR-T cells had already reached a contraction phase after antigen clearance.

We also investigated phenotype of endogenous $CD8^+$ and $CD4^+$ T cells, to assess whether this was an overall effect due to reduction in tumour size or a phenomenon specific for CAR-T cells.

Even though no significant differences were observed, GzmB expression (expressed as both percentage and MFI) was slightly higher in $CD8^+$ T cells from mice receiving combination therapy compared to cells from mice receiving CAR alone (Figure 6.10A and B; CAR alone: 21%$\pm$10, MFI 281$\pm$170; CAR+PD1: 35%$\pm$14, MFI 546$\pm$400). No differences were observed in the $CD4^+$ population (Figure 6.10A and B). On the other hand, similarly to CAR-T cells, both $CD8^+$ and $CD4^+$T cells from mice receiving combination therapy exhibited a lower percentage of $Ki67^+$ cells when compared to cells from mice receiving either CAR alone or PD1 blockade alone (Figure 6.10C), thus suggesting that $CD8^+$ T cells might also be in a contraction phase after tumour clearance.

Finally, percentages of $PD1^+LAG3^+$ cells did not significantly vary between groups (Figure 6.10D).

We also looked at TILs absolute numbers in all three compartments (CD4, CD8 and CAR). No statistically significant differences were observed at this time point (Figure 6.10E).

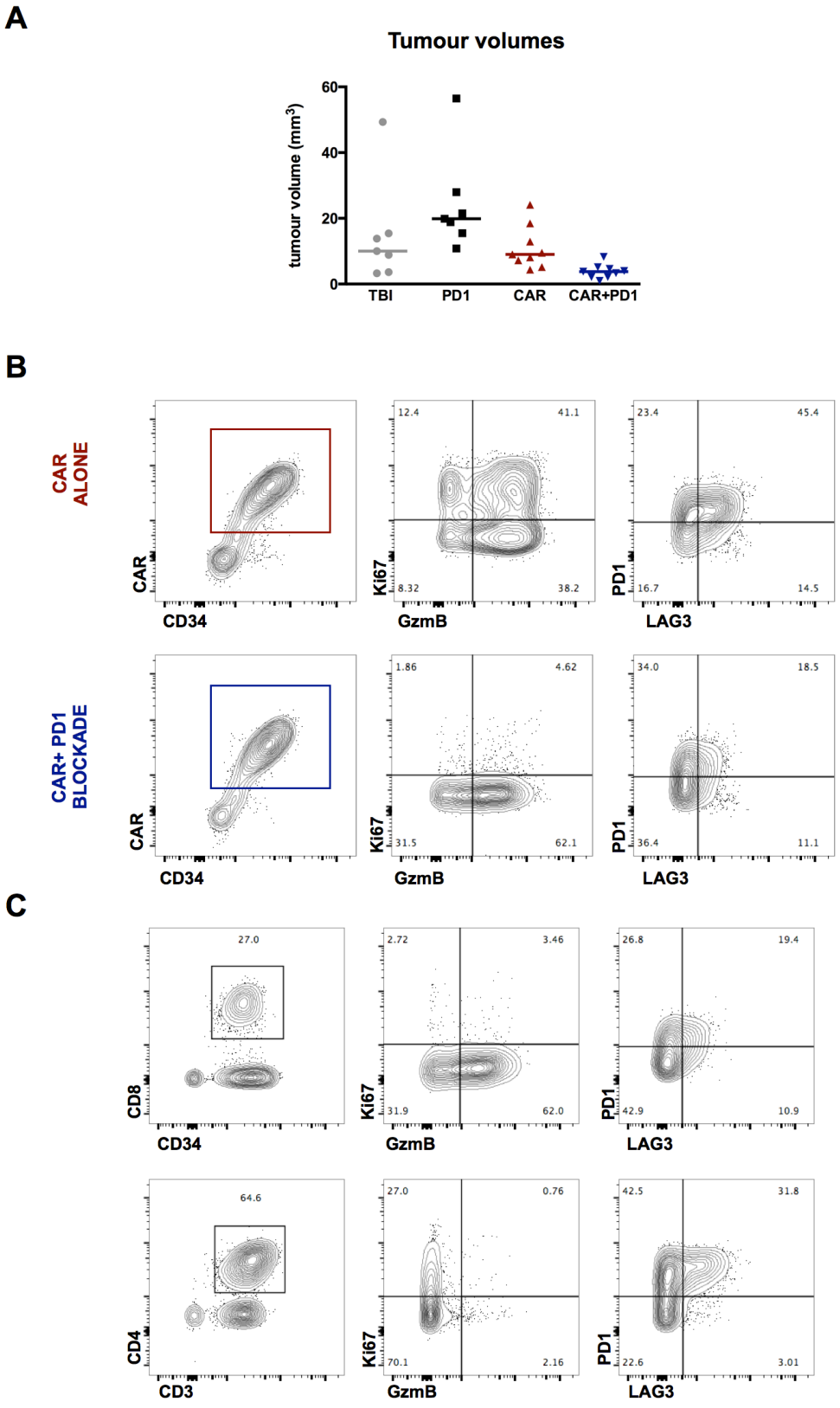

Figure 6.9 Phenotype of CAR-T cells and endogenous TILs: day 17 post infusion. Representative FACS plots

(**A**) Tumour volumes measured by MRI on the day before sacrifice (day 16 post T cells infusion).

(**B**) Gating strategy for $CD45.1^+$ transferred T cells.

(**C**) Gating strategy for $CD45.2^+$ endogenous $CD8^+$ and $CD4^+$ T cells.

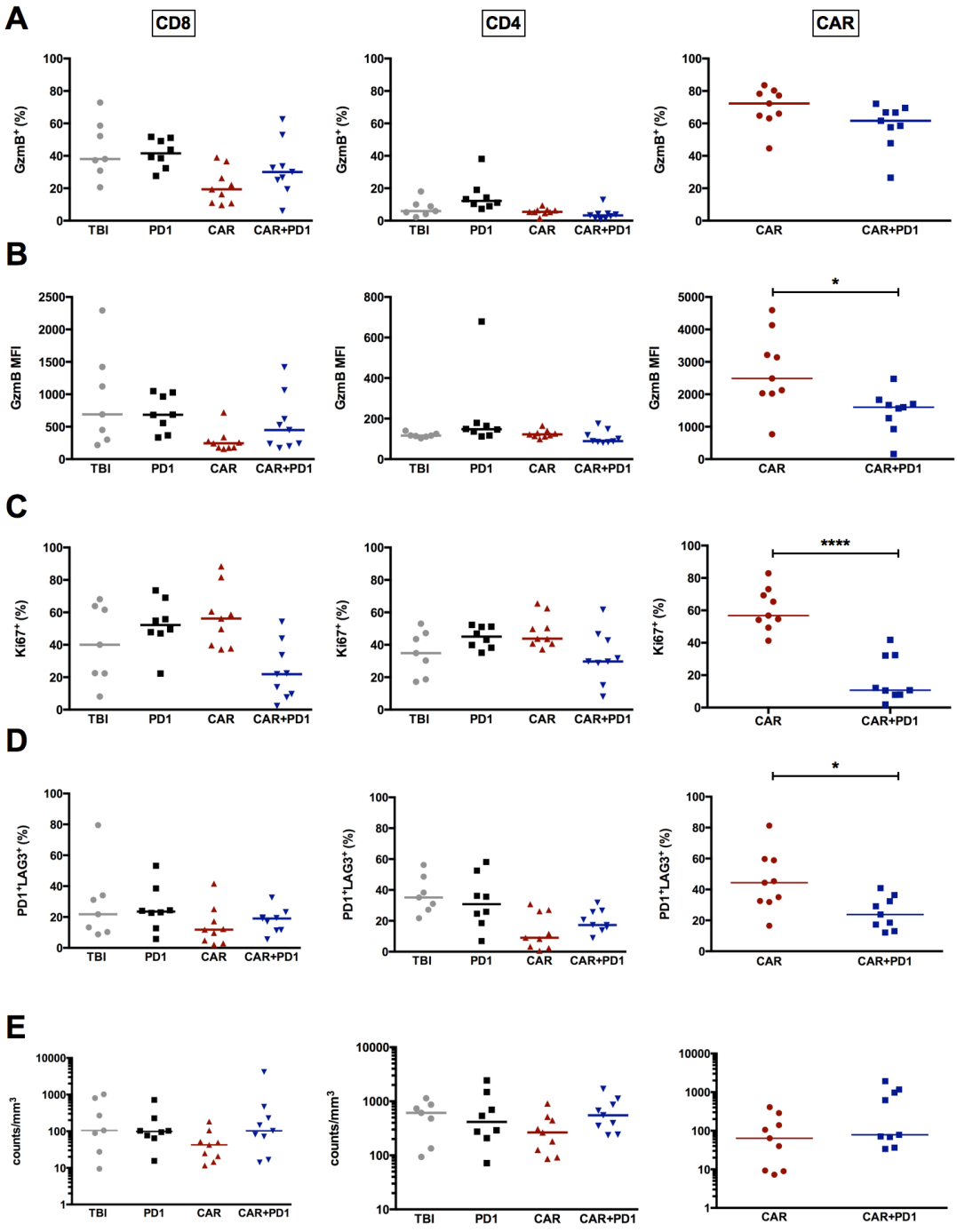

Figure 6.10 Phenotype of CAR-T cells and endogenous TILs at day 17 post infusion.

(**A**) GzmB percentage of expression in $CD8^+$, $CD4^+$ and transferred CAR-T cells.
(**B**) GzmB MFI in $CD8^+$, $CD4^+$ and transferred CAR-T cells.
(**C**) Ki67 percentage of expression in $CD8^+$, $CD4^+$ and transferred CAR-T cells.
(**D**) Percentage of cells double positive for PD1 and LAG3 in $CD8^+$, $CD4^+$ and transferred CAR-T cell
(**E**) Absolute numbers/mm^3 of endogenous $CD8^+$ and $CD4^+$ T cells and transferred Car-T cells
Shown are individual data point from x number of independent experiments as well as median as a horizontal line (* $p \leq 0.05$, unpaired T test).

6.5 Summary and conclusions

Data described in this chapter suggest that the combination of CAR-T cells with PD1 blockade may be an effective treatment for glioblastoma. However, the data set to date has not demonstrated enhanced efficacy of CAR T-cell therapy combined with PD-1 blockade as compared to PD-1 blockade alone. Nevertheless, it was shown that combination therapy was able to promote complete tumour clearance and long-term survival in a significant portion of treated mice. Mice with regressed tumour were monitored for up to 4 months and no signs of tumour growth were observed, suggesting that combination therapy can mediate a persistent and long-term response. Tumour clearance was confirmed by both MRI and histopathology.

We observed some degree of variability within the system, with one set of experiments showing mice not responding to combination therapy (Figure 6.2). The reason why combination therapy failed to control tumour growth remains unclear, as CAR-T cells appeared to infiltrate the tumour at the time of sacrifice (Figure 6.3). Since this pattern was only observed in one set of experiments, one could argue a technical problem occurred in that particular case. I am repeating an additional experiment to assess the efficacy of combination therapy in mediating complete tumour regression as compared to either CAR-T cells or PD-1 blockade alone.

The effect of PD1 blockade alone was not unexpected, as GL261 is a relatively immunogenic model due to its chemical induction (see section 4.1.1). Previous studies reported effective targeting of the PD1/PD-L1 pathway in pre-clinical models of GBM. Lesniak and colleagues showed that administration of a combination of PD-L1 and CTLA-4 blocking antibody and IDO inhibition was able to increase survival of mice intracranially implanted with GL261, through decreased T_{reg} infiltration and increased percentage of $IFN\gamma^+$ $CD8^+$ T cells (Wainwright et al., 2014). Moreover, in the same animal model, PD1 blockade combined with localised radiotherapy to the brain has been shown to promote long term survival in some mice (Zeng et al., 2013; Mathios et al., 2016).

Based on these observations, we sought to investigate whether the effect of combination therapy affected CAR-T cells directly or the endogenous compartment.

First, we explored the effect of PD1 blockade on persistence of CAR-T cells at the tumour site. Immunohistochemistry for CD34 at day 35 post treatment administration suggested that a longer persistence of CAR-T cells at tumour site might be one of the mechanisms mediating improved efficacy of CAR-T cells in the presence of PD1 blockade (Figure 6.3). Surprisingly, as mentioned above, presence of CAR-T cells within the tumour was observed also in those mice not responding to combination therapy, suggesting that other mechanisms may play a role in this context.

A recent study from Quezada and colleagues demonstrated that PD1 knock out in transferred tumour-reactive T cells increased the absolute numbers of $PD1^-$ T cells within the tumour (Menger et al., 2016). To investigate whether a similar mechanism was involved in the presence of PD1 blockade in these settings, we assessed the number of CAR-T cells and endogenous T cells by flow cytometry at day 9 and 17 post cells administration. We did not observe any statistically significant difference at either time point for any of the cell subsets investigated (CD8, CD4 and CAR T cells). At day 17 post infusion, however, CAR-T cells counts/mm^3 were significantly higher in 4 out of 9 mice receiving combination therapy compared to CAR-T cells only (Figure 6.10E). This was rather due to the significantly smaller tumour volumes measured in the combination therapy group, which therefore increased T cells density (Figure 6.9A). This observation correlates with IHC data showing infiltration of CAR-T cells early after tumour clearance (Figure 6.5). Taken together, this data may suggest that PD1 blockade could promote better persistence of tumour-specific CAR-T cells and consequent more efficient tumour clearance.

The phenotype of TILs – both endogenous and CAR^+– was also assessed at the same time points, to investigate whether a more active profile could be mediating a more effective tumour clearance.

However, phenotype analysis at day 9 post T cells infusion did not show synergistic effects of combination therapy, as both endogenous and CAR-T cells exhibited similar expression of GzmB and Ki67 with or without PD1 blockade. Interestingly, when looking at PD1 and LAG3 expression, we noticed that endogenous CTLs from combination therapy group exhibited a lower percentage of double positive population compared to mice receiving CAR only (Figure 6.8A), though differences were not statistically significant

(p=0.051). Since $PD1^{+}LAG3^{+}$ cells were also expressing higher levels of GzmB, we can conclude that positivity for these markers indicates a more active state rather than an exhaustion status (Fuertes Marraco et al., 2015). In this perspective, this data might suggest that concomitant administration of CAR-T cells and PD1 blockade can lead to a more potent activity of CAR-T cells, resulting in a lower activation of endogenous CTLs. Conversely, at day 17 post cells infusion, a general less active phenotype was observed in all groups (lower percentage of $GzmB^{+}$ and $PD1^{+}LAG3^{+}$ cells) (Figure 6.10). Mice receiving CAR only exhibited a more marked reduction in activation markers, suggesting a possible exhausted phenotype.

On the other hand, CAR-T cells form mice receiving combination therapy exhibited a marked reduction in GzmB MFI and Ki67 and PD1/LAG3 expression. This observation, combined with MRI data showing an almost complete tumour eradication, suggests that, at this stage, CAR-T cells had already reached a contraction phase.

Taken together, these data indicate that to depict possible differences between groups before the effect of treatment became obvious, TILs may need to be isolated at an earlier time point.

While in general tumour growth of GL261_EGFRvIII was consistent in this model, for this experiment, in the cohort of mice sacrificed at day 17 post T cell administration TBI-only controls exhibited very small tumours which resulted to be even smaller than mice receiving PD1 blockade (Figure 6.9). Although the main purpose of this experiment was to compare the phenotype of TILs in the presence of CAR-T cells with or without PD1 blockade, the unusual and unexpected behaviour of the control group should warn us to be careful in drawing conclusions from this experiment and hence this experiment will be repeated.

In conclusion, PD1 blockade can mediate efficient clearance of orthotopic tumours and mediate long term response. However, data presented in this chapter did not demonstrate a synergistic effect of CAR-T cell therapy and PD1 blockade, as survival experiments showed a marked effect of PD1 blockade alone (Figure 6.2), thus raising the question whether the effect observed in treated mice does not derive mainly by PD1 blockade alone. A subsequent experiment which was terminated at an early time point for FACS

analysis did show better tumour control by combination therapy as opposed to monotherapy, either CAR alone or PD1 blockade alone (Figure 6.4A). Further experiments are therefore needed to determine if observed efficacy is indeed resulting from a synergistic effect of CAR T-cell therapy and PD-1 blockade rather than from PD-1 blockade alone.

To study a possible effect of PD-1 blockade on CAR T-cell function, phenotype of TILs and CAR-T cells at different time points in mice treated with or without PD1 blockade was studied, to understand whether the additional antibody therapy acted mainly on CAR T cells directly or on the endogenous compartment. However, in this set of experiments it was not possible to identify specific patterns which could mediate a potential enhanced CAR T-cell function in the presence of anti-PD1 antibody.

Since recent studies have reported that downregulation of PD1 in tumour-specific T cells can rescue their activity and promote a more potent response (Menger et al., 2016; Cherkassky et al., 2016), future experiments should aim to depict whether this is the case the context of this animal model. To do so, we are planning to either use PD1 KO mice as donors for CAR-T cells or, alternatively, TALEN-mediated KO will be performed. Evaluation of efficacy of $PD1^{neg}$ T cells will enable to understand whether modulation of this pathway on CAR-T cells is enough to promote effective tumour clearance.

Chapter 7:
General discussion and future directions

7 General discussion and future directions

Immunotherapy for brain tumours shares many aspects with immunotherapy for non-CNS solid tumours, but, at the same time, poses unique questions and challenges related to the location and peculiar nature of this malignancy.

As first data from clinical trials on solid tumours are emerging, it is becoming clear that additional strategies will need to be pursued to improve efficacy in this context (Lim and June, 2017) (see section 1.4.3 and Figure 1.13). The four key aspects include:

- T cell trafficking
- Proliferation and persistence
- Overcoming an immunosuppressive environment
- Priming of the endogenous immune system

In this thesis, the development of an orthotopic immunocompetent model of glioma was described. This model allowed the study of the migration, persistence of an efficacy of CAR-T cells within the context of a functional immune system. The rationale of using an immunocompetent mouse model was that the response of CAR-T cells must be evaluated in the context of a complex tumour microenvironment, which a xenograft model would fail to provide.

7.1 T cell trafficking

Although the CNS has been historically considered an “immunological sanctuary”, it is now clear and well described that the immune system constantly patrols and scans this site and can actively migrate in case of infections or in case of autoimmune diseases such as multiple sclerosis (Ransohoff and Engelhardt, 2012; Engelhardt et al., 2017).

Based on this model, EGFRvIII-specific CAR-T cells should be able to actively infiltrate an EGFRvIII-expressing glioma within the brain. Data described in this thesis showed that systemically infused EGFRvIII-specific T cells efficiently migrated to and infiltrated EGFRvIII^{+} tumours within the brain. Bioluminescence imaging demonstrated that homing to the tumour was detectable from 72 hours after intravenous injection. Antigen recognition was required for persistent accumulation of CAR-T cells, since CAR-T cells specific

for an irrelevant antigen (human CD19), despite some initial background migration, did not accumulate to the same extent (Figure 4.2).

Other studies – including a recently published clinical trial report (Brown et al., 2016) – injected CAR-T cells directly into the tumour or the ventricles. In our hands, systemic administration was a suitable route of administration, as effective and consistent T cells trafficking was observed in this experimental setting. Considering the location within a delicate organ such as the brain, intravenous injection and a more physiological accumulation of CAR-T cells could be a safer option to avoid acute toxicities.

7.2 Proliferation and persistence

Two distinct aspects fall into this category: systemic engraftment and persistence within the tumour.

Persistence of CAR-T cells has been associated with efficacy in several clinical trials, both for haematological malignancies (Maude et al., 2014; Porter et al., 2015) and solid tumours (Louis et al., 2011). Intrinsic characteristics of $CD19^+$ malignancies such as ALL seem to have favoured a better engraftment and persistence of transferred T cells: CD19-specific T cells receive, in fact, constant stimulation by B cells, while localisation of tumour within the bone marrow provides easy access to T cells.

Choice of a tumour-specific antigen (as opposed to a tumour associated antigen such as CD19) has the advantage of reducing side effects due to on-target off-tumour recognition, but, at the same time, renders systemic engraftment more challenging.

Data described in this thesis suggest that, although efficiently infiltrating the tumour, CAR-T cells carrying a CD28ζ failed to systemically engraft, as transferred T cells were not observed either in draining cervical lymph nodes nor in the spleen (Figure 4.10 and Figure 5.4). Addition of 41BB as second co-stimulatory domain may have improved persistence, allowing for detection of a small population of CAR-T cells in the spleen.

These findings are in line with emerging data showing that 41BB promotes better long term persistence, through both modulation of exhaustion of T cells (Long et al., 2015; Sommermeyer et al., 2016) and preferential formation of memory T cells (Kawalekar et al., 2016).

Together with systemic engraftment, we observed poor persistence at tumour site, as demonstrated both by BLI and immunohistochemistry at the time of sacrifice (Figure 4.8). Phenotype analysis of TILs demonstrated that CAR-T cells do proliferate *in situ* (Ki67 expression) at day 9 post administration, suggesting early expansion of EGFRvIII-specific CAR-T cells. Conversely, at a later time point (17 days post infusion), CAR-T cells exhibited decreased Ki67 expression (Figure 4.9), suggesting that lack of persistence might be due to poor proliferative potential and exhaustion of transferred T cell. As observed for systemic engraftment, addition of 41BB as endodomain in the EGFRvIII-CAR did increase the percentage of $Ki67^+$ CAR-T cells at day 17 post infusion (Figure 5.5), confirming that addition of 41BB signalling may enhance CAR T-cell persistence within the tumour.

Future directions

Data described in this work indicate that a 41BB co-stimulatory domain may enhance persistence and proliferation of CAR-T cells *in vivo*. Since the combination of two co-stimulatory domains (CD28 and 41BB) in the form a third-generation CAR resulted in adverse side effects, future experiments will directly compare the two second-generation CARs carrying either CD28 or 41BB and evaluate their effect on persistence and activation within the tumour and their systemic engraftment.

Moreover, a different activation protocol for splenocytes (CD3 and CD28 stimulation) will be tested to obtain a more even ratio CD8/CD4. Increasing the proportion of CAR-expressing $CD4^+$ T_{helper} cells could provide cytokines necessary for sustained persistence within the tumour (Moeller et al., 2005, 2007).

Additionally, phenotype of transduced T cells will also be evaluated with this activation protocol to analyse the fraction of central memory T cells retained, as persistence has been associated with phenotype of CAR-T cells at the time of injection, with memory and less differentiated T cells being associated with better performance (Klebanoff et al., 2005; Gattinoni et al., 2011; Sommermeyer et al., 2016).

7.3 Overcoming an immunosuppressive environment

Solid tumours can efficiently downregulate the inflammatory response mounted by the immune system. Glioblastoma is known to be an immunosuppressive tumour. Immunosuppression is mediated by different pathways, including secretion of *indoleamine 2,3-dioxigenase* (IDO), TGFβ and IL10 and recruitment of T_{reg} cells (Fecci et al., 2006; Preusser et al., 2015). Amongst these mechanisms, the role of the PD1/PD-L1 pathway has also been recognised. Analysis on 135 glioblastoma patients showed PD-L1 expression in 88% of newly diagnosed tumours and 72% of recurrent cases (Berghoff et al., 2015). Interestingly, PD-L1 expression was also observed in tumour infiltrating monocytes (Bloch et al., 2013). The inflammatory infiltrates in GBM are generally sparse and mainly found in the perivascular areas (Preusser et al., 2015). They include $CD8^+$ CTLs, $CD4^+$ T_{helper}, T_{reg} cells, natural killer cells and macrophages. Of note, in two recent studies, a third of samples presented PD1 positivity on T cells (Berghoff et al., 2015; Nduom et al., 2016). These findings in humans correlate with preclinical data in mouse models showing that blockade of the PD1/PD-L1 pathway – mostly in combination with other immunotherapy approaches - results in improved survival of tumour bearing mice (Wainwright et al., 2014; Mathios et al., 2016; Antonios et al., 2016).

Despite these encouraging data, it is important to note that the success of checkpoint blockade observed in melanoma and lung cancer has been associated to the high mutational load and consequent presence of neo-antigens within these tumours. Glioblastomas, on the other hand, present on average 40 to 80 non-synonymous mutations, an order of magnitude lower than melanoma (Figure 1.14). Based on this observation, checkpoint blockade as monotherapy might not produce the striking results observed in other tumours. Interestingly, a recent clinical report has shown high response to PD1 blockade in two paediatric GBM patients which presented *biallelic mismatch repair deficiency* (bMMRD) and consequent hypermutation (Bouffet et al., 2016). These encouraging data further confirm that mutational load is a key factor for efficacy of checkpoint blockade.

It is important to note that the GL261 animal model - on which most of immunotherapy approaches have been tested – represents a more

immunogenic tumour due to its chemical induction, therefore pre-clinical results should be carefully translated to the clinical setting. This observation is corroborated by our data which show a marked effect of PD1 blockade alone. Despite the relatively low mutational load presented by glioblastoma, T cells infiltration can be increased and an immune response against GBM can be mounted, as it has been shown for tumour vaccines for EGFRvIII and IDH (Sampson et al., 2011; Schumacher et al., 2014). Moreover, current standard treatment with temozolomide or other chemotherapeutic agents can induce additional mutations within the tumour, thus resulting in a higher immunogenicity. These observations suggest that PD1 blockade could only be effective in the context of GBM if combined to other strategies to increase tumour infiltrates. Recent studies have shown that combination of PD1 blockade with local chemotherapy or dendritic cell vaccination (Mathios et al., 2016; Antonios et al., 2016) has a synergistic effect in increasing the immune response against orthotopic tumours. Similarly, CAR-T cell therapy could potentially break the immune tolerance for glioblastoma and drive the activation of the endogenous immune system, as suggested by our pre-clinical data.

In the context of adoptive cell therapy, blocking the PD1/PD-L1 pathway has been one of the approaches that have been explored to enhance T cells activity in solid tumours. A recent clinical study reported effective expansion and rescue of efficacy of CD19-specific CAR-T cells in a patient with refractory diffuse large B-cell lymphoma (Chong et al., 2017).

In pre-clinical studies, several strategies have been employed, including:

- Co-administration with PD1-blocking antibody (John et al., 2013)
- Local secretion of PD-L1 blocking antibody by CAR-T cells (Suarez et al., 2016)
- Genetic knock down, either by TALEN (Menger et al., 2016) or CRISPR/Cas9 (Ren et al., 2017)
- Use of a dominant negative form of PD1 (Cherkassky et al., 2016)
- Chimeric switch-receptor (PD1-CD28) which induces CD28 signalling in response to PD1 engagement (Ankri et al., 2013; Liu et al., 2016)

All these studies have demonstrated that adoptive T cells therapy combined with modulation of the PD1 pathway can improve efficacy in solid tumours.

Except for the first two approaches, the other reports have the advantage of blocking the PD1 pathway only in tumour-specific T cells, thus avoiding peripheral side effects which have been observed in antibody therapy.
However, PD1 modulation by systemic administration of blocking antibodies has the advantage of regulating this pathway on the endogenous immune system, which might be necessary to obtain an effective response.
In this work, we sought to investigate whether PD1 blockade had an effect on CAR-T cells persistence and, concomitantly, on endogenous TILs.
Quezada and colleagues showed that genetic knock down of PD1 in adoptively infused tumour-specific T cells promoted increase accumulation of $PD1^-$ cells, rather than enhancing their activity (Menger et al., 2016).
Our data shows that CAR-T cells express high levels of PD1 at both day 9 and day 17 post infusion (Figure 4.9). Inhibitory receptors such as PD1 and LAG3 are upregulated soon after activation as negative regulators of the immune response. As CAR-T cells showed high levels of GzmB *in vivo*, we hypothesised that, in the first instance, PD1 expression is a marker of activation (Zhu et al., 2011; Fuertes Marraco et al., 2015). However, failure of complete tumour clearance results into sustained antigen and a "chronic inflammation", comparable to chronic virus infection. In this context, PD-L1-expressing myeloid and tumour cells (Figure 6.1) engage PD1-expressing T cells, downregulating their function and possibly resulting in their exhaustion (Fuertes Marraco et al., 2015). This was confirmed when we looked at phenotype of TILs at day 17 post infusion, where CAR-T cells exhibited a marked decrease in activation and proliferation markers such as GzmB and Ki67 (Figure 4.9).
Analysis of TILs phenotype at day 17 post infusion demonstrated that not only CAR-T cells were possibly exhausted at that time point, but also endogenous $CD8^+$ T cells (Figure 4.9), suggesting that failure of controlling tumour growth at early time points results in an overall downregulation of the immune response and, eventually, tumour outgrowth.
Combination of CAR-T cells with PD1 blockade resulted in complete eradication of tumours and long term survival in the majority of mice treated with this combination therapy, although data so far have not demonstrated a significant survival advantage of combination therapy over PD1 blockade

alone. Immunohistochemistry for CD34 showed persistence of CAR-T cells in mice that rejected tumours (Figure 6.5), thus suggesting that modulation of the PD1 pathway may promote better persistence of CAR-T cells.

In our experimental settings, mice receiving PD1 only exhibited mixed responses: some mice did not respond, other initially responded then the tumour re-grew, while others had a complete response. These data indicate that the endogenous immune system also can play an important role in tumour rejection, as it has been indicated by previous studies (Zeng et al., 2013; Wainwright et al., 2014; Mathios et al., 2016).

Future directions

Phenotype analysis presented in this thesis did not completely answer the question regarding the mechanism driving a potential enhanced effect of combination over monotherapy. In our hands, PD1 blockade in combination with CAR-T cells did not induce an obvious increase in T cell infiltration nor their activity, both in the transferred and endogenous compartment. However, in this experimental setting, the effect of combination therapy was visible from day 14 post T cells injection, suggesting that the enhanced effect of CAR-T cells may take place soon after T cells infiltration within the tumour. An early accumulation and better proliferation of CAR-T cells could therefore increase the effector to target ratio and allow for efficient tumour clearance. To test this hypothesis, mice receiving either CAR T cells alone or in combination with PD1 blockade will be sacrificed at an early time point after infusion (6/7 days) for histopathology. Analysis of the degree of T cells infiltration in correlation to apoptosis of cancer cells will give insight into the early events that could drive a more potent and effective anti-tumour effect.

On a separate note, systemic PD1 blockade can have severe side effects due to over-activation of the immune system. Genetic downregulation of PD1 only on transferred T cells would be advantageous to avoid uncontrolled off-target toxicities. Recent studies have already shown feasibility and enhanced efficacy of transferred T cells (either with tumour-specific TCR or CAR). We plan to use a genetic knock down (as described in Menger et al., 2016), to ultimately demonstrate whether PD1 blockade mainly acts on CAR or on endogenous T cells (or a combination of both) and to determine the feasibility of this approach in the context of glioblastoma.

Finally, in this study, we focussed our attention on the phenotype of endogenous TILs ($CD8^+$ and $CD4^+$ T cells) and transferred CAR-T cells. However, it is known that solid tumours and, amongst them, glioblastoma contain myeloid cells which play an important role in immune suppression (Quail and Joyce, 2017). Investigating the effect that combination of CAR-T cells and PD1 blockade has on the myeloid compartment would be important to elucidate the broad effect of this therapy on the tumour microenvironment.

7.4 Priming of the endogenous immune system

This aspect has been relatively poorly investigated in the context of CAR-T cell therapy, since majority of studies have been performed in immunocompromised xenograft models.

Successful translation of CAR-T cell therapy to solid tumours will likely require ability of adoptively transferred T cells to induce an overall immune response against the tumour through bystander effect and to shift the tumour microenvironment towards a pro-inflammatory phenotype.

Data presented in this thesis suggest that CAR-T cells administration can mediate activation of endogenous T cells, both $CD8^+$ CTLs and $CD4^+$ T_{helper} cells, as demonstrated by increased GzmB expression (Figure 4.6), thus suggesting that CAR-T cells could promote a bystander effect through the induction of a pro-inflammatory environment.

A study from Johnson and colleagues showed that mice cured by EGFRvIII-targeted CAR-T cells were protected from re-challenge with $EGFRvIII^{neg}$ tumours (Sampson et al., 2014). These data suggest that CAR-T cells administration could promote memory formation and, moreover, antigen spreading, where EGFRvIII-targeted CAR-T cells can induce an endogenous immune response against other tumour antigens.

This aspect is particularly important to avoid antigen-escape and relapse with antigen-negative clones, a phenomenon that has been often observed in clinical trials for CD19-targeted adoptive cell therapy (Ghorashian et al., 2015). Moreover, GBM presents a marked intra-tumour heterogeneity which results in cells derived from different clones carrying different mutations and, therefore, expressing different antigens (Sottoriva et al., 2013). This feature makes targeted monotherapies particularly challenging (Jue and McDonald,

2016), as antigen escape is very likely to happen. This was the case also for EGFRvIII-targeted therapies, such as the peptide-based vaccine Rindopepimut® [EGFRvIII peptide conjugated to the adjuvant keyhole limpet hemocyanin (KLH) administered with granulocyte–macrophage colony-stimulating factor (GM-CSF)]. This was tested in a Phase I-II clinical trial and showed robust anti-tumour response (Sampson et al., 2010). Combination of the vaccine with high doses of temozolomide increased the immune response and increased both median progression-free survival and overall survival (Sampson et al., 2011). However, the vast majority of patients lost EGFRvIII expression within the tumour, indicating tumour escape (Sampson et al., 2010, 2011). Data from a phase III clinical trial did not show any increase in overall survival, which led to early closure of the trial (Weller et al., 2016).

In this perspective, combination with checkpoint blockade or secretion of pro-inflammatory cytokines such as IL12 (Pegram et al., 2012; Chmielewski et al., 2011) are particularly promising approaches as they can promote a broader anti-tumour response by activating the endogenous immune system to recognise several antigens with possible antigen spreading.

Future directions

Data presented in this work demonstrate that combination of CAR-T cells and PD1 blockade can promote long term survival in mice bearing EGFRvIII-expressing tumours. Since GL261 do not physiologically express EGFRvIII, cells were transduced with the extracellular portion of the receptor (Figure 3.1). This system does not recapitulate the clinical scenario and therefore cannot predict capability of CAR-T cell therapy to overcome antigen loss. Future experiments will use a combination of EGFRvIII^{pos} and EGFRvIII^{neg} GL261 as a surrogate for intra-tumour heterogeneity. Additionally, re-challenge of cured mice with EGFRvIII^{neg} GL261 will inform about memory formation and antigen spreading in treated mice.

7.5 Conclusions

In conclusion, data presented in this thesis demonstrate that CAR-T cell therapy can be a suitable strategy for the treatment of high grade gliomas.

We established a valuable animal model to study the complex interactions between transferred CAR-T cells and the endogenous immune system. This model allowed for a detailed characterisation of the kinetics and function of CAR-T cells within the tumour and provided useful insights to design alternative strategies to improve efficacy.

8 Appendix

MP15616. Extracellular EGFRvIII with transmembrane domain.

The extracellular portion of the mouse EGFR protein (including the variant III mutation) and its transmembrane domain were employed to produce EGFRvIII-positive GL261. As the intracellular signalling domain is missing the receptor is not active.

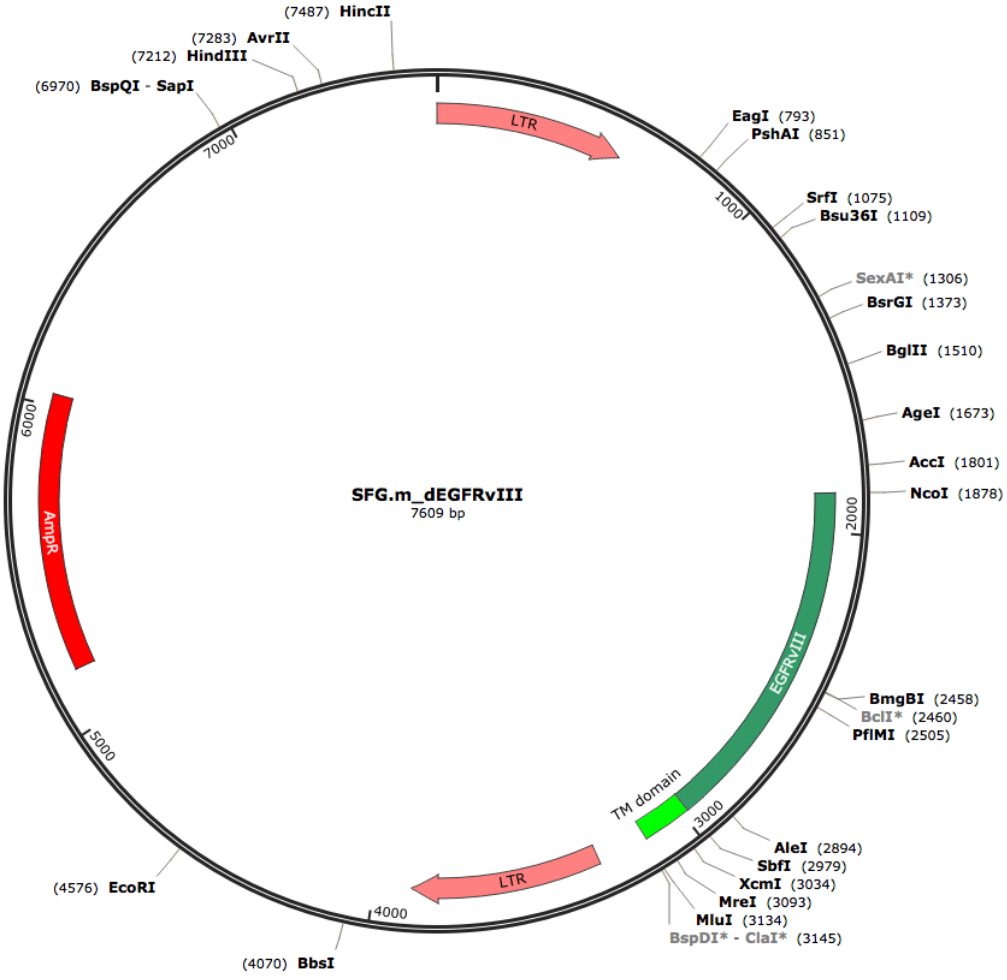

MP19711- N-terminus of mCD34 on glycosylphosphatidylinositol (GPI) anchor.

Open reading frame sequence

ATGGGCCAGGTGCACCGGGACACCCGGGCCGGCCTGCTGCTGCCCTGGCGGTGGGTGGCCCT
GTGCCTGATGAGCCTGCTGCACCTGAACAACCTGACCAGCGCCACCACCGAGACCAGCACCCA
GGGCATCAGCCCCAGCGTGCCCACCAACGAGAGCGTGGAGGAGAACATCACCAGCAGCATCC
CCGGCAGCACCAGCCACTACCTGATCTACCAGGACAGCAGCAAGACCACCCCAGCCATCAGC
GAGACAATGGTGAACTTCACCGTGACCAGCGGCATCCCCAGCGGCAGCGGCACCCCACACAC
CTTCAGCCAGCCCCAGACCAGCCCCACCGGCATCCTGCCCACCACCAGCGACAGCATCAGCAC
CAGCGAGATGACCTGGAAGAGCAGCCTGCCCAGCATCAACGTGAGCGACTACAGCCCCAACA
ACAGCAGCTTCGAGATGACCAGCCCCACCGAGCCCTACGCCTACACCAGCAGCAGCGCCCCA
AGCGGAGGCGGCGGAAGCGACGGCAGCCTGGGCAAGACCCCACTGCTGGGCACCAGCGTGCT
GGTGGCCATCCTGAACCTGTGCTTCCTGAGCCACCTGTGA

Red: signal peptide
Blue: N-terminus of CD34
Green: GPI-anchor from mCD59

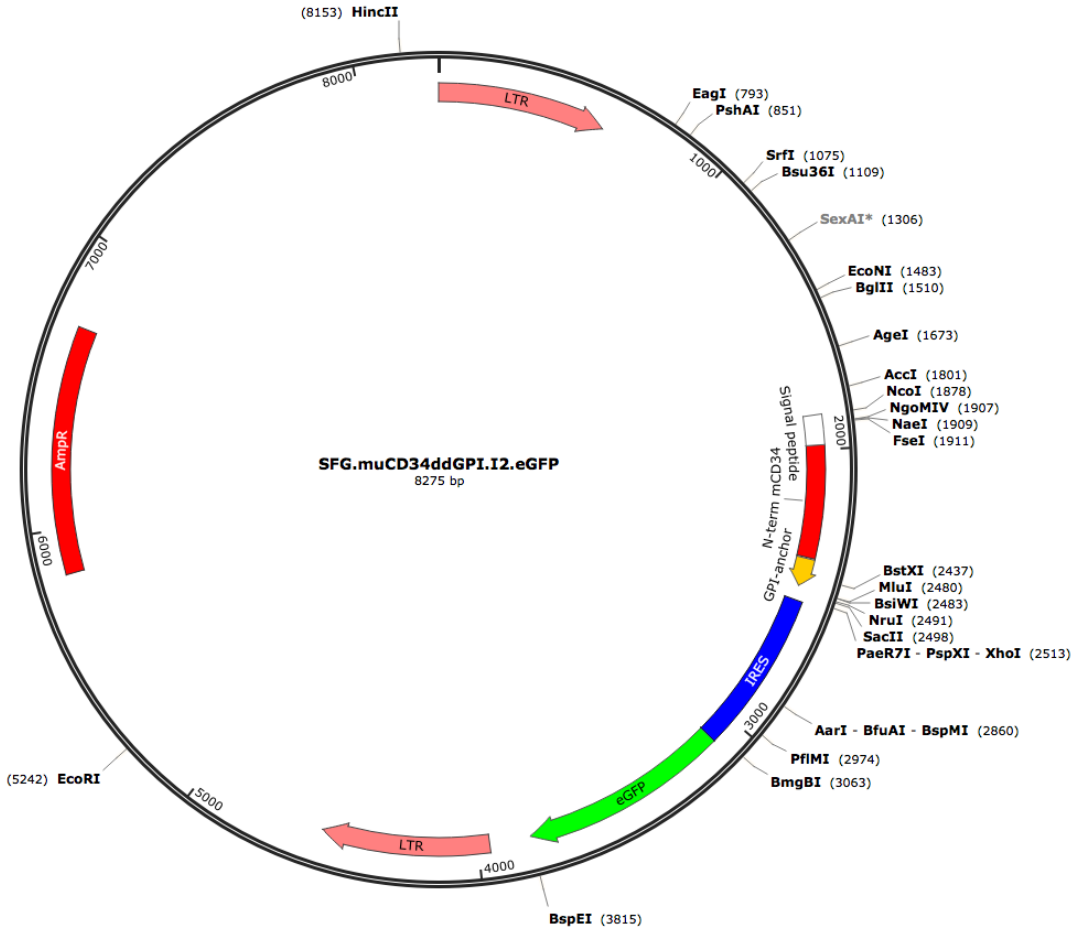

MP19712- C-terminus of mCD34 (type I transmembrane protein).

Open reading frame sequence

ATGGGCCAGGTGCACCGGGACACACGCGCCGGCCTGCTGCTGCCCTGGCGGTGGGTGGCCCT
GTGCCTGATGAGCCTGCTGCACCTGAACAACCTGACCAGCGCCCCAAGCGCCATCAAGGGCGA
GATCAAGTGCAGCGGCATCCGGGAGGTGCGGCTGGCCCAGGGCATCTGCCTGGAGCTGAGCG
AGGCCAGCAGCTGCGAGGAGTTCAAGAAGGAGAAGGGAGAGGACCTGATCCAGATCCTGTGC
GAGAAGGAGGAGGCCGAGGCCGACGCCGGTGCCAGCGTGTGCAGCCTGCTGCTGGCCCAGAG
CGAGGTGCGGCCCGAGTGCCTGCTGATGGTGCTGGCCAACAGCACCGAGCTGCCCAGCAAGC
TGCAGCTGATGGAGAAGCACCAGAGCGACCTGCGGAAGCTGGGCATCCAGAGCTTCAACAAG
CAGGACATCGGCAGCCACCAGAGCTACAGCCGGAAGACCCTGATCGCCCTGGTGACCAGCGG
CGTGCTGCTGGCCATCCTGGGCACCACCGGCTACTTCCTGATGAACCGGCGGAGCTGGAGCCC
CACCGGCGAGCGGCTGGGCGAGGACCCTGCCGCCACCGAGAACGGAGGCGGCCAGGGCTGA

Red: signal peptide
Blue: C-terminus of CD34
Violet: transmembrane domain
Orange: tyrosines converted into alanines to avoid downstream signalling

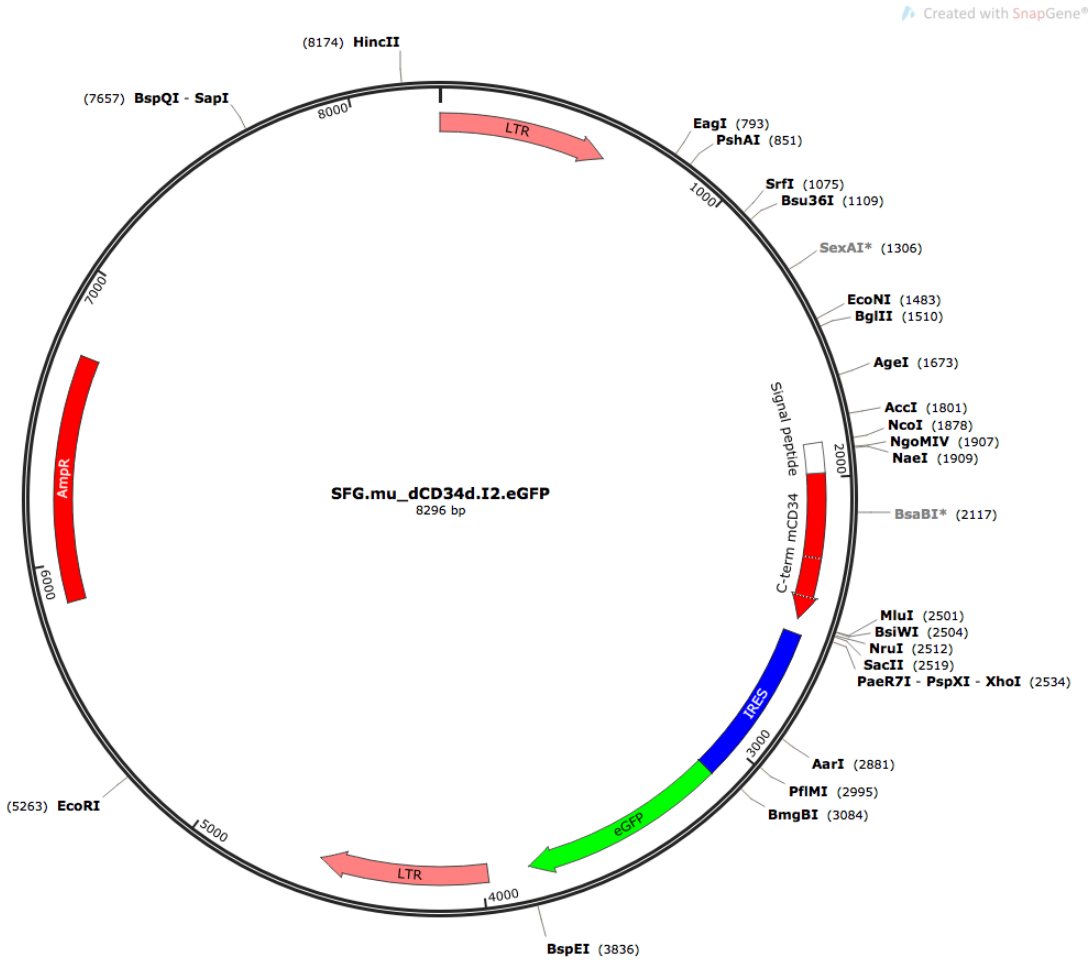

MP20493- Second generation anti EGFRVIII CAR: murine C-terminal CD34-T2A-MR1.1 ScFv-murine CD8stkCD28ζ.

MR1.1 ScFV sequence was obtained from (Beers et al., 2000b). MR1.1 is a mutant form obtained by mutagenesis of the complementary determining region (CDR) of the EGFRvIII-specific antibody MR1 (Lorimer et al., 1996). Second generation murine CAR consisting of a CD28-CD3ζ intracellular domain.

MR1.1 ScFv sequence:

ATGGAGACCGACACCCTGCTGCTGTGGGTGCTGCTGCTGTGGGTGCCCGGCAGCACCGGCCAG
GTGAAGCTGCAGCAGAGCGGCGGAGGCCTGGTGAAGCCCGGCGCCAGCCTGAAGCTGAGCTG
CGTGACCAGCGGCTTCACCTTCCGGAAGTTCGGCATGAGCTGGGTGCGGCAGACCAGCGACAA
GCGGCTGGAGTGGGTGGCCAGCATCAGCACCGGCGGCTACAACACCTACTACAGCGACAACG
TGAAGGGCCGGTTCACCATCAGCCGGGAGAACGCCAAGAACACCCTGTACCTGCAGATGAGCA
GCCTGAAGAGCGAGGACACCGCCCTGTACTACTGCACCCGGGGCTACAGCAGCACCAGCTAC
GCTATGGACTACTGGGGCCAGGGCACCACCGTGACAGTGAGCAGCGGCGGAGGAGGCAGTGG
TGGGGGTGGATCTGGCGGAGGTGGCAGCGACATCGAGCTGACCCAGAGCCCCGCCAGCCTGA
GCGTGGCCACCGGCGAGAAGGTGACCATCCGGTGCATGACCAGCACCGACATCGACGACGAC
ATGAACTGGTACCAGCAGAAGCCCGGCGAGCCCCCAAAGTTCCTGATCAGCGAGGGCAACAC
CCTGCGGCCCGGCGTGCCCAGCCGGTTCAGCAGCAGCGGCACCGGCACCGACTTCGTGTTCAC
CATCGAGAACACCCTGAGCGAGGACGTGGGCGACTACTACTGCCTGCAGAGCTTCAACGTGCC
CCTGACCTTCGGCGACGGCACCAAGCTGGAGATCAAGCGGTCG

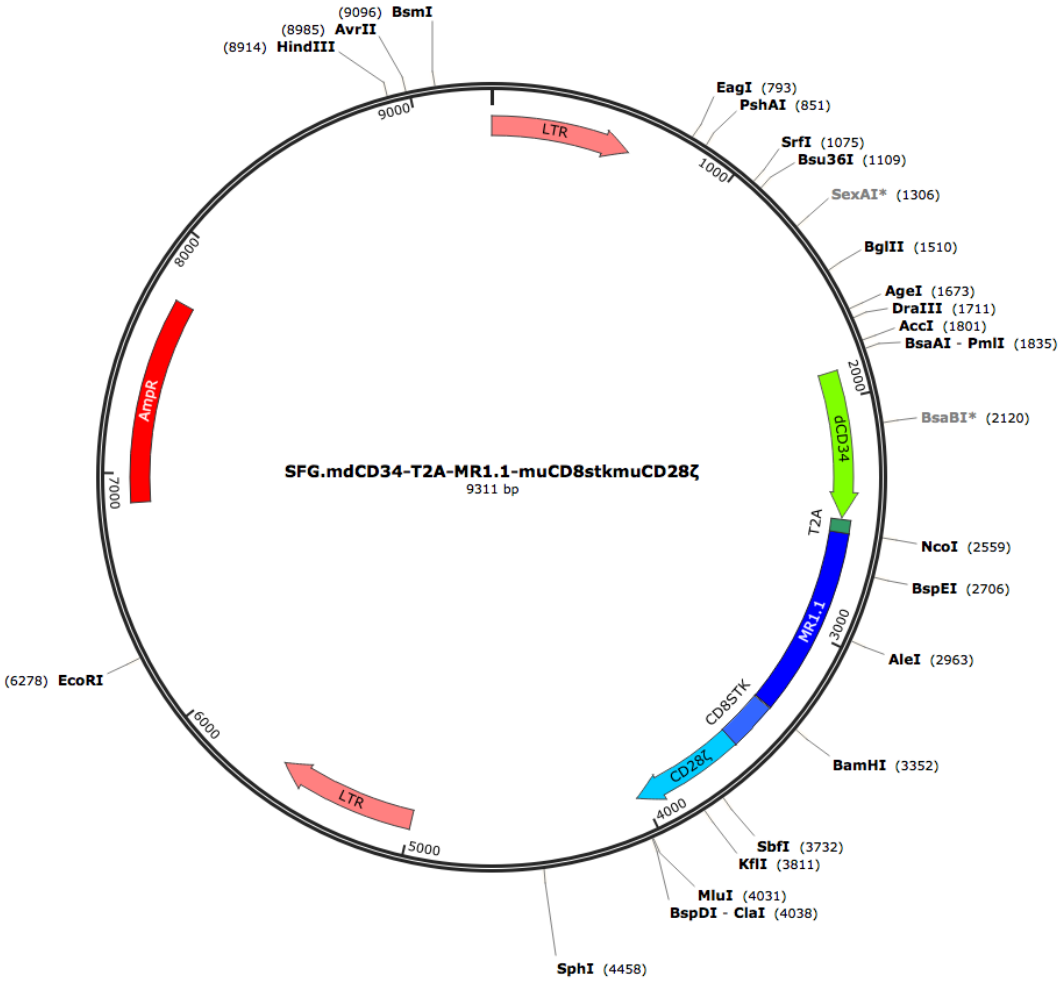

MP20504- Second generation anti EGFRVIII CAR: murine C-terminal CD34-T2A-MR1.1 ScFv-murine CD8stkCD28ζ-E2A-FLucX5red

For imaging purposes, firefly luciferase was included as reporter gene.

A stabilised luciferase carrying 5 point mutation was used, which make the enzyme more stable to both temperature and pH (Law et al., 2006). The luciferase was also red-shifted for better tissue penetration for imaging into C57Bl/6 mice (Branchini et al., 2005).

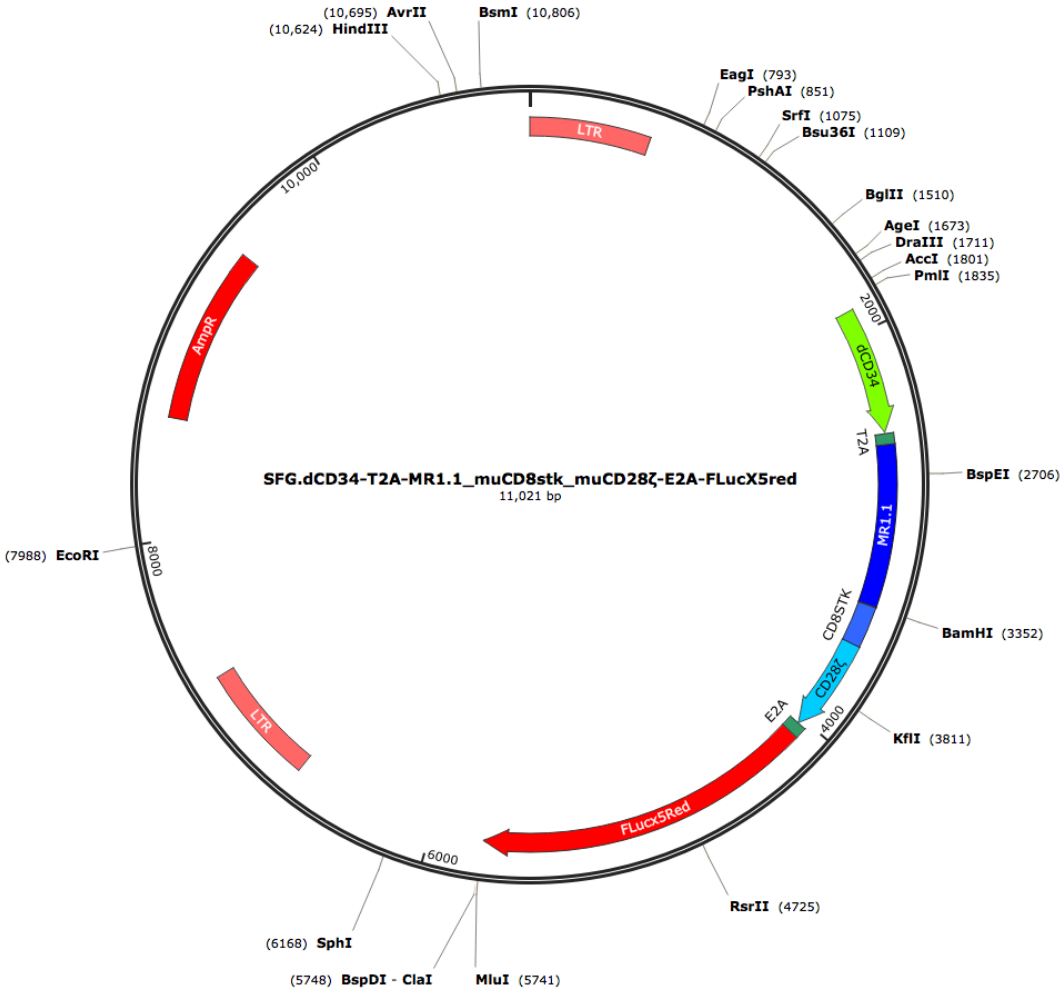

MP27962- Second generation anti human CD19 CAR: murine C-terminal CD34-T2A-MR1.1 ScFv-murine CD8stkCD28ζ-E2A-FLucX5red

Negative control CAR used in vivo. It possesses the same murine domains as MP20493 and MP20504, but the 4g7 ScFv confers specificity to human CD19.

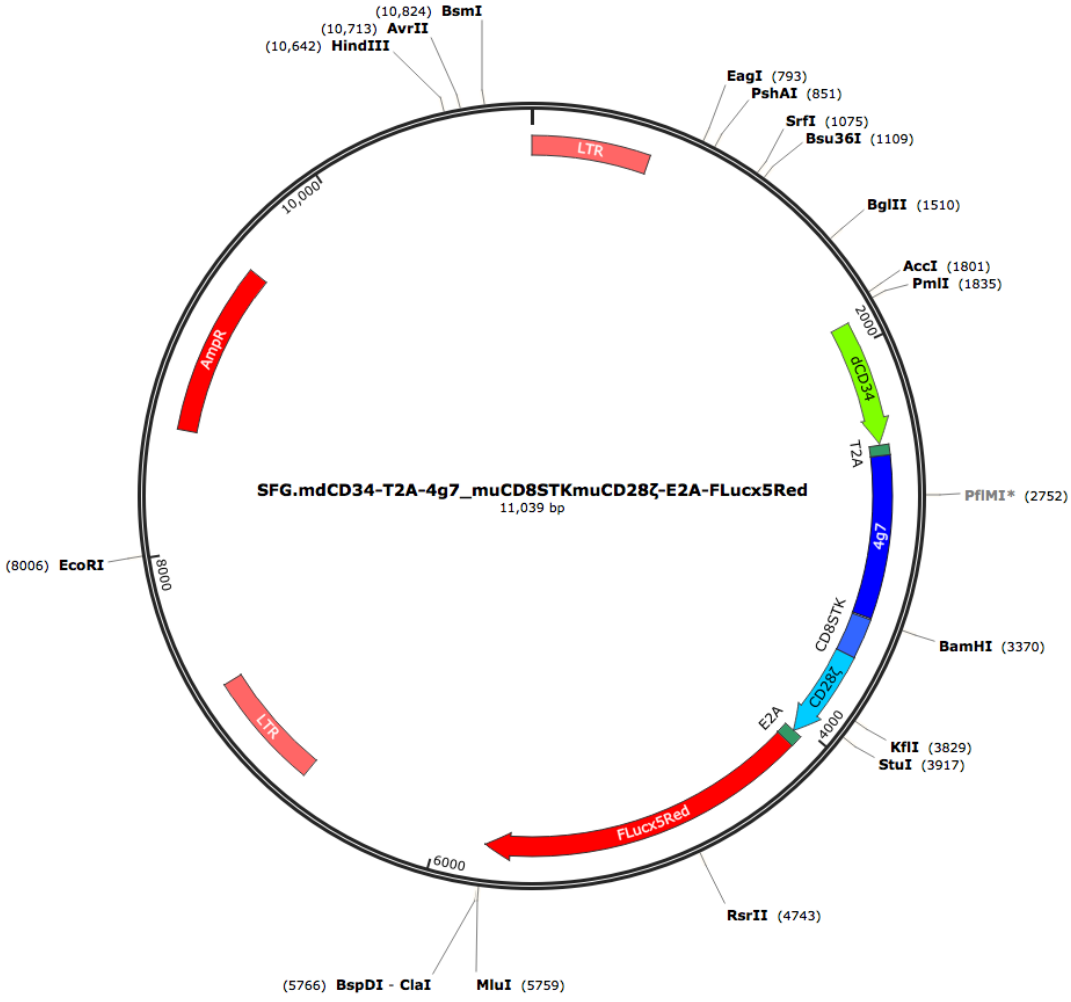

MP25063- Third generation anti EGFRVIII CAR: murine C-terminal CD34-T2A-MR1.1 ScFv-murine CD8stk41BBCD28ζ

Third generation murine CAR, consisting of a 41BB-CD28-CD3ζ intracellular domain.

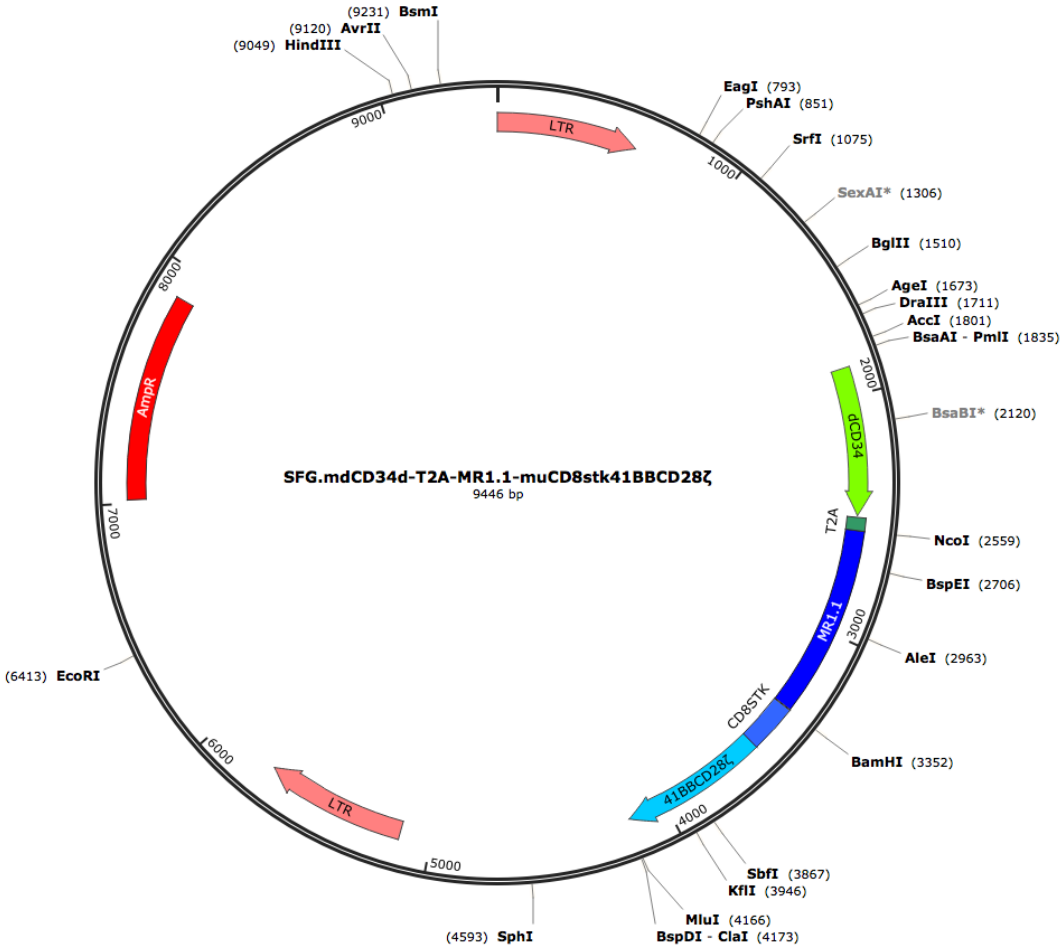

MP25128- Third generation anti EGFRVIII CAR: murine C-terminal CD34-T2A-MR1.1 ScFv-murine CD8stk41BBCD28ζ-E2A-FLucX5red.

Third generation murine CAR, consisting of a 41BB-CD28-CD3ζ intracellular domain. Red-shifted luciferase was co-expressed for *in vivo* tracking.

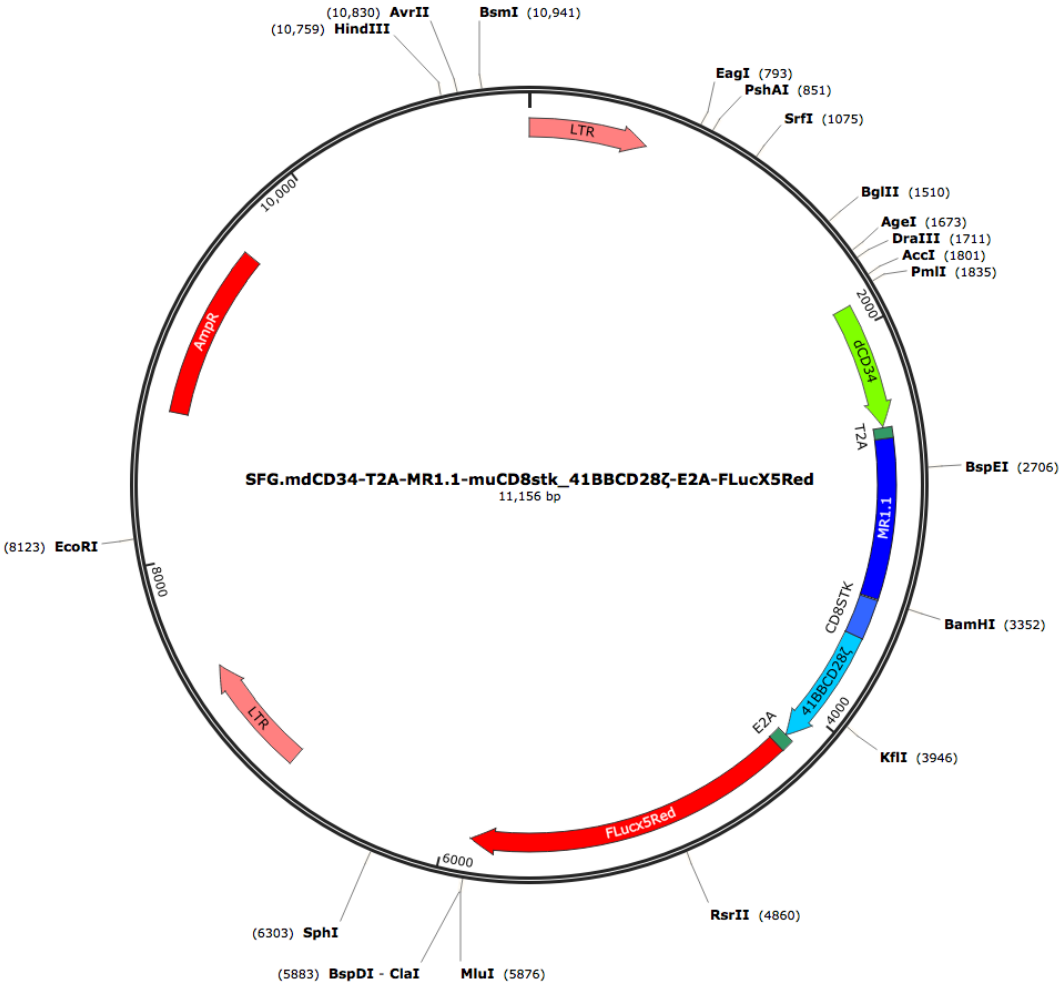

9 Bibliography

Adusumilli, P.S., L. Cherkassky, J. Villena-Vargas, C. Colovos, E. Servais, J. Plotkin, D.R. Jones, and M. Sadelain. 2014. Regional delivery of mesothelin-targeted CAR T cell therapy generates potent and long-lasting CD4-dependent tumor immunity. *Sci. Transl. Med.* 6:261ra151–261ra151.

Ahmed, N., V.S. Brawley, M. Hegde, C. Robertson, A. Ghazi, C. Gerken, E. Liu, O. Dakhova, A. Ashoori, A. Corder, T. Gray, M.-F. Wu, H. Liu, J. Hicks, N. Rainusso, G. Dotti, Z. Mei, B. Grilley, A. Gee, C.M. Rooney, M.K. Brenner, H.E. Heslop, W.S. Wels, L.L. Wang, P. Anderson, and S. Gottschalk. 2015. Human Epidermal Growth Factor Receptor 2 (HER2) –Specific Chimeric Antigen Receptor–Modified T Cells for the Immunotherapy of HER2-Positive Sarcoma. *J. Clin. Oncol.* 33:1688–1696. doi:10.1200/JCO.2014.58.0225.

Ahmed, N., V.S. Salsman, Y. Kew, D. Shaffer, S. Powell, Y.J. Zhang, R.G. Grossman, H.E. Heslop, and S. Gottschalk. 2010. HER2-Specific T Cells Target Primary Glioblastoma Stem Cells and Induce Regression of Autologous Experimental Tumors. *Clin. Cancer Res.* 16:474. doi:10.1158/1078-0432.CCR-09-1322.

Aldape, K., G. Zadeh, S. Mansouri, G. Reifenberger, and A. von Deimling. 2015. Glioblastoma: pathology, molecular mechanisms and markers. *Acta Neuropathol. (Berl.)*. 129:829–848. doi:10.1007/s00401-015-1432-1.

Alexandrov, L.B., S. Nik-Zainal, D.C. Wedge, S.A.J.R. Aparicio, S. Behjati, A.V. Biankin, G.R. Bignell, N. Bolli, A. Borg, A.-L. Borresen-Dale, S. Boyault, B. Burkhardt, A.P. Butler, C. Caldas, H.R. Davies, C. Desmedt, R. Eils, J.E. Eyfjord, J.A. Foekens, M. Greaves, F. Hosoda, B. Hutter, T. Ilicic, S. Imbeaud, M. Imielinsk, N. Jager, D.T.W. Jones, D. Jones, S. Knappskog, M. Kool, S.R. Lakhani, C. Lopez-Otin, S. Martin, N.C. Munshi, H. Nakamura, P.A. Northcott, M. Pajic, E. Papaemmanuil, A. Paradiso, J.V. Pearson, X.S. Puente, K. Raine, M. Ramakrishna, A.L. Richardson, J. Richter, P. Rosenstiel, M. Schlesner, T.N. Schumacher, P.N. Span, J.W. Teague, Y. Totoki, A.N.J. Tutt, R. Valdes-Mas, M.M. van Buuren, L. van /'t Veer, A. Vincent-Salomon, N. Waddell, L.R. Yates, Australian Pancreatic Cancer Genome Initiative, ICGC Breast Cancer Consortium, ICGC MMML-Seq Consortium, ICGC PedBrain, J. Zucman-Rossi, P. Andrew Futreal, U. McDermott, P. Lichter, M. Meyerson, S.M. Grimmond, R. Siebert, E. Campo, T. Shibata, S.M. Pfister, P.J. Campbell, and M.R. Stratton. 2013. Signatures of mutational processes in human cancer. *Nature*. 500:415–421.

Algarra, I., T. Cabrera, and F. Garrido. 2000. The HLA crossroad in tumor immunology. *Hum. Immunol.* 61:65–73. doi:10.1016/S0198-8859(99)00156-1.

Ali, S.A., V. Shi, I. Maric, M. Wang, D.F. Stroncek, J.J. Rose, J.N. Brudno, M. Stetler-Stevenson, S.A. Feldman, B.G. Hansen, V.S. Fellowes, F.T. Hakim, R.E. Gress, and J.N. Kochenderfer. 2016. T cells expressing an anti–B-cell maturation antigen chimeric antigen receptor cause remissions of multiple myeloma. *Blood*. 128:1688. doi:10.1182/blood-2016-04-711903.

Andersen, M.H., D. Schrama, P. thor Straten, and J.C. Becker. 2006. Cytotoxic T Cells. *J. Invest. Dermatol.* 126:32–41. doi:10.1038/sj.jid.5700001.

Anderson, M.S., E.S. Venanzi, L. Klein, Z. Chen, S.P. Berzins, S.J. Turley, H. von Boehmer, R. Bronson, A. Dierich, C. Benoist, and D. Mathis. 2002. Projection of an Immunological Self Shadow Within the Thymus by the Aire Protein. *Science*. 298:1395. doi:10.1126/science.1075958.

Ankri, C., K. Shamalov, M. Horovitz-Fried, S. Mauer, and C.J. Cohen. 2013. Human T Cells Engineered To Express a Programmed Death 1/28 Costimulatory Retargeting Molecule Display Enhanced Antitumor Activity. *J. Immunol.* 191:4121. doi:10.4049/jimmunol.1203085.

Antonios, J.P., H. Soto, R.G. Everson, J. Orpilla, D. Moughon, N. Shin, S. Sedighim, W.H. Yong, G. Li, T.F. Cloughesy, L.M. Liau, and R.M. Prins. 2016. PD-1 blockade enhances the vaccination-induced immune response in glioma. *JCI Insight*. 1:e87059. doi:10.1172/jci.insight.87059.

Artyomov, M.N., M. Lis, S. Devadas, M.M. Davis, and A.K. Chakraborty. 2010. CD4 and CD8 binding to MHC molecules primarily acts to enhance Lck delivery. *Proc. Natl. Acad. Sci.* 107:16916–16921. doi:10.1073/pnas.1010568107.

Aschenbrenner, K., L.M. D'Cruz, E.H. Vollmann, M. Hinterberger, J. Emmerich, L.K. Swee, A. Rolink, and L. Klein. 2007. Selection of Foxp3+ regulatory T cells specific for self antigen expressed and presented by Aire+ medullary thymic epithelial cells. *Nat Immunol*. 8:351–358. doi:10.1038/ni1444.

Ausman, J.I., W.R. Shapiro, and D.P. Rall. 1970. Studies on the Chemotherapy of Experimental Brain Tumors: Development of an Experimental Model. *Cancer Res.* 30:2394.

Baecher-Allan, C., E. Wolf, and D.A. Hafler. 2005. Functional analysis of highly defined, FACS-isolated populations of human regulatory CD4+CD25+ T cells. *FOCIS*. 115:10–18. doi:10.1016/j.clim.2005.02.018.

Baixeras, E., B. Huard, C. Miossec, S. Jitsukawa, M. Martin, T. Hercend, C. Auffray, F. Triebel, and D. Piatier-Tonneau. 1992. Characterization of the lymphocyte activation gene 3-encoded protein. A new ligand for human leukocyte antigen class II antigens. *J. Exp. Med.* 176:327. doi:10.1084/jem.176.2.327.

Bartkowiak, T., and M.A. Curran. 2015. 4-1BB Agonists: Multi-Potent Potentiators of Tumor Immunity. *Front. Oncol.* 5. doi:10.3389/fonc.2015.00117.

Beatty, G.L., A.R. Haas, M.V. Maus, D.A. Torigian, M.C. Soulen, G. Plesa, A. Chew, Y. Zhao, B.L. Levine, S.M. Albelda, M. Kalos, and C.H. June. 2014. Mesothelin-Specific Chimeric Antigen Receptor mRNA-Engineered T Cells Induce Antitumor Activity in Solid Malignancies. *Cancer Immunol. Res.* 2:112. doi:10.1158/2326-6066.CIR-13-0170.

Beers, R., P. Chowdhury, D. Bigner, and I. Pastan. 2000a. Immunotoxins with Increased Activity against Epidermal Growth Factor Receptor vIII-expressing Cells Produced by Antibody Phage Display. *Clin. Cancer Res.* 6:2835.

Beers, R., P. Chowdhury, D. Bigner, and I. Pastan. 2000b. Immunotoxins with Increased Activity against Epidermal Growth Factor Receptor vIII-expressing Cells Produced by Antibody Phage Display. *Clin. Cancer Res.* 6:2835.

Beers, R., P. Chowdhury, D. Bigner, and I. Pastan. 2000c. Immunotoxins with Increased Activity against Epidermal Growth Factor Receptor vIII-expressing Cells Produced by Antibody Phage Display. *Clin. Cancer Res.* 6:2835.

Bennett, C.L., J. Christie, F. Ramsdell, M.E. Brunkow, P.J. Ferguson, L. Whitesell, T.E. Kelly, F.T. Saulsbury, P.F. Chance, and H.D. Ochs. 2001. The immune dysregulation, polyendocrinopathy, enteropathy, X-linked syndrome (IPEX) is caused by mutations of FOXP3. *Nat Genet*. 27:20–21. doi:10.1038/83713.

vom Berg, J., M. Vrohlings, S. Haller, A. Haimovici, P. Kulig, A. Sledzinska, M. Weller, and B. Becher. 2013. Intratumoral IL-12 combined with CTLA-4 blockade elicits T cell–mediated glioma rejection. *J. Exp. Med.* 210:2803. doi:10.1084/jem.20130678.

Berger, C., M.C. Jensen, P.M. Lansdorp, M. Gough, C. Elliott, and S.R. Riddell. 2008. Adoptive transfer of effector CD8(+) T cells derived from central memory cells establishes persistent T cell memory in primates. *J. Clin. Invest.* 118:294–305. doi:10.1172/JCI32103.

Berghoff, A.S., B. Kiesel, G. Widhalm, O. Rajky, G. Ricken, A. Wöhrer, K. Dieckmann, M. Filipits, A. Brandstetter, M. Weller, S. Kurscheid, M.E. Hegi, C.C. Zielinski, C. Marosi, J.A. Hainfellner, M. Preusser, and W. Wick. 2015. Programmed death ligand 1 expression and tumor-infiltrating lymphocytes in glioblastoma. *Neuro-Oncol.* 17:1064–1075. doi:10.1093/neuonc/nou307.

Blank, C.U., J.B. Haanen, A. Ribas, and T.N. Schumacher. 2016. The “cancer immunogram.” *Science*. 352:658. doi:10.1126/science.aaf2834.

Bloch, O., C.A. Crane, R. Kaur, M. Safaee, M.J. Rutkowski, and A.T. Parsa. 2013. Gliomas Promote Immunosuppression through Induction of B7-

H1 Expression in Tumor-Associated Macrophages. *Clin. Cancer Res.* 19:3165. doi:10.1158/1078-0432.CCR-12-3314.

Bouffet, E., V. Larouche, B.B. Campbell, D. Merico, R. de Borja, M. Aronson, C. Durno, J. Krueger, V. Cabric, V. Ramaswamy, N. Zhukova, G. Mason, R. Farah, S. Afzal, M. Yalon, G. Rechavi, V. Magimairajan, M.F. Walsh, S. Constantini, R. Dvir, R. Elhasid, A. Reddy, M. Osborn, M. Sullivan, J. Hansford, A. Dodgshun, N. Klauber-Demore, L. Peterson, S. Patel, S. Lindhorst, J. Atkinson, Z. Cohen, R. Laframboise, P. Dirks, M. Taylor, D. Malkin, S. Albrecht, R.W.R. Dudley, N. Jabado, C.E. Hawkins, A. Shlien, and U. Tabori. 2016. Immune Checkpoint Inhibition for Hypermutant Glioblastoma Multiforme Resulting From Germline Biallelic Mismatch Repair Deficiency. *J. Clin. Oncol.* 34:2206–2211. doi:10.1200/JCO.2016.66.6552.

Branchini, B.R., T.L. Southworth, N.F. Khattak, E. Michelini, and A. Roda. 2005. Red- and green-emitting firefly luciferase mutants for bioluminescent reporter applications. *Anal. Biochem.* 345:140–148. doi:10.1016/j.ab.2005.07.015.

Brentjens, R.J., M.L. Davila, I. Riviere, J. Park, X. Wang, L.G. Cowell, S. Bartido, J. Stefanski, C. Taylor, M. Olszewska, O. Borquez-Ojeda, J. Qu, T. Wasielewska, Q. He, Y. Bernal, I.V. Rijo, C. Hedvat, R. Kobos, K. Curran, P. Steinherz, J. Jurcic, T. Rosenblat, P. Maslak, M. Frattini, and M. Sadelain. 2013. CD19-Targeted T Cells Rapidly Induce Molecular Remissions in Adults with Chemotherapy-Refractory Acute Lymphoblastic Leukemia. *Sci. Transl. Med.* 5:177ra38. doi:10.1126/scitranslmed.3005930.

Brentjens, R.J., I. Rivière, J.H. Park, M.L. Davila, X. Wang, J. Stefanski, C. Taylor, R. Yeh, S. Bartido, O. Borquez-Ojeda, M. Olszewska, Y. Bernal, H. Pegram, M. Przybylowski, D. Hollyman, Y. Usachenko, D. Pirraglia, J. Hosey, E. Santos, E. Halton, P. Maslak, D. Scheinberg, J. Jurcic, M. Heaney, G. Heller, M. Frattini, and M. Sadelain. 2011. Safety and persistence of adoptively transferred autologous CD19-targeted T cells in patients with relapsed or chemotherapy refractory B-cell leukemias. *Blood*. 118:4817. doi:10.1182/blood-2011-04-348540.

Brown, C.E., D. Alizadeh, R. Starr, L. Weng, J.R. Wagner, A. Naranjo, J.R. Ostberg, M.S. Blanchard, J. Kilpatrick, J. Simpson, A. Kurien, S.J. Priceman, X. Wang, T.L. Harshbarger, M. D'Apuzzo, J.A. Ressler, M.C. Jensen, M.E. Barish, M. Chen, J. Portnow, S.J. Forman, and B. Badie. 2016. Regression of Glioblastoma after Chimeric Antigen Receptor T-Cell Therapy. *N. Engl. J. Med.* 375:2561–2569. doi:10.1056/NEJMoa1610497.

Buchholz, V.R., M. Flossdorf, I. Hensel, L. Kretschmer, B. Weissbrich, P. Gräf, A. Verschoor, M. Schiemann, T. Höfer, and D.H. Busch. 2013. Disparate Individual Fates Compose Robust $CD8^+$ T Cell Immunity. *Science*. 340:630. doi:10.1126/science.1235454.

Burger, J.A., and J.G. Gribben. 2014. The microenvironment in chronic lymphocytic leukemia (CLL) and other B cell malignancies: Insight into disease biology and new targeted therapies. *Microenviron. Lymphomas*. 24:71–81. doi:10.1016/j.semcancer.2013.08.011.

Carpenito, C., M.C. Milone, R. Hassan, J.C. Simonet, M. Lakhal, M.M. Suhoski, A. Varela-Rohena, K.M. Haines, D.F. Heitjan, S.M. Albelda, R.G. Carroll, J.L. Riley, I. Pastan, and C.H. June. 2009. Control of large, established tumor xenografts with genetically retargeted human T cells containing CD28 and CD137 domains. *Proc. Natl. Acad. Sci.* 106:3360–3365. doi:10.1073/pnas.0813101106.

Carpenter, A.C., and R. Bosselut. 2010. Decision checkpoints in the thymus. *Nat Immunol*. 11:666–673. doi:10.1038/ni.1887.

Cherkassky, L., A. Morello, J. Villena-Vargas, Y. Feng, D.S. Dimitrov, D.R. Jones, M. Sadelain, and P.S. Adusumilli. 2016. Human CAR T cells with cell-intrinsic PD-1 checkpoint blockade resist tumor-mediated inhibition. *J. Clin. Invest.* 126:3130–3144. doi:10.1172/JCI83092.

Chmielewski, M., C. Kopecky, A.A. Hombach, and H. Abken. 2011. IL-12 Release by Engineered T Cells Expressing Chimeric Antigen Receptors Can Effectively Muster an Antigen-Independent Macrophage Response on Tumor Cells That Have Shut Down Tumor Antigen Expression. *Cancer Res.* 71:5697. doi:10.1158/0008-5472.CAN-11-0103.

Chong, E.A., J.J. Melenhorst, S.F. Lacey, D.E. Ambrose, V. Gonzalez, B.L. Levine, C.H. June, and S.J. Schuster. 2017. PD-1 blockade modulates chimeric antigen receptor (CAR)–modified T cells: refueling the CAR. *Blood*. 129:1039. doi:10.1182/blood-2016-09-738245.

Chow, K.K., S. Naik, S. Kakarla, V.S. Brawley, D.R. Shaffer, Z. Yi, N. Rainusso, M.-F. Wu, H. Liu, Y. Kew, R.G. Grossman, S. Powell, D. Lee, N. Ahmed, and S. Gottschalk. 2013. T Cells Redirected to EphA2 for the Immunotherapy of Glioblastoma. *Mol. Ther.* 21:629–637. doi:10.1038/mt.2012.210.

Comprehensive genomic characterization defines human glioblastoma genes and core pathways. 2008. *Nature*. 455:1061–1068. doi:10.1038/nature07385.

Corse, E., and J.P. Allison. 2012. Cutting Edge: CTLA-4 on Effector T Cells Inhibits In Trans. *J. Immunol.* 189:1123–1127. doi:10.4049/jimmunol.1200695.

Curran, K.J., B.A. Seinstra, Y. Nikhamin, R. Yeh, Y. Usachenko, D.G. van Leeuwen, T. Purdon, H.J. Pegram, and R.J. Brentjens. 2015. Enhancing Antitumor Efficacy of Chimeric Antigen Receptor T Cells Through Constitutive CD40L Expression. *Mol. Ther.* 23:769–778. doi:10.1038/mt.2015.4.

Davila, M.L., I. Riviere, X. Wang, S. Bartido, J. Park, K. Curran, S.S. Chung, J. Stefanski, O. Borquez-Ojeda, M. Olszewska, J. Qu, T. Wasielewska,

Q. He, M. Fink, H. Shinglot, M. Youssif, M. Satter, Y. Wang, J. Hosey, H. Quintanilla, E. Halton, Y. Bernal, D.C.G. Bouhassira, M.E. Arcila, M. Gonen, G.J. Roboz, P. Maslak, D. Douer, M.G. Frattini, S. Giralt, M. Sadelain, and R. Brentjens. 2014. Efficacy and Toxicity Management of 19-28z CAR T Cell Therapy in B Cell Acute Lymphoblastic Leukemia. *Sci. Transl. Med.* 6:224ra25. doi:10.1126/scitranslmed.3008226.

Davis, M.M., and P.J. Bjorkman. 1988. T-cell antigen receptor genes and T-cell recognition. *Nature*. 334:395–402. doi:10.1038/334395a0.

Di Stasi, A., B. De Angelis, C.M. Rooney, L. Zhang, A. Mahendravada, A.E. Foster, H.E. Heslop, M.K. Brenner, G. Dotti, and B. Savoldo. 2009. T lymphocytes coexpressing CCR4 and a chimeric antigen receptor targeting CD30 have improved homing and antitumor activity in a Hodgkin tumor model. *Blood*. 113:6392. doi:10.1182/blood-2009-03-209650.

Dudley, M.E., J.R. Wunderlich, P.F. Robbins, J.C. Yang, P. Hwu, D.J. Schwartzentruber, S.L. Topalian, R. Sherry, N.P. Restifo, A.M. Hubicki, M.R. Robinson, M. Raffeld, P. Duray, C.A. Seipp, L. Rogers-Freezer, K.E. Morton, S.A. Mavroukakis, D.E. White, and S.A. Rosenberg. 2002. Cancer Regression and Autoimmunity in Patients After Clonal Repopulation with Antitumor Lymphocytes. *Science*. 298:850. doi:10.1126/science.1076514.

Dudley, M.E., J.C. Yang, R. Sherry, M.S. Hughes, R. Royal, U. Kammula, P.F. Robbins, J. Huang, D.E. Citrin, S.F. Leitman, J. Wunderlich, N.P. Restifo, A. Thomasian, S.G. Downey, F.O. Smith, J. Klapper, K. Morton, C. Laurencot, D.E. White, and S.A. Rosenberg. 2008. Adoptive Cell Therapy for Patients With Metastatic Melanoma: Evaluation of Intensive Myeloablative Chemoradiation Preparative Regimens. *J. Clin. Oncol.* 26:5233–5239. doi:10.1200/JCO.2008.16.5449.

Dummer, W., A.G. Niethammer, R. Baccala, B.R. Lawson, N. Wagner, R.A. Reisfeld, and A.N. Theofilopoulos. 2002. T cell homeostatic proliferation elicits effective antitumor autoimmunity. *J. Clin. Invest.* 110:185–192. doi:10.1172/JCI15175.

Dunn, G.P., L.J. Old, and R.D. Schreiber. 2004. The immunobiology of cancer immunosurveillance and immunoediting. *Immunity*. 21:137–148.

Duong, C.P.M., C.S.M. Yong, M.H. Kershaw, C.Y. Slaney, and P.K. Darcy. 2015. Cancer immunotherapy utilizing gene-modified T cells: From the bench to the clinic. *Mol. Immunol.* 67:46–57. doi:10.1016/j.molimm.2014.12.009.

Engelhardt, B., P. Vajkoczy, and R.O. Weller. 2017. The movers and shapers in immune privilege of the CNS. *Nat Immunol*. 18:123–131.

Eshhar, Z., T. Waks, G. Gross, and D.G. Schindler. 1993. Specific activation and targeting of cytotoxic lymphocytes through chimeric single chains consisting of antibody-binding domains and the gamma or zeta subunits

of the immunoglobulin and T-cell receptors. *Proc. Natl. Acad. Sci.* 90:720–724.

Eyquem, J., J. Mansilla-Soto, T. Giavridis, S.J.C. van der Stegen, M. Hamieh, K.M. Cunanan, A. Odak, M. Gönen, and M. Sadelain. 2017. Targeting a CAR to the TRAC locus with CRISPR/Cas9 enhances tumour rejection. *Nature*. 543:113–117.

Fecci, P.E., D.A. Mitchell, J.F. Whitesides, W. Xie, A.H. Friedman, G.E. Archer, J.E. Herndon, D.D. Bigner, G. Dranoff, and J.H. Sampson. 2006. Increased Regulatory T-Cell Fraction Amidst a Diminished CD4 Compartment Explains Cellular Immune Defects in Patients with Malignant Glioma. *Cancer Res.* 66:3294. doi:10.1158/0008-5472.CAN-05-3773.

Finney, H.M., A.N. Akbar, and A.D.G. Lawson. 2003. Activation of Resting Human Primary T Cells with Chimeric Receptors: Costimulation from CD28, Inducible Costimulator, CD134, and CD137 in Series with Signals from the TCRζ Chain. *J. Immunol.* 172:104. doi:10.4049/jimmunol.172.1.104.

Finney, H.M., A.D.G. Lawson, C.R. Bebbington, and A.N.C. Weir. 1998. Chimeric Receptors Providing Both Primary and Costimulatory Signaling in T Cells from a Single Gene Product. *J. Immunol.* 161:2791.

Fontenot, J.D., M.A. Gavin, and A.Y. Rudensky. 2003. Foxp3 programs the development and function of CD4+CD25+ regulatory T cells. *Nat Immunol*. 4:330–336. doi:10.1038/ni904.

Fuertes Marraco, S.A., N.J. Neubert, G. Verdeil, and D.E. Speiser. 2015. Inhibitory Receptors Beyond T Cell Exhaustion. *Front. Immunol.* 6. doi:10.3389/fimmu.2015.00310.

Fulda, S. 2009. Tumor resistance to apoptosis. *Int. J. Cancer*. 124:511–515. doi:10.1002/ijc.24064.

Gabrilovich, D.I., and S. Nagaraj. 2009. Myeloid-derived suppressor cells as regulators of the immune system. *Nat Rev Immunol*. 9:162–174. doi:10.1038/nri2506.

Gan, H.K., A.H. Kaye, and R.B. Luwor. 2009. The EGFRvIII variant in glioblastoma multiforme. *J. Clin. Neurosci.* 16:748–754. doi:10.1016/j.jocn.2008.12.005.

Garcia, K.C., M. Degano, R.L. Stanfield, A. Brunmark, M.R. Jackson, P.A. Peterson, L. Teyton, and I.A. Wilson. 1996. An αβ T Cell Receptor Structure at 2.5 Å and Its Orientation in the TCR-MHC Complex. *Science*. 274:209. doi:10.1126/science.274.5285.209.

Garon, E.B., N.A. Rizvi, R. Hui, N. Leighl, A.S. Balmanoukian, J.P. Eder, A. Patnaik, C. Aggarwal, M. Gubens, L. Horn, E. Carcereny, M.-J. Ahn, E. Felip, J.-S. Lee, M.D. Hellmann, O. Hamid, J.W. Goldman, J.-C. Soria, M. Dolled-Filhart, R.Z. Rutledge, J. Zhang, J.K. Lunceford, R.

Rangwala, G.M. Lubiniecki, C. Roach, K. Emancipator, and L. Gandhi. 2015. Pembrolizumab for the Treatment of Non–Small-Cell Lung Cancer. *N. Engl. J. Med.* 372:2018–2028. doi:10.1056/NEJMoa1501824.

Gattinoni, L., S.E. Finkelstein, C.A. Klebanoff, P.A. Antony, D.C. Palmer, P.J. Spiess, L.N. Hwang, Z. Yu, C. Wrzesinski, D.M. Heimann, C.D. Surh, S.A. Rosenberg, and N.P. Restifo. 2005. Removal of homeostatic cytokine sinks by lymphodepletion enhances the efficacy of adoptively transferred tumor-specific CD8 $^{+}$ T cells. *J. Exp. Med.* 202:907–912. doi:10.1084/jem.20050732.

Gattinoni, L., E. Lugli, Y. Ji, Z. Pos, C.M. Paulos, M.F. Quigley, J.R. Almeida, E. Gostick, Z. Yu, C. Carpenito, E. Wang, D.C. Douek, D.A. Price, C.H. June, F.M. Marincola, M. Roederer, and N.P. Restifo. 2011. A human memory T cell subset with stem cell-like properties. *Nat Med*. 17:1290–1297. doi:10.1038/nm.2446.

Gerlach, C., J.C. Rohr, L. Perié, N. van Rooij, J.W.J. van Heijst, A. Velds, J. Urbanus, S.H. Naik, H. Jacobs, J.B. Beltman, R.J. de Boer, and T.N.M. Schumacher. 2013. Heterogeneous Differentiation Patterns of Individual $CD8^{+}$ T Cells. *Science*. 340:635. doi:10.1126/science.1235487.

Ghorashian, S., M. Pule, and P. Amrolia. 2015. CD19 chimeric antigen receptor T cell therapy for haematological malignancies. *Br. J. Haematol.* 169:463–478. doi:10.1111/bjh.13340.

Gordon, S., A. Plüddemann, and S. Mukhopadhyay. 2015. Sinusoidal Immunity: Macrophages at the Lymphohematopoietic Interface. *Cold Spring Harb. Perspect. Biol.* 7:a016378. doi:10.1101/cshperspect.a016378.

Gorman, J.V., and J.D. Colgan. 2014. Regulation of T cell responses by the receptor molecule Tim-3. *Immunol. Res.* 59:56–65. doi:10.1007/s12026-014-8524-1.

Grupp, S.A., M. Kalos, D. Barrett, R. Aplenc, D.L. Porter, S.R. Rheingold, D.T. Teachey, A. Chew, B. Hauck, J.F. Wright, M.C. Milone, B.L. Levine, and C.H. June. 2013. Chimeric Antigen Receptor–Modified T Cells for Acute Lymphoid Leukemia. *N. Engl. J. Med.* 368:1509–1518. doi:10.1056/NEJMoa1215134.

Hamid, O., C. Robert, A. Daud, F.S. Hodi, W.-J. Hwu, R. Kefford, J.D. Wolchok, P. Hersey, R.W. Joseph, J.S. Weber, R. Dronca, T.C. Gangadhar, A. Patnaik, H. Zarour, A.M. Joshua, K. Gergich, J. Elassaiss-Schaap, A. Algazi, C. Mateus, P. Boasberg, P.C. Tumeh, B. Chmielowski, S.W. Ebbinghaus, X.N. Li, S.P. Kang, and A. Ribas. 2013. Safety and Tumor Responses with Lambrolizumab (Anti–PD-1) in Melanoma. *N. Engl. J. Med.* 369:134–144. doi:10.1056/NEJMoa1305133.

Hannier, S., M. Tournier, G. Bismuth, and F. Triebel. 1998. CD3/TCR complex-associated lymphocyte activation gene-3 molecules inhibit CD3/TCR signaling. *J. Immunol.* 161:4058–4065.

Haso, W., D.W. Lee, N.N. Shah, M. Stetler-Stevenson, C.M. Yuan, I.H. Pastan, D.S. Dimitrov, R.A. Morgan, D.J. FitzGerald, D.M. Barrett, A.S. Wayne, C.L. Mackall, and R.J. Orentas. 2013. Anti-CD22–chimeric antigen receptors targeting B-cell precursor acute lymphoblastic leukemia. *Blood*. 121:1165. doi:10.1182/blood-2012-06-438002.

Haynes, N.M., J.A. Trapani, M.W.L. Teng, J.T. Jackson, L. Cerruti, S.M. Jane, M.H. Kershaw, M.J. Smyth, and P.K. Darcy. 2002. Single-chain antigen recognition receptors that costimulate potent rejection of established experimental tumors. *Blood*. 100:3155. doi:10.1182/blood-2002-04-1041.

Heemskerk, B., P. Kvistborg, and T.N.M. Schumacher. 2012. The cancer antigenome. *EMBO J.* 32:194. doi:10.1038/emboj.2012.333.

Hegde, M., M. Mukherjee, Z. Grada, A. Pignata, D. Landi, S.A. Navai, A. Wakefield, K. Fousek, K. Bielamowicz, K.K.H. Chow, V.S. Brawley, T.T. Byrd, S. Krebs, S. Gottschalk, W.S. Wels, M.L. Baker, G. Dotti, M. Mamonkin, M.K. Brenner, J.S. Orange, and N. Ahmed. 2016. Tandem CAR T cells targeting HER2 and IL13Rα2 mitigate tumor antigen escape. *J. Clin. Invest.* 126:3036–3052. doi:10.1172/JCI83416.

Hodi, F.S., S.J. O'Day, D.F. McDermott, R.W. Weber, J.A. Sosman, J.B. Haanen, R. Gonzalez, C. Robert, D. Schadendorf, J.C. Hassel, W. Akerley, A.J.M. van den Eertwegh, J. Lutzky, P. Lorigan, J.M. Vaubel, G.P. Linette, D. Hogg, C.H. Ottensmeier, C. Lebbé, C. Peschel, I. Quirt, J.I. Clark, J.D. Wolchok, J.S. Weber, J. Tian, M.J. Yellin, G.M. Nichol, A. Hoos, and W.J. Urba. 2010. Improved Survival with Ipilimumab in Patients with Metastatic Melanoma. *N. Engl. J. Med.* 363:711–723. doi:10.1056/NEJMoa1003466.

Hori, S., T. Nomura, and S. Sakaguchi. 2003. Control of Regulatory T Cell Development by the Transcription Factor Foxp3. *Science*. 299:1057. doi:10.1126/science.1079490.

Huang, H.-J.S., M. Nagane, C.K. Klingbeil, H. Lin, R. Nishikawa, X.-D. Ji, C.-M. Huang, G.N. Gill, H.S. Wiley, and W.K. Cavenee. 1997. The enhanced tumorigenic activity of a mutant epidermal growth factor receptor common in human cancers is mediated by threshold levels of constitutive tyrosine phosphorylation and unattenuated signaling. *J. Biol. Chem.* 272:2927–2935.

Huang, Y.-H., C. Zhu, Y. Kondo, A.C. Anderson, A. Gandhi, A. Russell, S.K. Dougan, B.-S. Petersen, E. Melum, T. Pertel, K.L. Clayton, M. Raab, Q. Chen, N. Beauchemin, P.J. Yazaki, M. Pyzik, M.A. Ostrowski, J.N. Glickman, C.E. Rudd, H.L. Ploegh, A. Franke, G.A. Petsko, V.K. Kuchroo, and R.S. Blumberg. 2015. CEACAM1 regulates TIM-3-mediated tolerance and exhaustion. *Nature*. 517:386–390.

Hui, E., J. Cheung, J. Zhu, X. Su, M.J. Taylor, H.A. Wallweber, D.K. Sasmal, J. Huang, J.M. Kim, I. Mellman, and others. 2017. T cell costimulatory receptor CD28 is a primary target for PD-1–mediated inhibition. *Science*. 355:1428–1433.

Imai, C., K. Mihara, M. Andreansky, I.C. Nicholson, C.-H. Pui, T.L. Geiger, and D. Campana. 2004. Chimeric receptors with 4-1BB signaling capacity provoke potent cytotoxicity against acute lymphoblastic leukemia. *Leukemia*. 18:676–684.

Jackson, H.J., S. Rafiq, and R.J. Brentjens. 2016. Driving CAR T-cells forward. *Nat. Rev. Clin. Oncol.* 13:370–383. doi:10.1038/nrclinonc.2016.36.

John, L.B., C. Devaud, C.P.M. Duong, C.S. Yong, P.A. Beavis, N.M. Haynes, M.T. Chow, M.J. Smyth, M.H. Kershaw, and P.K. Darcy. 2013. Anti-PD-1 Antibody Therapy Potently Enhances the Eradication of Established Tumors By Gene-Modified T Cells. *Clin. Cancer Res.* 19:5636. doi:10.1158/1078-0432.CCR-13-0458.

Johnson, L.A., R.A. Morgan, M.E. Dudley, L. Cassard, J.C. Yang, M.S. Hughes, U.S. Kammula, R.E. Royal, R.M. Sherry, J.R. Wunderlich, C.-C.R. Lee, N.P. Restifo, S.L. Schwarz, A.P. Cogdill, R.J. Bishop, H. Kim, C.C. Brewer, S.F. Rudy, C. VanWaes, J.L. Davis, A. Mathur, R.T. Ripley, D.A. Nathan, C.M. Laurencot, and S.A. Rosenberg. 2009. Gene therapy with human and mouse T-cell receptors mediates cancer regression and targets normal tissues expressing cognate antigen. *Blood*. 114:535. doi:10.1182/blood-2009-03-211714.

Johnson, L.A., J. Scholler, T. Ohkuri, A. Kosaka, P.R. Patel, S.E. McGettigan, A.K. Nace, T. Dentchev, P. Thekkat, A. Loew, A.C. Boesteanu, A.P. Cogdill, T. Chen, J.A. Fraietta, C.C. Kloss, A.D. Posey, B. Engels, R. Singh, T. Ezell, N. Idamakanti, M.H. Ramones, N. Li, L. Zhou, G. Plesa, J.T. Seykora, H. Okada, C.H. June, J.L. Brogdon, and M.V. Maus. 2015. Rational development and characterization of humanized anti–EGFR variant III chimeric antigen receptor T cells for glioblastoma. *Sci. Transl. Med.* 7:275ra22. doi:10.1126/scitranslmed.aaa4963.

Jones, R.B., L.C. Ndhlovu, J.D. Barbour, P.M. Sheth, A.R. Jha, B.R. Long, J.C. Wong, M. Satkunarajah, M. Schweneker, J.M. Chapman, G. Gyenes, B. Vali, M.D. Hyrcza, F.Y. Yue, C. Kovacs, A. Sassi, M. Loutfy, R. Halpenny, D. Persad, G. Spotts, F.M. Hecht, T.-W. Chun, J.M. McCune, R. Kaul, J.M. Rini, D.F. Nixon, and M.A. Ostrowski. 2008. Tim-3 expression defines a novel population of dysfunctional T cells with highly elevated frequencies in progressive HIV-1 infection. *J. Exp. Med.* 205:2763. doi:10.1084/jem.20081398.

Joyce, J.A., and D.T. Fearon. 2015. T cell exclusion, immune privilege, and the tumor microenvironment. *Science*. 348:74. doi:10.1126/science.aaa6204.

Jue, T.R., and K.L. McDonald. 2016. The challenges associated with molecular targeted therapies for glioblastoma. *J. Neurooncol.* 127:427–434. doi:10.1007/s11060-016-2080-6.

Kamphorst, A.O., A. Wieland, T. Nasti, S. Yang, R. Zhang, D.L. Barber, B.T. Konieczny, C.Z. Daugherty, L. Koenig, K. Yu, G.L. Sica, A.H. Sharpe, G.J. Freeman, B.R. Blazar, L.A. Turka, T.K. Owonikoko, R.N. Pillai, S.S. Ramalingam, K. Araki, and R. Ahmed. 2017. Rescue of exhausted CD8 T cells by PD-1–targeted therapies is CD28-dependent. *Science*. 355:1423. doi:10.1126/science.aaf0683.

Kaplan, D.H., V. Shankaran, A.S. Dighe, E. Stockert, M. Aguet, L.J. Old, and R.D. Schreiber. 1998. Demonstration of an interferon γ-dependent tumor surveillance system in immunocompetent mice. *Proc. Natl. Acad. Sci.* 95:7556–7561.

Kawalekar, O.U., R.S. O'Connor, J.A. Fraietta, L. Guo, S.E. McGettigan, A.D. Posey Jr., P.R. Patel, S. Guedan, J. Scholler, B. Keith, N.W. Snyder, I.A. Blair, M.C. Milone, and C.H. June. 2016. Distinct Signaling of Coreceptors Regulates Specific Metabolism Pathways and Impacts Memory Development in CAR T Cells. *Immunity*. 44:380–390. doi:10.1016/j.immuni.2016.01.021.

Kawamata, S., T. Hori, A. Imura, A. Takaori-Kondo, and T. Uchiyama. 1998. Activation of OX40 signal transduction pathways leads to tumor necrosis factor receptor-associated factor (TRAF) 2-and TRAF5-mediated NF-κB activation. *J. Biol. Chem.* 273:5808–5814.

Khong, H.T., and N.P. Restifo. 2002. Natural selection of tumor variants in the generation of "tumor escape" phenotypes. *Nat. Immunol.* 3:999–1005. doi:10.1038/ni1102-999.

Kinter, A.L., E.J. Godbout, J.P. McNally, I. Sereti, G.A. Roby, M.A. O'Shea, and A.S. Fauci. 2008. The Common γ-Chain Cytokines IL-2, IL-7, IL-15, and IL-21 Induce the Expression of Programmed Death-1 and Its Ligands. *J. Immunol.* 181:6738. doi:10.4049/jimmunol.181.10.6738.

Kitano, S., T. Tsuji, C. Liu, D. Hirschhorn-Cymerman, C. Kyi, Z. Mu, J.P. Allison, S. Gnjatic, J.D. Yuan, and J.D. Wolchok. 2013. Enhancement of Tumor-Reactive Cytotoxic $CD4^+$ T-cell Responses after Ipilimumab Treatment in Four Advanced Melanoma Patients. *Cancer Immunol. Res.* 1:235. doi:10.1158/2326-6066.CIR-13-0068.

Klausz, K., S. Berger, J.J. Lammerts van Bueren, S. Derer, S. Lohse, M. Dechant, J.G.J. van de Winkel, M. Peipp, P.W.H.I. Parren, and T. Valerius. 2011. Complement-mediated tumor-specific cell lysis by antibody combinations targeting epidermal growth factor receptor (EGFR) and its variant III (EGFRvIII). *Cancer Sci.* 102:1761–1768. doi:10.1111/j.1349-7006.2011.02019.x.

Klebanoff, C.A., L. Gattinoni, P. Torabi-Parizi, K. Kerstann, A.R. Cardones, S.E. Finkelstein, D.C. Palmer, P.A. Antony, S.T. Hwang, S.A.

Rosenberg, T.A. Waldmann, and N.P. Restifo. 2005. Central memory self/tumor-reactive CD8(+) T cells confer superior antitumor immunity compared with effector memory T cells. *Proc. Natl. Acad. Sci. U. S. A.* 102:9571–9576. doi:10.1073/pnas.0503726102.

Kochenderfer, J.N., M.E. Dudley, R.O. Carpenter, S.H. Kassim, J.J. Rose, W.G. Telford, F.T. Hakim, D.C. Halverson, D.H. Fowler, N.M. Hardy, A.R. Mato, D.D. Hickstein, J.C. Gea-Banacloche, S.Z. Pavletic, C. Sportes, I. Maric, S.A. Feldman, B.G. Hansen, J.S. Wilder, B. Blacklock-Schuver, B. Jena, M.R. Bishop, R.E. Gress, and S.A. Rosenberg. 2013. Donor-derived CD19-targeted T cells cause regression of malignancy persisting after allogeneic hematopoietic stem cell transplantation. *Blood*. 122:4129. doi:10.1182/blood-2013-08-519413.

Kochenderfer, J.N., S.A. Feldman, Y. Zhao, H. Xu, M.A. Black, R.A. Morgan, W.H. Wilson, and S.A. Rosenberg. 2009. Construction and Pre-clinical Evaluation of an Anti-CD19 Chimeric Antigen Receptor. *J. Immunother. Hagerstown Md 1997*. 32:689–702. doi:10.1097/CJI.0b013e3181ac6138.

Koebel, C.M., W. Vermi, J.B. Swann, N. Zerafa, S.J. Rodig, L.J. Old, M.J. Smyth, and R.D. Schreiber. 2007. Adaptive immunity maintains occult cancer in an equilibrium state. *Nature*. 450:903–907. doi:10.1038/nature06309.

Kong, S., S. Sengupta, B. Tyler, A.J. Bais, Q. Ma, S. Doucette, J. Zhou, A. Sahin, B.S. Carter, H. Brem, R.P. Junghans, and P. Sampath. 2012. Suppression of Human Glioma Xenografts with Second-Generation IL13R-Specific Chimeric Antigen Receptor–Modified T Cells. *Clin. Cancer Res.* 18:5949. doi:10.1158/1078-0432.CCR-12-0319.

Larkin, J., V. Chiarion-Sileni, R. Gonzalez, J.J. Grob, C.L. Cowey, C.D. Lao, D. Schadendorf, R. Dummer, M. Smylie, P. Rutkowski, P.F. Ferrucci, A. Hill, J. Wagstaff, M.S. Carlino, J.B. Haanen, M. Maio, I. Marquez-Rodas, G.A. McArthur, P.A. Ascierto, G.V. Long, M.K. Callahan, M.A. Postow, K. Grossmann, M. Sznol, B. Dreno, L. Bastholt, A. Yang, L.M. Rollin, C. Horak, F.S. Hodi, and J.D. Wolchok. 2015. Combined Nivolumab and Ipilimumab or Monotherapy in Untreated Melanoma. *N. Engl. J. Med.* 373:23–34. doi:10.1056/NEJMoa1504030.

Law, G.H.E., O.A. Gandelman, L.C. Tisi, C.R. Lowe, and J.A.H. Murray. 2006. Mutagenesis of solvent-exposed amino acids in *Photinus pyralis* luciferase improves thermostability and pH-tolerance. *Biochem. J.* 397:305–312. doi:10.1042/BJ20051847.

Lee, D.W., J.N. Kochenderfer, M. Stetler-Stevenson, Y.K. Cui, C. Delbrook, S.A. Feldman, T.J. Fry, R. Orentas, M. Sabatino, N.N. Shah, S.M. Steinberg, D. Stroncek, N. Tschernia, C. Yuan, H. Zhang, L. Zhang, S.A. Rosenberg, A.S. Wayne, and C.L. Mackall. 2015. T cells expressing CD19 chimeric antigen receptors for acute lymphoblastic leukaemia in children and young adults: A phase 1 dose-escalation trial. *The Lancet*. 385:517–528. doi:10.1016/S0140-6736(14)61403-3.

Lee, J., S. Kotliarova, Y. Kotliarov, A. Li, Q. Su, N.M. Donin, S. Pastorino, B.W. Purow, N. Christopher, W. Zhang, J.K. Park, and H.A. Fine. 2006. Tumor stem cells derived from glioblastomas cultured in bFGF and EGF more closely mirror the phenotype and genotype of primary tumors than do serum-cultured cell lines. *Cancer Cell*. 9:391–403. doi:10.1016/j.ccr.2006.03.030.

Lewis, P.W., M.M. Müller, M.S. Koletsky, F. Cordero, S. Lin, L.A. Banaszynski, B.A. Garcia, T.W. Muir, O.J. Becher, and C.D. Allis. 2013. Inhibition of PRC2 Activity by a Gain-of-Function H3 Mutation Found in Pediatric Glioblastoma. *Science*. 340:857–861. doi:10.1126/science.1232245.

Li, A., J. Walling, Y. Kotliarov, A. Center, M.E. Steed, S.J. Ahn, M. Rosenblum, T. Mikkelsen, J.C. Zenklusen, and H.A. Fine. 2008. Genomic Changes and Gene Expression Profiles Reveal That Established Glioma Cell Lines Are Poorly Representative of Primary Human Gliomas. *Mol. Cancer Res.* 6:21. doi:10.1158/1541-7786.MCR-07-0280.

Li, M.O., and A.Y. Rudensky. 2016. T cell receptor signalling in the control of regulatory T cell differentiation and function. *Nat Rev Immunol*. 16:220–233.

Lim, W.A., and C.H. June. 2017. The Principles of Engineering Immune Cells to Treat Cancer. *Cell*. 168:724–740. doi:10.1016/j.cell.2017.01.016.

Liu, W., A.L. Putnam, Z. Xu-yu, G.L. Szot, M.R. Lee, S. Zhu, P.A. Gottlieb, P. Kapranov, T.R. Gingeras, B.F. de St. Groth, C. Clayberger, D.M. Soper, S.F. Ziegler, and J.A. Bluestone. 2006. CD127 expression inversely correlates with FoxP3 and suppressive function of human $CD4^+$ T reg cells. *J. Exp. Med.* 203:1701. doi:10.1084/jem.20060772.

Liu, X., R. Ranganathan, S. Jiang, C. Fang, J. Sun, S. Kim, K. Newick, A. Lo, C.H. June, Y. Zhao, and E.K. Moon. 2016. A Chimeric Switch-Receptor Targeting PD1 Augments the Efficacy of Second-Generation CAR T Cells in Advanced Solid Tumors. *Cancer Res.* 76:1578. doi:10.1158/0008-5472.CAN-15-2524.

Long, A.H., W.M. Haso, J.F. Shern, K.M. Wanhainen, M. Murgai, M. Ingaramo, J.P. Smith, A.J. Walker, M.E. Kohler, V.R. Venkateshwara, R.N. Kaplan, G.H. Patterson, T.J. Fry, R.J. Orentas, and C.L. Mackall. 2015. 4-1BB costimulation ameliorates T cell exhaustion induced by tonic signaling of chimeric antigen receptors. *Nat Med*. 21:581–590.

Lopez, J.A., M.R. Jenkins, J.A. Rudd-Schmidt, A.J. Brennan, J.C. Danne, S.I. Mannering, J.A. Trapani, and I. Voskoboinik. 2013. Rapid and Unidirectional Perforin Pore Delivery at the Cytotoxic Immune Synapse. *J. Immunol.* 191:2328. doi:10.4049/jimmunol.1301205.

Lorimer, I.A.J., A. Keppler-Hafkemeyer, R.A. Beers, C.N. Pegram, D.D. Bigner, and I. Pastan. 1996. Recombinant immunotoxins specific for a mutant epidermal growth factor receptor: Targeting with a single chain

antibody variable domain isolated by phage display. *Proc. Natl. Acad. Sci.* 93:14815–14820.

Louis, C.U., B. Savoldo, G. Dotti, M. Pule, E. Yvon, G.D. Myers, C. Rossig, H.V. Russell, O. Diouf, E. Liu, H. Liu, M.-F. Wu, A.P. Gee, Z. Mei, C.M. Rooney, H.E. Heslop, and M.K. Brenner. 2011. Antitumor activity and long-term fate of chimeric antigen receptor–positive T cells in patients with neuroblastoma. *Blood*. 118:6050. doi:10.1182/blood-2011-05-354449.

Louis, D.N., A. Perry, G. Reifenberger, A. von Deimling, D. Figarella-Branger, W.K. Cavenee, H. Ohgaki, O.D. Wiestler, P. Kleihues, and D.W. Ellison. 2016. The 2016 World Health Organization Classification of Tumors of the Central Nervous System: a summary. *Acta Neuropathol. (Berl.)*. 131:803–820. doi:10.1007/s00401-016-1545-1.

Ludwig, K., and H.I. Kornblum. 2017. Molecular markers in glioma. *J. Neurooncol.* doi:10.1007/s11060-017-2379-y.

Maes, W., and S.W. Van Gool. 2011. Experimental immunotherapy for malignant glioma: lessons from two decades of research in the GL261 model. *Cancer Immunol. Immunother.* 60:153–160. doi:10.1007/s00262-010-0946-6.

Maher, J., R.J. Brentjens, G. Gunset, I. Riviere, and M. Sadelain. 2002. Human T-lymphocyte cytotoxicity and proliferation directed by a single chimeric TCR[zeta] /CD28 receptor. *Nat Biotech*. 20:70–75. doi:10.1038/nbt0102-70.

Malissen, B., and P. Bongrand. 2015. Early T Cell Activation: Integrating Biochemical, Structural, and Biophysical Cues. *Annu. Rev. Immunol.* 33:539–561. doi:10.1146/annurev-immunol-032414-112158.

Mantovani, A., S. Sozzani, M. Locati, P. Allavena, and A. Sica. 2002. Macrophage polarization: tumor-associated macrophages as a paradigm for polarized M2 mononuclear phagocytes. *Trends Immunol.* 23:549–555. doi:10.1016/S1471-4906(02)02302-5.

Mao, H., D.G. LeBrun, J. Yang, V.F. Zhu, and M. Li. 2012. Deregulated Signaling Pathways in Glioblastoma Multiforme: Molecular Mechanisms and Therapeutic Targets. *Cancer Invest.* 30:48–56. doi:10.3109/07357907.2011.630050.

Mathios, D., J.E. Kim, A. Mangraviti, J. Phallen, C.-K. Park, C.M. Jackson, T. Garzon-Muvdi, E. Kim, D. Theodros, M. Polanczyk, A.M. Martin, I. Suk, X. Ye, B. Tyler, C. Bettegowda, H. Brem, D.M. Pardoll, and M. Lim. 2016. Anti–PD-1 antitumor immunity is enhanced by local and abrogated by systemic chemotherapy in GBM. *Sci. Transl. Med.* 8:370ra180. doi:10.1126/scitranslmed.aag2942.

Maude, S.L., N. Frey, P.A. Shaw, R. Aplenc, D.M. Barrett, N.J. Bunin, A. Chew, V.E. Gonzalez, Z. Zheng, S.F. Lacey, Y.D. Mahnke, J.J. Melenhorst, S.R. Rheingold, A. Shen, D.T. Teachey, B.L. Levine, C.H. June, D.L.

Porter, and S.A. Grupp. 2014. Chimeric Antigen Receptor T Cells for Sustained Remissions in Leukemia. *N. Engl. J. Med.* 371:1507–1517. doi:10.1056/NEJMoa1407222.

Mead, K.I., Y. Zheng, C.N. Manzotti, L.C.A. Perry, M.K.P. Liu, F. Burke, D.J. Powner, M.J.O. Wakelam, and D.M. Sansom. 2005. Exocytosis of CTLA-4 Is Dependent on Phospholipase D and ADP Ribosylation Factor-1 and Stimulated during Activation of Regulatory T Cells. *J. Immunol.* 174:4803. doi:10.4049/jimmunol.174.8.4803.

MEEKER, T.C., R.A. MILLER, M.P. LINK, J. BINDL, R. WARNKE, and R. LEVY. 1984. A Unique Human B Lymphocyte Antigen Defined by a Monoclonal Antibody. *Hybridoma*. 3:305–320. doi:10.1089/hyb.1984.3.305.

Menger, L., A. Sledzinska, K. Bergerhoff, F.A. Vargas, J. Smith, L. Poirot, M. Pule, J. Herrero, K.S. Peggs, and S.A. Quezada. 2016. TALEN-Mediated Inactivation of PD-1 in Tumor-Reactive Lymphocytes Promotes Intratumoral T-cell Persistence and Rejection of Established Tumors. *Cancer Res.* 76:2087. doi:10.1158/0008-5472.CAN-15-3352.

Milone, M.C., J.D. Fish, C. Carpenito, R.G. Carroll, G.K. Binder, D. Teachey, M. Samanta, M. Lakhal, B. Gloss, G. Danet-Desnoyers, D. Campana, J.L. Riley, S.A. Grupp, and C.H. June. 2009. Chimeric Receptors Containing CD137 Signal Transduction Domains Mediate Enhanced Survival of T Cells and Increased Antileukemic Efficacy In Vivo. *Mol. Ther.* 17:1453–1464. doi:10.1038/mt.2009.83.

Moeller, M., N.M. Haynes, M.H. Kershaw, J.T. Jackson, M.W.L. Teng, S.E. Street, L. Cerutti, S.M. Jane, J.A. Trapani, M.J. Smyth, and P.K. Darcy. 2005. Adoptive transfer of gene-engineered $CD4^+$ helper T cells induces potent primary and secondary tumor rejection. *Blood*. 106:2995. doi:10.1182/blood-2004-12-4906.

Moeller, M., M.H. Kershaw, R. Cameron, J.A. Westwood, J.A. Trapani, M.J. Smyth, and P.K. Darcy. 2007. Sustained Antigen-Specific Antitumor Recall Response Mediated by Gene-Modified $CD4^+$ T Helper-1 and $CD8^+$ T Cells. *Cancer Res.* 67:11428. doi:10.1158/0008-5472.CAN-07-1141.

Moon, E.K., C. Carpenito, J. Sun, L.-C.S. Wang, V. Kapoor, J. Predina, D.J. Powell, J.L. Riley, C.H. June, and S.M. Albelda. 2011. Expression of a Functional CCR2 Receptor Enhances Tumor Localization and Tumor Eradication by Retargeted Human T cells Expressing a Mesothelin-Specific Chimeric Antibody Receptor. *Clin. Cancer Res.* 17:4719. doi:10.1158/1078-0432.CCR-11-0351.

Morgan, R.A., N. Chinnasamy, D.D. Abate-Daga, A. Gros, P.F. Robbins, Z. Zheng, S.A. Feldman, J.C. Yang, R.M. Sherry, G.Q. Phan, M.S. Hughes, U.S. Kammula, A.D. Miller, C.J. Hessman, A.A. Stewart, N.P. Restifo, M.M. Quezado, M. Alimchandani, A.Z. Rosenberg, A. Nath, T. Wang, B. Bielekova, S.C. Wuest, A. Nirmala, F.J. McMahon, S. Wilde,

B. Mosetter, D.J. Schendel, C.M. Laurencot, and S.A. Rosenberg. 2013. Cancer regression and neurologic toxicity following anti-MAGE-A3 TCR gene therapy. *J. Immunother. Hagerstown Md 1997*. 36:133–151. doi:10.1097/CJI.0b013e3182829903.

Morgan, R.A., M.E. Dudley, J.R. Wunderlich, M.S. Hughes, J.C. Yang, R.M. Sherry, R.E. Royal, S.L. Topalian, U.S. Kammula, N.P. Restifo, Z. Zheng, A. Nahvi, C.R. de Vries, L.J. Rogers-Freezer, S.A. Mavroukakis, and S.A. Rosenberg. 2006. Cancer Regression in Patients After Transfer of Genetically Engineered Lymphocytes. *Science*. 314:126. doi:10.1126/science.1129003.

Morgan, R.A., J.C. Yang, M. Kitano, M.E. Dudley, C.M. Laurencot, and S.A. Rosenberg. 2010. Case Report of a Serious Adverse Event Following the Administration of T Cells Transduced With a Chimeric Antigen Receptor Recognizing ERBB2. *Mol. Ther.* 18:843–851. doi:10.1038/mt.2010.24.

Motzer, R.J., B. Escudier, D.F. McDermott, S. George, H.J. Hammers, S. Srinivas, S.S. Tykodi, J.A. Sosman, G. Procopio, E.R. Plimack, D. Castellano, T.K. Choueiri, H. Gurney, F. Donskov, P. Bono, J. Wagstaff, T.C. Gauler, T. Ueda, Y. Tomita, F.A. Schutz, C. Kollmannsberger, J. Larkin, A. Ravaud, J.S. Simon, L.-A. Xu, I.M. Waxman, and P. Sharma. 2015. Nivolumab versus Everolimus in Advanced Renal-Cell Carcinoma. *N. Engl. J. Med.* 373:1803–1813. doi:10.1056/NEJMoa1510665.

Narita, Y., M. Nagane, K. Mishima, H.-J.S. Huang, F.B. Furnari, and W.K. Cavenee. 2002. Mutant Epidermal Growth Factor Receptor Signaling Down-Regulates p27 through Activation of the Phosphatidylinositol 3-Kinase/Akt Pathway in Glioblastomas. *Cancer Res.* 62:6764.

Nduom, E.K., J. Wei, N.K. Yaghi, N. Huang, L.-Y. Kong, K. Gabrusiewicz, X. Ling, S. Zhou, C. Ivan, J.Q. Chen, J.K. Burks, G.N. Fuller, G.A. Calin, C.A. Conrad, C. Creasy, K. Ritthipichai, L. Radvanyi, and A.B. Heimberger. 2016. PD-L1 expression and prognostic impact in glioblastoma. *Neuro-Oncol.* 18:195–205. doi:10.1093/neuonc/nov172.

Neyns, B., J. Sadones, E. Joosens, F. Bouttens, L. Verbeke, J.-F. Baurain, L. D'Hondt, T. Strauven, C. Chaskis, P. In't Veld, A. Michotte, and J. De Greve. 2009. Stratified phase II trial of cetuximab in patients with recurrent high-grade glioma. *Ann. Oncol.* 20:1596–1603. doi:10.1093/annonc/mdp032.

Noushmehr, H., D.J. Weisenberger, K. Diefes, H.S. Phillips, K. Pujara, B.P. Berman, F. Pan, C.E. Pelloski, E.P. Sulman, K.P. Bhat, R.G.W. Verhaak, K.A. Hoadley, D.N. Hayes, C.M. Perou, H.K. Schmidt, L. Ding, R.K. Wilson, D. Van Den Berg, H. Shen, H. Bengtsson, P. Neuvial, L.M. Cope, J. Buckley, J.G. Herman, S.B. Baylin, P.W. Laird, and K. Aldape. Identification of a CpG Island Methylator Phenotype that Defines a Distinct Subgroup of Glioma. *Cancer Cell*. 17:510–522. doi:10.1016/j.ccr.2010.03.017.

Ochiai, H., G.E. Archer, J.E. Herndon, C.-T. Kuan, D.A. Mitchell, D.D. Bigner, I.H. Pastan, and J.H. Sampson. 2008. EGFRvIII-targeted immunotoxin induces antitumor immunity that is inhibited in the absence of CD4+ and CD8+ T cells. *Cancer Immunol. Immunother.* 57:115–121. doi:10.1007/s00262-007-0363-7.

Oh, T., S. Fakurnejad, E.T. Sayegh, A.J. Clark, M.E. Ivan, M.Z. Sun, M. Safaee, O. Bloch, C.D. James, and A.T. Parsa. 2014. Immunocompetent murine models for the study of glioblastoma immunotherapy. *J. Transl. Med.* 12:107–107. doi:10.1186/1479-5876-12-107.

Osswald, M., E. Jung, F. Sahm, G. Solecki, V. Venkataramani, J. Blaes, S. Weil, H. Horstmann, B. Wiestler, M. Syed, L. Huang, M. Ratliff, K. Karimian Jazi, F.T. Kurz, T. Schmenger, D. Lemke, M. Gömmel, M. Pauli, Y. Liao, P. Häring, S. Pusch, V. Herl, C. Steinhäuser, D. Krunic, M. Jarahian, H. Miletic, A.S. Berghoff, O. Griesbeck, G. Kalamakis, O. Garaschuk, M. Preusser, S. Weiss, H. Liu, S. Heiland, M. Platten, P.E. Huber, T. Kuner, A. von Deimling, W. Wick, and F. Winkler. 2015. Brain tumour cells interconnect to a functional and resistant network. *Nature*. doi:10.1038/nature16071.

Ousman, S.S., and P. Kubes. 2012. Immune surveillance in the central nervous system. *Nat Neurosci*. 15:1096–1101.

Park, T.-J., K. Boyd, and T. Curran. 2006. Cardiovascular and Craniofacial Defects in Crk-Null Mice. *Mol. Cell. Biol.* 26:6272–6282. doi:10.1128/MCB.00472-06.

Parkhurst, M.R., J.C. Yang, R.C. Langan, M.E. Dudley, D.-A.N. Nathan, S.A. Feldman, J.L. Davis, R.A. Morgan, M.J. Merino, R.M. Sherry, M.S. Hughes, U.S. Kammula, G.Q. Phan, R.M. Lim, S.A. Wank, N.P. Restifo, P.F. Robbins, C.M. Laurencot, and S.A. Rosenberg. 2011. T Cells Targeting Carcinoembryonic Antigen Can Mediate Regression of Metastatic Colorectal Cancer but Induce Severe Transient Colitis. *Mol. Ther.* 19:620–626. doi:10.1038/mt.2010.272.

Pegram, H.J., J.C. Lee, E.G. Hayman, G.H. Imperato, T.F. Tedder, M. Sadelain, and R.J. Brentjens. 2012. Tumor-targeted T cells modified to secrete IL-12 eradicate systemic tumors without need for prior conditioning. *Blood*. 119:4133. doi:10.1182/blood-2011-12-400044.

Peng, W., C. Liu, C. Xu, Y. Lou, J. Chen, Y. Yang, H. Yagita, W.W. Overwijk, G. Lizee, L. Radvanyi, and P. Hwu. 2012. PD-1 Blockade Enhances T-cell Migration to Tumors by Elevating IFN- Inducible Chemokines. *Cancer Res.* 72:5209–5218. doi:10.1158/0008-5472.CAN-12-1187.

Pollard, S.M., K. Yoshikawa, I.D. Clarke, D. Danovi, S. Stricker, R. Russell, J. Bayani, R. Head, M. Lee, M. Bernstein, J.A. Squire, A. Smith, and P. Dirks. 2009. Glioma Stem Cell Lines Expanded in Adherent Culture Have Tumor-Specific Phenotypes and Are Suitable for Chemical and

Genetic Screens. *Cell Stem Cell*. 4:568–580. doi:10.1016/j.stem.2009.03.014.

Porter, D.L., W.-T. Hwang, N.V. Frey, S.F. Lacey, P.A. Shaw, A.W. Loren, A. Bagg, K.T. Marcucci, A. Shen, V. Gonzalez, D. Ambrose, S.A. Grupp, A. Chew, Z. Zheng, M.C. Milone, B.L. Levine, J.J. Melenhorst, and C.H. June. 2015. Chimeric antigen receptor T cells persist and induce sustained remissions in relapsed refractory chronic lymphocytic leukemia. *Sci. Transl. Med.* 7:303ra139. doi:10.1126/scitranslmed.aac5415.

Porter, D.L., B.L. Levine, M. Kalos, A. Bagg, and C.H. June. 2011. Chimeric Antigen Receptor–Modified T Cells in Chronic Lymphoid Leukemia. *N. Engl. J. Med.* 365:725–733. doi:10.1056/NEJMoa1103849.

Porter, K.R., B.J. McCarthy, S. Freels, Y. Kim, and F.G. Davis. 2010. Prevalence estimates for primary brain tumors in the United States by age, gender, behavior, and histology. *Neuro-Oncol.* 12:520–527. doi:10.1093/neuonc/nop066.

Preusser, M., M. Lim, D.A. Hafler, D.A. Reardon, and J.H. Sampson. 2015. Prospects of immune checkpoint modulators in the treatment of glioblastoma. *Nat Rev Neurol*. 11:504–514.

Pule, M.A., B. Savoldo, G.D. Myers, C. Rossig, H.V. Russell, G. Dotti, M.H. Huls, E. Liu, A.P. Gee, Z. Mei, E. Yvon, H.L. Weiss, H. Liu, C.M. Rooney, H.E. Heslop, and M.K. Brenner. 2008. Virus-specific T cells engineered to coexpress tumor-specific receptors: persistence and antitumor activity in individuals with neuroblastoma. *Nat Med*. 14:1264–1270. doi:10.1038/nm.1882.

Pulè, M.A., K.C. Straathof, G. Dotti, H.E. Heslop, C.M. Rooney, and M.K. Brenner. 2005. A chimeric T cell antigen receptor that augments cytokine release and supports clonal expansion of primary human T cells. *Mol. Ther.* 12:933–941. doi:10.1016/j.ymthe.2005.04.016.

Quail, D.F., and J.A. Joyce. 2017. The Microenvironmental Landscape of Brain Tumors. *Cancer Cell*. 31:326–341. doi:10.1016/j.ccell.2017.02.009.

Qureshi, O.S., Y. Zheng, K. Nakamura, K. Attridge, C. Manzotti, E.M. Schmidt, J. Baker, L.E. Jeffery, S. Kaur, Z. Briggs, and others. 2011. Trans-endocytosis of CD80 and CD86: a molecular basis for the cell-extrinsic function of CTLA-4. *Science*. 332:600–603.

Radtke, F., N. Fasnacht, and H.R. MacDonald. 2010. Notch Signaling in the Immune System. *Immunity*. 32:14–27. doi:10.1016/j.immuni.2010.01.004.

Ransohoff, R.M., and B. Engelhardt. 2012. The anatomical and cellular basis of immune surveillance in the central nervous system. *Nat Rev Immunol*. 12:623–635. doi:10.1038/nri3265.

Ren, J., X. Liu, C. Fang, S. Jiang, C.H. June, and Y. Zhao. 2017. Multiplex Genome Editing to Generate Universal CAR T Cells Resistant to PD1 Inhibition. *Clin. Cancer Res.* 23:2255. doi:10.1158/1078-0432.CCR-16-1300.

Restifo, N.P., M.E. Dudley, and S.A. Rosenberg. 2012. Adoptive immunotherapy for cancer: harnessing the T cell response. *Nat Rev Immunol*. 12:269–281. doi:10.1038/nri3191.

Restifo, N.P., and L. Gattinoni. 2013. Lineage relationship of effector and memory T cells. *Curr. Opin. Immunol.* 25:556–563. doi:10.1016/j.coi.2013.09.003.

Ribas, A., R. Kefford, M.A. Marshall, C.J.A. Punt, J.B. Haanen, M. Marmol, C. Garbe, H. Gogas, J. Schachter, G. Linette, P. Lorigan, K.L. Kendra, M. Maio, U. Trefzer, M. Smylie, G.A. McArthur, B. Dreno, P.D. Nathan, J. Mackiewicz, J.M. Kirkwood, J. Gomez-Navarro, B. Huang, D. Pavlov, and A. Hauschild. 2013. Phase III Randomized Clinical Trial Comparing Tremelimumab With Standard-of-Care Chemotherapy in Patients With Advanced Melanoma. *J. Clin. Oncol.* 31:616–622. doi:10.1200/JCO.2012.44.6112.

Riley, J.L. 2009. PD-1 signaling in primary T cells. *Immunol. Rev.* 229:114–125. doi:10.1111/j.1600-065X.2009.00767.x.

Robbins, P.F., R.A. Morgan, S.A. Feldman, J.C. Yang, R.M. Sherry, M.E. Dudley, J.R. Wunderlich, A.V. Nahvi, L.J. Helman, C.L. Mackall, U.S. Kammula, M.S. Hughes, N.P. Restifo, M. Raffeld, C.-C.R. Lee, C.L. Levy, Y.F. Li, M. El-Gamil, S.L. Schwarz, C. Laurencot, and S.A. Rosenberg. 2011. Tumor Regression in Patients With Metastatic Synovial Cell Sarcoma and Melanoma Using Genetically Engineered Lymphocytes Reactive With NY-ESO-1. *J. Clin. Oncol.* 29:917–924. doi:10.1200/JCO.2010.32.2537.

Rosenberg, S.A., J.C. Yang, R.M. Sherry, U.S. Kammula, M.S. Hughes, G.Q. Phan, D.E. Citrin, N.P. Restifo, P.F. Robbins, J.R. Wunderlich, K.E. Morton, C.M. Laurencot, S.M. Steinberg, D.E. White, and M.E. Dudley. 2011. Durable Complete Responses in Heavily Pretreated Patients with Metastatic Melanoma Using T-Cell Transfer Immunotherapy. *Clin. Cancer Res.* 17:4550. doi:10.1158/1078-0432.CCR-11-0116.

Rossig, C., M. Pule, B. Altvater, S. Saiagh, G. Wright, S. Ghorashian, L. Clifton-Hadley, K. Champion, Z. Sattar, B. Popova, A. Hackshaw, P. Smith, T. Roberts, E. Biagi, B. Dreno, R. Rousseau, S. Kailayangiri, M. Ahlmann, R. Hough, B. Kremens, M.G. Sauer, P. Veys, N. Goulden, M. Cummins, and P.J. Amrolia. 2017. Vaccination to improve the persistence of CD19CAR gene-modified T cells in relapsed pediatric acute lymphoblastic leukemia. *Leukemia*. 31:1087–1095.

Sakaguchi, S., M. Miyara, C.M. Costantino, and D.A. Hafler. 2010. FOXP3+ regulatory T cells in the human immune system. *Nat. Rev. Immunol.* 10:490–500. doi:10.1038/nri2785.

Sampson, J.H., K.D. Aldape, G.E. Archer, A. Coan, A. Desjardins, A.H. Friedman, H.S. Friedman, M.R. Gilbert, J.E. Herndon, R.E. McLendon, D.A. Mitchell, D.A. Reardon, R. Sawaya, R. Schmittling, W. Shi, J.J. Vredenburgh, D.D. Bigner, and A.B. Heimberger. 2011. Greater chemotherapy-induced lymphopenia enhances tumor-specific immune responses that eliminate EGFRvIII-expressing tumor cells in patients with glioblastoma. *Neuro-Oncol.* 13:324–333. doi:10.1093/neuonc/noq157.

Sampson, J.H., B.D. Choi, L. Sanchez-Perez, C.M. Suryadevara, D.J. Snyder, C.T. Flores, R.J. Schmittling, S.K. Nair, E.A. Reap, P.K. Norberg, J.E. Herndon, C.-T. Kuan, R.A. Morgan, S.A. Rosenberg, and L.A. Johnson. 2014. EGFRvIII mCAR-Modified T-Cell Therapy Cures Mice with Established Intracerebral Glioma and Generates Host Immunity against Tumor-Antigen Loss. *Clin. Cancer Res.* 20:972. doi:10.1158/1078-0432.CCR-13-0709.

Sampson, J.H., A.B. Heimberger, G.E. Archer, K.D. Aldape, A.H. Friedman, H.S. Friedman, M.R. Gilbert, J.E. Herndon, R.E. McLendon, D.A. Mitchell, D.A. Reardon, R. Sawaya, R.J. Schmittling, W. Shi, J.J. Vredenburgh, and D.D. Bigner. 2010. Immunologic Escape After Prolonged Progression-Free Survival With Epidermal Growth Factor Receptor Variant III Peptide Vaccination in Patients With Newly Diagnosed Glioblastoma. *J. Clin. Oncol.* 28:4722–4729. doi:10.1200/JCO.2010.28.6963.

Savoldo, B., C.A. Ramos, E. Liu, M.P. Mims, M.J. Keating, G. Carrum, R.T. Kamble, C.M. Bollard, A.P. Gee, Z. Mei, H. Liu, B. Grilley, C.M. Rooney, H.E. Heslop, M.K. Brenner, and G. Dotti. 2011. CD28 costimulation improves expansion and persistence of chimeric antigen receptor–modified T cells in lymphoma patients. *J. Clin. Invest.* 121:1822–1826. doi:10.1172/JCI46110.

Schatz, D.G., M.A. Oettinger, and M.S. Schlissel. 1992. V(D)J Recombination: Molecular Biology and Regulation. *Annu. Rev. Immunol.* 10:359–383. doi:10.1146/annurev.iy.10.040192.002043.

Scholler, J., T.L. Brady, G. Binder-Scholl, W.-T. Hwang, G. Plesa, K.M. Hege, A.N. Vogel, M. Kalos, J.L. Riley, S.G. Deeks, R.T. Mitsuyasu, W.B. Bernstein, N.E. Aronson, B.L. Levine, F.D. Bushman, and C.H. June. 2012. Decade-Long Safety and Function of Retroviral-Modified Chimeric Antigen Receptor T Cells. *Sci. Transl. Med.* 4:132ra53. doi:10.1126/scitranslmed.3003761.

Schumacher, T., L. Bunse, S. Pusch, F. Sahm, B. Wiestler, J. Quandt, O. Menn, M. Osswald, I. Oezen, M. Ott, M. Keil, J. Balsz, K. Rauschenbach, A.K. Grabowska, I. Vogler, J. Diekmann, N. Trautwein, S.B. Eichmuller, J. Okun, S. Stevanovic, A.B. Riemer, U. Sahin, M.A. Friese, P. Beckhove, A. von Deimling, W. Wick, and M. Platten. 2014. A vaccine targeting mutant IDH1 induces antitumour immunity. *Nature*. 512:324–327.

Schwartzentruber, J., A. Korshunov, X.-Y. Liu, D.T.W. Jones, E. Pfaff, K. Jacob, D. Sturm, A.M. Fontebasso, D.-A.K. Quang, M. Tonjes, V. Hovestadt, S. Albrecht, M. Kool, A. Nantel, C. Konermann, A. Lindroth, N. Jager, T. Rausch, M. Ryzhova, J.O. Korbel, T. Hielscher, P. Hauser, M. Garami, A. Klekner, L. Bognar, M. Ebinger, M.U. Schuhmann, W. Scheurlen, A. Pekrun, M.C. Fruhwald, W. Roggendorf, C. Kramm, M. Durken, J. Atkinson, P. Lepage, A. Montpetit, M. Zakrzewska, K. Zakrzewski, P.P. Liberski, Z. Dong, P. Siegel, A.E. Kulozik, M. Zapatka, A. Guha, D. Malkin, J. Felsberg, G. Reifenberger, A. von Deimling, K. Ichimura, V.P. Collins, H. Witt, T. Milde, O. Witt, C. Zhang, P. Castelo-Branco, P. Lichter, D. Faury, U. Tabori, C. Plass, J. Majewski, S.M. Pfister, and N. Jabado. 2012. Driver mutations in histone H3.3 and chromatin remodelling genes in paediatric glioblastoma. *Nature*. 482:226–231. doi:10.1038/nature10833.

Seddiki, N., B. Santner-Nanan, J. Martinson, J. Zaunders, S. Sasson, A. Landay, M. Solomon, W. Selby, S.I. Alexander, R. Nanan, A. Kelleher, and B.F. de St. Groth. 2006. Expression of interleukin (IL)-2 and IL-7 receptors discriminates between human regulatory and activated T cells. *J. Exp. Med.* 203:1693. doi:10.1084/jem.20060468.

Sehrawat, S., P.B.J. Reddy, N. Rajasagi, A. Suryawanshi, M. Hirashima, and B.T. Rouse. 2010. Galectin-9/TIM-3 Interaction Regulates Virus-Specific Primary and Memory CD8+ T Cell Response. *PLOS Pathog.* 6:e1000882. doi:10.1371/journal.ppat.1000882.

Seliger, B., U. Wollscheid, F. Momburg, T. Blankenstein, and C. Huber. 2001. Characterization of the Major Histocompatibility Complex Class I Deficiencies in B16 Melanoma Cells. *Cancer Res.* 61:1095.

Seligman, A.M., M.J. Shear, and L. Alexander. 1939. Studies in carcinogenesis: VIII. Experimental production of brain tumors in mice with methylcholanthrene. *Am. J. Cancer*. 37:364–395.

Simpson, T.R., F. Li, W. Montalvo-Ortiz, M.A. Sepulveda, K. Bergerhoff, F. Arce, C. Roddie, J.Y. Henry, H. Yagita, J.D. Wolchok, K.S. Peggs, J.V. Ravetch, J.P. Allison, and S.A. Quezada. 2013. Fc-dependent depletion of tumor-infiltrating regulatory T cells co-defines the efficacy of anti–CTLA-4 therapy against melanoma. *J. Exp. Med.* 210:1695. doi:10.1084/jem.20130579.

Śledzińska, A., L. Menger, K. Bergerhoff, K.S. Peggs, and S.A. Quezada. 2015. Negative immune checkpoints on T lymphocytes and their relevance to cancer immunotherapy. *Cancer Immunother.* 9:1936–1965. doi:10.1016/j.molonc.2015.10.008.

Smith-Garvin, J.E., G.A. Koretzky, and M.S. Jordan. 2009. T Cell Activation. *Annu. Rev. Immunol.* 27:591–619. doi:10.1146/annurev.immunol.021908.132706.

So, T., J. Song, K. Sugie, A. Altman, and M. Croft. 2006. Signals from OX40 regulate nuclear factor of activated T cells c1 and T cell helper 2 lineage

commitment. *Proc. Natl. Acad. Sci. U. S. A.* 103:3740–3745. doi:10.1073/pnas.0600205103.

Sommermeyer, D., M. Hudecek, P.L. Kosasih, T. Gogishvili, D.G. Maloney, C.J. Turtle, and S.R. Riddell. 2016. Chimeric antigen receptor-modified T cells derived from defined CD8+ and CD4+ subsets confer superior antitumor reactivity in vivo. *Leukemia*. 30:492–500.

Song, J., T. So, M. Cheng, X. Tang, and M. Croft. 2005. Sustained Survivin Expression from OX40 Costimulatory Signals Drives T Cell Clonal Expansion. *Immunity*. 22:621–631. doi:10.1016/j.immuni.2005.03.012.

Sottoriva, A., I. Spiteri, S.G.M. Piccirillo, A. Touloumis, V.P. Collins, J.C. Marioni, C. Curtis, C. Watts, and S. Tavaré. 2013. Intratumor heterogeneity in human glioblastoma reflects cancer evolutionary dynamics. *Proc. Natl. Acad. Sci.* 110:4009–4014. doi:10.1073/pnas.1219747110.

Stupp, R., W.P. Mason, M.J. van den Bent, M. Weller, B. Fisher, M.J.B. Taphoorn, K. Belanger, A.A. Brandes, C. Marosi, U. Bogdahn, J. Curschmann, R.C. Janzer, S.K. Ludwin, T. Gorlia, A. Allgeier, D. Lacombe, J.G. Cairncross, E. Eisenhauer, and R.O. Mirimanoff. 2005. Radiotherapy plus Concomitant and Adjuvant Temozolomide for Glioblastoma. *N. Engl. J. Med.* 352:987–996. doi:10.1056/NEJMoa043330.

Stylli, S.S., R.B. Luwor, T.M.B. Ware, F. Tan, and A.H. Kaye. 2015. Mouse models of glioma. *J. Clin. Neurosci.* 22:619–626. doi:10.1016/j.jocn.2014.10.013.

Suarez, E.R., D.-K. Chang, J. Sun, J. Sui, G.J. Freeman, S. Signoretti, Q. Zhu, and W.A. Marasco. 2016. Chimeric antigen receptor T cells secreting anti-PD-L1 antibodies more effectively regress renal cell carcinoma in a humanized mouse model. *Oncotarget*. 7:34341.

Szatmári, T., K. Lumniczky, S. Désaknai, S. Trajcevski, E.J. Hídvégi, H. Hamada, and G. Sáfrány. 2006. Detailed characterization of the mouse glioma 261 tumor model for experimental glioblastoma therapy. *Cancer Sci.* 97:546–553. doi:10.1111/j.1349-7006.2006.00208.x.

Sznol, M., and L. Chen. 2013. Antagonist Antibodies to PD-1 and B7-H1 (PD-L1) in the Treatment of Advanced Human Cancer. *Clin. Cancer Res.* 19:1021. doi:10.1158/1078-0432.CCR-12-2063.

Szymczak, A.L., C.J. Workman, Y. Wang, K.M. Vignali, S. Dilioglou, E.F. Vanin, and D.A.A. Vignali. 2004. Correction of multi-gene deficiency in vivo using a single “self-cleaving” 2A peptide-based retroviral vector. *Nat Biotech*. 22:589–594. doi:10.1038/nbt957.

Tai, X., F. Van Laethem, L. Pobezinsky, T. Guinter, S.O. Sharrow, A. Adams, L. Granger, M. Kruhlak, T. Lindsten, C.B. Thompson, L. Feigenbaum, and A. Singer. 2012. Basis of CTLA-4 function in regulatory and

conventional CD4$^+$ T cells. *Blood*. 119:5155. doi:10.1182/blood-2011-11-388918.

Takaba, H., Y. Morishita, Y. Tomofuji, L. Danks, T. Nitta, N. Komatsu, T. Kodama, and H. Takayanagi. 2015. Fezf2 Orchestrates a Thymic Program of Self-Antigen Expression for Immune Tolerance. *Cell*. 163:975–987. doi:10.1016/j.cell.2015.10.013.

Till, B.G., M.C. Jensen, J. Wang, X. Qian, A.K. Gopal, D.G. Maloney, C.G. Lindgren, Y. Lin, J.M. Pagel, L.E. Budde, A. Raubitschek, S.J. Forman, P.D. Greenberg, S.R. Riddell, and O.W. Press. 2012. CD20-specific adoptive immunotherapy for lymphoma using a chimeric antigen receptor with both CD28 and 4-1BB domains: pilot clinical trial results. *Blood*. 119:3940. doi:10.1182/blood-2011-10-387969.

Topalian, S.L., C.G. Drake, and D.M. Pardoll. 2015. Immune Checkpoint Blockade: A Common Denominator Approach to Cancer Therapy. *Cancer Cell*. 27:450–461. doi:10.1016/j.ccell.2015.03.001.

Träger, U., S. Sierro, G. Djordjevic, B. Bouzo, S. Khandwala, A. Meloni, M. Mortensen, and A.K. Simon. 2012. The Immune Response to Melanoma Is Limited by Thymic Selection of Self-Antigens. *PLOS ONE*. 7:e35005. doi:10.1371/journal.pone.0035005.

Trapani, J.A., and M.J. Smyth. 2002. Functional significance of the perforin/granzyme cell death pathway. *Nat Rev Immunol*. 2:735–747. doi:10.1038/nri911.

Triebel, F., S. Jitsukawa, E. Baixeras, S. Roman-Roman, C. Genevee, E. Viegas-Pequignot, and T. Hercend. 1990. LAG-3, a novel lymphocyte activation gene closely related to CD4. *J. Exp. Med.* 171:1393. doi:10.1084/jem.171.5.1393.

Tumeh, P.C., C.L. Harview, J.H. Yearley, I.P. Shintaku, E.J.M. Taylor, L. Robert, B. Chmielowski, M. Spasic, G. Henry, V. Ciobanu, A.N. West, M. Carmona, C. Kivork, E. Seja, G. Cherry, A.J. Gutierrez, T.R. Grogan, C. Mateus, G. Tomasic, J.A. Glaspy, R.O. Emerson, H. Robins, R.H. Pierce, D.A. Elashoff, C. Robert, and A. Ribas. 2014. PD-1 blockade induces responses by inhibiting adaptive immune resistance. *Nature*. 515:568–571. doi:10.1038/nature13954.

Turtle, C.J., L.-A. Hanafi, C. Berger, M. Hudecek, B. Pender, E. Robinson, R. Hawkins, C. Chaney, S. Cherian, X. Chen, L. Soma, B. Wood, D. Li, S. Heimfeld, S.R. Riddell, and D.G. Maloney. 2016. Immunotherapy of non-Hodgkin's lymphoma with a defined ratio of CD8$^+$ and CD4$^+$ CD19-specific chimeric antigen receptor–modified T cells. *Sci. Transl. Med.* 8:355ra116. doi:10.1126/scitranslmed.aaf8621.

Vibhakar, R., G. Juan, F. Traganos, Z. Darzynkiewicz, and L.R. Finger. 1997. Activation-Induced Expression of Human Programmed Death-1 Gene in T-Lymphocytes. *Exp. Cell Res.* 232:25–28. doi:10.1006/excr.1997.3493.

Vlahovic, G., P.E. Fecci, D. Reardon, and J.H. Sampson. 2015. Programmed death ligand 1 (PD-L1) as an immunotherapy target in patients with glioblastoma. *Neuro-Oncol.* 17:1043–1045. doi:10.1093/neuonc/nov071.

Wainwright, D.A., A.L. Chang, M. Dey, I.V. Balyasnikova, C.K. Kim, A. Tobias, Y. Cheng, J.W. Kim, J. Qiao, L. Zhang, Y. Han, and M.S. Lesniak. 2014. Durable Therapeutic Efficacy Utilizing Combinatorial Blockade against IDO, CTLA-4, and PD-L1 in Mice with Brain Tumors. *Clin. Cancer Res.* 20:5290. doi:10.1158/1078-0432.CCR-14-0514.

Wan, Y.Y., and R.A. Flavell. 2009. How Diverse—CD4 Effector T Cells and their Functions. *J. Mol. Cell Biol.* 1:20–36. doi:10.1093/jmcb/mjp001.

Wang, X., and I. Rivière. 2016. Clinical manufacturing of CAR T cells: foundation of a promising therapy. *Mol. Ther. - Oncolytics*. 3:16015. doi:10.1038/mto.2016.15.

Watts, T.H. 2005. TNF/TNFR FAMILY MEMBERS IN COSTIMULATION OF T CELL RESPONSES. *Annu. Rev. Immunol.* 23:23–68. doi:10.1146/annurev.immunol.23.021704.115839.

Weller, M., N. Butowski, D. Tran, L. Recht, M. Lim, H. Hirte, L. Ashby, L. Mechtler, S. Goldlust, F. Iwamoto, J. Drappatz, D. O'Rourke, M. Wong, G. Finocchiaro, J. Perry, W. Wick, Y. He, T. Davis, R. Stupp, and J. Sampson. 2016. ATIM-03. ACT IV: AN INTERNATIONAL, DOUBLE-BLIND, PHASE 3 TRIAL OF RINDOPEPIMUT IN NEWLY DIAGNOSED, EGFRvIII-EXPRESSING GLIOBLASTOMA. *Neuro-Oncol.* 18:vi17-vi18. doi:10.1093/neuonc/now212.068.

Wherry, E.J., S.-J. Ha, S.M. Kaech, W.N. Haining, S. Sarkar, V. Kalia, S. Subramaniam, J.N. Blattman, D.L. Barber, and R. Ahmed. 2007. Molecular Signature of CD8+ T Cell Exhaustion during Chronic Viral Infection. *Immunity*. 27:670–684. doi:10.1016/j.immuni.2007.09.006.

Wildin, R.S., F. Ramsdell, J. Peake, F. Faravelli, J.-L. Casanova, N. Buist, E. Levy-Lahad, M. Mazzella, O. Goulet, L. Perroni, F. Dagna Bricarelli, G. Byrne, M. McEuen, S. Proll, M. Appleby, and M.E. Brunkow. 2001. X-linked neonatal diabetes mellitus, enteropathy and endocrinopathy syndrome is the human equivalent of mouse scurfy. *Nat Genet*. 27:18–20. doi:10.1038/83707.

Willoughby, J., J. Griffiths, I. Tews, and M.S. Cragg. 2017. OX40: Structure and function – What questions remain? *Mol. Immunol.* 83:13–22. doi:10.1016/j.molimm.2017.01.006.

de Witte, M.A., A. Jorritsma, A. Kaiser, M.D. van den Boom, M. Dokter, G.M. Bendle, J.B.A.G. Haanen, and T.N.M. Schumacher. 2008. Requirements for Effective Antitumor Responses of TCR Transduced T Cells. *J. Immunol.* 181:5128–5136. doi:10.4049/jimmunol.181.7.5128.

Workman, C.J., K.J. Dugger, and D.A.A. Vignali. 2002. Cutting Edge: Molecular Analysis of the Negative Regulatory Function of Lymphocyte

Activation Gene-3. *J. Immunol.* 169:5392. doi:10.4049/jimmunol.169.10.5392.

Workman, C.J., and D.A.A. Vignali. 2005. Negative Regulation of T Cell Homeostasis by Lymphocyte Activation Gene-3 (CD223). *J. Immunol.* 174:688. doi:10.4049/jimmunol.174.2.688.

Wu, G., A. Broniscer, T.A. McEachron, C. Lu, B.S. Paugh, J. Becksfort, C. Qu, L. Ding, R. Huether, M. Parker, J. Zhang, A. Gajjar, M.A. Dyer, C.G. Mullighan, R.J. Gilbertson, E.R. Mardis, R.K. Wilson, J.R. Downing, D.W. Ellison, J. Zhang, and S.J. Baker. 2012. Somatic histone H3 alterations in pediatric diffuse intrinsic pontine gliomas and non-brainstem glioblastomas. *Nat. Genet.* 44:251–253. doi:10.1038/ng.1102.

Yin, Y., X.X. Wang, and R.A. Mariuzza. 2012. Crystal structure of a complete ternary complex of T-cell receptor, peptide–MHC, and CD4. *Proc. Natl. Acad. Sci.* 109:5405–5410. doi:10.1073/pnas.1118801109.

Youngblood, B., J.S. Hale, and R. Ahmed. 2013. T-cell memory differentiation: insights from transcriptional signatures and epigenetics. *Immunology*. 139:277–284. doi:10.1111/imm.12074.

Yu, H., E. Sotillo, C. Harrington, G. Wertheim, M. Paessler, S.L. Maude, S.R. Rheingold, S.A. Grupp, A. Thomas-Tikhonenko, and V. Pillai. 2017. Repeated loss of target surface antigen after immunotherapy in primary mediastinal large B cell lymphoma. *Am. J. Hematol.* 92:E11–E13. doi:10.1002/ajh.24594.

Yu, X., K. Harden, L. C Gonzalez, M. Francesco, E. Chiang, B. Irving, I. Tom, S. Ivelja, C.J. Refino, H. Clark, D. Eaton, and J.L. Grogan. 2009. The surface protein TIGIT suppresses T cell activation by promoting the generation of mature immunoregulatory dendritic cells. *Nat Immunol*. 10:48–57. doi:10.1038/ni.1674.

Zagzag, D., D.C. Miller, L. Chiriboga, H. Yee, and E.W. Newcomb. 2003. Green Fluorescent Protein Immunohistochemistry as a Novel Experimental Tool for the Detection of Glioma Cell Invasion In Vivo. *Brain Pathol.* 13:34–37. doi:10.1111/j.1750-3639.2003.tb00004.x.

Zambrano-Zaragoza, J.F., E.J. Romo-Martínez, M. de J. Durán-Avelar, N. García-Magallanes, and N. Vibanco-Pérez. 2014. Th17 Cells in Autoimmune and Infectious Diseases. *Int. J. Inflamm.* 2014:651503. doi:10.1155/2014/651503.

Zeng, J., A.P. See, J. Phallen, C.M. Jackson, Z. Belcaid, J. Ruzevick, N. Durham, C. Meyer, T.J. Harris, E. Albesiano, G. Pradilla, E. Ford, J. Wong, H.-J. Hammers, D. Mathios, B. Tyler, H. Brem, P.T. Tran, D. Pardoll, C.G. Drake, and M. Lim. 2013. Anti-PD-1 Blockade and Stereotactic Radiation Produce Long-Term Survival in Mice With Intracranial Gliomas. *Int. J. Radiat. Oncol.* 86:343–349. doi:10.1016/j.ijrobp.2012.12.025.

Zhao, Z., M. Condomines, S.J.C. van der Stegen, F. Perna, C.C. Kloss, G. Gunset, J. Plotkin, and M. Sadelain. 2015. Structural Design of Engineered Costimulation Determines Tumor Rejection Kinetics and Persistence of CAR T Cells. *Cancer Cell*. 28:415–428. doi:10.1016/j.ccell.2015.09.004.

Zhong, X.-S., M. Matsushita, J. Plotkin, I. Riviere, and M. Sadelain. 2010. Chimeric Antigen Receptors Combining 4-1BB and CD28 Signaling Domains Augment PI3kinase/AKT/Bcl-XL Activation and CD8+ T Cell–mediated Tumor Eradication. *Mol. Ther.* 18:413–420. doi:10.1038/mt.2009.210.

Zhu, C., A.C. Anderson, A. Schubart, H. Xiong, J. Imitola, S.J. Khoury, X.X. Zheng, T.B. Strom, and V.K. Kuchroo. 2005. The Tim-3 ligand galectin-9 negatively regulates T helper type 1 immunity. *Nat. Immunol.* 6:1245–1252. doi:10.1038/ni1271.

Zhu, M.-L., A. Nagavalli, and M.A. Su. 2013. Aire Deficiency Promotes TRP-1–Specific Immune Rejection of Melanoma. *Cancer Res.* 73:2104. doi:10.1158/0008-5472.CAN-12-3781.

Zhu, Y., S. Yao, and L. Chen. 2011. Cell Surface Signaling Molecules in the Control of Immune Responses: A Tide Model. *Immunity*. 34:466–478. doi:10.1016/j.immuni.2011.04.008.